DEUTERON-91

PROCEEDINGS
OF THE INTERNATIONAL WORKSHOP

ОБЪЕДИНЕННЫЙ ИНСТИТУТ ЯДЕРНЫХ ИССЛЕДОВАНИЙ

E2-92-25

МАТЕРИАЛЫ МЕЖДУНАРОДНОГО РАБОЧЕГО СОВЕЩАНИЯ

ДУБНА ДЕЙТРОН-91

Дубна, 11—13 июня 1991 года

PROCEEDINGS OF THE INTERNATIONAL WORKSHOP

DUBNA DEUTERON-91

Dubna, 11—13 June 1991

Дубна 1992

С О Д Е Р Ж А Н И Е

INTRODUCTION

B. Kuehn

The Dubna Deuteron Workshop was organized by a broad collaboration, which concentrates on the investigation of the deuteron structure at small distances or large internal momenta. This collaboration arose similar to a selforganizing system partly around the experimental-technical basis at the Laboratory of High Energies in Dubna, partly initiated by the large group of physicists at LIYAF in Gatchina engaged in this field and is strongly stimulated and supported by many theoreticians at JINR and many other institutes of the USSR.

The research programme of the Laboratory of High Energies is concentrated on the problem of quantum chromodynamics at large distances. Up to now this section of the universal theory of elementary particles (standard model) is still least investigated and least understood. One of the parts of this program is the investigation of the deuteron structure.

The deuteron is the simplest nuclear system. It is composed of two nucleons, which themselves are complicated systems. They are overlapping at small distances forming a 6q-state. So in the deuteron a whole complex of problems can be studied:

- the nucleon-nucleon interaction at small distances,
- properties of overlapping bags,
- quark-gluon degrees of freedom;
- the nature of the confinement,
- determination and explanation of the static properties of the deuteron,
- and as a feed back effect additional features of the nucleon structure.

A more conventional output is the further completion of our knowledge of the deuteron wave function. Up to now the different potential models fail in giving a unique answer concerning the relative D-state

amplitude at distances smaller than 1.5 fm. Moreover inside the core the wave function is a matter of extrapolation or speculation. As we will see, our experiments offer possibilities for a considerable progress in the solution of this problem and will provide new constraints for the construction of potential models or, generally speaking, of the NN interaction.

At present in the research of the deuteron structure in Dubna are involved the following groups:

Experiments at the Synchrophasotron of LHE:

- INESS-ALPHA (LHE), a magnetic two-arm spectrometer for the study of fragmentation processes in inclusive and exclusive measurements and suitable as polarimeter and for polarization experiments;
- MASPIC (LCTA), a magnetic two-arm spectrometer with one arm for fast particles in forward direction and one arm at large angles;
- DISK (LHE), a two-arm magnetic spectrometer with a broad angular region of both arms;
- ANOMALON (LSHE), a magnetic spectrometer for forward directed particles with a large solid angle;
- Hydrogen Bubble Chamber UBK 100 (LHE), a $4\tilde{\pi}$ -detector for fragmentation processes, particle production and for polarization measurements.
- Polaris (LHE), the source of polarized deuterons.

These setups are installed at the beam lines of the Synchrophasotron and can be supplied with every beam from this accelerator including polarized deuterons with momenta up to 9 GeV/c. They are equipped with liquid hydrogen or deuterium targets. The polarized deuteron beam is produced by the cryogenic ion source POLARIS installed 6 years ago by the cryogenic group of Yu.K.Pilipenko. Vector- and tensor-polarized deuterons are available. The experimental work with the polarized beam is fully established and reliable.

The experimental groups are strongly supported by the theoretical groups of V.K.Lukyanov at the Laboratory of Theoretical Physics and of G.I.Lykasov at the Laboratory of Nuclear Problems.

The quoted groups are united in a central research project of JINR called:

"Search and Investigation of Non-Nucleon Degrees of Freedom and Spin Effects in Few Body Systems".

This work in Dubna is supported and supplemented by further groups at other institutes in the Soviet Union. Experimental work with an old

tradition is performed at LIYAF, Gatchina, at the 1 GeV proton synchrocyclotron, at the electron accelerators at the Kharkov Physical-Technical Institute and at the Institute of Nuclear Physics of the Sibirian Section of the Academy of Sciences in Novosibirsk. Theoretical groups are working in this field at the Moscow State University, at the Institute of Theoretical Physics in Kiev, at the Tashkent State University, at the Far East University in Vladivostok, at the Moscow Institute of Theoretical and Experimental Physics and at the Physical Institute of Academy of Sciences.

Recently the scientific council of the Nuclear Physics section of the Academy of Sciences has stated the high scientific significance of the research in our field in Dubna and the other institutes and recommended its further financial support.

Institutes of other states, members of JINR, such as Bulgaria, Czechoslovakia, Germany, Poland and Rumania are also involved in our program. Joint experiments with SATURNE, France and at the COSY installation in Yulich, FRG are being in preparation.

The technical basis here in LHE is still the Synchrophasotron. It will be replaced in the near future by the new cryogenic synchrotron NUCLOTRON, which is in the state of assembly. The prospects of the investigation of the deuteron and of polarization experiments will be presented in detail by the following speakers.

These prospects need the support of our community to get the necessary funding. Therefore the organizing committee proposes our collaborants to agree at the end of the meeting a short statement concerning the scientific significance of our research and the development of the technical basis. We cordially invite our guests to take part in the discussion of such a statement.

Now some words about the construction of our program.

We have to deal with a system consisting of two nucleons, which are also composite particles of complicated structure and are overlapping at small distances. So our problem has a dialectic aspect: the deuteron has to be understood, as well as a composite, as an entire object. To illustrate this situation I would like to quote a poem of the famous German poet, thinker and scientist J.W. von Goethe [1]. He meditated just on such an aspect concerning the leaves of the Gingo tree, which are splitted in the shown manner (Fig.1)

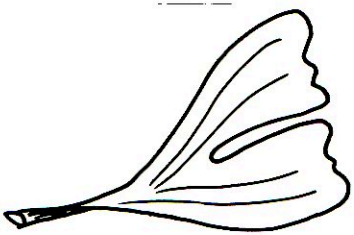

Fig. 1. Leave of the Gingo tree.

Gingo Biloba

Dieses Baumes Blatt, der von Osten
Meinem Garten anvertraut,
Gibt geheimen Sinn zu kosten,
Wie's dem Wissenden erbaut.

Ist es ein lebendig Wesen,
Das sich in sich selbst getrennt?
Sind es zwei, die sich erlesen,
Dass man sie als eines kennt?

Solche Fragen zu erwidern
Fand ich wohl den rechten Sinn;
Fühlst Du nicht in meinen Liedern,
Dass ich eins und doppelt bin?

The leaves of the Gingo tree, which from the east
Was entrusted to my garden,
Give to taste me secret sense
How it satisfies the wise.

Have we here a living being,
Which divided self itself?
Are there two, which give to know,
That they are a single one?

Search an answer to such questions,
As I found, makes real sense;
Don't you feel it in my songs
That I'm as well one as double?

Outgoing from the point of view "Are there two, which give to know, that they are a single one", we decided to include into our program a review talk on the status of our knowledge of the nucleon structure. After this it is natural to dedicate a session to that, what makes them a "single one", that means to the NN-interaction in the light of phenomenological potentials, bag models and QCD.

The main part of the program is devoted to the experimental study of the deuteron structure by means of hadronic probes, i.e. by nucleons and pions, and the theoretical interpretation of these experiments. These are the central activities here in Dubna

By these means we are studying essentially the dynamical properties of the deuteron. The static properties of an object, its geometry, configuration, symmetries, etc., are important but cannot present the complete picture.

This I want to demonstrate by surely the only experiment, which we will see live at this workshop (Fig.2). The considered system consists

of one double conus, which I will call "bolus", and two inclined rails in a specific configuration, the "antibolus". These particles together are forming none other than the "diabolus". The "diabolus" is characterized by its geometrical parameters and by one axis and several planes

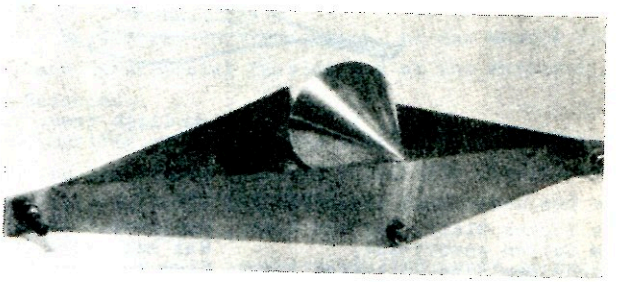

Fig.2. The two particle system "diabolus"

of symmetry. But from this we are learning not very much about the nature of this system. To study the dynamical behaviour we must excite the system. So I kick the "bolus" off its position on the top of the rails. It goes down, but soon it climbes back to the top, goes over the top down on the other side of the rails, comes back to the top and so on. It oscillates obviously around its stable position, which is paradoxically just on the top. We of course easily find the explanation of this strange behaviour and understand that the static picture of our system was extremely incomplete. We need a further particle to explain the dynamics of the "diabolus" and this is not more and not less than the earth, which supplies us with the gravitation, responsible for the observed motion. The analysis of these dynamics allows us to determine the role of the different parameters of the system, their mutual dependence, the limits of parameters within which we find a certain behaviour. That means we get only from such an experiment the full understanding of the object.

The same is true for our study of the deuteron. We need its static parameters and we need the dynamical behaviour of it, that means the interaction with other particles, its fragmentation under certain conditions, for instance in a polarized state, formation of highly excited states (dibarions, narrow resonances) or the interaction of it as a cumulative particle, as "a single one".

The investigation of the deuteron by hadronic probes is supplemented by experiments at electron beams. The study of the deuteron is an important part of the research programs at SLAC, CEBAF, at Novosibirsk,

Kharkov and at other electron accelerators. The results of these experiments are of extreme importance for our knowledge of the deuteron structure. So our workshop would be rather incomplete, if we wouldn't take into account these investigations.

Unfortunately the problem of the relativistic description of the deuteron up to now is not uniquely solved. This is a principal difficulty for all relativistic many body systems. In our case it is a crucial point for all interpretations of our experiments. Different procedures of relativisation result in different predictions. Therefore we included a special session for the discussion of this fundamental problem.

Last but not least we organized two talks, a theoretical one and an experimental one, on the spin structure of the nucleons, which is studied nowadays at high energies. It should strongly affect the spin structure of the deuteron at small distances. So we are immediately connected with this problem and, perhaps, will have the possibility to seriously contribute to these investigations.

After this short survey of our program let us start our work. I wish you an interesting meeting with many stimulating discussions.

Reference

[1] Johann Wolfgang v. Goethe (1749-1832), West-Oestlicher Divan, translation by B.Kuehn.

PREPARATION OF THE JOINT DUBNA-SACLAY $\Delta\sigma_{L,T}(\vec{n},\vec{p})$-EXPERIMENT WITH POLARIZED BEAM AND TARGET AT THE JINR LABORATORY OF HIGH ENERGIES

Dubna - Saclay - Geneva - Villigen - Freiburg - - Prague Collaboration

J.Ball[1], N.S.Borisov[2], J.Bystricky[3], A.N.Chernikov[4], E.V.Chernykh[5], P.Demierre[6], S.V.Dzhemukhadze[5], A.N.Fedorov[4], J.M.Fontaine[7], G.Gaillard[6], L.B.Golovanov[5], R.Hess[6], Z.Janout[8], Yu.M.Kazarinov[2], A.D.Kirillov[5], Yu.F.Kiselev[4], A.Klett[9], J.Konichek[8], B.Kuehn[5], V.P.Ladygin[5], C.Lechanoine-Leluc[6], F.Lehar[3], A.de Lesquen[3], M.C.Mallet-Lemaire[1], S.Mango[10], P.K.Maniakov[5], E.A.Matyushevsky[5], B.C.Neganov[4], A.A.Nomofilov[5], V.V.Perelygin[4], V.F.Peresedov[5], S.A.Popov[4], D.Rapin[6], E.Rossle[9], P.A.Rukoyatkin[5], H.Schmitt[9], V.I.Sharov[5], L.N.Strunov[5], A.L.Svetov[5], S.A.Zaporozhets[5], A.V.Zarubin[4], L.S.Zolin[5]

1 LNS, CEN-Saclay, France
2 LYaP, JINR Dubna
3 DPhPE, CEN-Saclay, France
4 PPL, JINR, Dubna
5 LHE, JINR, Dubna
6 DPNS, University of Geneva, Switzerland
7 DPhN/ME,CEN-Saclay, France
8 Politechnical Institute, Prague, ChSFR
9 University of Freiburg, FRG
10 PSI, Villigen, Switzerland

We would like to tell, briefly, about the project of experiments, its status, organization and preparation of necessary equipment. The proposal of experiments was entitled as: "Measurement of $\Delta\sigma_L$ and $\Delta\sigma_T$ Total Cross Section Differences in Transmission Experiments at Energies of 1 - 4.5 GeV/N of Polarized Deuteron Beam at the Dubna Synchrophasotron and Nuclotron".

We propose to start systematic investigations of spin effects in NN-, dN-, and dd-scattering over this energy region. Systematic investigations of NN-scattering in a several GeV energy region are fundamentally important for understanding of the NN-force nature and nuclear core spin structure. In addition, it will be interesting to discover some anomalies in energy dependence of spin observables (they can be related to nonnucleonic degrees of freedom of nuclear matter).

The presence of the polarized deuteron beam (up to 10 GeV/c) at the Dubna Synchrophasotron of the High Energy Laboratory (JINR) allowed to obtain first data concerning the spin structure of deuteron core and gives unique conditions for the advance of studies in the field of relativistic nuclear physics (investigation of the lightest nuclei structure at small distances) and for experiments on NN-scattering. Measurements of the differences $\Delta\sigma_L$ and $\Delta\sigma_T$ of pure spin state total cross sections for np-interactions at incident neutron energies of 1-4.5 GeV are the first experiment of the planned programme. Results of this experiment will immediately allow us to estimate how large spin effects are and whether the structure of the energy dependence $\Delta\sigma_{L,T}$ exists in this energy region.

The intention of the $\Delta\sigma$ -experiment had been given in the main by Professor F.Lehar as a natural extention of the Saturne II NN-programme to a higher energy region. For example, we attract your attention to extracts from the status report of the Saturne II Nucleon-Nucleon group[1]:"It will be useful to mention a possible extention of the np spin dependent total cross section differences above the Saturne II energy region in context with checks of a possible structure observed in $\Delta\sigma_L$ energy dependence by ANL-HEP physicists. At present, the unique accelerator providing a polarized deuteron beam is the Dubna JINR-LHEP synchrophasotron. A variable momentum of the Dubna accelerator reaches up to 9.5 GeV/c. The intensity of this beam is more than 10^9 deuterons/ spill which may provide more than 10^5 neutrons/ spill on the target. This allows to use the stable low-efficiency transmission detector...".

$\Delta\sigma_{L,T}$ Project Status

- several times the project was reported to scientific audience;
- it had obtained positive references of critics and high appreciations of experts of the LHE Scientific Technical Council;
- it had beenapproved by the LHE Scientific-Technical Council and the JINR Scientific-Coordinated Council;
- it had been included in the JINR Problem-Subject Plan of 1991;
- the realization of this project was started from the end of 1990.

Formalism

The description of the nucleon-nucleon experiment formalism had been given on the whole by J.Bystricky, F.Lehar and P.Winternitz /2/. The total nucleon-nucleon cross section is written down as the sum:

$$\sigma_{tot} = \sigma_{0,tot} + \sigma_{1,tot}\cdot(\vec{P}_B\cdot\vec{P}_T) + \sigma_{2,tot}(\vec{P}_B\cdot\vec{k})(\vec{P}_T\cdot\vec{k}), \quad (1)$$

where $\vec{P}_B$ and $\vec{P}_T$ are the polarization vectors of beam and target, respectively, $\vec{k}$ is a unit vector in the beam direction, and $\sigma_{0,tot}$ is the unpolarized total cross section. The two other cross sections are related to the observables $\Delta\sigma_L$ and $\Delta\sigma_T$ by

$$\Delta\sigma_L = \sigma(\rightleftarrows) - \sigma(\rightrightarrows) = -2(\sigma_{1,tot} + \sigma_{2,tot}) \quad (2)$$

$$\Delta\sigma_T = \sigma(\downarrow\uparrow) - \sigma(\uparrow\uparrow) = -2\sigma_{1,tot}, \quad (3)$$

where $\Delta\sigma_L$ and $\Delta\sigma_T$ are the cross section differences measured with beam and target polarization vectors parallel and antiparallel to each other, and oriented longitudinally ($\Delta\sigma_L$) or transversally ($\Delta\sigma_T$) with respect to the beam.

The isoscalar parts of $\Delta\sigma_L$ and $\Delta\sigma_T$ can be evaluated according to equations:

$$\Delta\sigma_{L,T}(I=0) = 2\Delta\sigma_{L,T}(np) - \Delta\sigma_{L,T}(pp). \quad (4)$$

To demonstrate the values of the measured total cross section differences, we show (see Fig.1 and Fig.2) the existing $\Delta\sigma_{L,T}$ data for np-interactions from the SaturneII Nucleon-Nucleon group papers/1,3,4/. As is seen, the values of total cross section differences are of several millibarns.

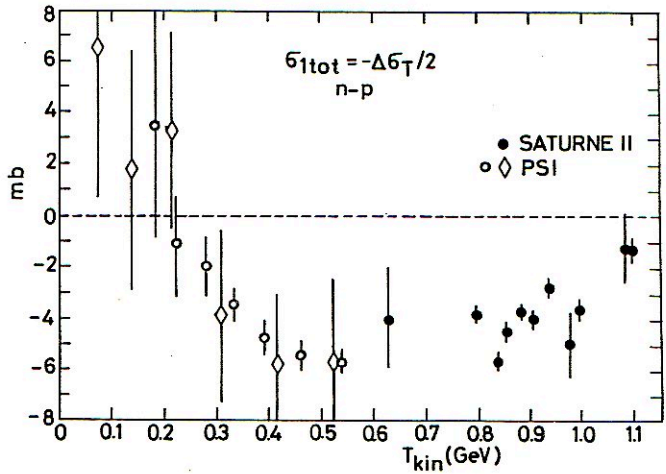

Fig. 1.- $\sigma_{1tot} = -\Delta\sigma_T/2$ energy dependence.
● ..... SATURNE II.
○ ..... ref.[6].

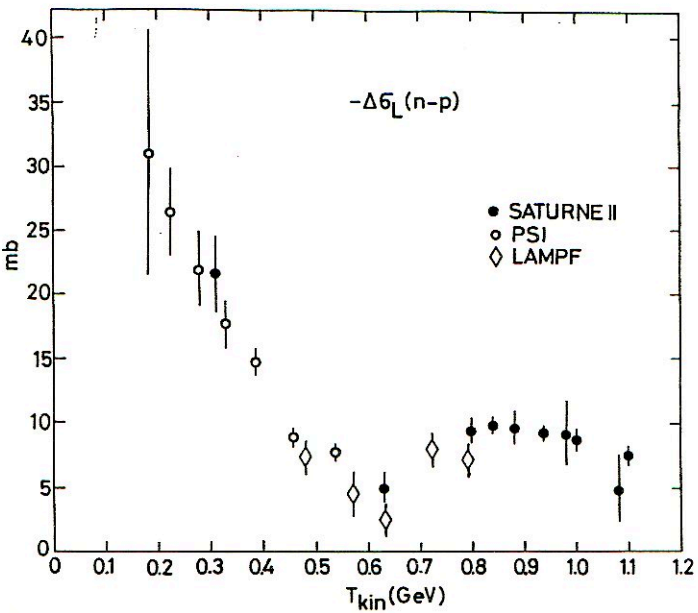

Fig. 2. - $-\Delta\sigma_L$ energy dependence.
● ..... SATURNE II.
○ ..... ref.[6].

Organization of the $\Delta\sigma$ -Experiment

Figure 3 shows a scheme of an experimental set-up. The elements of this scheme are the following:

DP - the two arm deuteron beam polarimeter;

T_s - the Be or C neutron production target;

DM - the cleaning dipole magnet for sweeping charged particles (protons, deuterons,...) from the neutron beam direction;

CD - blocks of biological defence; collimator for forming of the necessary cross section of the polarized neutron beam (about 30 mm in diameter);

SPM - the spin-precessing magnet;

PPT - the polarized proton target;

I - the neutron beam intensity monitor before the polarized target;

TD - the transmission detector to measure the neutron intensity behind the PPT;

and, lastly, NP - the neutron beam polarimeter for controlling the T or L neutron polarization directions.

The polarized beam of free neutrons is generated by the polarized deuteron break-up on the production target T_S. The spin-dependent cross-sections are measured by the attenuation of the polarized neutron beam passing through the polarized proton target PPT. For measuring $\Delta\sigma_T$ the spin-precessing magnet is turned off. The vertical direction of the neutron beam polarization vector remains as an accelerated and extracted deuteron beam one. For measuring $\Delta\sigma_L$ the spin-precessing magnet is turned on and neutron spins are precessed into the longitudinal direction. The PPT polarization must also be oriented in the vertical (for $\Delta\sigma_T$) and longitudinal (for $\Delta\sigma_L$) directions.

Now, let us fix your attention on some characteristics of the planned set-up elements and equipment which are necessary for the set-up running.

Polarized Deuteron Beam

We shall use polarized deuterons of the slowly extracted beam lines MV1 and VP1 at Experimental Hall 205 at the High Energy Laboratory of the JINR. The beam momentum can be changed from approximately 1 GeV/c up to roughly 9 GeV/c. At present, the intensity of the polarized deuteron beam is approximately $2 \cdot 10^9$ deuteron/cycle. The value of the beam vector polarization is approximately $P_z \simeq 0.4$, that is $\sim$ 60% from maximum value only for the vector polarized beam. The sign of the beam polarization can be changed cycle by cycle.

Beam Line Deuteron Polarimeter

We shall use the working polarimeter of the ALPHA set-up. This is the fast two-arm deuteron polarimeter[5] at focus F5 of the VP1 beam line. For measuring of two values $+p_z$ and $-p_z$ with 5% accuracy only ~15 minutes are necessary at the deuteron beam intensity of 10^9 deuteron/cycle. The polarization components of the polarized deuteron beam are determined in the elastic forward scattering of 3 GeV/c deuterons on hydrogen because in this case calibration data for the analyzing powers are known with a good accuracy. Elastically scattered deuterons on protons (liquid hydrogen is used) are detected in a set of scintillator counters in forward directions in coincidence with recoil protons using Δ E-E scintillation telescopes.

The incident beam monitoring is carried out with the gas ionization chamber.

Neutron Beam

An intense polarized neutron beam with well defined orientation of polarization and small energy spread will be obtained by a break-up of polarized deuterons on a production target. The neutron beam axes can be chosen either as the direction of the beam line VP1 or the 4V one before the 2SP12 magnet. At present, the VP1 direction is more preferable for a better biological defence.

The neutron generation target T_s (approximately 20 cm thick Be or C) will be placed before the 3SP12 magnet, i.e. cleaning magnet. The calculations show that for the deuteron beam intensity of 10^9d/cycle at the 15 m distance from the 20 cm thick C target, the neutron flux through a cross section of 2.5 cm in diameter will be 2.4×10^5 neutron/cycle for the deuteron momentum of 3 GeV/c and 2.2×10^6 neutron/cycle for the deuteron momentum of 9 GeV/c.

In the 4V beam direction the testing runs for tracing of the neutron beam axes and measuring of the neutron flux were made at the end of December 1990 and March 1991. The neutron flux at the PPT placing area for the above mentioned conditions was estimated as 10^6 neutron/cycle for the deuteron momentum of 9 GeV/c.

Without a collimator and with the cleaning magnet turned on the charged particle background at the PPT placing region was estimated as 5% from the neutron flux. Now the collimator mounting is being made at the end of the VP1 direction.

Spin-Precessing Magnet

In order to precess neutron spins from the vertical direction to the longitudinal one, it is necessary to have a dipole magnet with a side-way magnetic field direction and a magnetic field integral of about 2.5 Teslameter. It will be obtained using a usual "warm" magnet of the SP94 type.

Intensity Monitor and Transmission Detector

To measure $\Delta\sigma_{T,L}$, the same method as Saturne II and PSI by F.Lehar et al.[1,6] will be used. Detectors for monitoring the incident collimated neutron beam and the neutrons having passed through the target are CH_2 convertors and scintillation counters. The convertors are placed immediately behind a large veto scintillator and charged particles emitted forward are detected by two counters in coincidence. This method is less efficient but provides better stability of detection efficiency compared to the live-target one.

Transmission measurements of the deuteron-proton total cross sections can be also made with a high rate if the whole deuteron beam intensity and integral type detectors (ionization chambers or current regime scintillation counters) will be used. This method allows one to measure quickly and with high statistical precision the energy dependence of the deuteron-proton and deuteron-deuteron total cross section differences. It is important for the problem to search for high excited states of 3N- and 4N-systems.

Polarized Proton Target

Various possibilities to get a sufficient volume PPT were studied. There are two ways: either we use PPT from other scientific centers or create an own large volume PPT at the JINR. The JINR specialists suggested the project of creating a frozen spin mode polarized proton target with a volume of about 0.5 ℓ. This "big" target is planned to be put into operation at the end of 1994.

The possibility of bringing PPT from other scientific centers to the first stage of experiment is studied. So, it is possible to use the Argonne - Saclay PPT (~ 140 cm^3)[7] which may be brought from the FNAL.

Let us fix your attention to some statistic estimations. To get one value of $\Delta\sigma$(np) at fixed energy with the statistical error of about 0.1 mb using the 30 cm length PPT, one needs 50 hours for the value of the polarized deuteron beam intensity $I \sim 1 \times 10^9$/cycle. If integral

type detectors are used, the same $\Delta\sigma$ (dp) statistical error can be obtained for the 4 cm length PPT within 20 minutes.

Data Acquisition System

The system of automatization accepts data from the computer of the beam control and the beam channel group, the direction of the beam polarization data from the automatization subsystem of the ALPHA polarimeter and data from deuteron beam position and dimension detectors located in several beam trajectory points. Every one-cycle and summary run information may be monitored visually with the help of graphic displays.

If necessary current target parameters such as polarization, temperature and magnetic field parameters must be included in the monitoring data. In this case the system of automatization is linked with the target monitoring subsystem. After each cycle the monitoring data must be recorded together with the main data.

The main data are an array of monitoring numbers, about 20 16-bit words being read from CAMAC scalers. Parallel with statistics being obtained, the pulse height distribution measurement for each counter of the neutron detecting system is triggered additionally to control information with the help of charge-digital converters.

The system consists of an IBM PC XT/AT computer based on a microcomputer and a CAMAC parallel branch driver interface in the PC input-output system. In accordance with the EUR 4600 document the driver is able to drive a branch with 7 crates. The driver is manufactured as a CAMAC unit and located in one of the branch crates. Colour TV monitors controlled by interfaces in CAMAC crates are used to present the information in a graphic form. For the system control and tests a toggle-switch and parallel input-output CAMAC registers are used.

An on-line programme in PC controls the set-up. The operator interface of the system is based on an electronic table: the hardware configuration, i.e. types, characteristics and station numbers of CAMAC modules, statistics obtaining regimes, types of graphics to output on TV screens and other input system parameters are specified as elements of the electronic table.

By data acquisition the IBM PC accepts data from the CAMAC to the PC RAM, then together with the transputer processes the data and transmits the information in a graphic form on the PC display or TV monitors. The information is written down on a fast tape cartridge or through the EC 1010 (Mitra 15) minicomputer on a magnetic tape with standard density.

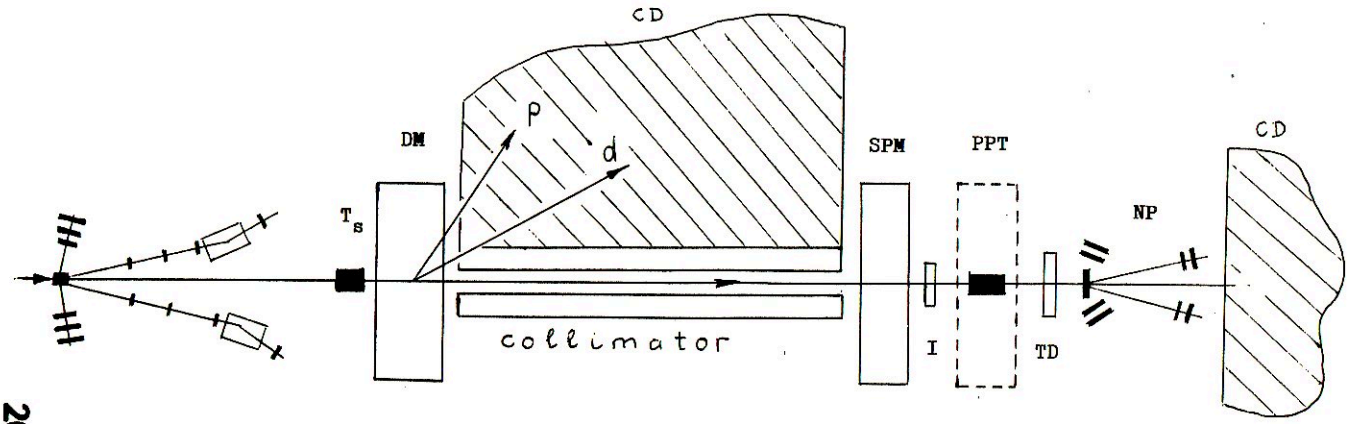

Fig.3. SCHEME OF THE EXPERIMENTAL SET-UP.

DP - two arm deuteron polarimeter

T_s - Be neuteron production target

DM - deflecting dipole magnet

SPM - spin precessing magnet

PPT - polarized proton target

I - intensity monitoring detector

TD - transmission detector

NP - neutron polarimeter

References

1. P.Bach, J.Ball et al. Exp. 144. Group Nucleon-Nucleon Status Report. 15-10-1990.
2. J.Bystricky, F.Lehar and P.Winternitz. Journal de Physique (Paris)39, p.1, 1978.
3. F.Lehar. Invited Talks on the Paris and Bonn Conferences (1990).
4. F.Lehar. Invited Talk on the Specialists' Meeting on Neutron Cross Section Standards for the Energy Region above 20 MeV. May 1991. Uppsala, Sweden.
5. V.G.Ableev et al. Nucl.Instr.&Meth. A306, p.73, 1991.
6. R.Binz et al. Nucl.Phys.A508, p.267, 1990.
7. J.Ball et al. Preprint CEN-Saclay DPhPE84-15, 1984.

NN INTERACTION FROM QUARK MODELS AND QCD

H.J. Weber*

University of Virginia, Charlottesville, VA 22901, USA

1. Introduction

Since nuclei are composed of nucleons it has been a goal of nuclear physics to explain nuclear properties starting from the nucleon-nucleon (NN) interaction. Thus, NN scattering has been studied intensely and for more than fifty years.

Yukawa's pion exchange (OPE[1]) has provided the first mechanism for the nuclear force. The OPE potential is the component of longest range because the pion is the lightest meson and the mass of the exchanged meson is inversely proportional to the range of the force. From peripheral phase shifts and accurately measured deuteron properties, such as its quadrupole moment and asymptotic D/S wave function ratio, the pion-nucleon coupling constant $g_{\pi NN}$ is known within a few percent, and the OPEP has been disentangled from the remaining (two-pion, TPE, and vector-) meson exchanges and other non-mesonic contributions at shorter internucleon distances. The pionic exchange current (MEC) is a direct consequence and prediction of the OPE mechanism. It has been clearly observed in the electro-disintegration of the deuteron near threshold at large momentum transfer ($\simeq_1 4.5$ fm^{-1}), where the pion-MEC fills in a zero in the transition to the $^1S_0$ wave. This confirmation of the pion-MEC has put the OPEP on firm grounds, albeit as an effective degree of freedom of the strong interaction at low energy [2].

The pion-nucleon (and all other meson-nucleon) vertex form factor is less well understood as it is related to the internal structure of the nucleon. Nucleons and mesons are long known to be composed of quarks. The constituent quark model (NQM) gives a fair account of their internal structure. The exclusion principle for quarks has led to the color concept as analog of charge for the strong interaction between quarks, where each quark carries one of three colors. Since the early 1970's quantum chromodynamics (QCD, [3]) has evolved as the SU(3)-color gauge theory of the strong interaction, in which quarks and eight gauge bosons, called gluons, are the fundamental pointlike particles. QCD has two interrelated unusual properties. Asymptotic freedom says that its running coupling constant, $\alpha_s(q^2) = g^2/4\pi$, becomes small at high momentum transfer q^2, so that perturbation theory applies there, while it grows larger at low q^2, thereby helping to confine quarks and gluons inside color singlet hadrons.

As the nuclear forces are the long range part of the strong interaction, there have been numerous attempts to derive them from QCD. Some involve effective quark-antiquark exchange motivated by the corresponding valence quark content of mesons. This will be discussed in Sect. 2, and non-mesonic quark interaction models in Sect. 3. Another fruitful approach involves the large color limit of a SU(N_c), $N_c \to \infty$, gauge theory where meson dynamics is reproduced and baryons become topologically stable meson configurations [4]. Such a theory of pions and a nucleon soliton was first proposed by Skyrme [5]. More recently isospin-SU(2) instantons have been used to construct approximate Skyrmion solutions, [6]. These aspects will be discussed in Sect. 4.

*Supported in part by the U.S. National Science Foundation.

2. Quark-Antiquark Exchange

The nuclear force is known to be charge independent, and the neutron and proton masses are nearly the same. They represent a doublet, and the three pions a triplet, of the underlying SU(2) isospin symmetry of QCD, which is broken by the electromagnetic interaction to a few percent. The small pion mass compared to all other hadrons can be understood by the chiral symmetry of QCD, which leaves the quark helicities (their spin projection along their direction of motion) invariant. Or equivalently for zero mass quarks, the axial and vector currents are conserved. The non-zero pion decay constant $f_\pi = 93$ MeV in the axialvector matrix element $<0|A^\mu|\pi(p)> \sim i f_\pi p^\mu$ signals the spontaneous breakdown of chiral symmetry in QCD. This is qualitatively well described by the Gell-Mann - Lévy sigma model which has a Mexican hat-type potential for the quartet $(\sigma,\vec{\pi})$ of scalar fields so that the isoscalar σ develops a non-zero vacuum expectation value σ_0 at the rim of the hat [7]. The pseudo-scalar isovector pion field becomes the Goldstone boson associated with the degenerate ground state along the rim of the hat. Quarks acquire a constituent mass $m_q = gf_\pi = g\sigma_0$, where g is the common σ-$\vec{\pi}$ coupling constant. However, a far smaller scalar coupling constant is needed in the NN potential for the spin-isospin independent attraction at medium distances, if it is parameterized in terms of a σ-meson exchange with a mass of about 0.55 GeV.

In the MIT bag model (usually) massless free quarks and gluons are confined inside a sphere that is surrounded by the QCD vacuum. Inside there is a perturbative vacuum so that asymptotic freedom holds; outside chiral symmetry is broken spontaneously. At the bag boundary r=R, there is no radial current, $\hat{r}\cdot\bar{q}\vec{\gamma}q=0$, which corresponds to an infinite square well confinement potential and the boundary condition

$$-i\hat{r}\cdot\vec{\gamma}q=q, \quad r=R. \tag{1}$$

When a quark reflects from this surface, its spin will not be turned around so that its helicity is not conserved there. To remedy this violation of chiral symmetry the pion field is coupled to quarks at the surface r=R in order to chirally rotate their spin (chirality is equivalent to helicity for massless quarks). Thus, eq.(1) is replaced by

$$-i\hat{r}\cdot\vec{\gamma}q=\exp(i\vec{\pi}\cdot\vec{\tau}\gamma_5/f_\pi)q, \quad r=R. \tag{2}$$

The continuation of the axial current $\hat{r}\cdot\bar{q}\gamma_5\vec{\gamma}\vec{\tau}q/2$ inside (for the lowest Dirac wave function with S-wave large component) to $f_\pi\hat{r}\cdot\vec{\nabla}\vec{\pi}$ outside determines the pion-quark coupling constant from which the pion-nucleon coupling constant follows [8]. A nucleon bag with a pion source on its surface will generate the conventional OPEP (and TPEP) of the NN force, when the pion is allowed to propagate inside the bag. In that case chiral symmetry is spontaneously broken also inside the bag, so that there will be constituent quarks rather than current quarks, just like in the naive quark model. Although the bag was designed as a relativistic model of asymptotic freedom and confinement in QCD, it is not Lorentz invariant (neither quarks nor the bag can be boosted properly; alternative covariant quark models are developed on the light cone [9]) and it appears to be inconsistent with QCD sum rules. From the latter we know the value of the gluon condensate

$$<(gF^c_{\mu\nu})^2>_0 \simeq 0.5\ \text{GeV}^4, \qquad (3)$$

which, using the trace anomaly of QCD, gives an estimate for the energy density difference between the hadron and the vacuum around it [10], which is given by the bag constant B in the bag model,

$$\varepsilon_{vac}=tr(T_{\mu\nu})/4 = -(33-2N_f)<(gF^c_{\mu\nu})^2>_0/3\pi^2 2^7 \simeq -0.5\ \text{GeV/fm}^3 \simeq -10B. \qquad (4)$$

This means that B is ten times too small and the concept of a perturbative vacuum inside at low energy is not correct, constituent quarks (in an instanton vacuum) are required to restore the energy balance. Nonetheless, from chiral bag models we learn that the chiral symmetry of QCD for confined quarks requires a pion cloud around hadrons. It provides the link with nuclear forces at long and intermediate ranges.

A more general treatment allows including other mesons as well upon starting from the generating functional of QCD (without the gauge fixing and ghost terms)

$$Z(J,\eta,\bar\eta) = N\int DAD\bar qDq\Delta_F \exp\{i\int d^4x\ [L+J\cdot A+\bar q\eta+\bar\eta q]\} \qquad (5)$$

$$L=-\tfrac{1}{4}F^c_{\mu\nu}F^{\mu\nu,c}+\bar q\gamma^\mu(i\partial_\mu-g\tfrac{\lambda^c}{2}A^c_\mu), \quad F^c_{\mu\nu}=\partial_\mu A^c_\nu-\partial_\nu A^c_\mu+gf^{cab}A^a_\mu A^b_\nu . \qquad (6)$$

We know that the nonlinear terms in the field tensor $F^c_{\mu\nu}$ and L are ultimately responsible for asymptotic freedom at high momentum and for color confinement at low momentum. If we ignore them, the gluon fields can be integrated out leading to the quark action L_q in the functional $W=\exp(iL_q/2)$ with the quark current $J^\mu = g\bar q\gamma^\mu\lambda^c q/2$ in

$$L_q = \int\int d^4x d^4y J^\mu(x) G_{\mu\nu}(x-y) J^\nu(y) \qquad (7)$$

and the gluon propagator $G_{\mu\nu}$. Upon modifying the short range components of $G_{\mu\nu}$ so as to reproduce asymptotic freedom and those at long range to generate a linear confinement potential, one can put back into the effective gluon propagator $G_{\mu\nu}$ in eq.(7) the most important nonlinear effects of (5). With that in mind, let us consider two quarks, one from each surface of two colliding nucleons. If the nucleons do not overlap, color confinement precludes the direct term in eq. (7) from contributing to their interaction. Upon Fierz transforming the exchange term

$$\bar q_2,\gamma^\mu\lambda^c q_1\cdot\bar q_1,\gamma_\mu\lambda^c q_2=\tfrac{8}{9}(\bar q_2,q_2\ \bar q_1,q_1+\bar q_2,i\gamma_5\vec\tau q_2\cdot\bar q_1,i\gamma_5\vec\tau q_1$$

$$+\bar q_2,i\gamma_5 q_2\ \bar q_1,i\gamma_5 q_1+\bar q_2,\vec\tau q_2\cdot\bar q_1,\vec\tau q_1)$$

$$+\tfrac{4}{9}(\bar q_2,i\gamma^\nu\vec\tau q_2\cdot\bar q_1,i\gamma_\nu\vec\tau q_1+\bar q_2,i\gamma_5\gamma^\nu\vec\tau q_2\cdot\bar q_1,i\gamma_5\gamma_\nu\vec\tau q_1)+... \qquad (8)$$

were repeated indices are summed over as usual, it displays its color singlet, chiral invariant quark transitions [11]. This approach has been generalized to a bosonization of QCD in terms of meson fields [12] ignoring correlations from instantons. If eq. (8) is restricted to a single point x, i.e. $G_{\mu\nu}$ is dominated by a contact term, eq. (8) would represent the interaction Lagrangian of a Nambu-Jona-Lasinio model [13]

which is known to drive meson dynamics and exhibit spontaneous breakdown of chiral symmetry. For the σ and π channels there is support for a nearly pointlike four-quark interaction from instantons and for vector-mesons from the hidden SU(2) symmetry [13].

Instantons are non-perturbative self-dual Yang-Mills solutions of finite energy in 4-dimensional Euclidean space of any SU(2) subgroup of SU(3)-color [14]. They do not confine, but appear to stabilize at the small size of about 1/3 fm. Assuming a quark condensate, $\langle\bar{q}q\rangle_0 \neq 0$ inducing a rearrangement of the vacuum leading to a spontaneous chiral symmetry breakdown, quarks in an instanton vacuum are known to become constituent quarks. The relevant Lagrangian [15] is

$$L = \bar{q}(i\gamma\cdot\partial - m_q)q + G\{(\bar{q}q)^2 + (\bar{q}i\gamma_5\vec{\tau}q)^2 - (\bar{q}i\gamma_5 q)^2 - (\bar{q}\vec{\tau}q)^2\}, \qquad (9)$$

where all quarks are located within the size of about 1/3 fm of a typical instanton and G depends on the instanton density. Thus, the quark contact approximation seems realistic for the scalar-isoscalar (σ) and the pseudoscalar-isovector ($\vec{\pi}$) channels upon comparing eqs.(8) and (9).

Using bag model quark wave functions as a confinement model we can infer from eq.(8) meson-quark couplings in lowest quark loop order e.g.

$$\Gamma_{\pi NN} = G\langle N|\int d^3r(\bar{q}i\gamma_5\vec{\tau}q)\exp(i\vec{q}\cdot\vec{r})|N\rangle, \qquad (10)$$

$$\Gamma_{\rho NN} = (G/\sqrt{2})\langle N|\int d^3r(\bar{q}i\gamma^\mu\vec{\tau}q)\exp(i\vec{q}\cdot\vec{r})|N\rangle \text{ , etc.} \qquad (11)$$

where G is a common quark-meson coupling constant, the integration is over the bag interior and $|N\rangle$ denotes the spin-isospin three-quark nucleon wave function. Numerical results in Table 1 for the bag model and other confinement models, such as the NQM with relativistic corrections (CQM) or a linear confinement potential, show encouraging similarities with meson-nucleon coupling constants extracted from NN data and the vector dominance model [16]. While there is one coupling constant and one D/F ratio for each mesonic SU(3) flavor octet, the only parameter G of the quark interchange model follows from the Goldberger-Treiman relation. This model has also been extended to hyperons [17].

TABLE. Comparison of meson-nucleon coupling constants from various confinement models. Tensor couplings are in parentheses

Meson (J^π,I)	Mass (GeV)	MIT Bag	Linear conf.pot.	CQM	Bonn Pot.
ε (0^+,0)	1.2	3.89	4.53	6.79	
a_0(0^+,1)	0.98	0.44	0.5	0.75	1.69
η (0^-,0)	0.5488	4.87	5.32	4.83	
π (0^-,1)	0.1385	13.4	14.8	13.4	14.08
ω (1^-,0)	0.783	6.0 (-0.4)	3.78(-0.5)	9.44(-0.49)	10.6 (0)
ρ (1^-,1)	0.77	0.67 (2.2)	0.42 (3.2)	1.05 (1.53)	0.41(6.1)
f_1(1^+,0)	1.285	0.6	0.22	0.56	
a_1(1^+,1)	1.26	1.1	0.6	1.57	

The vector-meson couplings of the quark interchange model eq. (11) etc. with broken SU(6) flavor symmetry are also consistent with those of the hidden SU(2) symmetry, where the vector-mesons are effective gauge bosons of the chiral $SU(2)_L \times SU(2)_R$ of QCD [13].

3. Short-Range NN Interaction

The meson-nucleon vertex form factors are given by various 3-quark overlap integrals and are soft as a consequence of the nucleon three-quark size of about 2/3 fm in the NQM, which is somewhat larger than an estimated 0.5 fm of the quark core from vector-meson dominance and the hidden SU(2) symmetry [13].As a result, meson-exchange potentials based on quark models become small inside inter-nucleon distances of about 1 fm, whereas conventional mesonic NN potentials become large and highly cutoff (Λ) dependent there [18] with a too small core $\sqrt{6}/\Lambda \sim 1/3$ fm from the fit of vertex form factors. Due to this strong damping, non-mesonic quark interactions can be naturally included at short distances and boundary condition (R- or P-matrix) methods are applicable. A boundary r=b is chosen that separates an external mesonic NN potential and wave function from an internal sphere with a six-quark core potential V_q and wave function ψ_q in a two-channel system

$$(T+V_h-E)\psi_h=-V_{hq}\psi_q \ , \quad (T+V_q-E)\psi_q=-V_{qh}\psi_h . \tag{12}$$

with a hadronic NN potential V_h and wave function ψ_h. Since the six-quark wave functions are mostly color octet, ψ_{88}, the core potential V_q must be confining. For example, when all six quarks are in the lowest S state in the deuteron channel, the spatially symmetric six-quark wave function can be expanded as

$$\psi_q = \frac{1}{3}\ \psi_{NN} + \sqrt{\frac{4}{45}}\ \psi_{\Delta\Delta} + \sqrt{\frac{4}{5}}\ \psi_{88} . \tag{13}$$

The internal six-quark spectrum E_ν is discrete solving $(T+V_q-E_\nu)|E_\nu>=0$. Eliminating the internal degrees of freedom, an optical potential is obtained as core potential with approximately linear energy dependence,

$$V_h(\vec{r},\vec{r}';E) = \sum_\nu <NN,\vec{r}|V_{hq}|E_\nu><E_\nu|V_{qh}|NN,\vec{r}'>/(E-E_\nu) . \tag{14}$$

The six-quark energies E_ν are also poles of the P-matrix which, for an uncoupled NN channel, is defined as the logarithmic derivative at r = b of the radial wave function. Since the NN wave function has a node for such a pole value of k, it may match a confined six-quark state $|E_\nu>$. For an appropriate b that is directly related to the three-quark bag radius, poles of P may thus be identified as multiquark states $|E_\nu>$ which can but need not be S-matrix poles (e.g., di-baryon resonances). Since the P-matrix is usually determined from the external mesonic NN wave function at r=b, its lowest pole E_0 and residue can be extracted from the energy dependence of the S-wave phase shifts between 0.5 and 1

GeV. For a large b=1.4 fm [19] and one pole E_0 at 283 MeV, the $^1S_0$ phase shift fits the data well up to 1 GeV lab energy except below 0.25 GeV, where more attraction is needed which is supplied by the meson-exchange potential when it is allowed to penetrate inside down to NN distance r=0.65 fm. A second pole gives equally good fits (cutting off the meson-exchange potential at b = 1.4 fm), but its energy is very uncertain. In ref. 11 an energy dependent six-quark potential modeled after the P-matrix approach was used to complete the construction of the NN potential at short distances. From the magnetic deuteron form factor B, b =1 fm has been extracted. The corresponding six-quark probability is about 2.3 %. Thus, reasonable fits of NN data are possible in such models. At such lower values of b (=1 fm) the lowest pole depends more on the meson-exchange potential and moves up in energy [20]. Different non pole back-ground P-matrix parameterizations correspond to different non mesonic 6-quark interactions at short range, which are better analyzed in 6-quark cluster models.

The quark cluster model (CQM, [21]) has only a rather crude mesonic potential consisting of a central and tensor term with pion exchange tails and a Gaussian that is adjusted to scattering lengths and effective ranges in each S wave channel. Its main ingredients are a two-body confinement potential and the color magnetic hyperfine interaction. The latter is repulsive for the totally symmetric spatial [6] representation, where all six quarks are in the lowest S orbit, and is attractive for the [42] state with two quarks in the P shell, so that these configurations become nearly degenerate and mix. A pure [42], as well as an admixed [42], has an energy independent node r_0 in the relative NN wave function at small NN separation acting like a hard core with S wave phase shift $\delta_0 \simeq -kr_0$, similar to the Pauli repulsion in $\alpha\alpha$ scattering at short range. Since a few years, however, evidence has been mounting against the spin dependent color magnetic two-body interaction from perturbative QCD as the only spin-splitting force in the hadron spectroscopy with a strength that is more than five times a more realistic $\alpha_s = 0.3$. In fact, the instanton generated force that supports the meson exchange picture mentioned in Sect.2 works equally well in the single hadron spectroscopy [22]. It has no problems with the unwanted spin-orbit interaction and allows reducing the strength (and problems) of the chf interaction to its perturbative level. Hence the QCM needs to be redone with such a more realistic quark interaction for V_q in the two-channel framework of Sect.2 that is consistent with a P-matrix analysis so that it gives the linear energy dependence of the NN potential at short distances and the proper energy dependence of S-wave phase shifts up to about 1 GeV, and with a quark-model based meson potential at longer distances.

4. Skyrme Models, Chiral Symmetry And Instantons

The Skyrme model has attracted much attention as part of an effective QCD Lagrangian in the large color limit, $N_c \to \infty$, at low energy [4] that starts from that of the non-linear σ-model [7]

$$L_\sigma = (f_\pi^2/4)\mathrm{Tr}[\partial_\mu U \partial^\mu U^\dagger] + \cdots \qquad (15)$$

with the non-linear pion field $U = \exp(i\vec{\tau}\cdot\vec{\pi}/f_\pi)$ in SU(2) isospin. In the Skyrme model [5] baryons are constructed as topological solitons of an SU(2) field $U(\vec{r})$ with well defined winding number, which is the baryon number A. In the hedgehog ansatz

$$U(\vec{r}) = \exp(i\theta(r)\hat{r}\cdot\vec{\tau}); \ \theta(0)=\pi, \ \theta\to 0 \text{ as } r\to\infty, \qquad (16)$$

the chiral angle θ is the solution of a variational equation obtained from the Skyrme Lagrangian (consisting of L_σ and a 4'th order derivative to stabilize the soliton) by minimizing the energy of a nucleon. This model gives a qualitatively correct picture of baryon structure and meson dynamics. For A=2 the much developed product ansatz $U(\vec{r}_1,\vec{r}_2) = U(\vec{r}_1)U(\vec{r}_2)$ provides the OPEP at long range and repulsion at short range in the static limit, but misses the spin-isospin independent attraction at medium range. When a Skyrmion is quantized as a spin 1/2 rotator, including the Roper resonance as a vibrator, a weak NN attraction has been obtained [23]. Recently [6] A = 1 and 2 Skyrmion fields have been generated from instantons, self-dual SU(2) Yang-Mills fields of topological charge 2 in Euclidean four-dimensional space. Here the SU(2) is the isospin group and not a subgroup of SU(3) color. The key is the Wilson line

$$U(\vec{r}) = T\exp(-\int_{-\infty}^{\infty} A_4(\vec{r},t)dt) \qquad (17)$$

with Euclidean time t which suggests defining a Skyrmion $U(\vec{r})=V(\vec{r},\infty)$ in terms of the solution V of $(\partial V/\partial t)V^{-1}=-A_4$ with $V(\vec{r},-\infty)=1$. For A=1,2 all instantons are conformal generalizations of 't Hooft's instantons [14],

$$A_0 = i(\vec{\nabla}\rho\cdot\vec{\tau})/2\rho, \quad \rho(x)= \sum_{i=1,A+1} \lambda_i/(x-X_i)^2, \ x=(\vec{r},t) \qquad (18)$$

where $X_i = (\vec{X}_i,T)$ is the i'th pole (which can be removed by a gauge transformation) with positive weight λ_i . Hosaki et al. [6] find the NN potential by projection that is strictly valid only for large r. Their instanton construction generates a tensor and spin interaction similar to the product ansatz for r>2 fm. Its tensor force is close to that of the OPEP. Its central force at medium range is far less repulsive than that from the product ansatz, but is still not attractive, and it gives repulsion at short range, just like the product ansatz. The Skyrmions from the instanton construction can be considered as variational approximations of the exact Skyrmion solution that reduce to the product ansatz at large r. In general they are closer to a rescaled product ansatz except for the torus, in which the identity of both A=1 Skyrmions is completely lost and which has no such product ansatz. For A = 1 the exact and instanton generated Skyrmions differ only slightly. If all poles are at the origin at different times $T_1 = -T_2 = T$, $T_3 = 0$ with weights $\lambda_1=\lambda_2=1$, $\lambda_3=\lambda$, then the Wilson line integral is elementary for the A =2 case. A hedgehog with twice the chiral angle of the A = 1 case obtains. Its energy is only 1% higher than the exact solution. Well separated A= 1 Skyrmions are obtained from A =2 instantons with well separated poles X_1, X_2 in space with much smaller weights than that of the pole at X_3. They are distinguished by the relative orientation of the well separa-

ted hedgehogs. The most attractive case has a relative rotation of about an axis perpendicular to the line joining them, which can be smoothly varied to the torus case.

Finally, Weinberg [24] studied nuclear forces from the point of view of chiral Lagrangians. The most general Lagrangian L involving pions and low energy nucleons (with momenta less than some $Q < m_\rho$) and consistent with spontaneously broken chiral symmetry is an infinite series with increasing numbers of derivatives of N fields. Other degrees of freedom (such as vector-mesons, Δ's, N^*'s, $\bar{N}$', ...) are integrated out. Their contribution is contained in the coefficients of the expansion. This L is non-linear and non-renormalizable, but allows for easy derivation of soft-pion theorems in the tree approximation. When loops are included, soft-pion processes can be calculated to any order. Ultraviolet divergences can be absorbed into redefined coefficients of L. Upon counting the powers ν of Q from a Feynman diagram with E_N external N-lines, L loops, V_i vertices of type i with n_i N-fields and d_i derivatives or m_π factors gives the relation

$$\nu=2L+2-E_N/2+\sum_i V_i(d_i-2+n_i/2), \qquad (19)$$

where $d_i-2+n_i/2\geq 0$. The leading term will be without loops and $d_i-2+n_i/2 = 0$, i. e. $d_i=1$ and $n_i=2$ or $d_i=0$ and $n_i=4$. For two nucleons graphs with pure nucleon intermediate states must be summed by solving a Lippmann-Schwinger equation to avoid infrared divergences. For two nucleons then the effective potential is given simply by the OPEP and a four-N contact interaction. This is a very crude simulation of the NN medium range attraction, but does not give the repusion at short range yet. For three nucleons the disconnected graphs (two-body interactions) are more important by a factor Q^{-2}, so that the three-nucleon effective potential enters only as a correction of higher order in Q. In the interaction of a single slowly varying external electroweak field with nucleons and pions, the minimum value of $d_i-2+n_i/2=-1$, [25], so that the leading terms involve only a single nucleon and no four-N contact term. Thus, there is no short-ranged two-body current in leading order, and only soft-one-pion exchange terms contribute to the two-body current. This justifies the chiral filter hypothesis from chiral Lagrangians.

References

1. H. Yukawa, Proc. Phys. Math. Soc. Japan, 17 (1935) 48; reprinted in Selected Papers In Foundations Of Nuclear Physics, ed. R. T. Beyer, Dover Publ. (N.Y. 1949) p.139.
2. T.E.O. Ericson and M. Rosa-Clot, Ann. Rev. Nucl. Part. Sci. 35 (1985) 271.
3. I.J.R. Aitchison and A.J.G.Hey, Gauge Theories in Particle Physics, Adam Hilger (Bristol 1989).
4. G.'t Hooft, Nucl. Phys. B72 (1974) 461; E. Witten, Nucl. Phys. B72 (1978) 445.

5. T.H.R. Skyrme, Nucl. Phys. 31 (1962) 556. E. Witten, Nucl. Phys. B160 (1979) 57.

6. M. F. Atiyah and N. S. Manton, Phys. Lett. B222 (1989) 438; A. Hosaka, M. Oka and R.D. Amado, Univ.Pennsylvania preprint UPR-0122-MT Febr.(1991).

7. M. Gell-Mann and M. Lévy, Nuovo Cimento 16 (1960) 705.

8. F. Myhrer and J. Wroldsen, Rev. Mod. Phys. 60 (1988) 629 and references therein.

9. W. Konen and H. J. Weber, Phys. Rev. D41 (1990) 2201; Z. Dziembowski et al., Phys. Rev. D39 (1989) 3257; and references therein; H.J. Weber, Phys. Lett. B233 (1989) 267.

10. E.V. Shuryak, Nucl. Phys. B203 (1982) 116.

11. M. Beyer and H.J. Weber, Phys. Lett. B146 (1984) 383 and Phys. Rev. C35 (1987) 14.

12. C.D. Roberts, R. T. Cahill and J. Praschifka, Ann. Phys. (N.Y.) 188 (1988) 20.

13. U.-G. Meissner, Phys. Rept. 161 (1988) 213 and references therein.

14. G. 't Hooft, Phys. Lett. B37 (1976) 8 and Phys. Rev. D14 (1976) 3432; A.A. Belavin et al., Phys. Lett. B59 (1975)85.

15. D.I. Diakonov and V.Yu. Petrov, Nucl. Phys. B272 (1986) 457; S.I. Kruglov, Acta Phys. Pol. B21 (1990) 985 and references therein.

16. J.J. Sakurai, Currents and Mesons, Univ. Chicago Press (1969).

17. M. Bozoian et al., Phys. Lett. B122 (1983) 138.

18. R. Machleidt et al., Phys. Rept. 149 (1987) 1 and references therein.

19. C. Fasano and T.-S.H. Lee, Phys. Rev. C36 (1987) 1906.

20. B.L.G. Bakker, I.L. Grach and I.M. Narodetskii, Nucl. Phys. A424 (1984) 563. B.L.G. Bakker, in Dubna Conf. (1990) Proc., World Sci.

21. S. Takeuchi, K. Shimizu and K. Yazaki, Nucl. Phys. A504 (1989) 777.

22. E.V. Shuryak and J.L. Rosner, Phys. Lett. B218 (1989) 72; N.I. Kochelev, Yad.Fiz. 41 (1985) 456 [Sov.J. Nucl. Phys. 41 (1985) 291]

23. G. Kälbermann and J.M. Eisenberg, Phys. Lett. B257 (1991) 259.

24. S. Weinberg, Phys. Lett. B251 (1990) 288; Univ. Texas preprint UTTG-03-91.

25. M. Rho, Phys. Rev. Lett. 66 (1991) 1275.

QCD AND DEUTERON STRUCTURE AT SMALL DISTANCES

A.P. Kobushkin

Institute for Theoretical Physics, Kiev, Ukraine

1. Introduction

The connection between the quantum chromodynamics (QCD) and deuteron structure at small distances remains one of the most intriguing problems in the nuclear physics of the last decade. A lot of experimental data for different processes at intermediate and high energies have been obtained during this period of time. To explain them, a lot of theoretical models were proposed, which take into account deuteron color degrees of freedom: constituent counting rules[1], hybrid model for deuteron wave function[2], reduced nuclear amplitudes in QCD[3], etc. Unfortunately, for reactions with unpolarized deuterons, no conclusive discrimination between quark-constituent and traditional nucleon-meson models was observed.

For example, a shoulder[+)] in the differential cross section of the A (d,p) reaction with proton emission at 0°, which was observed at the range $k > 0.2$GeV/c of an internal momentum in the deuteron, can be explained in a framework of different models, such as the manifestation of nonnucleon (quark) degrees of freedom[4-7], the final state interaction near the region of Δ -isobar excitation[8], inelastic interactions[9] and so on.

Some predictions for an energy dependence of an exclusive reactions, e.g., $d(\gamma,p)n$ at $\theta_{cm} \sim 90^{\circ}$, were done[11] using the model of reduced nuclear amplitudes in QCD. The recent data[10] suggests that at $E_{\gamma} \geq 1.2$ GeV the energy behavior of the cross section is

---

[+)] For the first time it was observed at Dubna[4] (see also ref.5) at 9 GeV/c and was confirmed in Saturne[6] at lower energies.

that of simple constituent counting rules for the deuteron as a six-quark object as well as that of the reduced nuclear amplitude model; but due to the ambiguity of theoretical calculations in terms of the traditional nucleon-meson approaches, it is impossible to clearly demonstrate its unsoundness.

To distinguish between models for the deuteron structure at small distances, one needs additional data at somewhat higher energy and/or polarized observables at present or somewhat lower energies (see, e.g. ref.12). In the present talk I would like to discuss the present situation in the experimental study of a deuteron structure at small distances as well as some theoretical models with the aim of understanding the tendency in future experimental investigations in few-body systems at high and intermediate energies.

First (sect.2), we shall discuss the results of recent measurements of polarized observables in the elastic ed-scattering. In sect.3 the analysis of data for the $d(\gamma,p)n$ deuteron break-up reaction will be reviewed. The analysis of measurements in the (d,p) break-up reaction with unpolarized and polarized deuteron beams is done in sect.4. Concluding remarks are given in sect.5.

2. Polarized observables in elastic ed-scattering. Theory and experiment

In elastic ed-scattering experiments with unpolarized particles the measurable quantities are structure functions $A(Q^2)$ and $B(Q^2)$ which can be expressed as linear combinations of the deuteron monopole (charge) G_C, quadrupole G_Q and magnetic G_M form factors:

$$A(Q^2) = G_C^2 + \frac{8}{9}\eta G_Q^2 + \frac{2}{3}\eta G_M^2 = G_E^2 + \frac{2}{3}\eta G_M^2, \qquad (1)$$

$$B(Q^2) = \frac{4}{3}\eta(1+\eta) G_M^2, \qquad (2)$$

where $\eta = Q^2/(4m_d^2)$; m_d is the deuteron mass and $Q^2 = -q^2$; q is the energy-momentum transfer. Thus, such experiments supplied only information of the electrical G_E and magnetic G_M form factors of the deuteron. But the knowledge of its monopole G_C and quadrupole G_Q form factors is essential in detailed study of NN-interaction as well as possible nonnucleon degrees of freedom in the deuteron. For example, at $Q^2 < 0.3$ $(GeV/c)^2$ the behavior of G_C is governed mainly by S-wave part of the deuteron wave function, while

the behavior of G_Q is essentially determined by D-wave part of the one. At higher Q^2 the behavior of form factor G_C was shown to be sensitive for mechanisms beyond the impulse approximation (IA) and thus it can be used to distinguish between different models.

To separate the deuteron monopole G_C and quadrupole G_Q form factors the measurement of at least one spin observable is needed. One of such quantities is the tensor analysing power of the elastic ed-scattering

$$T_{20} = -\sqrt{2}\,\frac{x(x+2)}{1+2x^2}\,, \qquad x = \frac{2}{3}\eta\,\frac{G_Q}{G_C}\,, \qquad (3)$$

which is measured in experiments with tensor polarizing deuteron target. (In experiments, where unpolarized deuteron target is used, the recoil tensor polarization of the deuteron can be measured, which gives the same combination of the form factors as eq.(3)).

The separation of the form factors at $Q^2 \leq 0.495$ (GeV/c)^2 was done in ref.13 and is displayed in fig.1.

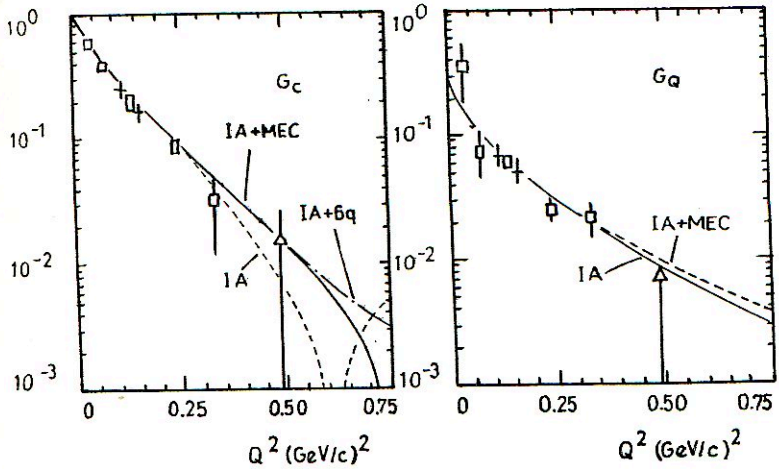

Fig.1. Charge G_C and quadrupole G_Q form factors of the deuteron /13/. To separate G_C and G_Q the following data for T_{20} were used: + - Bates; □ - Novosibirsk; Δ - Bonn. For all curves IA was performed with the RSC wave function of the deuteron; IA+MEC from ref.14; IA+6q - from ref.2 (Kobushkin; Kobushkin and Shelest).

The results of some models are also presented. Traditional models without quark degrees of freedom predict (see, e.g., ref.14) a minimum of G_c around Q^2 =0.6 to 0.8 $(GeV/c)^2$. On the contrary, the hybrid model[12] leads to smooth falloff of this form factor. Unfortunately, the experimental results are not of sufficient accuracy to confirm the presence of the meson-exchange currents (MEC) or 6-quark contribution. But it must be noted that the recent preliminary data from Bates[15] at $\sqrt{Q^2}$ =3.78, 4.22 and 4.62 fm^{-1} shows a tendency of T_{20} to the results of the IA with the Reid soft core wave function (fig.2)

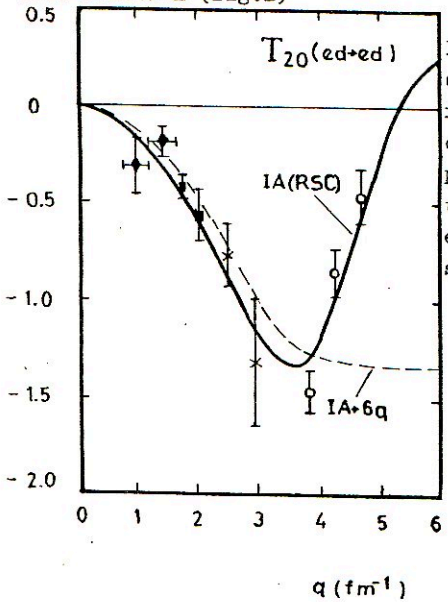

Fig.2. Comparison with experiment of two theoretical models (IA - full curve and IA+6quarks - dotted curve) for the tensor analysing power T_{20} of the elastic ed-scattering. Three points at the highest q are recent preliminary results from Bates[15].

If the deuteron can be considered at large Q^2 as a 6-quark object, QCD predicts[16] that $x \to 1$ when $Q^2 \to \infty$ and the tensor analysing power T_{20} tends in the limit to minimal possible value $T_{20} = -\sqrt{2}$. It also predicts that the ratio $R = p_x/p_{xz}$ of the vector and tensor polarization of the deuteron

$$R = \frac{2\sqrt{1+\eta}\,\sin\theta/2}{3\sqrt{1+\eta\sin^2\theta/2}}\left(1+2x^{-1}\right) \to \frac{2}{3}\left(\frac{1+\eta}{1+\eta\sin^2\theta/2}\right)^{1/2}\sin\theta/2, \quad (4)$$

where θ is the electron scattering angle. An experimantal study of such behaviors of T_{20} and R must be distinctive signature of QCD in the nuclear physics. But the problem is that such a behavior can be reached at rather high $Q^2 \sim$ few $(GeV/c)^2$. This is argued by fig.3 which displays the comparison of the so-called reduced form factor of the deuteron[3]

$$f_d(Q^2) = \frac{A^{1/2}(Q^2)}{F_N^2(Q^2/4)} \qquad (5)$$

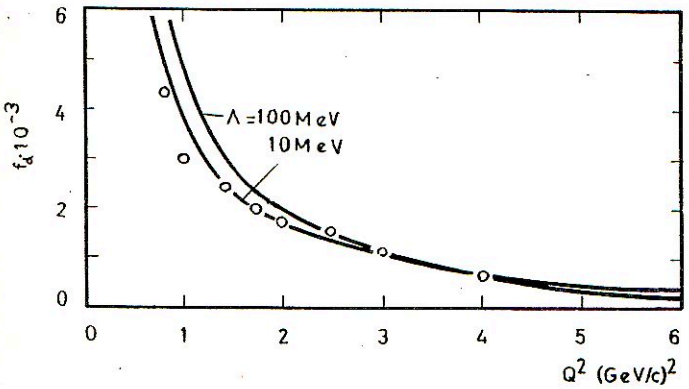

Fig.3. Comparison of the reduced form factor of the deuteron (for definition see eq.(5)) with the QCD prediction (6).

with the QCD prediction[17]

$$f_d(Q^2) \sim \frac{\alpha_s(Q^2)}{Q^2} \left(\ln \frac{Q^2}{\Lambda}\right)^{-\frac{8}{145}}. \qquad (6)$$

In eqs. (5) and (6) we are using the following notation: $F_N(Q^2) = \left(1 + Q^2/0.71\,(GeV/c)^2\right)^{-2}$ is the nucleon form factor; $\alpha_s(Q^2)$ is an effective QCD constant and Λ is an infrared cutoff parameter in QCD.

Concluding this section it must be said that no distinctive manifestation of the quark degrees of freedom of the deuteron was found up to now in the elastic ed-scattering. In the nearest

future it seems too unrealistic to reach a kinematic region, where QCD can be tested in polarized elastic ed-scattering.

3. $d(\gamma,p)n$ -reaction and QCD

The method of the reduced nuclear amplitudes /3/ was applied by Brodsky and Hiller /11/ to $d(\gamma,p)n$ cross section at $\theta_{cm}\sim 90°$. The reduced amplitude for this reaction was written as

$$m_{\gamma d\to pn} = \frac{M_{\gamma d\to pn}}{F_n(\hat{t}_n)\,F_p(\hat{t}_p)}, \qquad (7)$$

where $\hat{t}_n = (p_n - \frac{1}{2}p_d)^2$, $\hat{t}_p = (p_p - \frac{1}{2}p_d)^2$; $M_{\gamma d\to pn}$ is amplitude for the reaction; p_n, p_p and p_d are neutron, proton and deuteron momenta, respectively. The differential cross section in terms of the reduced amplitude is

$$\frac{d\sigma}{d\Omega_{cm}} \sim \frac{1}{s-m_d^2}\,F_p^2(\hat{t}_p)\,F_n^2(\hat{t}_n)\,|m_{\gamma d\to pn}|^2. \qquad (8)$$

The form factors $F_n(\hat{t}_n)$ and $F_p(\hat{t}_p)$ effectively remove the falloff of the nuclear amplitude $M_{\gamma d\to pn}$ due to the internal degrees of freedom of the nucleons. The behavior of the reduced amplitude $m_{\gamma d\to pn}$ is defined by dimensional counting rules /1/ regarding the neutron and proton as structureless particles:

$$m_{\gamma d\to pn} \sim p_T^{4-n}\,f(\theta_{cm}), \qquad (9)$$

where $n=5$ is the number of "elementary" fields in the external states: incoming (two nucleons and one photon) and outcoming (two nucleons) particles. So the energy behavior of the cross section at fixed θ_{cm} is defined to be

$$\frac{d\sigma}{d\Omega_{cm}} \sim \frac{1}{s-m_d^2}\,F_p^2(\hat{t}_p)\,F_n^2(\hat{t}_n)\,p_T^{-2}\,f(\theta_{cm}). \qquad (10)$$

At sufficiently large energy $F_p(\hat{t}_p) \sim F_n(\hat{t}_n) \sim s^{-2}$ and the behavior given by eq. (10) is reduced to the prediction of the counting rules[1]:

$$\frac{d\sigma}{d\Omega_{cm}} \sim s^{-11} \tilde{f}(\theta_{cm}). \qquad (11)$$

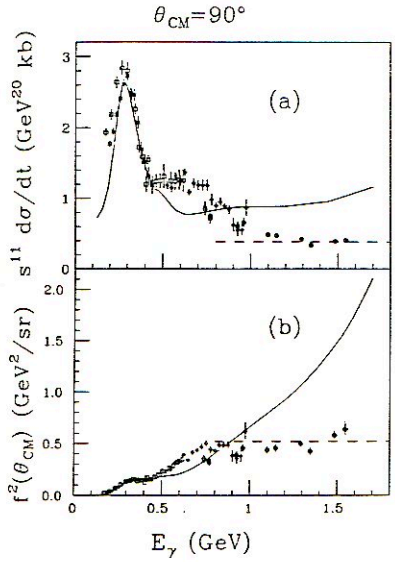

Fig.4. Comparison of experimental data[10] for cross section of $d(\gamma,p)n$ reaction with two models: constituent counting rules (a) and reduced nuclear amplitudes in QCD (b). Full curves correspond to theoretical calculations[18] in the framework of nucleon-meson approach.

Fig.4 shows a comparison of three models (traditional calculations in terms of nucleons and mesons[18], the reduced nuclear amplitude and the counting rules) with experiment[10]. One sees that the behavior of the cross section supports the hypothesis about the 6-quark structure of the deuteron at small distances. But due to a lot of uncertainties in the calculations[18] based on the "traditional" approach authors of ref.10 stressed that their data cannot be taken as a clear evidence that the latest one fails.

4. Study of deuteron structure in A (d,p) experiments at relativistic energy

The differential cross section of a fragmentation reaction A(d,p) of the 9 GeV/c deuteron into the proton at 0° was measured[4,5] in a wide region of the proton-spectator momentum. Assuming the impulse approximation one can extract from this data "momentum distribution" (MD) of nucleons in the deuteron. This has been done[4,5] in a framework of the light-cone dynamics[7]. At the range $0.2 < k < 0.6$ GeV/c of the internal momentum in the deuteron a significant deviation of the measured MD from ones, calculated using some popular NN-potentials, was shown.

The momentum k is defined in the light-cone dynamic as follows

$$k = \left(\frac{m^2 + k_\perp^2}{4\alpha(1-\alpha)} - m^2 \right)^{1/2}, \quad \alpha = \frac{E_p + p_z}{E_d + d_z}, \quad \vec{k}_T = \vec{p}_T, \quad \vec{d}_T = 0, \qquad (12)$$

where m is the proton mass; E_p and E_d are energies and $\vec{p}$ and $\vec{d}$ are momenta (in the lab. frame) of the proton-spectator and the deuteron, respectively. The momentum k is reduced to the proton momentum in the deuteron rest frame only at $p_z \sim \frac{1}{2} d_z$ (i.e., when $\alpha \sim \frac{1}{2}$).

The same effect was also observed[6] at lower deuteron beam momentum ($d = 3.1$ GeV/c).

In my report I shall dwell upon only one possible theoretical point of view (the reduced nuclear amplitude in QCD), which explains such behavior of the MD in the deuteron, as well as the recent data[6,19] for the tensor analysing power $T_{20}(k)$ of the reaction. Some alternative approaches will be reviewed by other authors at this Workshop.

The model of reduced nuclear amplitude in QCD assumes that all the quarks of the deuteron carry momentum $\frac{1}{6}\vec{d}$ and a hard proton is produced by a hard gluon exchange between two of them (see, e.g., fig. 5a). Absorbing high momentum, the quark averages it between all quarks which form the observed proton. As a result, every quark of the final proton carries momentum $\frac{1}{3}\vec{p}$, where $\vec{p}$ is the total proton momentum. But to simplify the calculations, the model does not consider the individual quarks and deals with gluon exchange between 3-quark colour blocks of the totally colour-

less "deuteron." The quark momenta averaging at the 3-quark final system (proton) is taken into account by some form factor $F(k^2)$ at appropriate (3q)-(3q)-gluon vertex. As a result, a sum of quark diagrams like fig.5a is reduced to the diagram of fig.5b, where lines B_8 and B_8' correspond to color 3-quark subsystems of the "deuteron".

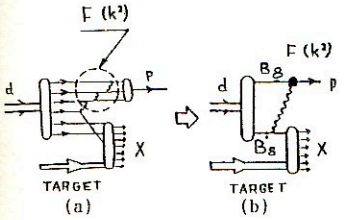

Fig.5. One possible quark diagram (a) and the reduced diagram (b) for a hard proton creation in the (d,p) reaction.

The decomposition of the 6-quark configuration S^6 with the deuteron quantum numbers is given by:

$$|S^6\rangle = \sum_{B,B'}{}' \beta_{BB'} |B\rangle|B'\rangle =$$

$$= \sqrt{\frac{1}{9}} \left|\tfrac{1}{2}\tfrac{1}{2}\underline{1}\right\rangle\left|\tfrac{1}{2}\tfrac{1}{2}\underline{1}\right\rangle - \sqrt{\frac{4}{45}} \left|\tfrac{3}{2}\tfrac{3}{2}\underline{1}\right\rangle\left|\tfrac{3}{2}\tfrac{3}{2}\underline{1}\right\rangle +$$

$$+ \sqrt{\frac{2}{9}} \left|\tfrac{1}{2}\tfrac{1}{2}\underline{8}\right\rangle\left|\tfrac{1}{2}\tfrac{1}{2}\underline{8}\right\rangle + \sqrt{\frac{2}{9}} \left|\tfrac{3}{2}\tfrac{1}{2}\underline{8}\right\rangle\left|\tfrac{1}{2}\tfrac{1}{2}\underline{8}\right\rangle - \sqrt{\frac{2}{9}} \left|\tfrac{1}{2}\tfrac{1}{2}\underline{8}\right\rangle\left|\tfrac{3}{2}\tfrac{1}{2}\underline{8}\right\rangle + \tag{13}$$

$$+ \sqrt{\frac{1}{9}} \left|\tfrac{1}{2}\tfrac{3}{2}\underline{8}\right\rangle\left|\tfrac{1}{2}\tfrac{3}{2}\underline{8}\right\rangle + \sqrt{\frac{1}{45}} \left|\tfrac{3}{2}\tfrac{1}{2}\underline{8}\right\rangle\left|\tfrac{3}{2}\tfrac{1}{2}\underline{8}\right\rangle,$$

where $|B\rangle = |j t \mu\rangle$ and $|B'\rangle = |j' t' \mu'\rangle$ mean the spin-isospin-color wave functions of the 3-quark clusters with spin j (j'), isospin t (t') and colour representation μ (μ'), respectively. The distribution of the hard proton will be described by $6q \to p + n$ transition amplitude $t_{J_3}(\alpha, \vec{k}_\perp = 0)$, which is expressed through some nonperturbative (soft) distribution amplitude $\phi(\beta, \vec{\ell}_T)$ for the color 3-quark clusters in the deuteron:

$$t_{J_3}(\alpha, \vec{k}_T = 0) = \alpha_s(k^2)\, F(k^2) \cdot$$

$$\cdot \int_0^\alpha d\beta \int d^2\ell \; K_{J_3} \frac{[\alpha(1-\alpha)\beta(1-\beta)]^{1/2}}{(\alpha-\beta)\left(m_d^2 - \frac{m^2}{1-\alpha} - \frac{m^2 + \ell_T^2}{1-\beta}\right)} \phi(\beta, \vec{\ell}_T), \tag{14}$$

$$K_{J_3} = \sum_{B_8 B_8'} \beta_{B_8 B_8'} \cdot$$

$$\cdot \left\{ \langle N | \langle N | \right\}_{J=1, J_3, T=0, T_3=0} \Gamma_\mu^a(1) \Gamma^{\nu a}(2) \left\{ |B_8\rangle |B_8\rangle \right\}_{J=1, J_3, T=0, T_3=0} , \tag{15}$$

where J_3 is z-projection of the deuteron spin, $\Gamma_\mu^a(1) =$

$= \sum_{i=1}^{3} \frac{\lambda_a^{(i)}}{2} \gamma_\mu^{(i)}$, $\Gamma_\mu^a(2) = \sum_{i=4}^{6} \frac{\lambda_a^{(i)}}{2} \gamma_\nu^{(i)}$ and $\left\{ |j t \mu\rangle |j' t' \mu'\rangle \right\}_{J J_3 T T_3}$

means a colorless state with total spin J and isospin T which is constructed from two 3-quark clusters $|B\rangle = |j t \mu\rangle$ and $|B'\rangle = |j' t' \mu'\rangle$ by using the Clebsh-Gordan coefficients. From eq.(14) one obtains the asymptotic behavior for the transition amplitude at

$$t_{J_3}(\alpha, \vec{k}_T = 0) = C_{J_3} \alpha(k^2) F(k^2) (1-\alpha)^{3/2}, \tag{16}$$

$$C_{J_3} = K_{J_3} \int_0^1 d\beta \int d^2\ell \left(\frac{\beta}{1-\beta} \right)^{\frac{1}{2}} \phi(\beta, \vec{\ell}_T), \tag{17}$$

and thus the MD of nucleons in the deuteron $|\Psi(k)|^2$ and the tensor analysing power tend to be:

$$|\Psi(k)|^2 \sim (1-\alpha)^{\frac{1}{2}} \sum_{J_3} |t_{J_3}|^2 \sim (1-\alpha)^{7/2} \alpha_s^2(k^2) F^2(k^2), \tag{18}$$

$$T_{20} = -0.42, \tag{19}$$

respectively.

In fig.6 we present the ratio of the meaured MD to the predicted asymptotic expression. One concludes that at $k > 0.5$ GeV/c the cross section reaches the asymptotic behavior predicted by this model. At the same region the data[6,19] shows (fig.7a) that T_{20}

tends to the constant value near -0.5, which is in a qualitative agreement with the model results. At the same time traditional calculations based on the NN-potentials give a positive value of T_{20} at this region.

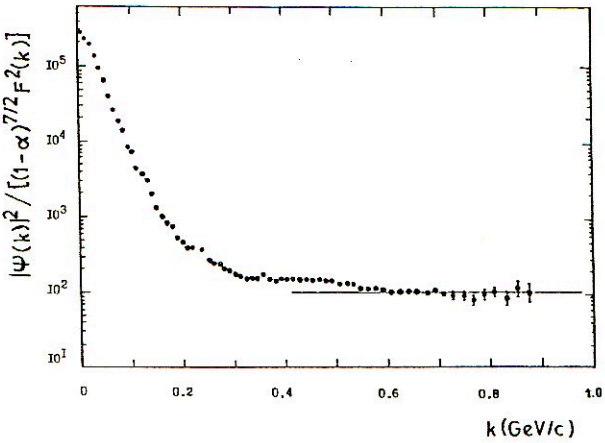

Fig.6. Ratio of measured momentum distribution of nucleons in the deuteron (refs.4,5) to QCD prediction (18). Dipole form factor $(1 + k^2/0.71\ (GeV/c)^2)^{-2}$ was used for $F(k^2)$.

At fig.7b the tensor analysing power of the elastic ed-scattering is compared with the one of the (d,p) reaction. A scale for the $\sqrt{Q^2}$-axis is chosed to localize the minimum point $T_{20} = -\sqrt{2}$ predicted by the IA for both reactions, at the same position. The comparison of this reactions teaches us that measurements of the polarized observables in the elastic ed-scattering at $Q^2>1\ (GeV/c)^2$ could cover the region of new physics of deuteron, where the basic fields are not nucleons and mesons but quarks and gluons.

5. Conclusions

A lot of effects observed in reactions with unpolarized deuterons at intermediate and high energies (behavior of the structure function $A(Q^2)$ of the elastic ed-scattering, the (d,p)-fragmentation with 0° proton emission, energy dependence of the cross section of the $d(\gamma,p)n$ reaction at 90° in the c.m. system) can be explained treating the deuteron as a six-quark object. But due to

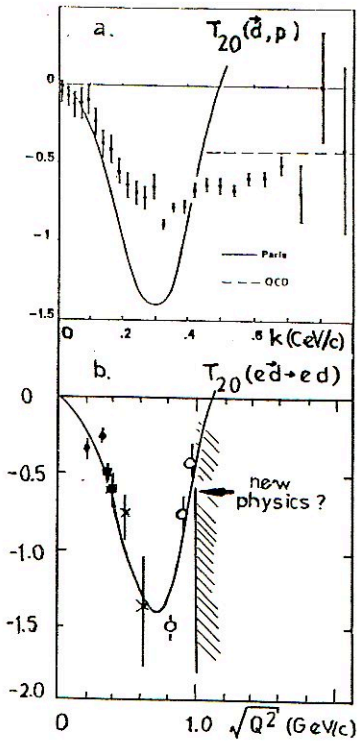

Fig.7. Behaviors of T_{20} for (d,p) reaction (a) and elastic ed-scattering (b). Dashed line is the prediction (19) of the QCD model (see text); solid lines correspond to IA.

a lot of ambiguities in the traditional nucleon-meson theoretical approaches a breakdown of the nucleon-mesonic point of view cannot be clearly demonstrated.

The recent data for T_{20} in the elastic ed-scattering are in discrepancy with the naive hybrid model for the deuteron wave function and can be described best of all by the nonrelativistic impulse approximation with the Reid soft-core deuteron wave function. The comparison of the data for the elastic ed-scattering with the data for T_{20} in the (d,p) reaction shows that the QCD could be tested at higher Q^2 in electron scattering experiments with polarized deuteron targets.

We would like to stress here, that theoretical analysis of ed-reactions is not simpler then one of reactions studied in experiments with deuteron relativistic beams at Dubna and Saturne:

a relativistic description of the deuteron structure cannot be ignored in consistent theory of both types of reactions, as well as a lot of mechanisms beyond the impulse approximation (final state interaction, pion production at intermediate states and so on).

But there is one advantage of experiments with relativistic deuteron beams: due to luminosity the much smaller distance in the deuteron becomes to be allowable for Dubna and Saturne experiments, than for experiments with high energy electron beams (see fig.7).

Finally, it can be recommended to measure cross section, T_{20} and polarization transmission $\varkappa$ for pd-backward scattering at the Dubna synchrophasatron: this reaction is assumed to be dominated by one-neuteron-exchange mechanism[20] and can be used to obtain information about the deuteron structure at $k > 1$ GeV/c. At somewhat lower energies the cross section and T_{20} have been measured at Saturne. It seems to be rather important to complete such data by a knowledge of $\varkappa$-behavior for this reaction.

References

1. V.A. Matveev, R.M. Muradjan, and A.N. Tavkhelidze, Lett. Nuov. Cim. 7, 719 (1973); S.J. Brodsky and G.R. Farrar, Phys. Rev. Lett. 31, 1153 (1973); S.J. Brodsky and G.R. Farrar, Phys, Rev. D11, 1309 (1975)
2. A.P. Kobushkin, Yad. Fiz. 28, 495 (1978); A.P. Kobushkin and V.P. Shelest, Sov. J. Part. Nucl. 14, 483 (1983); Y. Kizukury, M. Namiki, and K.Okano, Prog. Theor. Phys., 61, 559 (1979).
3. R.G. Arnold et al., Phys. Rev. Lett. 35, 776 (1975); S.J. Brodsky and B.T. Chertok, Phys. Rev. Lett. 37, 269 (1976); S.J. Brodsky and B.T. Chertok, Phys. Rev. D14, 3003 (1976).
4. V.G. Ableev et al., Nucl. Phys. A393, 491 (1983); ibid A411, 541 (E) (1984).
5. V.G. Ableev et al., Proc Int. Conf. on Theory of Few Body and Quark-Hadron Systems, Dubna, June 16-20, 1987, JINR, Dubna D4-87-692, p. 140 (1987); preprint of Zentralinstitut für Kernforschung ZfK-666, Rossendorf, 1989.
6. C.F. Perdrisat et al., Phys. Rev. Lett. 59, 2840 (1987).
7. A.P. Kobushkin and L. Vizireva, J. Phys. G: Nucl. Phys. 8, 893 (1983).
8. M.G. Dolidze and G.I. Lykasov, Contribution to the 7-th Int. Conf. on Polarized Phenomena in Nuclear Physics, Paris, July 9-13, 1990.

9. H. Müller, Z. Phys. A-Atomic Nuclei, 336, 103 (1990).
10. J. Napolitano et al., Nucl. Phys., A508, 455c (1990).
11. S.J. Brodsky, J.R. Hiller, Phys. Rev., C28, 475 (1983).
12. A.P. Kobushkin, Report at the 9-th Int. Symp. on High Energy Spin Physics, Bonn, September 10-15, 1990.
13. B. Boden et al., Bonn University preprint BONN-ME-90-06; H.-D. Schablitzky, Report at the 9-th Int. Symp. on High Energy Spin Physics, Bonn, September 10-15, 1990.
14. M. Gari and H. Hyuga, Nucl. Phys., A264, 409 (1976).
15. S. Kowalsky, Invited talk at the 9-th Int. Symp. on High Engergy Spin Physics, Bonn, September 10-15, 1990.
16. C.E. Carlson and F. Gross, Phys. Rev. Lett., 53, 127 (1984).
17. S.J. Brodsky, C.-R. Li, and G.P. Lepage, Phys. Rev. Lett., 51, 83 (1983).
18. T.-S. H. Lee, Argonne National Laboratory, Physics Division, Report No PHY-5253-TH-88 (1988).
19. V.G. Ableev et al., Pisma v ZhETF, 47, 558 (1988); JINR Rapid Communication, No4, p.5 (1990); Report at the 9-th Int. Symp. on High Energy Spin Physics, Bonn, September 10-15, 1990.
20. A.P. Kobushkin, J. Phys. G: Nucl. Phys. 12, 487 (1986).

THE GOTTFRIED SUM RULE AND NUCLEAR STRUCTURE CORRECTIONS

Kaptari L.P.
Laboratory of Theoretical Physics, Joint Institute for Nuclear Research, Head Post Office, Box 79, Moscow, Russia
Umnikov A.Yu.
Far Eastern State University, Sukhanov-str. 8, Vladivostok, Russia

I. Recently, the NMC data[1, 2] on the ratio F_2^n/F_2^p have been applied to derive the difference $F_2^p - F_2^n$ and to estimate the Gottfried Sum (GS) $S_G \equiv \int (F_2^p - F_2^n)dx/x$[3] experimentally. Its value has been found to be below the quark-parton model expectation of 1/3, namely:

$$S_G = 0.240 \pm 0.016\,. \tag{1}$$

Serious theoretical speculations have appeared as a consequence of this discrepancy, e.g. the strong isospin violation in the proton sea-quark distributions[4] or the postponement of the onset of the Regge behavior to much smaller x values than have currently been sampled experimentally[5].

Note that the experimental value of the GS is sensitive to the procedure of extraction of the ratio F_2^n/F_2^p from the combined data on the deuteron and proton. Since the deuteron is a more complicated system than a simple sum of two free nucleons, a number of structure factors may change the ratio F_2^n/F_2^p. At least one should be careful while considering the influence of widely discussed nuclear effects, such as fermi motion, binding effects and mesonic exchanges in nuclei. Though in the integral characteristics of nuclear structure functions (SF) these corrections are small, it is not evident that they can be neglected in the procedure of determination of the neutron SF $F_2^n(x)$ from the nuclear data. Moreover, the recent analysis of BCDMS data on the proton and the deuteron performed in ref.[6] has shown the noticeable influence of the deuteron structure factors on the extracted neutron SF and the ratio F_2^n/F_2^p. It seems, the same corrections can also be expected for the NMC data.

The aim of this paper is to demonstrate that in the framework of the theoretical approach suggested in refs.[7] it is possible to extract the neutron SF so that the

obtained value of the GS doesn't dramatically contradict the quark-parton predictions. It is shown that the nuclear corrections change the behavior of the difference $(F_2^p - F_2^n)$ as $x \to 0$ as compared with the prediction of the NMC experimental data fit.

II. Since the SF have been measured not in the whole region of the scale variable x, it is useful to define the x-dependent Gottfried integral:

$$I_G(x_1 \div x_2) = \int_{x_1}^{x_2} (F_2^p - F_2^n)\, dx/x, \tag{2}$$

and separately evaluate it in the measured and unmeasured regions of x. Thus, the GS may be written as a sum of three integrals (2) corresponding to three regions considered in ref.[1]:

$$\begin{array}{ccccccc} S_G & = & I_G^{NMC}(0 \div 0.004) & + & I_G^{NMC}(0.004 \div 0.8) & + & I_G^{NMC}(0.8 \div 1) \\ (0.240 \pm 0.016) & & (0.011 \pm 0.003) & & (0.227 \pm 0.014) & & (\ 0.002 \pm 0.001\ ). \end{array} \tag{3}$$

The second term in (3) has been estimated experimentally using the F_2^D from the fit of the published deuteron data and the ratio F_2^n/F_2^p has been taken from the *unsmeared* NMC experimental results[2]. The first and third terms correspond to the unmeasured regions and have been estimated by extrapolation procedure. Thus, in all these three integrals the nuclear corrections have been missed. Let $F_2^{D\,(exp.)}$ be the experimental deuteron SF (that obviously includes all the nuclear and other effects) and $F_2^{p(exp.)}$ the corresponding proton SF. Then the unsmeared neutron SF defined by:

$$\tilde{F}_2^n = 2F_2^{D(exp.)} - F_2^{p(exp.)} \tag{4}$$

is overestimated due to the mesonic contributions to the deuteron SF. A more correct way to determine the neutron SF is to solve the integral equation[1]:

$$F_2^n(x,Q^2) = \left[2F_2^{D(exp.)}(x,Q^2) - \delta F_2^{mes.}(x,Q^2) - S_p^{-1}(x,Q^2)F_2^{p(exp.)}(x,Q^2)\right] S_n(x,Q^2), \tag{5}$$

$$S_{p(n)} = \frac{F_2^{p(n)}(x,Q^2)}{\int F_2^{p(n)}(x/y,Q^2) f_{N/D}(y)dy},$$

for $F_2^n(x)$. Here $\delta F_2^{mes.}(x,Q^2)$ is the meson contribution, $f_{N/D}(y)$ is the distribution function of the nucleons carrying out the y-fraction of the total deuteron momentum. The distribution function $f_{N/D}(y)$ is straightforward connected with the usual

[1] in this approach we take into account the nuclear corrections coming from the fermi-motion and meson exchange currents in the deuteron. A more complete analysis should include also the shadowing as $x \to 0$ and the contributions of other non-nucleon degrees of freedom (multiquarks, Δ-isobar ...) as $x \to 1$.

deuteron wave function (computed in a realistic Paris or Bonn group potential) and includes the boundness of the nucleons inside the deuteron. The explicit expression of the $\delta F_2^{mes.}(x, Q^2)$ has been computed in ref.[7]. Fig.1. illustrates the contribution $\delta F_2^{mes.}$ for different mesons π, ω, σ in the deuteron. To extract the neutron SF by solving the integral equation (5),

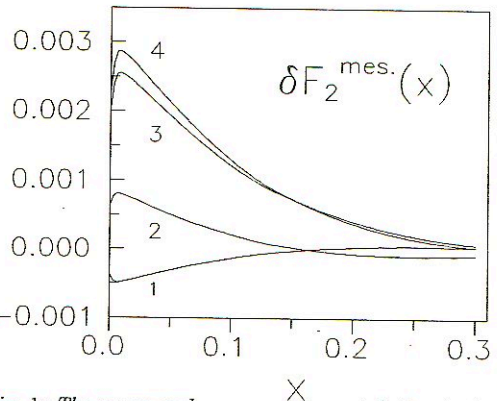

Fig. 1: *The meson exchange currents contribution to the deuteron structure function [7]. Curves 1-3 correspond to the contribution of $\omega-, \sigma-$ and $\pi-$mesons respectively; curve 4 is the sum over all the mesons.*

we should parametrize the proton, deuteron and neutron SF in the full region of x and experimental values of Q^2. At this moment we are free in the choice of the parameters and we can from the very beginning constrain them to obey the Gottfried Sum Rule exactly. That kind of analysis has been done in[6] to extract the neutron SF from the combined BCDMS data. From that analysis we can compute the corresponding Gottfried integrals (3):

$$\begin{aligned} I_G^{BCDMS}(0 \div 0.004) &= 0.036 \\ I_G^{BCDMS}(0.004 \div 0.8) &= 0.297 \\ I_G^{BCDMS}(0.8 \div 1) &= 0.0004. \end{aligned} \tag{6}$$

Note that in eq.(6) the Gottfried Sum Rule is exactly fulfilled. Comparison of (6) with (3) shows that here is a systematic difference in the NMC treatment of the experimental data with the results obtained from BCDMS experiments. To achieve the agreement between them, it is necessary to take into account the following:

i) In the region $0.004 \leq x \leq 0.8$ where the role of the fermi motion is negligible small it is sufficient to correct the difference $F_2^p - F_2^n$ by adding the function $\delta F_2^{mes.}(x)$. As a result the Gottfried integral in this region increases by adding:

$$\delta I_G^{(mes.)}(0.004 \div 0.8) = \int_{0.004}^{0.8} \delta F_2^{mes.}(x)\, dx/x = 0.03 \pm 0.01. \tag{7}$$

To estimate the integral $I_G^{(mes.)}(0.004 \div 0.8)$ (7) we have used the numerical results for the mesonic corrections computed in ref.[7] (see also Fig.1). In ref.[7] it was noted that the numerically mesonic contribution to the deuteron SF $\delta F_2^{mes.}(x)$ was underestimated by $\sim 40\%$, owing to the approximate form of the current operator. This circumstance is reflected in (7) as a systematic error. ii) Besides, the meson corrections change the behavior of $F_2^p - F_2^n$ as $x \to 0$. Usually in the region $x \leq 0.004$ one assumes the "non-singlet" power behavior of the difference $F_2^p - F_2^n$ as ax^α. The fit of the NMC data at small x ($x = 0.004 - 0.15$) gives $a = 0.21 \pm 0.03$, $\alpha = 0.62 \pm 0.05$ [1]. This yields $I_G(0 \div 0.004)$ as is shown in(3). Upon taking into account the mesonic corrections to the NMC data the parameters became $a = 0.143 \pm 0.013$, $\alpha = 0.423 \pm 0.048$. This situation is shown in Fig.2 where the dashed lines correspond to the new behavior of the data and the shadow area displays the ambiguities in $\delta F_2^{mes.}(x)$ pointed above.

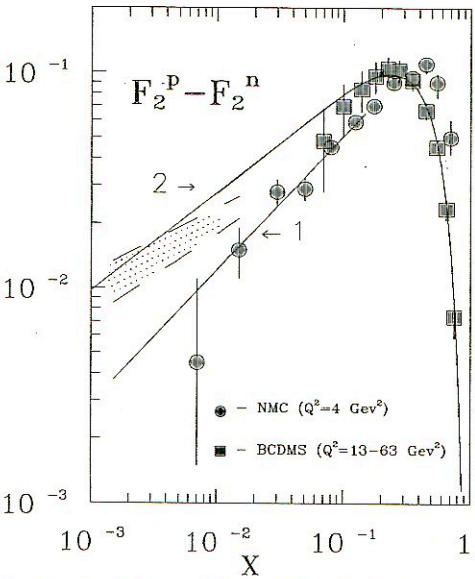

Fig. 2: *The difference $F_2^p(x) - F_2^n(x)$. Solid lines: 1 - NMC data fit[1]; 2 - parametrization from ref.[6]. Dashed lines and shadow area - corrected NMC data fit with the taking into account of the mesonic corrections (see text). Data: circles - NMC[1], squares - BCDMS[8].*

Thus, the part of the Gottfried integral computed with the new parameters a and α becomes: $I_G(0 \div 0.004) = 0.0340 \pm 0.010$. iii) At last in the region $0.8 \leq x \leq 1$ the mesonic contribution is negligible. Other nuclear effects, viz. fermi motion and binding effects, in this region may be significant in the functional dependence of SF. However, since here the absolute values of the SF are small, it is clear that their contributions to the integral characteristics are insignificant.

Gathering together the corrected integrals we obtain the corrected estimation of the GS instead of (1):

$$S_G = (0.034 \pm 0.01) + (0.227 \pm 0.014) + (0.03 \pm 0.01) + (0.002 \pm 0.001) = 0.29 \pm 0.03, \quad (8)$$

that is close to the quark-parton predictions of 1/3.

III. Concluding remarks:

a) The procedure of extraction of the neutron SF from the nuclear data is model-dependent. Thereby the estimation of the Gottfried Sum is model-dependent too. A more accurate analysis should be based on the solution of the integral equation (5). In accordance with the definition of the functions $S_{p(n)}$ in (5), a theoretical model within which one describes the nucleus (deuteron) as well as the main characteristics of deep inelastic processes is required. Obviously, the suggested model is far to be complete. Besides the consideration in (5) of the mesonic corrections, binding and fermi-motion effects, other nuclear structure factors may be relevant (nuclear shadowing[9], six-quark[10], Δ-isobar admixtures in the deuteron[11] ...).

b) The most important factor to be included into our analysis is the nuclear shadowing as $x \to 0$ [9]. This correction is opposite in sign with the mesonic contribution and they may cancel each other at very small x. This circumstance may be checked experimentally by checking the sign of the unsmeared difference $F_2^p - F_2^n$ as $x \to 0$: the sign will be negative (positive) if the shadowing is smaller (larger) than the mesonic contribution.

c) The shadowing effects may modify our prediction concerning the behavior of the difference $F_2^p - F_2^n$ $x \to 0$ given in Fig.2 and may slightly change our estimation of the Gottfried integral $I_G(0 \div 0.004)$.

d) In our opinion, at this time the experimental situation is not quite clear to claim whether the Gottfried Sum Rule is fulfilled experimentally or not. In principle, high precision neutrino experiments may clarify this problem.

IV. We thank Profs. K. Rith and G.I. Smirnov for stimulating discussions.

References

[1] NMCollab.: P.Amaudruz et al. CERN-PPE/91-05.

[2] NMCollab.: D.Allasia et al., Phys. Lett. **B242** (1990) 366.

[3] K.Gottfried, Phys. Rev. Lett. **18** (1967) 1174.

[4] G.Preparata, P.G. Ratcliffe and J. Soffer, Phys. Rev.Lett. **66** (1991) 683.

[5] S.D. Ellis and W.J. Stirling, Phys. Lett. **B256** (1991) 258.

[6] L.P.Kaptari and A.Yu.Umnikov, Phys. Lett. **259B** (1991) 155.

[7] L.P. Kaptari, B.L. Reznik, A.I. Titov, A.Yu. Umnikov, JETP Lett., **47**(9) (1988) 428;
L.P. Kaptari, A.I. Titov, E.L. Bratkovskaya, A.Yu. Umnikov, Nucl. Phys., **A512** (1990) 684;

[8] BCDMS Collab.: A.C. Benvenuti et al., Phys. Lett., **B237** (1990) 592; *ibid.*, 599.
A.C. Benvenuti et al., Preprint CERN-EP/89-170, 1989; CERN-EP/89-171, 1989.

[9] N.N.Nikolaev and V.I.Zakharov, Phys. Lett. **B55** (1975) 397.

[10] L.P. Kaptari, A.Yu. Umnikov, JINR Rapid Comm., No. 6[32]-88, Dubna (1988) 17.

[11] L.P. Kaptari and A.Yu. Umnikov, Z. fur Phys. **A** (1991) to be published.

THE STUDY OF DEUTERON 6q-STRUCTURE IN THE PROCESSES OF INELASTIC ELECTRON SCATTERING AND POSSIBILITY OF POTENTIAL DESCRIPTION OF N* - N SYSTEM

L.Ya.Glozman

Alma-Ata Power Engineering Institute, Kosmonavtov 126, Alma-Ata, 480013, Kazakhstan

1.The feasibility for the short-range NN interaction to be of the quark origin has long been discussed elsewhere; nevertheless, the quark approach proper was argued for but passively. Indeed, various data (NN scattering phase shifts, electromagnetic form factors, etc.) have been shown to be compatible with the quark concepts [1-5] in case the given data are also compatible with the conventional NN phenomenology extended by including the meson exchange currents (MEC) [6].

For the quark concepts to get convincing actuality, such concepts have to be able of being used to predict, or to account for, quite a number of different properties of the NN-system and of heavier nuclei which cannot be interpreted in any other way or, at least, cannot be described in terms of any unified interpretation.

2.To understand what nontrivial consequences of the deuteron 6q-structure can be expected, let us consider this structure in some details. The NN system in the S-wave in the nucleon overlap region has been shown to be a superposition of the quark configurations s^6 and s^4p^2- s^52s [4-5]. The latter configurations [7] comprise a few states differing in their spatial $[f_X]$ and colour-spin $[f_{CS}]$ (or spin- flavor $[f_{ST}]$) symmetries [8,9]. It is of importance in this case that the superposition of the states in the s^4p^2-s^52s shells, which is realized for the low-energy NN-system in the s-wave of relative motion, may be presented in a compact manner to be a quark-antisymmetrized nodal 2N-function [10]. So the deuteron and NN -system wave function at moderate energies in continuum may be presented to be a sum of two mutually-orthogonal components [4]:

$$\Psi = |NN> + |s^6>, \quad <NN|s^6> = 0, \tag{1}$$

where the "NN-component"

$$|NN> = \hat{A}\{N(1,2,3)N(4,5,6)\chi_{NN}(\vec{r})\} \tag{2}$$

is the quark-antisymmetrized function of the "NN-channel" in two-nucleon system; s^6-is a 6-quark system resembling a bag.

The orthogonality condition (1) means that the "NN-channel" in the nucleon overlap region includes a superposition of the orbitally-excited configurations in the s^4p^2-s^52s shells, with each of the configurations being orthogonal to s^6. Besides, the function χ_{NN} in (2) must have a node in S-wave at 0.5-0.6 fm. The region of intermediate and long ranges in (2),where the quark exchanges do not occur, is treated in terms of the conventional meson exchanges.

All the above conditions are met by the function χ_{NN},obtainable with the Moscow deep attractive NN potential [11] where a deuteron is in correspondence with the first excited (nodal) 2S-state in the deep attractive well (see fig.1). At the same time, the deep-lying (node-free) ground state was treated as a forbidden (extra) state and had only an auxiliary function.

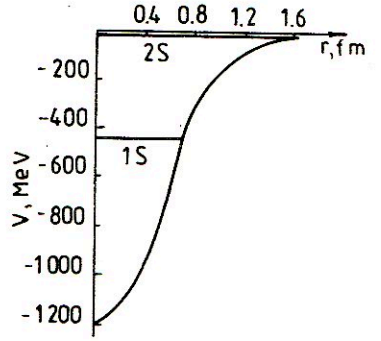

Fig. 1.

Central part of the Moscow NN potential for the S-wave (last version)

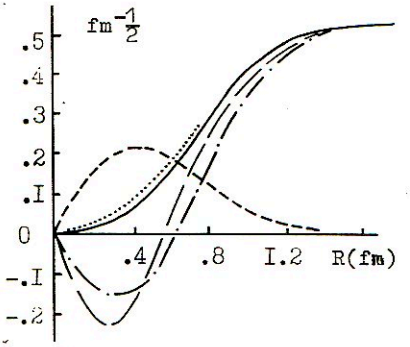

Fig. 2.

Long-dashed line—deuteron Moscow $^3S_1$ wave function;
dash-dotted line—function χ_{NN} in (2) (deuteron Moscow NN wave function modified at short ranges to satisfy the condition of normalizing the full 6q-function (1) to unit);
short-dashed line—s^6 wave function $\kappa\sqrt{\frac{9}{10}}\phi_{0S}(\vec{r})$ ($|s^6>=\kappa\sqrt{\frac{9}{10}}\hat{A}\{\phi_N(1,2,3)\phi_N(4,5,6)\phi_{0S}(\vec{r})\}$);
dotted line—deuteron Paris $^3S_1$ wave function

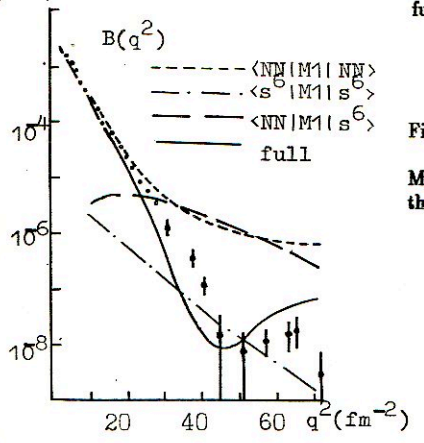

Fig. 3.

Magnetic structure function $B(q^2)$ for the process d(e,e')d

The NN wave function behaviour at short ranges, which is conventional for the NN potentials with repulsive core and under which the wave function amplitude in S-wave attenuates gradually when penetrating into the core zone,occurs in this case due to destructive interference of the NN and s^6 channels [3-5] in (1) (see fig.2) and may be traced in quite a pictorial way using the example of the deuteron magnetic form factors [4] (see fig.3).

3.The deuteron 6q-function (1) contains a rich cluster world. For example, the result has been well-known which consists in that the s^6 configuration is a superposition of three cluster components

$$N(1,2,3)N(4,5,6)\phi_{0S}(\vec{r})\ ;\ \Delta(1,2,3)\Delta(4,5,6)\phi_{0S}(\vec{r})\ ;\ C(1,2,3)C(4,5,6)\phi_{0S}(\vec{r})\ .$$

In the $s^4p^2 - s^52s$ configurations, which we are interested in, two oscillatory excitation quanta may be distributed not only to the relative motion of two clusters, but also to the internal Jakobi coordinates of clusters. This is in correspondence with the fact that these configurations comprise not only the components

$$N(1,2,3)N(4,5,6)\phi_{2S}(\vec{r})\ ;\ \Delta(1,2,3)\Delta(4,5,6)\phi_{2S}(\vec{r})\ ;\ C(1,2,3)C(4,5,6)\phi_{2S}(\vec{r})\ ,$$

but also the terms

$$N(1,2,3)N^{**}(4,5,6)\phi_{0S}(\vec{r})\ ;\ N^{*}(1,2,3)N^{*}(4,5,6)\phi_{0S}(\vec{r})\ ;$$

$$N(1,2,3)N^{*}(4,5,6)\phi_{1P}(\vec{r})\ ;\Delta^{**}(1,2,3)\Delta(4,5,6)\phi_{0S}(\vec{r})\ ;...$$

where the number of asterisks indicates the number of the internal excitation quanta.The cluster content of each shell component can be analyzed by the use of fractional parentage expansion [8,9].

4.We propose to examine the 6q-structure directly using the $d(e,e'p)N^{*}or\Delta$ process where some states of baryon-spectator $N^{*}or\Delta$ are expected to be discriminated by the missing mass technique [12].

In the quasi-elastic region, where the knocked-out proton is fast ($E_p > 1GeV$) and the resonance-spectator "R" is slow, nuclear electromagnetic current may be presented as

$$J^{\nu}_{fi} \sim \sum_{A} j^{\nu}_{A\to p}\Phi^{d}_{AR}(\vec{K}_R)\ , \qquad (3)$$

where "A" is the intermediate baryon (3q-cluster) absorbing photon (see fig.4[a]); $j^{\nu}_{A\to p}$ is the hadronic electromagnetic current which can be calculated on the quark level.

All the information about quark-cluster structure of the deuteron is contained in the function

$$\Phi^{d}_{AR}(\vec{K}_R) = \frac{1}{(2\pi)^{3/2}}\int d\vec{r}e^{i\vec{K}_R\vec{r}}\sqrt{\frac{6!}{3!3!}} < A(1,2,3)R(4,5,6)|\Psi^{d}(1,2,...,6) > \qquad (4)$$

here $\vec{K}_R$ is momentum of baryon-spectator "R".

When calculating this function we limited ourselves to the dominant components of the baryon wave-functions:$N \simeq |s^3[3]_X[21]_{CS}L = 0S = \frac{1}{2}J = \frac{1}{2}T = \frac{1}{2} > ;\Delta \simeq |s^3[3]_X[1^3]_{CS}L = 0S = \frac{3}{2}J = \frac{3}{2}T = \frac{3}{2} > ;N^{*}(1440) \simeq |sp^2[3]_X[21]_{CS}L = 0S = \frac{1}{2}J = \frac{1}{2}T = \frac{1}{2} > ;N^{*}(1535) \simeq |s^2p[21]_X[21]_{CS}L = 1S = \frac{1}{2}J = \frac{1}{2}T = \frac{1}{2} > ;N^{*}(1520) \simeq$

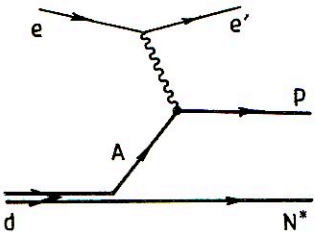

Fig. 4^a.

Diagram for the spectator mechanism of the $d(e,e'p)N^*$ process

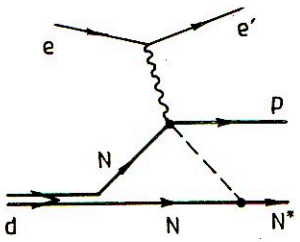

Fig. 4^b.

Diagram for the nonspectator mechanism of the $d(e,e'p)N^*$ process

$|s^2p[21]_X[21]_{CS}L = 1S = \frac{1}{2}J = \frac{3}{2}T = \frac{1}{2}>$, where center-of-mass oscillator motion is excluded.

The most simple situation takes place when the only state "A" in (4) is possible or one of them is dominant. In these cases the cross-section may be presented as a product of relative motion momentum distribution $\rho_{AR}(\vec{K}_R)$ and off-shell cross-section $\sigma_{e+A\to e+p}$:

$$\frac{d\sigma}{d\vec{K}_e d\vec{K}_p} = \frac{1}{K_e^2}\sigma_{e+A\to e+p}(\vec{K}_e,\vec{K}_p)\rho_{AR}(\vec{K}_R)\delta(E_i - E_f)\ , \tag{5}$$

where momentum distribution

$$\rho_{AR}(\vec{K}_R) = \frac{1}{2J_d+1}\sum_{M_d M_A M_R}|\Phi^d_{AR}(\vec{K}_R)|^2 \tag{6}$$

is normalized to the spectroscopic factor

$$S^d_{AR} = \int d\vec{K}_R \rho_{AR}(\vec{K}_R) \tag{7}$$

which represents the effective number of baryon pairs A-R in the deuteron.

This situation is typical of the processes $d(e,e'p)N^*(1440)$ (where the elementary process is $e+p\to e'+p$) and $d(e,e'p)\Delta$ (here the elementary process is $e+\Delta\to e'+p$).

The weight of the $N - N^*(1440)$ component is very sensitive to the exact contributions of different configurations $s^4p^2[6]_X[2^3]_{CS}$; $s^4p^2[42]_X[42]_{CS}$;... in the deuteron 6q-wave function. So we may present now only a wide range for the corresponding spectroscopic factor

$$S^d_{NN^*(1440)} = 10^{-5} - 20\cdot 10^{-5}\ .$$

In contrast, the $\Delta\Delta$ component is mainly conditioned by the s^6 configuration in the deuteron (influence of the s^4p^2 configurations here is one order of magnitude less). For

the weight of the s^6 configuration in the deuteron from 2.5

$$S^d_{\Delta\Delta} = 10^{-2} - 1.6 \cdot 10^{-2}.$$

The functions $\Phi^d_{AR}(\vec{K}_R)$ (4) for the $NN^*(1440)$ and $\Delta\Delta$ pairs up to $\vec{K}_R = 0.5 GeV/c$ have 0S- oscillator character (because of the high binding energy) and the corresponding momentum distribution (6) is displayed in fig.5.

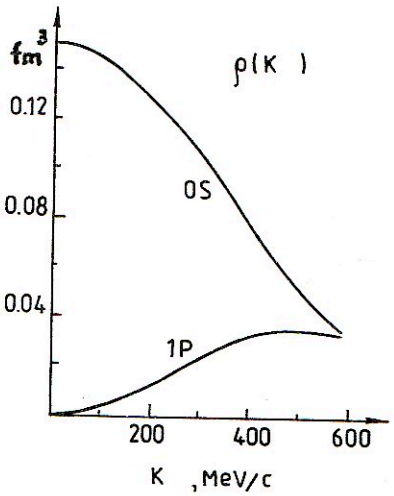

Fig. 5.

Momentum distributions for the $d(e,e'p)N^*or\Delta$ processes (in order to develop the given momentum distribution it is necessary to multiply vertical scale by corresponding spectroscopic factor)

A more complicated situation takes place when describing the processes $d(e,e'p)N^*(1520)$ and $d(e,e'p)N^*(1535)$. Here we have the interference of some terms in (3).For instance, for the first of the processes: $J^\nu_{fi} \sim$

$$\sim j^\nu_{p\to p}\Phi^d_{NN^*(1520)} + j^\nu_{N^*(1520)\to p}\Phi^d_{N^*(1520)N^*(1520)} + j^\nu_{N^*(1535)\to p}\Phi^d_{N^*(1535)N^*(1520)}. \quad (8)$$

At momentum transfer $q \sim 1 - 2 GeV/c$ the baryon electromagnetic de-excitation amplitudes $e + N^*(1535) \to e' + p$ and $e + N^*(1520) \to e' + p$ are comparable or exceed to some extent the amplitude of elastic scattering $e + p \to e' + p$. Moreover,the corresponding spectroscopic factors are comparable to each other too:

$$S^d_{NN^*(1535)} = 10^{-3} - 2 \cdot 10^{-3}$$

$$S^d_{NN^*(1520)} = 2 S^d_{NN^*(1535)}$$

$$S^d_{N^*(1535)N^*(1535)} = 2 \cdot 10^{-4} - 3 \cdot 10^{-4}$$

$$S^d_{N^*(1520)N^*(1520)} = 10 S^d_{N^*(1535)N^*(1535)}$$

$$S^d_{N^*(1535)N^*(1520)} = 8 S^d_{N^*(1535)N^*(1535)} .$$

So, in a wide range of recoil momentum $K_R = 0 - 500 MeV/c$ we don't have a dominant term and as a consequence the factorization (5) doesn't take place. But the behaviour of $\Phi^d_{NN^*(1535)}(\vec{K}_R)$ and $\Phi^d_{NN^*(1520)}(\vec{K}_R)$,on the one hand, have 1P- oscillator character. On the other hand, $\Phi^d_{N^*(1520)N^*(1520)}(\vec{K}_R)$,$\Phi^d_{N^*(1535)N^*(1535)}(\vec{K}_R)$ and $\Phi^d_{N^*(1535)N^*(1520)}(\vec{K}_R)$ have 0S - behaviour (see the corresponding momentum distributions in fig.5). As a result,close to the point $K_R = 0$ $(K_R \leq 100 MeV/c)$ the cross-section of these processes is conditioned by the baryon de-excitation and being measured permits us to infer the corresponding spectroscopic factors from the experiment.

Finally,mention should be made that the process displayed in fig.4^b must be evaluated. This process is conditioned only by the usual NN component in the deuteron and can mask the 6q-structure of the deuteron.

5.Let us discuss the possibility of potential description of the N^*N system. For simplicity a many-particle oscillatory Hamiltonian is used in the treatment below because such a Hamiltonian permits analytical transformations under the transition from one-particle coordinates to the Jacobi coordinates. By choosing the internal Jacobi coordinates of two 3q-clusters , together with the coordinate $\vec{r}$ of the relative motion of the two clusters, to be the required set of the Jacobi coordinates, we devide the oscillatory Hamiltonian into three parts. Two parts correspond to the internal motion in the 3q-clusters while the third part is in correspondence with the relative motion of the clusters in the oscillatory potential (besides, the center-of-mass vibrations occur which are excluded exactly in the translation-invariant-shell model).

Had the interactions among the quarks reduced to the confinement forces $\sim r^2$ only, we would have dealt with the oscillatory baryon-baryon potential which is universal for different pairs of 3q-clusters NN, $\Delta\Delta$,N^*N,...

Since,however,the interactions among the quarks are defined also by other forces (which depend on spins,etc.) of perturbative and nonperturbative character, such a "degeneracy of potentials" is avoided. At the same time, the degeneracy must be preserved as before for the cluster pairs which,in terms of the quark model, are of the identical internal 3q spatially-spin-flavor symmetry and of the same symmetry with respect to the quark permutation from one cluster to another.The latter symmetry is also defined by the appropriate Young schemes in the 6q-system.

In view of the above,we are interested in the baryon pairs NN and $NN^*(1440)$. The component $\phi_N\phi_N\phi_{2S}(\vec{r})$ with the nodal function of relative motion $\phi_{2S}(\vec{r})$ and the component $\phi_{N^*(1440)}\phi_N\phi_{0S}(\vec{r})$ with the node-free function of relative motion $\phi_{0S}(\vec{r})$ have to accompany each other in different 2-quantum $s^4p^2 - s^52s$ configurations. In other words, a given shell cannot comprise any configuration which would include the component $\phi_N\phi_N\phi_{2S}(\vec{r})$ and would not include the component $\phi_{N^*(1440)}\phi_N\phi_{0S}(\vec{r})$,and vice versa. This circumstance is readily understandable because the respective fractional parentage coefficients are defined by the same Clebsh-Gordan coefficients for different SU(n) groups [8,9],excluding SU(3) oscillatory symmetry.

All this means that a unified at short ranges potential can be constructed for the NN and $N^*(1440)N$ systems. This potential must be of such a depth that two levels would be contained in the $^3S_1$-wave therein,with the lower level corresponding to the node-free

bound state of the $N^*(1440)N$ system at binding energy $\sim m_{N^*(1440)} + m_N - m_d$,and the upper level to the nodal state of the NN system at an energy equaling the deuteron binding energy in two-nucleon channel. By treating potentially the interaction in the $N^*(1440)N$ system in such a manner,we can describe the above-mentioned component in the deuteron through the wave function of the deep-bound $^3S_1$ state (the 1S level) in the Moscow NN potential (see fig.1).

Finally,let us consider the following. The Moscow NN-potential model can describe only the first component of the two-nucleon system in representation (1). But a full description of the deuteron means using both nodal potential component and s^6 compound state [4]. In this connection,the deep (of a 1 GeV depth) attractive potential yields a particularly-adequate description of the $N^*(1440)N$ system at low energies because the $N^*(1440)N$ component in the deuteron is microscopically coupled to the $s^4p^2 - s^52s$ quark shell alone (for the S-wave) and,of course, is not contained in the s^6 configuration. By its physical origin,the deep attractive potential is bound up just to describing the interactions of the clusters formed within the $s^4p^2 - s^52s$ and higher configurations but not s^6.The potentials of this type will be quite adequate for the baryon pairs such as $N^*(1440)N$,$N^*(1535)N^*(1535)$,$N^*(1520)N^*(1520)$, $N^*(1535)N^*(1520)$,...

References

1.M.Oka, K.Yazaki.Progr.Theor.Phys. 66(1981)556;Nucl.Phys. A402(1983)477
2.A.Faessler et al.Nucl.Phys. A402(1983)555;A496(1989)621
3.Y.Yamauchi et al.Nucl.Phys. A443(1985)628;A457(1986)621
4.L.Ya.Glozman et al.Z.Phys.A332(1989)339
5.I.T.Obukhovsky,A.M.Kusainov.Phys.Lett. B238(1990)142; Yad.Fiz. 51(1990)1655
6.J.F.Mathiot.Phys.Rep. 173(1989)63;D.O.Riska Phys.Rep. 181(1989)207
7.V.G.Neudatchin et al.Progr.Theor.Phys. 58(1977)1072
8.M.Harvey.Nucl.Phys. A352(1981)301;326
9.I.T.Obukhovsky et al.J.Phys. A15(1983)27;Z.Phys.A308(1982)253
10.I.T.Obukhovsky A.M.Kusainov.Yad.Fiz.47(1988)494
11.V.I.Kukulin et al.Phys.Lett. B135(1984)20;B165(1985)7
12.L.Ya.Glozman,V.G.Neudatchin,I.T.Obukhovsky A.A.Sakharuk.Phys.Lett. B252(1990)23

NONNUCLEON COMPONENTS IN THE DEUTERON AND THE QUARK-CLUSTER APPROACH TO THE N-N INTERACTION

V.G.Neudatchin and I.T.Obukhovsky

Institute of Nuclear Physics, Moscow State University,

Moscow,119899

The problem of the quark effects in the NN-interaction is being widely discussed (see the reviews /1,2/ and the references therein). An undoubtful advantage of the quark approach, which has not as yet been appraised at its true worth, is the simplicity in the interpretation of intricate phenomena which in the traditional approach would require the introduction of the multi-meson and baryon contributions. For example, the repulsive core in the NN-interaction and the suppression of the quark effects in the deuteron magnetic form factors were very easily explained - through the destructive interference of the quark configurations s^6 and s^4p^2 in the NN-system wave function at low energies (including the deuteron)/3,4/. At higher energies this simple model makes predictions at a qualitative level. As the energy increases, the contribution of the excited configuration s^4p^2 to the S-wave NN scattering gets larger, leading to changes in the short-range NN-interaction. At intermediate energy it becomes more appropriate to describe the NN-interaction using, instead of the commonly used phenomenological repulsive core, the deep attractive potential containing one extra bound state which is regarded as forbidden /5,6/ (the bound OS-state would correspond to the configuration s^6 which is suppressed in the present case).

So the quark microscopic approach is formulated here through the quark shell configurations /7,8/, which contain a very capacious information about the influence of the antisymmetrization upon the BB-system (NN, $\Delta\Delta$, $N\Delta$, etc.). For example, the question as to the virtual baryons B^*, B^{**} with one or two oscillator quanta of internal excitation in the NN interaction is answered with ease in terms of the configurations s^5, s^5p, s^4p^2, s^3p^3, etc. Note that these excited states can be observed as real particles in the quasi-elastic knock-out of a nucleon from the deuteron, $d(e,e'p)N^*$ or $A(d,N^*)X$, where N^* is the excited nucleon-spectator, and can give valuable independent information about the presence of the configuration s^4p^2 in the deuteron.

In the present paper these problems are studied on the basis of the

Hamiltonian:

$$H_q = \sum_i \left(m_i - \frac{\nabla_i^2}{2m_i}\right) + \sum_{i<j} V_{ij}(\rho), \quad \rho = r_i - r_j \qquad (1)$$

proceeding from the assumption about the two-particle interaction of quarks. The role of the configuration s^6 and s^4p^2 in the S-wave NN scattering in a wide energy range $0<E_{lab}\leq 1\text{-}2$ GeV was considered. We extended the energy range and made a number of improvements in the model with the pair qq-interactions (the interactions of constituent quarks with the π- and σ-effective fields and the form factors at the πqq- and σqq-vertices were taken into account, in some variants we introduced the contact four-fermion interactions of different operator form, etc.). This enabled us to describe simultaneously the baryon spectrum with allowance for one- and two-quantum excited states (N, Δ, N^*, N^{**}), the NN-scattering data in a comparable energy interval and non-nucleon components in the deuteron.

Just as in the standard RGM approach /9,10/, we derive the equations of motion proceeding from the Hulthen-Kohn variational principle. The trial function is written as an expansion in the two-center shell configurations $S_+^3(R)S_-^3(R)$ /11/ which for the L-th partial wave is written as:

$$\frac{1}{r}Y_{LM}(\hat{r})u_{6q}^{LST}(k,r;\rho_1,\xi_1,\rho_2,\xi_2,X) =$$

$$= \sum_f \int_0^\infty \chi_f^L(k,R)\left[N_f^L(R,R)\right]^{-1/2}\left|S_+^3(R)S_-^3(R)[f_X][f_{CS}]LST\right\rangle RdR\,. \qquad (2)$$

In the representation (2) the summation is made over all the Young schemes $[f_X]$, $[f_{CS}]$, satisfying the Pauli exclusion principle, in the coordinate (X) and colour-spin (CS) space which is briefly designated from here on by a symbol f. $S_\pm(R)$ denotes the quark OS-orbitals, centered at points $\pm\frac{R}{2}$,

$$S_\pm(r_i,R) = (\pi b^2)^{-3/4}\exp\left[-\frac{1}{2b^2}(r_i \mp \frac{R}{2})^2\right]\chi(C_i,S_i,T_i) \qquad (3)$$

Thus, R is a generator coordinate /11/ and the other variables in (2) are Jacobi coordinates,

$$r = \frac{1}{3}\sum_{i=1}^{3} r_i - \frac{1}{3}\sum_{j=4}^{6} r_j, \quad X = \frac{1}{6}\sum_{i=1}^{6} r_i, \quad \rho_1 = r_1 - r_2, \quad \xi_1 = \frac{1}{2}(r_1+r_2) - r_3,$$

etc. In the expression (2) we need not to use the antisymmetrization operator with respect to permutations of quarks from different nucleons,

$$A = \frac{1}{10}\left(1 - \sum_{i=1}^{3}\sum_{j=4}^{6} P_{ij}\right), \quad A^2 = A$$

since the basis two-center functions in (2) are completely antisymmetrized. They are constructed, using the Clebsch-Gordan coefficients of the groups $SU(n)$ from the reduction chain of subgroups

$$SU(24)_{XCST} \supset SU(2)_X \times SU(12)_{CST},$$

$$SU(12)_{CST} \supset SU(6)_{CS} \times SU(2)_T \supset SU(3)_C \times SU(2)_S \times SU(2)_T \qquad (4)$$

and the Young schemes $[f_{XCST}]=[1^6]$, $[f_X]$, $[f_{CST}]=[\tilde{f}_X]$, $[f_{CS}]$, $[f_C]=[2^3]$, $[f_S]$, $[f_T]$ are invariants of these subgroups. The method of construction of the basis and the calculation of the Clebsch-Gordan and fractional parentage coefficients (the method of scalar factors /2,12/) were described by us in /2,8,12,13/. In the representation (2) the expansion is performed over the functions, normalized to unit at any fixed value of R,

$$\langle S^3_+(R)S^3_-(R)[f]LST|S^3_+(R')S^3_-(R')[f']L'S'T'\rangle = \delta_{ff'}\delta_{LL'}\delta_{SS'}\delta_{TT'}N^L_{f_X}(R,R'). \qquad (5)$$

The convenience of the normalized basis consists in that at $R\to 0$ the basis vectors $\left[N^L_f(R,R)\right]^{-1/2}|S^3_+S^3_-[f]LST\rangle$ change over to usual shell configurations /11/ $|s^m p^n[f]LST\rangle$, $m+n=6$. Considering that for even L the Young scheme $[f_X]$ takes on in (2) two values, $[6]_X$ and $[42]_X$, we get in the channel under study $L=0$, $S=1$, $T=0$ (instead of the limit $R\to 0$ we record the integral of the δ-function)

$$\int_0^\infty \frac{\delta(R)}{R}\left[N^{L=0}_{f_X}(R,R)\right]^{-1/2}|S^3_+(R)S^3_-(R)[f]L{=}0S{=}1T{=}0\rangle RdR \qquad (6)$$

$$= \begin{cases} |s^6[6]_X[2^3]_{CS}L{=}0S{=}1T{=}0\rangle & \text{if } [f_X]=[6], \\ |s^4p^2[42]_X[f]_{CS}L{=}0S{=}1T{=}0\rangle & \text{if } [f_X]=[42], \end{cases}$$

where $[f_{CS}]=[42]$, $[321]$, $[2^3]$, $[31^3]$, $[24^4]$ are all the possible Young scheme from the Clebsch-Gordan series for the inner product $[2^3]_C\cdot[42]_S$.

As it has been noted, the configurations s^6 and s^4p^2 are the most essential components of the NN-system wave function in the internal region and, therefore, in our modified RGM approach we recorded the trial functions $\chi^L_f(k,R)$ in (2) as an expansion

$$\chi^L_f(k,R) = \mathcal{A}^L_f(k)\frac{\delta(R)}{R}+U^{NN}_f\left[C^L_{f_X}(k,R)+\cot\delta_L(k)\,S^L_{f_X}(k,R)\right]. \qquad (7)$$

The expansion (7) includes only the "basis" internal states $\frac{\delta(R)}{R}$ and the asymptotic states $S^L_{f_X}(k,R)$, $C^L_{f_X}(k,R)$, which in the limit $r\to\infty$ describe the free motion of $3q$-clusters. In the expressions (7) U^{NN}_f are elements

of unitary matrix $U_f^{B_1B_2}$ which realizes in the CST space the transformation from the baryon quantum numbers $B_1(S_1T_1C_1)B_2(S_2T_2C_2)$ to the quantum numbers of the $6q$-system - the Young schemes $[f_X]$ and $[f_{CS}]$. The coefficients α_f^L and $\cot\delta_L$ in (2) and (7) are variational parameters. The trial functional of the Hulthen-Kohn variational principle:

$$\mathcal{J}_E^{LST}\left(\left\{\alpha_f^L\right\},\cot\delta_L\right) = \frac{\hbar^2k^2}{3m_q}\frac{\operatorname{ctg}\delta_L}{k^3} + \int Y^*_{LM}(\hat{r})\frac{1}{r}u_{6q}^{LST}(k,r;\rho_1,\ldots X)(H_q-E)$$

$$\times\, Y_{LM}(\hat{r})u_{6q}^{LST}(k,r;\rho_1,\ldots X)d^3r d^3\rho_1\ldots d^3X \qquad (8)$$

is quadratic in α_f^L, $\cot\delta_L$, and we get from the stationary conditions $\partial\mathcal{J}_E^{LST}/\partial\alpha_f^L=0$, $\partial\mathcal{J}_E^{LST}/\partial\cot\delta_L=0$ a set of linear algebraic equations for $\left\{\alpha_f^L\right\}$ and $\cot\delta_L$ /3/.

In the quark-cluster approach to the nucleon-nucleon interaction it is usually assumed that the Hamiltonian (1) describes not only the hadronic system but also the interaction of hadrons as quark clusters/10/. This makes possible a comparison between different quark interactions and a wide range of experimental data.

It is known that the splitting in the spectrum of light hadrons is well described by the colour-exchange potentials carried over from the charmonium spectroscopy /14/ (the spin-orbital forces are omitted)

$$V_{ij}^{OGE}(\rho) = \alpha_g\frac{\lambda_i\lambda_j}{4}\left[\frac{1}{\rho}-\frac{\pi}{m_q^2}\left(1+\frac{2}{3}\sigma_i\sigma_j\right)\delta(\rho)-\frac{1}{m_q^2\rho^3}S_{ij}(\hat{\rho})\right], \qquad (9)$$

$$S_{ij}(\hat{\rho}) = 3(\sigma_i\hat{\rho})(\sigma_j\hat{\rho})-\sigma_i\sigma_j,$$

$$V_{ij}^{conf} = -\frac{\lambda_i\lambda_j}{4}(\alpha_c\rho-V_0). \qquad (10)$$

but in this case the constants α_g, α_c, m_q should be considered as phenomenological parameters. This "renormalization" of the QCD constants merely imitates the nonperturbative contributions and is inconsistent even on the NN system where the interaction (9), (10) leads to the short range repulsion and fails to account for the mutual attraction of nucleons in a medium range $0.5\leqslant r\leqslant 1.5$ fm. Though it is not a priori clear that the universal potentials, describing both the $3q$- and $6q$-system, are existent, the construction of the phenomenological potentials V_{ij}, which take into account the nonperturbative dynamics, is quite justified and led to certain positive results /9,10,15,16/. In the framework of the "naive nonperturbative"

models /15,17/, allowing for the π- and σ-exchanges at the quark level, the success was achieved due to introduction of new parameters (such as m_σ, $g_{\sigma qq}$ etc.) which were fitted directly to the NN data. However, the fitfitting of the parameters cannot lead to a better understanding of the dynamics. In the present work we did not fit parameters of the chiral interaction H_{ch} specially to the NN data or the baryon spectrum but we used the constrains upon the πqq and σqq interactions which follow from known models of the spontaneous breaking of chiral symmetry (SBCS) /18,19/ in QCD vacuum. According to known Nambu-Jona-Lasinio results/18/ the effective fields interaction is of the chiral-invariant form, $H_{ch} \sim g_{ch}\,\bar{\psi}(\sigma + i\gamma_5\tau\pi)\psi$; the constrains upon the masses of the effective fields - pseudo scalar (π), scalar (σ) and fermion (in our case it is the constituent quarks with the mass $m_q \approx m_N/3$) are $m_\pi \approx 0$, $m_\sigma \approx 2m_q$. Besides, we followed the papers /19/ and kept it mind that the description of the interaction in terms of the effective fields (π, σ, q) makes sense only at distances greater - than the characteristic size ρ_c of the instanton fluctuations responsible for SBCS (according to refs. /19,20/ $\rho_c \approx 0.3$ fm). In the presence of the instanton fluctuations of the gluon field the light QCD quarks ($m_{u,d} \approx 0$) acquire the dynamic mass $m_q(Q^2)$ which depends on the momentum transfer Q /19/. At large momenta, when $Q \geq Q_c \approx \rho_c^{-1}$, this mass $m_q(Q^2) \to m_{u,d} \approx 0$ and only at small momenta $Q \to 0$ it equals the constituent mass $m_q(0) = m_q \approx m_N/3$. The interaction with the effective chiral field $\phi(x)$ can be recorded in the form, suggested in refs. /19/:

$$H_{ch} = m_q(Q^2)\bar{\psi}\, exp(i\gamma_5\tau\phi/f_\pi)\psi \,. \qquad (11)$$

At $Q \geq Q_c \approx 0.6$ GeV/c the interaction is automatically switched off. We used the expression (11) in the linear approximation in $\pi = \hat{\phi} f_\pi \sin(\phi/f_\pi)$ and $\sigma = f_\pi(\cos(\phi/f_\pi) - 1)$

$$H_{ch} \approx m_q\bar{\psi}\psi + g_{ch}F(Q^2)\bar{\psi}(\sigma + i\gamma_5\tau\pi)\psi \,. \qquad (12)$$

where $m_q = m_q(0)$, $g_{ch} = \frac{m_q}{f_\pi}$, $F(Q^2) = m_q(Q^2)/m_q(0)$. The expression (12) differs from the Hamiltonian of the linear σ-model only in that the vertex constant g_{ch} is reduced by the form factor $F(Q^2)$.

The form factor $F(Q^2)$ from /19/ was here approximated by the analytic expression

$$F(Q^2) = \left[1 + \sum_{k=1}^{n} C_k \frac{Q^2 + m_\pi^2}{Q^2 + \Lambda_k^2}\right]^{1/2} \qquad (13)$$

The convenience of (13) is in that it enables us to record immediately the π and σ exchange potential generated by the Hamiltonian (12)

$$V_{ij}^{ch}(\rho) = \frac{1}{3}\alpha_{ch} m_\pi \Big\{ \tau_i \tau_j \sigma_i \sigma_j \Big[Y_0(m_\pi \rho) + \sum_{k=1}^{n} C_k \frac{\Lambda_k^3}{m_\pi^3} Y_0(\Lambda_k \rho) + \Big(1 + \sum_{k=1}^{n} C_k\Big) \frac{4\pi}{m_k^3} \delta(\rho) \Big] + \tau_i \tau_j S_{ij}(\hat{\rho}) \Big[Y_0(m_\pi \rho) + \sum_{k=1}^{n} C_k \frac{\Lambda_k^3}{m_\pi^3} Y_0(\Lambda_k \rho) \Big] \quad (14)$$

$$-3\Big(\frac{4m_q^2}{m_\pi^2}\Big)\Big[\frac{m_\sigma}{m_\pi}\Big(1 + \sum_{k=1}^{n} C_k \frac{m_\pi^2 - m_\sigma^2}{\Lambda_k^2 - m_\sigma^2}\Big) Y_0(m_\sigma \rho) + \sum_{k=1}^{n} C_k \Big(\frac{\Lambda_k^2 - m_\pi^2}{\Lambda_k^2 - m_\sigma^2}\Big) Y_0(\Lambda_k \rho)\Big]\Big\},$$

$$Y_0(x) = e^{-x}/x, \; Y_2(x) = (3/x^2 + 3/x + 1) Y_0(x)$$

Combining the potential V_{ij}^{ch} with the colour exchange interactions V_{ij}^{OGE} and V_{ij}^{conf}, we get a potential model,

$$V_{ij} = V_{ij}^{OGE} + V_{ij}^{conf} + V_{ij}^{ch}, \quad (15)$$

which uses in fact different types of interaction in three different regions $0<\rho\leq\rho_c$, $\rho_c\leq\rho\leq r_{conf}$ and $r_{conf}\leq\rho<\infty$. Hence, this model has two characteristic scales: ρ_c and r_{conf} and gives stable observables as other model parameters are varied.

It has already been noted that the masses of the effective fields (q, π, σ) in our model are fixed

$$m_q = \frac{1}{3} m_N, \; m_\pi = 140 \; MeV, \; m_\sigma = 2m_q \quad (16)$$

and are not adjustable parameters, just as is not the constant $\alpha_{ch} = \frac{g_{ch}^2}{4\pi} \times \frac{m_\pi^2}{4m_q^2}$, which is normalized to known constant of the pseudo scalar πNN - coupling $g_{\pi NN}^2/4\pi = 14.2$ (see, for example, /10,15/)

Table 1a. Parameters of the qq-interaction

№	b (fm)	α_s	α_c $\left(\frac{MeV}{fm}\right)$	V_0 (MeV)	α_{ch}
I	0.55	1.33	411.35	300.6	0
Ia*)	0.475	0.97	246.4	-	0
II	0.525	0.78	161.78	94.44	0.0284
III	0.50	0.57	253.74	231.46	0.0284

*) from ref. /10/

$$\alpha_{ch} = \Big(\frac{3}{5}\Big)^2 \frac{g_{\pi NN}^2}{4\pi} \cdot \frac{m_\pi^2}{4m_N^2} = 0.0284. \quad (17)$$

The adjustable parameters of the interaction (15) were, as usual, only the constants α_s, α_c and V_0, which were chosen to provide the best description of the nucleon mass, the Δ isobar and the masses of the nucleon

Table 1b. The nucleon excitation spectra for variants I-III

№	m_N (MeV)	m_Δ (MeV)	$m_N^*\left(J^P=\frac{1}{2}^+\right)$ (MeV)		$m_N^*\left(J^P=\frac{1}{2}^-\right)$ (MeV)			m_Δ^* (MeV)
I	939	1234	1454	2037	1345	1501	2005	2188
Ia	939	1232	–	–	–	–	–	–
II	939	1235	1412	1848	1426	1628	1951	2157
III	939	1232	1497	1884	1483	1682	2077	2181
Exp	939	1232±2	1440±40	1710±30	1540±20	1650±30	2100(?)	(?)

excited states of positive and negative parity $N^*_{1/2^-}$ (1535) $N^{**}_{1/2^+}$ (1440), etc. (table 1). Despite the fact that the model parameters were not specially fitted to the NN-data, we obtained a not bad description of the $^3S_1$-phase shifts in the whole energy interval $0<E_{lab}\leq 1$ GeV which supplied the reliable phase-shift data /21/. (The underrated values of the

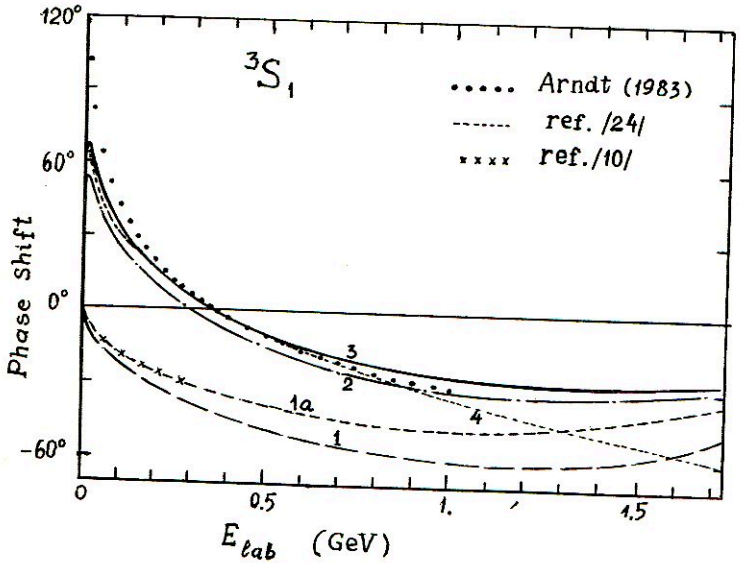

Fig. 1. $^3S_1$-wave phase shifts.

$^3S_1$-phases at $E_{lab} \leqslant 0.2$ GeV can be accounted for by the fact that the calculation didn't include the tensor forces and the $^3S_1$-$^3D_1$ - mixing). The best description of the phase shifts in the region $0 < E_{lab} \leqslant 1$ GeV is obtained for variants II and III, i.e. for the cases when the baryon spectrum is described most accurately.

We solve the problem of the projection of the six-quark wave function onto the NN-channel (and other baryon channels) by means of the fractional parentage technique (or Racah's method) which is employed as a rule to calculate the cluster spectroscopic factors S_x, widely used in nuclear physics for the analysis of the direct reactions on light nuclei /22/. The completely antisymmetrized wave function (for example, a superposition of the configurations s^6, s^4p^2, etc.) is expanded as a finite series in the nonantisymmetrized, but orthogonal basis consisting of the product of clusters with fixed quark numbers.

$$\Psi^{A}_{6q}(12\ldots6) = \sum_{B_iB_j} \Gamma^{CST}_{B_iB_j}\, \Phi_{B_iB_j}(r)\, B_i(123)\, B_j(456). \qquad (18)$$

For example, the configuration $s^4p^2[42]_X[42]_{CS}$, which was first discussed in refs. /7,8/ is expanded in the orthogonal basis

$$|s^4p^2[42]_X[42]_{CS}\ L{=}0\ S{=}1\ T{=}0\rangle_{TISM} = \sqrt{\tfrac{1}{25}}\left\{N(123)N(456)\right\}_{ST}\varphi_{20}(r)$$

$$+\sqrt{\tfrac{2}{225}}\left\{C_1(123)C_1(456)\right\}_{ST}\varphi_{20}(r) - \sqrt{\tfrac{4}{225}}\left\{C_2(123)C_2(456)\right\}_{ST}\varphi_{20}(r)$$

$$-\sqrt{\tfrac{1}{450}}\left\{C_1^{**}(123)C_1(456)\right\}_{ST}\varphi_{00}(r) + \sqrt{\tfrac{1}{225}}\left\{C_1^{**}(123)C_2(456)\right\}_{ST}\varphi_{00}(r)$$

$$-\sqrt{\tfrac{1}{180}}\left\{C_2^{**}(123)C_2(456)\right\}_{ST}\varphi_{00}(r) + \sqrt{\tfrac{1}{50}}\left\{N(123)\tilde{N}^{**}(456)\right\}_{ST}\varphi_{00}(r)$$

$$+\ldots \quad (31 \text{ terms as a whole}) \qquad (19)$$

Here N, N^*, $\tilde{N}^{**}$, Δ^*, C_i, C_i^*, C_i^{**}, $C_i'^*$ are baryons possessing different spin-isospin and colour structure (the number of asterisks corresponds to the number of the oscillator quanta of excitation; the complete enumeration of quantum numbers would occupy much space). In (19) the generalized fractional parentage coefficient is the function of relative motion of baryons ($\varphi_{00}(r)$, $\varphi_{20}(r)$, ...), multiplied by the fractional parentage coefficient in the $XCST$-space. In the general case, it is a certain function

$\Phi_{B_iB_j}(r)$, which describes the relative motion of baryons $B_i(123)$ and $B_j(456)$.

$$\Phi_{B_iB_j}(r) = \sqrt{\frac{6!}{3!3!2}} \left\{ \langle B_i(123) | \langle B_j(456) | \right\}_{ST} | \psi^{LST}_{6q}(123456) \rangle \cdot \qquad (20)$$

The functions $\Phi_{B_iB_j}(r)$ are quite analogous to the function of relative motion of cluster and residual nucleus, for example, in the quasielastic α-particle knock-out $A(p,p'\alpha)(A-4)$ /22/. Namely, we can write Eq. (19) for the six-quark deuteron by the general form, commonly used in the low-energy nuclear physics /2,13,22/

$$\Phi_{B_iB_j}(\mathbf{r}) = \begin{bmatrix} 6 \\ 3 \end{bmatrix}^{1/2} \Gamma^{CST}_{B_iB_j} \, \Phi_{B_iB_j}(\mathbf{r}) \qquad (21)$$

The quasi-elastic knock-out experiments $d(e,e'p)N^*$ and the deuteron fragmentation reactions $A(d,N^*)X$ at the intermediate energies (see for example refs. /23/) offer an excellent possibility of the immediate experimental observation of individual terms in the expansion (19), as far as the high value of the final state relative momentum $k \gtrsim 1$ GeV/c makes the final state quark antisymmetrization not essential ($k \gg b^{-1}$, where $b \approx 0.5$ fm is the characteristic size of the three-quark system).

Here, the spectator N^* momentum distribution (i.e. the initial state momentum distribution of the B_1B_2 mutual motion) is described, ideally, by the square of the Fourier transform of the function (20)

$$\bar{\Phi}_{B_1B_2}(\mathbf{k}) = (2\pi)^{-3/2} \int \Phi_{B_1B_2}(\mathbf{r}) \, e^{i\mathbf{kr}} \, d^3r \, . \qquad (22)$$

Its normalization integral provides us with the corresponding "effective number" of baryons, mentioned above.

Using the technique of projection onto the NN and other BB-channels (20), we show in figs. 2 a,b the NN-scattering wave functions for the energy $E_{lab}=200$ MeV and in fig.3 the wave function of the deuteron for variant III which gives the phase shifts most close to the experimental. Figures 2a,b and 3 show in the form of projections onto the NN channel the complete wave function $u^{L=0ST}_{6q}$ and its components:

1) the shell component $s^6[6]_X[2^3]_{CS}$ which is symmetric in the x-space;
2) the additional component $\tilde{u}^{LST}_{6q}$ which belongs to mixed symmetry in the x-space

$$\tilde{u}^{LST}_{6q} = u^{LST}_{6q} - \tilde{a}_{[6]_X} | s^6[6]_X[2^3]_{CS} LST \rangle \cdot \qquad (23)$$

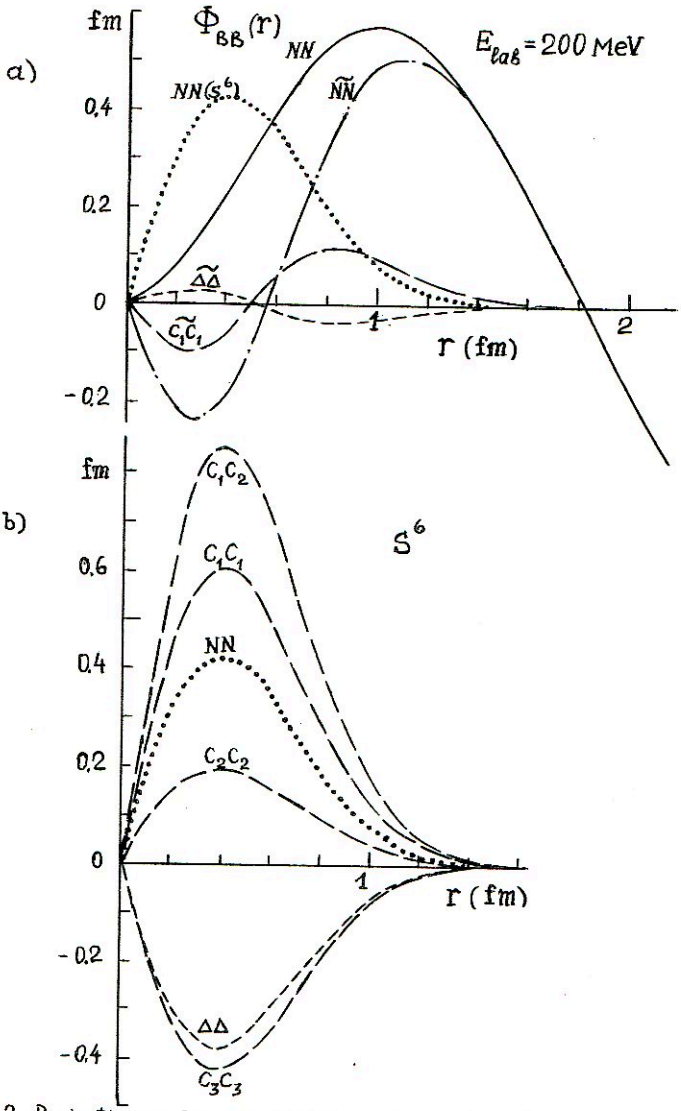

Fig. 2. Projections of the 6q-wave functions onto BB-channels.

By definition, these components are orthogonal to each other $\langle \tilde{u}^{LST}_{6q} | s^6[6]_X[2^3]_{CS} LST\rangle = 0$ and the component $\tilde{u}^{LST}_{6q}$ consists of the asymptotic part of wave function which will be written in what follows as $A\left\{\psi_N\psi_N\chi_{as}(r)\right\}$, without specifying the form of $\chi_{as}(r)$ and the superpositions of the remaining 5 states of the shell configuration $s^4p^2[42]_X$

$$\tilde{u}^{LST}_{6q} = \sum_{f_{CS}} \tilde{a}_f | s^4p^2[42]_X[f_{CS}]LST\rangle + A\left\{\psi_N\psi_N\chi_{as}(r)\right\} \qquad (24)$$

(Here the coefficients $\tilde{a}_f$ differ from the calculated a_f. The coefficients $\tilde{a}_f$ include the correction for the overlap of the configurations s^6 and $s^4p^2[42]_X$ with the asymptotic part of the wave function).

Figure 2b shows the projections of the component $\tilde{a}_{[6]_X} | s^6[6]_X[2^3]_{CS} LST\rangle$ onto the NN-, $\Delta\Delta$-, and CC-channels and figure 2a - the analogous projections for the component $\tilde{u}^{LST}_{6q}$ at an energy E_{lab}=200 MeV. (At other energies the relation between the projections NN, $\Delta\Delta$, CC does not change qualitatively). We see that the components $s^6[6]_X$ and $\tilde{u}^{LST}_{6q}$ differ qualitatively in relative value of the amplitudes of the functions $\Phi_{NN}(r)$ and $\Phi_{BB}(r)$, where BB=$\Delta\Delta$, C_iC_j. The symmetric component $s^6[6]_X$ is projected onto any of the baryon channels NN, CC with the weights close to unity (i.e. none of the baryon channels is predominant) whereas the component $\tilde{u}^{LST}_{6q}$ is projected mainly onto the NN-channel ($\tilde{\Phi}_{NN} \gg \tilde{\Phi}_{\Delta\Delta}, \tilde{\Phi}_{CC}$) not only in the asymptotic region but in the overlap region, $r \leqslant r_{conf}$ as well. This means that in the configuration $s^4p^2[42]_X$ there forms (dynamically) such a superposition of states $[f_{CS}]$, which corresponds to the predominantly clustered wave function in the form of N + N with the other nonexcited baryon cluster, $\Delta + \Delta$ and $C_i + C_j$, being suppressed.

Thus, upon solving the set of equations for a_f we get that the NN-scattering wave function in a wide energy range has a characteristic structure - it consists of two qualitatively different components. The component $\tilde{u}^{LST}_{6q}$, defined in (23), is the clustered NN state which in the region of small distances is described by the superposition of states in the configuration s^4p^2 (see (24)) and has (in the projection onto the NN channel) a node at distances $r \sim b$ (see fig. 2). The second component is the symmetric shell state $s^6[6]_X$ which is more like a $6q$-bag (none of the baryon channels is predominant in it). Both the components coexist in the region of distances $r \leqslant 2b$ and for the understanding of the NN-dynamics at small distances this effect of mixing of the configurations s^6 and s^4p^2 is very

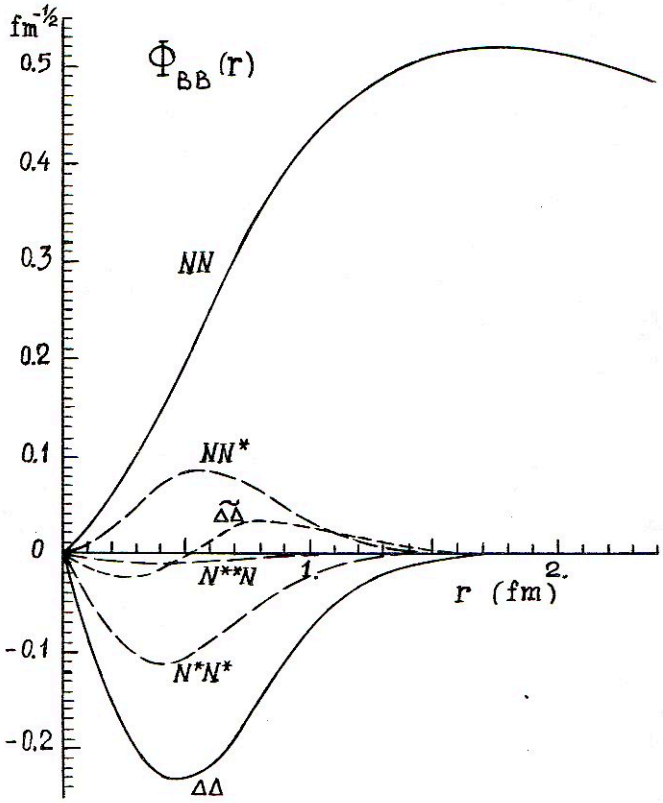

Fig.3. Projections of the 6q-wave function of the deuteron onto BB-channels.

essential (this was first noted in the paper of Harvey /11/).

Here we note that the configuration s^4p^2 plays the significant role in the NN-scattering. The nodal position of the wave function

$$\tilde{\Phi}_{NN}(r) = \sqrt{10}\langle N(123)|N(456)|\tilde{u}^{LST}_{6q}\rangle \qquad (25)$$

at small distances $r \approx b$ is stable in a wide energy interval $0 < E_{lab} \leq 1.2$ GeV which accounts for the negative slope of the phase shifts in the $^3S_1$-waves up to energies $E_{lab} \leq 1.2$ GeV. These nodal wave functions $\tilde{\Phi}_{NN}(r)$ could play a key role in the optical model description of NN scattering /5,6,24/ mentioned in the Introduction.

In the present work we obtained not only the absolute values of the amplitudes of the configurations s^6 and s^4p^2, entering into the wave function of the NN-system, but also their relative sign (negative) which remains unchanged up to energies $E_{lab} \approx 1$-1.2 GeV. In the deuteron the relative sign is also negative. The latter is especially important since it permits one to understand that in the deuteron electromagnetic form factors the contributions of the s^6 and s^4p^2 configurations will interfere destructively /4,25/. Just because of the destructive interference of the quark contributions the deuteron magnetic form factor takes on a zero value in the region $Q^2 \approx 2$ GeV$^2/c^2$ and, accordingly, rapidly decreases in absolute value at $Q^2 \leq 0.8$-1 GeV$^2/c^2$. This behaviour of the magnetic form factor is quite different from the previous predictions made in the hybrid model/26/ in which the $6q$-bag (configuration s^6) and the NN-component are spaced apart and their contributions interfere weakly in the electromagnetic processes.

One of the interesting qualitative effects predicted by the model with excited six quark configurations (s^6, s^4p^2, *etc.*) is obviously short range non-nucleon components $\Delta\Delta$, NN^*, NN^{**}, etc. in the deuteron. A visualization of the specific momentum distribution of such components in the deuteron will be a crucial check on the six quark origin of NN interaction. Mesurements of the momentum distribution of a baryon-spectator in deuteron fragmentation reactions will be such crucial experiments.

The fragmentation cross section of the deuteron into forward proton was studied in Dubna in the reaction $^{12}C(d,p)X$ /27/. It is assumed that the spectator mechanism is predominant in the region $\alpha_N \geq 0.6$ and so the expression for the invariant cross section takes a simple form /28/

$$E_N \frac{d^3\sigma}{dp_N^3} = C \frac{1}{2(1-\alpha_N)m_N} \sqrt{\frac{m_N^2+p_T^2}{4\alpha_N(1-\alpha_N)}} \left| \bar{\Phi}_{NN}\left(\frac{m_N^2+p_T^2}{4\alpha_N(1-\alpha_N)} - m_N^2\right)\right|^2 f(\alpha_N), \quad (26)$$

where $\alpha_N = \frac{E_N + p_L}{E_d + p_d}$ is a part of deuteron momentum carried by a nucleon in the deuteron infinite momentum frame /28,29/, $\vec{p}_N = (\vec{p}_T, p_L)$ is a momentum of the nucleon-spectator, $\bar{\Phi}_{NN}(k_L^2+k_T^2)$ is the Fourier transform (22) of the nonrelativistic wave function $\Phi_{NN}(\vec{r})$ (in our case $\bar{\Phi}_{NN}$ is the projection of the six quark wave function onto NN channel (20)). It is postulated that

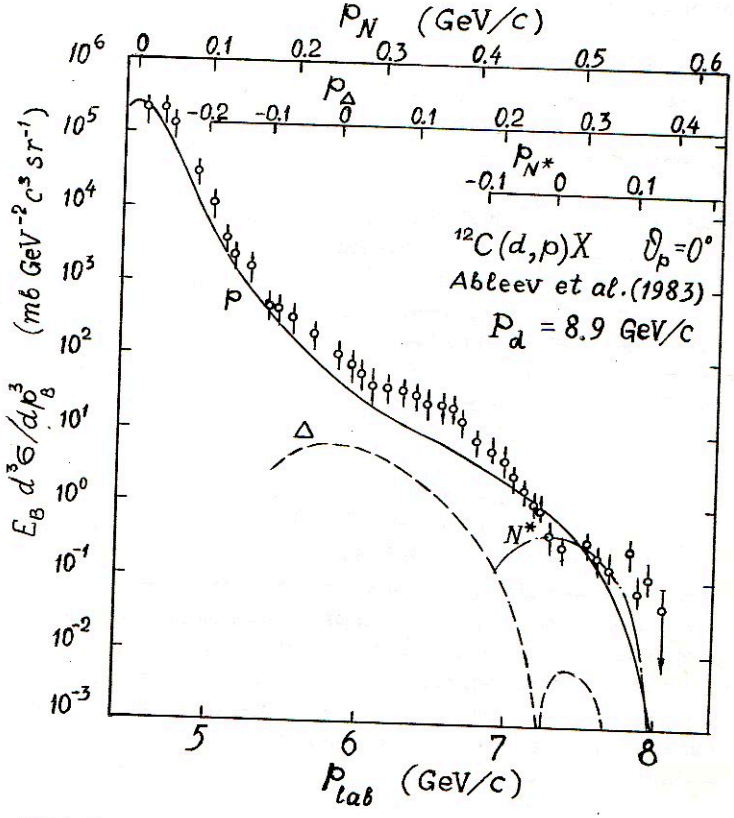

Fig.4. The fragmentation cross sections of the deuteron

Φ_{NN} is a function of the virtual two-nucleon mass $m_{NN}=2\sqrt{m_N^2+\vec{k}_T^2+k_L^2}$ and so the light front variables are k_T and $\alpha_N=(\sqrt{m_N^2+\vec{k}_T^2+k_L^2}+k_L)/m_{NN}$ /28/. The constant C in eq.(26) is proportional to the inelastic nucleon-nucleus cross section $C\cong C_d\,\sigma_{NA}^{in}((1-\alpha_N)E_d)$, where $C_d=(\sigma_{NA}^{tot}-\sigma_{dA}^{el})/\sigma_{NA}^{tot}$, and $f(\alpha)$ is the factor of a form of the cross section near the kinematical limit $f(\alpha)=(\alpha_{max}-\alpha)(1-\alpha)^{-1}(2\alpha_{max}-1)^{-1}$ (see for example /28/). In the case of baryon-spectator B_1 we can use the simple substitutions $m_{NN}\to m_{B_1B_2}=(p_{B_1}^2+m_{B_1}^2)^{1/2}+(p_{B_2}^2+m_{B_2}^2)^{1/2}$ and $\alpha_{B_1}=[(p_{B_1}^2+m_{B_1}^2)^{1/2}+p_{B_1L}]/(E_d+P_d)$ in the eq.(26). The fig.4 shows the fragmentation cross sections of the deuteron into forward proton, Δ-isobar and $N^*(1535)$ for the kinematics of the Dubna experiment /27/ on nucleus ^{12}C at the momentum P_d=8.9 GeV/c. (Upper scales in the fig.4 show momenta of the barion -spectators in the deuteron rest frame.)

References

1. F.Myhrer, J.Wroldsen, Rev.Mod.Phys. 60,629(1988)
2. V.G.Neudatchin, I.T.Obukhovsky, Yu.F.Smirnov, Particles and Nuclei. (Moscow, Energoatomizdat, 1984) vol. 15, p. 1165 (in Russian)
3. I.T.Obukhovsky, A.M.Kusainov, Phys.Lett. B238,142 (1990)
4. L.Ya.Glozman, N.A.Burkova, E.I.Kuchina, Z.Phys.A232,339(1989)
5. V.G.Neudatchin, I.T.Obukhovsky, V.I.Kukulin, N.F.Golovanova, Phys.Rev. C 11,128(1975)
6. V.M.Krasnopol'sky, V.I.Kukulin, V.N.Pomerantzev, P.B.Sazonov, Phys. Lett. B165,7(1985)
7. V.G.Neudatchin, Yu.F.Smirnov, R.Tamagaki, Progr.Theor.Phys. 58,1072 (1977)
8. I.T.Obukhovsky, V.G.Neudatchin, Yu.F.Smirnov, Yu.M.Tchuvil'sky, Phys. Lett. B88,231(1979)
9. M.Oka, K.Yazaki, Nucl.Phys. A402,477(1983)
10. A.Faessler, F.Fernandez, G.Lübeck, K.Shimizu, Phys.Lett. B112,201 (1983); ibid Nucl.Phys. A402,555(1983)
11. M.Harvey, Nucl.Phys. A352,301(1981); ibid 326(1981)
12. I.T.Obukhovsky, Z.Phys. A306,253(1982)
13. I.T.Obukhovsky, Yu.F.Smirnov, Yu.M.Tchuvil'sky, Z.Phys. A15,7 (1982)
14. A.De Rujula, H.Georgi, S.L.Glashow, Phys.Rev. D 12,147(1975)
15. H.Ito, A.Faessler, Nucl.Phys. A470,626(1987)
16. Y.Yamauchi, M.Wakamatzu, Nucl.Phys. A457,621(1986)

17. J.Burger, R.Müller, K.Tragl, H.M.Hofmann. Nucl.Phys. A493,427 (1989)
18. Y.Nambu, G.Jona-Lasinio, Phys.Rev. 122,345(1961)
19. D.I.Dyakonov, V.Yu.Petrov, Nucl.Phys. B272,457(1986); D.I.Dyakonov, V,Yu.Petrov, P.V.Pobylitsa, Nucl.Phys. B306,809 (1988)
20. E.V.Shuryak, Phys.Reports 115,151(1984)
21. R.A.Arndt, L.D.Roper, R.A.Bryan, R.B.Clark, B.S.Ver West, P.Signell, Phys. Rev. D 28,97(1983)
22. Yu.A.Kudeyarov, I.V.Kurdumov, V.G.Neudatchin, Yu.F.Smirnov, Nucl.Phys. A163,316(1971); M.Ichimura, A.Arima, D.Halbert and T.Terazawa, Nucl. Phys. A204,225(1973)
23. V.G.Ableev et al., Pisma JETP 45,467(1987); ibid 47,558(1988)
24 Yu.Dorodnykh, V.G.Neudatchin, N.P.Yudin, I.T.Obukhovsky, Phys.Rev. C43,2499 (1991)
25 I.T.Obukhovsky, in Few-Body and Quark-Hadronic Systems (Proc. of Intern. Conf. edited by Sapojnikov M.G. and Hanhasaev M.H., JINR, D4,87,692, Dubna, USSR, 1987) p. 200
26. Y.Kisukuri, M.Namiki, K.Okano, N.Oshimo, Progr.Theor.Phys. G4,1478 (1980)
27. V.G.Ableev et al., Nucl.Phys. A393,491(1983)
28. A.P.Kobushkin, V.P.Shelest, Particles and Nuclei. (Moscow, Energoatomizdat, 1983) vol.14, p.1146 (in Russian)
29. L.Frankfurt, M.Strikman, Particles and Nuclei. (Moscow, Energoatomizdat, 1980) vol.11, p.571 (in Russian)

RELATIVISTIC DEUTERON STRUCTURE IN THE LIGHT FRONT DYNAMICS

Karmanov V.A.

Lebedev Physical Institute,
Leninsky Prospect 53, Moscow 117924, Russia

1. Introduction

Finding from the first principles the nuclear wave function at relative nucleon momenta of the order of their mass ($q \sim m$) is practically impossible. This is connected with the fact that NN-potential (for example, OBEP), which is valid at relatively large inter-nucleon distances, becomes invalid in relativistic region, whereas the true relativistic NN-interaction hardly can be calculated reliably. Therefore we can use only general properties of relativistic wave function independing of unknown details of interaction. Under these circumstances we should work in the formalism which uses as a relativistic wave function a natural generalization of more or less known nonrelativistic wave function and at the same time satisfies the general principles of relativistic dynamics (i.e., the correct transformation properties, dependence on natural relativistic variables and so on). Review of this formalism based on the explicitly covariant light front wave functions and developed in the papers [1,2] is given in this report.

We will show that at $q \sim m$ parametrization of the wave function is changed considerably: 1) wave function becomes to

depend on new natural variables, having the sence of relativistic relative momenta; 2) besides that the wave function depends on another extra variable having the form of a unit vector $\vec{n}$. These two facts lead to qualitative observable phenomena which do not depend on unknown details of behaviour of the relativistic deuteron wave function.

Below we explain the physical reasons of qualitative change of the wave function parametrization in relativistic region, describe the properties of the light front deuteron wave function and give qualitative predictions for the cross section of the deuteron electrodisintegration.

2. Parametrization of a relativistic wave function

Transformation properties of any relativistic wave function follow from the field theory and Poincare group. However below we obtain these properties from rather transparent qualitative physical consideration. A reader interested in more strict proof can find it in the review paper [2].

Let us consider the wave function of a system (for definiteness we consider the deuteron) with the total momentum $\vec{p}$: $\psi = \psi(\vec{k}_1, \vec{k}_2, \vec{p})$, where $\vec{k}_1$ and $\vec{k}_2$ are the nucleon momenta, $\vec{k}_1 + \vec{k}_2 = \vec{p}$. In coordinate space this wave function is the probability amplitude $\psi(\vec{r}_1, \vec{r}_2, t)$ to find in the deuteron the nucleons in the points $\vec{r}_1$ and $\vec{r}_2$ at one and the same time moment t. Let us define the relative momentum $\vec{q}$ as the momentum of one of the nucleons (let $\vec{q} = \vec{k}_1$) in the reference frame where $\vec{k}_1 + \vec{k}_2 = 0$. This momentum is expressed through energy squared s in c.m.-system: $\vec{q}^2 = s/4 - m^2$, where $s = (k_1 + k_2)^2 = 4(\vec{q}^2 + m^2)$, m is the nucleon mass. We emphasize the following very important and for the first glance paradoxical fact: this relative momentum does not coincide with the nucleon momentum in the deuteron rest system. Indeed, inspite of the fact that the sum of the nucleon momenta is equal to the deuteron momentum: $\vec{k}_1 + \vec{k}_2 = \vec{p}$, the sum of the nucleon energies is not equal to the deuteron energy: $\varepsilon(\vec{k}_1) + \varepsilon(\vec{k}_2) \neq \varepsilon_D(\vec{p})$, where $\varepsilon(\vec{k}) = (m^2 + \vec{k}^2)^{1/2}$, $\varepsilon_D(\vec{p}) = (M^2 + \vec{p}^2)^{1/2}$, M is the deuteron mass. Therefore, if in any given system of reference

we have the equality $\vec{k}_1 + \vec{k}_2 = \vec{p}$ (i.e., not complete equality of the four-dimensional vectors, but only the equality of their projections on three-dimensional subspace), then in other system of reference this equality is desrtoyed. So the shadows of two non-equal trees can turn out to be equal at a certain time of day, but they become different at other position of the sun. In order to go over from initial system, where $\vec{k}_1 + \vec{k}_2 = \vec{p}$, to the system where $\vec{k}_1 + \vec{k}_2 = 0$, one should apply the Lorentz boost corresponding to the velocity $\vec{v}_1 = (\vec{k}_1 + \vec{k}_2)/(\varepsilon(\vec{k}_1) + \varepsilon(\vec{k}_2)) = \vec{p}/(\varepsilon(\vec{k}_1) + \varepsilon(\vec{k}_2))$. On the other hand the transformation to the system, where $\vec{p} = 0$, corresponds to the boost with other velocity $\vec{v}_2 = \vec{p}/\varepsilon_D(\vec{p}) \neq v_1$. In the first system of reference we have $\vec{k}_1 + \vec{k}_2 = 0$, $\vec{k}_1 = -\vec{k}_2 = \vec{q}$, but $\vec{p} \neq 0$; in the second system of reference we have $\vec{p} = 0$, but $\vec{k}_1 + \vec{k}_2 \neq 0$ and hence $\vec{k}_1 \neq \vec{q}$. The nucleon momentum in this system we denote as $\vec{p}_n$, keeping in mind that it will be the momentum of the neutron-spectator in the reaction D(e,e'p)n.

So, we introduce the variable $\vec{q} \neq \vec{p}_n$, but as we shall see now this variable does not exhauts all the set of variables. Speaking about the relativistic equal-time wave function with arguments connected by the equality $\vec{k}_1 + \vec{k}_2 = \vec{p}$, we always should point out the corresponding system of reference where this wave function is defined and where this equality is valid. Namely in this system the events in the points $\vec{r}_1$ and $\vec{r}_2$ are simultaneous. In other system of reference they are not simultaneous and correspond to different moments of time t_1 and t_2. Corresponding wave function becomes equal-time one in this new system, if we put the time difference to zero: $\Delta t = t_1 - t_2 = 0$. But the wave function depends dynamically on Δt, having different values in different systems of reference. This means that the wave function depends dynamically on the system of reference. In the momentum space this fact corresponds to its dynamical dependence not only on the relative momentum $\vec{q}$, but on the total momentum $\vec{p}$ (since in different systems a particle moves with different momenta $\vec{p}$): $\psi = \psi(\vec{q}, \vec{p})$.

More rigorously this phenomenon can be elucidated as follows. Since Hamiltonian of a system (which is the zero component P_0 of the four-momentum operator P_μ) contains

interaction, then the components J_{i0} ($i = 1,2,3$) of the four-dimensional angular momentum tensor $J_{\mu\nu}$ contain the interaction as well (in order to provide the correct transformation properties of the energy P_0 under the Lorentz transformations realized by the generators J_{i0}). Therefore the Lorentz transformations of the wave function $\psi(\vec{q}, \vec{p})$ which are also realized by J_{i0} and transform the wave function from one system of reference (where the total momentum of the deuterom is $\vec{p}$) to other one (with momentum $\vec{p}'$) are the dynamical ones. Hence the wave function $\psi(\vec{q}, \vec{p})$ depends dynamically on the total momentum $\vec{p}$.

It is well known that most convenient system of reference is the infinite momentum frame (IMF). The virtual creation of particles from vacuum is suppressed in IMF, since the life time of these vacuum fluctuations $t \sim \hbar/\Delta E$ tends to zero when ΔE tends to infinity in IMF. Therefore in IMF we observe namely those particles which constitute the composite system. In the limit $\vec{p} \dashrightarrow \infty$ the dependence of the wave function on $|\vec{p}|$ disappeares, but dependence on the direction $\vec{n} = \vec{p}/|\vec{p}|$ survives. By this way we come to the result mentioned in the introduction:

$$\psi = \psi(\vec{q}, \vec{n}). \qquad (1)$$

The physical reason of dependence of the wave function (1) on the variable $\vec{n}$ is impossibility in principle to separate the center-of-mass motion of a relativistic interacting system from the internal motion. This property just manifests itself in dependence of the equal-time wave function not only on the relative momentum $\vec{q}$ (internal motion), but as well as on the total momentum $\vec{p}$ (center-of-mass motion). The inter-influence of the internal and center-of-mass motion is inherent to any interacting relativistic systems, but it still never has been observed.

It is convenient to represent the nucleon momenta in IMF (i.e., at $\vec{p} \dashrightarrow \infty$) in the form:

$$\vec{k}_1 = \vec{k}_\perp + x\vec{p}, \quad \vec{k}_2 = -\vec{k}_\perp + (1 - x)\vec{p}, \quad 0 < x < 1. \qquad (2)$$

For the wave function we obtain: $\psi = \psi(\vec{k}_\perp, x)$. The variables $\vec{q}$, $\vec{n}$ in eq. (1) are connected with well-known variables $\vec{k}_\perp$, x. Substituting eq. (2) in $s = (\varepsilon(\vec{k}_1) + \varepsilon(\vec{k}_2))^2 - (\vec{k}_1 + \vec{k}_2)^2$ and taking into account that at $\vec{p} \dashrightarrow \infty$ $\varepsilon(\vec{k}_1) \approx xp + \frac{m^2 + \vec{k}_\perp^2}{2xp}$ and similary for $\varepsilon(\vec{k}_2)$, we find:

$$\vec{q}^{\,2} = \frac{\vec{k}_\perp^{\,2} + m^2}{4x(1-x)} - m^2 . \qquad (3)$$

Analogously to eq. (3) one can find:

$$\vec{n}\vec{q} = \left[\frac{\vec{k}_\perp^{\,2} + m^2}{x(1-x)} \right]^{1/2} \left(\frac{1}{2} - x \right). \qquad (4)$$

Note that in accordance with the statement given above, if the equality $\vec{k}_1 + \vec{k}_2 = \vec{p}$ is valid in the system with $\vec{p} \to \infty$, then in the reference system, where $\vec{k}_1 + \vec{k}_2 = 0$, the momentum $\vec{p}$ turns into the momentum $\vec{p}'$ which is not equal to zero. It can be easy calculated by the Lorentz transformation corresponding to the velocity $\vec{v}_1$ defined above ($v_1 \to c$ at $\vec{p} \to \infty$): $\vec{p}' = (\vec{p} - \vec{v}_1 \varepsilon(\vec{p})/c)/(1 - \vec{v}_1^{\,2}/c^2)^{1/2}$. At $\vec{p} \to \infty$ we obtain that in the system where $\vec{k}_1 + \vec{k}_2 = 0$ the total momentum has finite nonzero value: $\vec{p}' = -\vec{n}(s - M^2)/2\sqrt{s}$, where $\vec{n} = -\vec{p}/|\vec{p}|$.

3. The light front wave function

Above we considered the wave function giving the probability amplitude at one and the same time moment for all the particles in a certain fixed frame of reference (namely, in IMF). In order not to be connected with fixed reference frame, instead of this wave function we can use the equivalent non-equal-time wave function defined on the light front surface $z + t = 0$ but in arbitrary frame of reference. Thus, in the coordinate space we have $\psi = \psi(\vec{x}_1, t_1, \vec{x}_2, t_2)$, where $t_1 = -z_1$, $t_2 = -z_2$. However in this approach we still have no complete independence of the reference frame, since the equation of the surface $z + t = 0$ is not invariant and therefore is tied to a definite frame of reference. Explicit covariance of the nuclear wave function is necessary to construct the states with definite angular momentum and spin.

Theoretical approach leading to explicitly covariant wave functions was developed in the papers [1] (see the

review [2]). In the approach [1,2] the state vector is defined on the light front surface $\omega x = 0$, where $\omega^2 = \omega_0^2 - \vec{\omega}^2 = 0$. The theory becomes explicitly covariant but keeps in itself all the physical properties of the wave functions discussed above including their dependence on the variable $\vec{n}$. In contrast to the IMF approach in the framework of new formalism the vector $\vec{n}$ is directed not in the direction $\vec{p}$ (the momentum $\vec{p}$ is finite now) but in the direction $\vec{\omega}$.

The light front wave function is a coefficient in the expansion of the state vector $\Phi(p)$ defined on the covariant light front hypersurface:

$$\Phi(p) = \int \Psi(k_1, k_2, P, \omega\tau)\,\delta^{(4)}(k_1 + k_2 - p - \omega\tau) \cdot$$

$$\cdot a^+(\vec{k}_1)\, a^+(\vec{k}_2)|0\rangle\, d\tau\, \frac{d^3k_1}{\sqrt{2\varepsilon_1}} \cdot \frac{d^3k_2}{\sqrt{2\varepsilon_2}} + \ldots \qquad (5)$$

We emphasize that all the four-vectors are on respective mass shells: $p^2 = M^2$, $(\omega\tau)^2 = 0$ (τ is a scalar parameter), $k_1^2 = k_2^2 = m^2$ and are constrained by the relation: $k_1 + k_2 = p + \omega\tau$. The latter relation, as well as the three-momentum conservation in the equal-time wave function, follows from the translation invariance of the theory. Hence the paramertization of the light front wave function formally coincides with the parametrization of the scattering amplitude $1 + 2 \dashrightarrow 3 + 4$. In c.m.-system ($\vec{k}_1 + \vec{k}_2 = 0$) it depends on the relative momentum q and the "scattering angle" θ_{nq} between $\vec{q}$ and $\vec{n}$. So we return to parametrization (1).

The equation for the wave function has the form very close to the Schroedinger equation in the momentum space:

$$\left(4(\vec{q}^{\,2} + m^2) - M^2\right)\Psi(\vec{q}, \vec{n}) =$$

$$= -\frac{m^2}{2\pi^3}\int \Psi(\vec{q}', \vec{n})\, V(\vec{q}', \vec{q}, \vec{n}, M^2)\, \frac{d^3q'}{\varepsilon(q')}\,. \qquad (6)$$

The kernal V in eq.(6) depends on the vector parameter $\vec{n}$. This dependence automatically appeares in any calculation of the kernal in the light front dynamics and leads to $\vec{n}$-dependence of the wave function. In the variables $\vec{k}_\perp$ and x the equation (6) is transcribed in the form coinciding with the Weinberg equation [3]:

$$\left(\frac{\vec{k}_\perp^{\,2}+m^2}{x(1-x)}-M^2\right)\Psi(\vec{k}_\perp,x)=$$

$$=-\frac{m^2}{2\pi^3}\int\Psi(\vec{k}_\perp',x')V(\vec{k}_\perp',x',\vec{k}_\perp,x,M^2)\frac{d^2k_\perp'\,dx'}{2x'(1-x')}. \quad (7)$$

As an example let us consider the system consisting of two spinless particles interacting in the ladder approximation by exchange of the massless and spinless particle (Wick-Cutkosky model [4,5]). The corresponding interaction kernal calculated by the light front modification [1a,d] of the graph technique developed in ref. [6] has the form:

$$V(\vec{q}',\vec{q},\vec{n},M^2)=-4\pi\alpha\Big[(\vec{q}'-\vec{q})^2$$

$$-(\vec{n}\vec{q}')(\vec{n}\vec{q})\frac{(\varepsilon(\vec{q}')-\varepsilon(\vec{q}))^2}{\varepsilon(\vec{q}')\,\varepsilon(\vec{q})}$$

$$+\left(\varepsilon^2(\vec{q}')+\varepsilon^2(\vec{q})-\frac{1}{2}M^2\right)\left|\frac{\vec{n}\vec{q}'}{\varepsilon(\vec{q}')}-\frac{\vec{n}\vec{q}}{\varepsilon(\vec{q})}\right|\Big]^{-1}. \quad (8)$$

The solution of eq. (6) with the kernal (8) for the ground state is given by the formula [1d]:

$$\Psi(\vec{q},\vec{n})=\frac{2^3\pi^{1/2}\varkappa^{5/2}}{(\vec{q}^{\,2}+\varkappa^2)^2\left(1+\dfrac{|\vec{n}\vec{q}|}{\varepsilon(\vec{q})}\right)}, \quad (9)$$

where $\varkappa^2=m|\varepsilon_B|$, ε_B is the binding energy and $\varepsilon(\vec{q})=(\vec{q}^{\,2}+m^2)^{1/2}$. At $q \ll m$ the factor $(1+|\vec{n}\vec{q}|/\varepsilon(\vec{q}))^{-1}$ in eq. (9) (arising, as it was explained above, due to inter-influence of internal and center-of-mass motion) turns into 1, and we return to well known Coulomb wave function of the ground state. At $q \sim m$ this factor is important and leads to observable phenomena.

Calculations of the electromagnetic form-factor of this bound system by two methods: (i) through the light front wave function; (ii) through the Bethe-Salpeter function [7]; give the coinciding results. This shows that the light front approach is self-consistent, as well as the Bethe-Salpeter approach, but more convenient in practice for the aims of

nuclear physics. The Bethe-Salpeter function for the deuteron was calculated in ref. [8].

In the case of the states with nonzero angular momentum the vector $\vec{n}$ participates in construction of the angular momentum on the equal ground with the vector $\vec{q}$, since the transformation properties of $\vec{n}$ and $\vec{q}$ under rotations and the Lorentz transformations of coordinate system coincide with each other (in both cases $\vec{q}$ and $\vec{n}$ are rotated only). Therefore the relativistic deuteron wave function on the light front has more rich spin structure than non-relativistic one:

$$\begin{aligned}\Psi(\vec{q},\vec{n}) = \Big(& f_1\sqrt{\tfrac{1}{2}}\,\vec{\sigma} + f_2\,\tfrac{1}{2}\left(3\,\frac{\vec{q}(\vec{q}\vec{\sigma})}{q^2} - \vec{\sigma}\right) \\ & + f_3\,\tfrac{1}{2}\left(3\vec{n}(\vec{n}\vec{\sigma}) - \vec{\sigma}\right) \\ & + f_4\,\frac{1}{2q}\left(3\vec{q}(\vec{n}\vec{\sigma}) + 3\vec{n}(\vec{q}\vec{\sigma}) - 2(\vec{q}\vec{n})\vec{\sigma}\right) \\ & + f_5\, i\sqrt{\tfrac{3}{2}}\,[\vec{q}\times\vec{n}]/q \\ & + f_6\,\frac{\sqrt{3}}{2q}\left[[\vec{q}\times\vec{n}]\times\vec{\sigma}\right]\Big)\sigma_y . \end{aligned} \qquad (10)$$

The functions f_{1-6} depend on q and on $\vec{n}\vec{q}$. Estimations of the functions f_{1-6} in the framework of the one boson exchange model (but not in the potential approximation) were obtained in ref. [1e]. In nonrelativistic region $q \ll m$ the functions f_{3-6} become neglegible, the functions $f_{1,2}$ become independent of $\vec{n}$ and coincide with usual S- and D-waves, and we return to well known nonrelativistic deuteron wave function.

In order to obtain the deuteron wave function in relativistic region it seems resonable as a first step to take a nonrelativistic wave function (for example, calculated in Paris potential) and to replace its argument (nonrelativistic relative momentum) by relativistic relative momentum $\vec{q}$. This allows to take into account correctly the relativistic kinematics and so to guess partially the true wave function at $q \sim m$ (neglecting its $\vec{n}$-dependence). Example considered above shows that this replacement in the nonrelativistic Coulomb

wave function leads to the correct relativistic wave function (with accuracy of its $\vec{n}$-dependence). Of course, this almost exact coincidence is a property of the model. This procedure is already realized in a number of papers devoted to nuclear reactions with high momentum transfer where relativistic effects in deuteron are important (e.g., fragmentation of relativistic deuterons on nuclear taget, electrodisintegration of deuteron and so on, see Lykasov's report at the present workshop).

4. Experimental consequences

What do the qualitative observable phenomena (which can not be imitated by other processes) follow from dependence of the deuteron wave function on variable $\vec{n}$? Let us consider the reaction D(e,e'p)n. For simplicity we start from the impulse approximation, in which the cross section is proportional to the wave function squared: $d\sigma/d\Omega_p d\Omega_e dE' \sim |\psi(q, \cos\theta_{nq})|^2$. Since the deuteron wave function is not changed at the replacement $\vec{q} \to -\vec{q}$ (this follows from the Pauli principle), the wave function squared is symmetric relative to $\theta_{nq} = 90^\circ$. The variables q and θ_{nq} are expressed through the momenta and scattering angles of the particles participating in the reaction (see refs.[1f,g]). One can find such the kinematical conditions for experiment that the value q will be constant, but the angle θ_{nq} will vary. In usual kinematical conditions (i.e., at fixed values of the electron scattering angle θ_e and its final energy E') the cross section versus the proton emission angle θ_p (or, equivalently, versus the neutron momentum p_n) is measured. In order to provide the condition q = constant one should vary θ_p and E' simultaneously according to a certain relation between them (ref.[1f]). For kinematics of CEBAF the relation between θ_p and E' was calculated in ref.[1g]. For $\theta_e = 12^\circ$, 13° and 14° it is shown in fig.1. Corresponding cross section is shown in fig. 2 (the curve 1). The peak at this curve appeares due to the fact that the wave function being symmetric relative to $\theta_{nq} = 90^\circ$ has inevitably the maximum (or minimum) at this value of θ_{nq} and at corresponding value of θ_p. Estimations

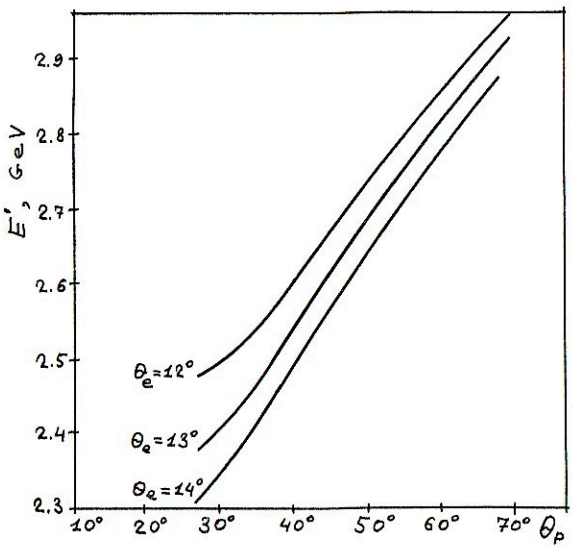

Fig. 1. The relation between the proton emission angle θ_p (relative to the beam direction) and the final electron energy E', ensuring the constant value of the light front wave function's argument q = 0.7 GeV/c. The beam energy is 4 GeV.

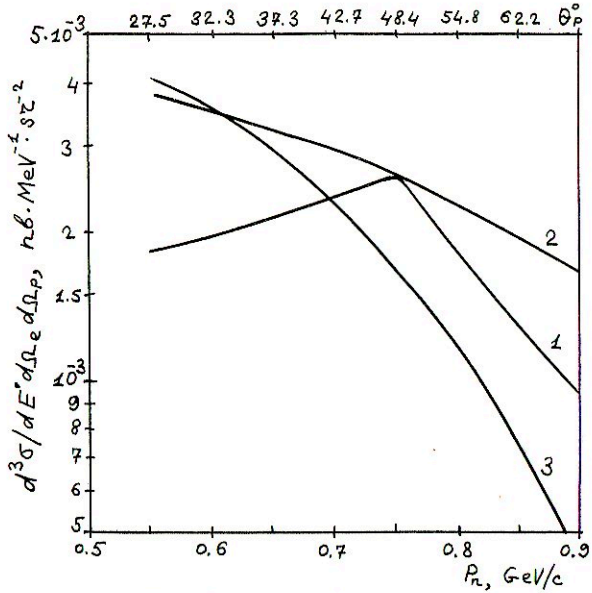

Fig. 2. The D(e,e'p)n reaction cross section in impulse approximation at E = 4 GeV, θ_e = 12°, q = 0.7 GeV/c and at the relation between θ_p and E' shown in fig. 1. The curve 1 is calculated with the light front wave function depending on two variables q and M; the curve 2 is the same but neglecting dependence of the wave function on variable M; the curve 3 is the same with the Gross wave function.

[1e] show that we have namely maximum. The wave function (9) has the same behaviour (at $\theta_{nq} = 90^\circ$ the factor $(1 + |\vec{nq}|/\varepsilon(\vec{q}))^{-1}$ reaches its maximal value equal to 1). The curve 2 in fig.2 shows the cross section calculated by neglecting the wave function dependence on variable $\vec{n}$. In this kinematics the wave function $\psi(q)$ is constant and the corresponding cross section is monotonic one (it depends on θ_p due to eN cross section and kinematical factors).

Another theoretical approach to the problem of the relativistic deuteron wave function is based on the Feynman vertex with the off-shell momentum of one of the particles (the Gross wave function [9]). In this approach the wave function depends only on one variable (neutron momentum spectator p_n in the reaction D(e,e'p)n in impulse approximation) and does not result in the peak in the cross section (curve 3 in fig.2).

Our estimations of influence of the final state interaction carried out in refs.[1f,g] show that the final state interaction though distorts the form of the curves in fig.2, but does not delete the peak. Reliable quantitative calculations in the region under consideration seem to us impossible because of high relative energy in the final nucleon state (of the order of 1 GeV). However the arguments given above indicate that influence of the center-of-mass motion on the internal motion can be dicovered.

References

1) V.A.Karmanov. ZhETF, a) 71 (1976) 399; b) 75 (1978) 1187; c)76 (1979) 1884. Nucl. Phys. d) B166 (1980) 378; e) A362 (1981) 331; f) A453 (1986) 707; g) Lebedev Phys. Inst. preprint No.74 (1989).
2) V.A.Karmanov. Fiz. EChAYa, 19 (1988) 525 [Transl.: Sov. J. Particles and Nuclei, 19 (1988) 228.
3) S.Weinberg. Phys. Rev. 150 (1966) 1313.
4) G.C.Wick. Phys. Rev., 96 (1954) 1124.
5) R.E.Cutcosky. Phys. Rev. 96 (1954) 1135.
6) V.G.Kadyshevsky. ZhETF, 46 (1964) 654, 872; Nucl. Phys. 6 (1968) 125.
7) E.E.Salpeter, H.A.Bethe. Phys. Rev. 84 (1951) 1232.
8) M.I.Zuilhot, I.A.Tjon. Phys. Rev. C22 (1980) 2369.
9) W.Buck, F.Gross. Phys. Rev. D20 (1979) 2361.

RELATIVISTIC DEUTERON AND CHARACTERISTICS OF PROCESSES WITH ITS PARTICIPATION

M.V.Tokarev
Physics Department, Tashkent State University,
Tashkent,700095, Russia

1. INTRODUCTION

The investigation of hardron-deuteron and lepton-deuteron interactions at high energies yields independent information on the relativistic deuteron structure and its constituents.

Recent experimental data on momentum dependence of cross section for the D-p fragmentation processes are given in Ref.[1-3] and on structure function $B(Q^2)$ for elastic e-D scattering in Ref.[4]. This data is widely used both for testing available deuteron models and for a future development of the theory of the relativistic nuclear systems.

However the analysis of the unpolarized characteristics, for example, given in Refs.[1-4], of the considered processes is not sufficient to conclude unambiguously on the advantage of any relativistic approach to be used to describe both the deuteron itself and the processes involving it and does not allow us to consider unambiguously the relative contribution of varion mechanisms of the processes (impulse approximation (IA), pion enhancement, final state interaction, meson exchange current, etc.).

The measurement of polarization characteristics - tensor analyzing power T_{20} and vector polarization transfer coefficient of the D-p fragmentation process [3,5,6] and tensor analyzing power T_{20} [7] of the elastic e-D scattering also allows us to analyze these processes more correctly and to conclude that together with the scheme of the deuteron wave function relativisation the relativistic description of the processes themselves is of importance as well.

In the present paper some polarization and unpolarization characteristics of $p+D \to (h,p)+X$, $p+D \to h+X$, $e+D \to e+D$ processes are considered in the framework of the covariant formalism in the light cone variables on the basis of the relativistic deuteron wave function (RDWF) with one of the nucleons on mass-shell [8-10].

2. RELATIVISTIC DEUTERON WAVE FUNCTION

We use the relativistic description of the deuteron proposed in Refs. [8-10]. The RDWF $\Psi_\alpha(x,k_\perp)$ in the light cone variables $(x,k_\perp)$ is defined by the DNN vertex function Γ_α with one of the nucleons and the deuteron on mass shell

$$\Gamma_\alpha = k_\alpha \cdot [a_1 + a_2 \cdot (m+\hat{k})] + \gamma_\alpha \cdot [a_3 + a_4 \cdot (m+\hat{k})] . \qquad (1)$$

Function Γ_α is parameterized by four scalar functions $a_i(i=1-4)$, depending on the variable - the nucleon virtuality k^2. The latter one is a function of x and $k_\perp$

$$k^2 = x \cdot M_D^2 - (x \cdot m^2 + k_\perp^2)/(1-x) . \qquad (2)$$

In Ref.[11] the relativistic equation for Ψ_α was constructed. The explicit form of the RDWF and its parameterization was determined in Refs.[8-10]. While constructing the RDWF we used some assumptions on its negative components in nonrelativistic region, a correct asymptotic behaviour in the nonrelativistic limit, coincided with a known deuteron wave function (Paris [12], M.Gourdin [13], Mc Gee [14]) and the description of static deuteron momenta.

The constructed RDWF is used to describe electromagnetic deuteron form-factors, structure functions of elastic and deep-inelastic e-D scattering. In Ref.[15] the RDWF was used to describe the cross section of the D(e,e'p)n exclusive deuteron electrodisintegration process.

The obtained results show that the developed cavariant approach in the light cone variables and the derivation of the RDWF may be used for the analysis of the great number of processes with the deuteron participation.

3. DOUBLE INCLUSIVE p+D → (h,p)+X PROCESS

The comparison of experimental data [3,5,6] with theoretical calculations, for example,in Refs.[16-18], shows that tensor analysing power T_{20} and vector polarization transfer coefficient K of the D+A → p+X process cannot be described by the spectator mechanism

only, though its contribution is considerable, therefore to extract direct information on the RDWF structure in the region of the dynamic D-wave enhancement is impossible. The latter conclusion is justified in Ref.[18] by the fact that the region of minimal T_{20} is filled by the contribution of pion enhancement mechanism. That is why the experiments on measurements of T_{20} and K of the double inclusive p+D → (h,p)+X process with registrating a fast particle ($h=\pi^{\pm},K^{\pm},\bar{p}$) scattered within a large angle ($\theta_h>90^{\circ}$) and back scattered proton-spectator may be in our opinion more informative. In this case the contribution of the pion enhancement mechanism is kinematically suppressed and one may expect to obtain direct information on the momentum distribution of nucleons in the deuteron and polarization RDWF structure in the region of dynamic D-wave enhancement.

The amplitude of the process considered in the IA is described by a diagram (Fig.1).

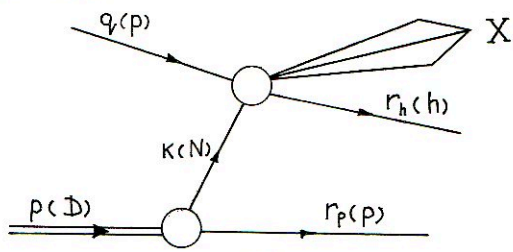

Fig. 1

Here q, p, k, r^h, r^p are momenta of the incident proton (p), deuteron (D) active nucleon (N), registered particle (h), and proton-spectator (p), respectively. The top block describes the amplitude of the p+N → h+X process, the bottom block describes the DNN vertex Γ_α with one nucleon on mass-shell. Under this approximation tensor analyzing power T_{20} of the p+D → (h,p)+X reaction in the framework of the covariant formalism in the light-cone variables with the RDWF [12-14] is defined by the formula

$$T_{20}= -\frac{\sqrt{2}}{3}\cdot t_D^{hp}/\rho_D^{hp}, \qquad (3)$$

where $t_D^{hp} = \Phi^{zz}(x,k_\perp)\cdot S_{zz}\cdot\rho_N^h(x^h/x,\ r_\perp^h - x^h/x\cdot k_\perp)$

$$\rho_D^{hp} = \Phi^{\alpha\beta}(x,k_\perp)\cdot\rho_{\alpha\beta}\cdot\rho_N^h(x^h/x,\ r_\perp^h - x^h/x\cdot k_\perp)\ .$$

Here $x^h = r_+^h/p_+$, $x = k_+/p_+$, $x^p = 1 - x$, $r_\perp^h$, $k_\perp$, $r_\perp^p$ are the fraction of the deuteron momentum and transverse momentum carried away by the particle h , active nucleon N, proton-spectator p, respectively; $S_{\alpha\beta}$ is a quadrupole part of the polarization deuteron density matrix ($S_{\alpha\beta} = S_{\beta\alpha}$, $S_{\alpha\alpha} = 0$, $p_\alpha\cdot S^{\alpha\beta} = 0$);

$\rho_{\alpha\beta} = -(g_{\alpha\beta} - p_\alpha p_\beta/M_D^2)/3$ is an unpolarized part of the polarization deuteron density matrix; M_D is a deuteron mass; ρ_N^h is the inclusive cross-section for the p+D → h+X process.

Tensor $\Phi_{\alpha\beta}$ is expressed via a vertex function Γ_α as follows:

$$\Phi_{\alpha\beta} = Sp\ \{(m+\hat{k})^{-1}\cdot\bar{\Gamma}_\alpha(k)\cdot(m+\hat{r}_p)\cdot\Gamma_\beta(k)\cdot(m+\hat{k})^{-1}\cdot(m+\hat{q})\}\ . \qquad (4)$$

Fig.2 shows the results of our calculation of the dependence of T_{20} of the process $p+\vec{D} \to (\pi^+,p)+X$ on the momentum of backward scattered proton-spectator with the registration of a fast π^+ - meson ($r_{\pi^+} = 0.2$ GeV/c) at the angle of $\theta_{\pi^+} = 90^\circ$. Curves 1,2,3 and 4 denote calculations using the RDWF [10] with the core for the momenta of the incident proton q = 4.55, 8.9, 50.,1000. (GeV/c), respectively.

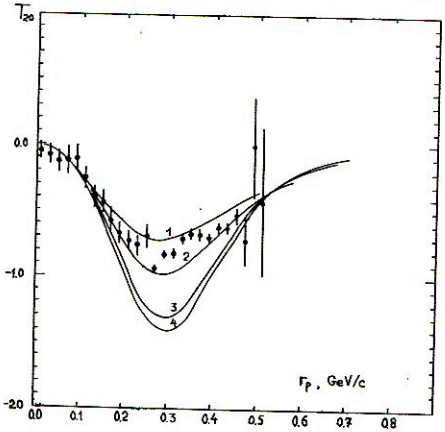

Fig.2. Tensor analyzing power T_{20} of the $p+\vec{D}\to(\pi^+,p)+X$ process in the relativistic impulse approximation.
Experimental data from[5].

Fig.2 shows a noticeable dependence of T_{20} on the incident proton momentum; with the increase of q the value of T_{20} tending to the asymptotic behavior. This is consistent with the results from Ref.[16] for $s = (p+q)^2 \to \infty$ with taking no account of mass terms resulting from (m+q) in the formula (2).

Note, that the formula (1) under the IA for T_{20} coincides with T_{20} of the $p+\vec{D} \to p+X$ process. Therefore, it is natural to compare results of our calculations with experimental data on T_{20} [3,5].

Fig.2 shows experimental points [5] for comparison.

Good agreement between the theoretical results and experimental data is observed.

Experimental verification of the predicted momentum dependence of T_{20} in the region of the dynamic D-wave enhancement is of interest. This may lead to the reconsideration of the role of the pion enhancement mechanism in this region.

Another characteristic that is able to give independent information on the polarization structure of the relativistic deuteron is the vector polarization transfer coefficient - K. It defines the value of polarization transfer from a vector-polarized deuteron to a registered polarized proton.

The K in the IA of the $p+\vec{D} \to (h,\vec{p})+X$ process in the framework of the covariant formalism in the light-cone variables [8-10] is defined as follows:

$$K = V_D^{hp} / \rho_D^{hp}, \qquad (5)$$

where $V_D^{hp} = \Phi^V_{\alpha\beta}(x,k_\perp) \cdot \rho_V^{\alpha\beta} \cdot \rho_N^h(x^h/x\,,\ r_\perp^h - x^h/x \cdot k_\perp)$.

Here $\rho_{\alpha\beta} = i \cdot \varepsilon_{\alpha\beta\mu\nu} \cdot s^\mu \cdot p^\nu / 2 \cdot M_D$ is the vector part of the polarization deuteron density matrix; s is four vector of the deuteron spin ($s_\alpha^2 = -1$, $p_\alpha \cdot s^\alpha = 0$).

Tensor $\Phi^V_{\alpha\beta}$ as well as tensor $\Phi_{\alpha\beta}$ in the (2) is expressed via the vertex function Γ_α with one nucleon on the mass-shell

$$\Phi^V_{\alpha\beta} = Sp\ ((m+\hat{k})^{-1} \cdot \Gamma_\alpha(k) \cdot \gamma_5 \cdot \hat{s}_p \cdot (m+\hat{r}_p) \cdot \Gamma_\beta(k) \cdot (m+\hat{k})^{-1} \cdot (m+\hat{q})) \qquad (6)$$

The magnitude s_p is the four vector of the registered proton-spectator spin.

Fig.3(a) shows the results of our calculation of K for the $p+\vec{D} \to (\pi^+,\vec{p})+X$ process vs the momentum r_p of the backward scattered proton-spectator ($\theta_p = 180^\circ$) and the momentum r_{π^+} of the fast π^+- meson, scattered at the angle of $\theta_{\pi^+} = 90^\circ$. Curves 1,2,3 and 4 are calculations using the RDWF [10] with the core for momenta of the incident proton q = 4.55, 8.9, 50.,1000. (GeV/c), respectively. The angle $\theta_{\vec{q}\vec{s}_D}$ between the incident proton momentum $\vec{q}$ and the vector of the deuteron spin $\vec{s}$ is 90°. Dashed lines 1,2,3,4 are calculations using the RDWF [8] with no core.Fig.3(a) shows that the qualitative effect - the absence of zero in the S-wave of the RDWF is manifested in the displacement of K's zero into the region of $r_p > 0.3$ (GeV/c).

The dependence of K on the incident proton momentum q both for r_p more and less 0.3 (GeV/c) is clearly observed. With increasing q the curve of K tends to the asymptotic behavior. This agrees with the result [17] for K obtained under the IA for the $\vec{D} + {}^{12}C \to p+X$ process in the $s = (p+q)^2 \to \infty$ limit. Fig.3(a) also shows experimental data [6] of K for this process.

The experimental points are seen to lie systematically upper than theoretical curves even for q =1000. (GeV/c).

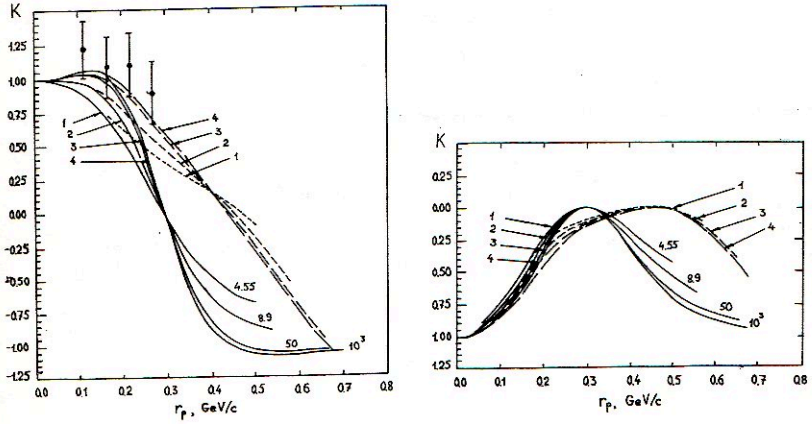

Fig.3. Vector polarization transfer coefficient K of the $p+\vec{D} \to (h,\vec{p})+X$ process in the relativistic impulse approximation: (a) $\theta_{\vec{q}\vec{s}_D} = 90^\circ$, (b) $\theta_{\vec{q}\vec{s}_D} = 0^\circ$. Experimental data from [6].

Fig.3(b) shows the calculated results of K for the case of $\theta_{\vec{q}\vec{p}_D} = 0^\circ$. Notation is the same as in Fig.3(a). With increasing q the flexure in the curve of K both for r_p less and more 0.3 (GeV/c) is observed and K = 0 for r_p = 0.3 (GeV/c). The calculation using the RDWF [18] without core, shows the displacement of the maximum of the dependence of K into the region of r_p > 0.3 (GeV/c).

4. SINGLE INCLUSIVE p+D → h+X PROCESS

It is known that the production of the cumulative particle h($\pi^\pm$, $K^\pm$, $\bar{p}$) for the p+D → h+X process are mainly due to the direct mechanism, though some contribution comes also from rescattering. The direct mechanism is associated with the cumulative production of a particle h on one of the nucleon nucleus having a large Fermi momentum. The contribution of this mechanism is due to the high momentum component of the RDWF. Another mechanism involves both nucleons in the a cumulative particle production and is independent of the existence of such a component.

In Refs.[16,19] in the framework of the approach [8-10] the experimental data [20] on inclusive cross section of cumulative π^+ - meson production was described by the direct mechanism. So it is natural to consider this mechanism in the same approach for the calculation of the tensor analyzing power T_{20} of the p+$\vec{D}$ → h+X process, as well.

Under this approximation T_{20} of the p+$\vec{D}$ → h+X process is defined by formula

$$T_{20} = -\frac{\sqrt{2}}{3}\cdot t_D^h(x^h, r_\perp^h) \,/\, \rho_D^h(x^h, r_\perp^h), \qquad (7)$$

where $$t_D^h = \int_{x^h}^1 \frac{dx}{1-x} \int d^2k_\perp \cdot \Phi^{zz}(x,k_\perp)\cdot S_{zz}\cdot \rho_N^h(x^h/x,\ r_\perp^h - x^h/x\cdot k_\perp)$$

$$\rho_D^h = \int_{x^h}^1 \frac{dx}{1-x} \int d^2k_\perp \cdot \Phi^{\alpha\beta}(x,k_\perp)\cdot \rho_{\alpha\beta}\cdot \rho_N^h(x^h/x,\ r_\perp^h - x^h/x\cdot k_\perp)\cdot$$

Here notation is the same as in formula (1).

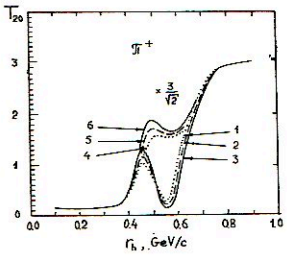

a)

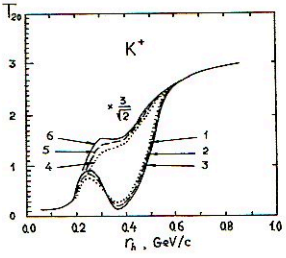

b)

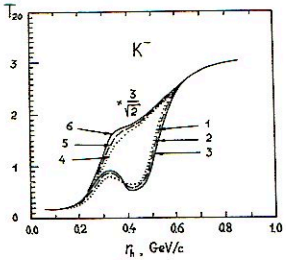

c)

Fig. 4. Tensor analyzing power T_{20} of the $p+\vec{D} \to h+X$ process in the relativistic impulse approximation: a) $h = \pi^+$; b) $h = K^+$; c) $h = K^-$.

The calculation results of the momentum dependence T_{20} of the $p+\vec{D} \to h+X$ process for the angle $\theta_h = 180^o$ and values of momenta of the projectile proton q = 8.9, 20., 500. (GeV/c) are shown in Fig.4. Parameterizations of the inclusive cross section $\rho_p^h(x,k_\perp)$ for the production of h (π^+, $K^\pm$) on the proton were taken from Ref.[21] and it was assumed that $\rho_N^h = \rho_p^h$. The last assumption does not much affect the qualitative behavior of ρ_D^h but it is more sensitive to the behavior of T_{20} near $x \simeq 1$. The tensor analyzing power T_{20} is independent of the absolute cross section.

Fig. 4(a,b,c) demonstrates T_{20} of the $p+\vec{D} \to h+X$ process as a function of the momentum r_h. We calculated it using the RDWF [10] with core (curves 1,2,3) and the RDWF[8] without core (curves 4,5,6) for momenta of the incident proton q =8.9, 20., 500.(GeV/c),respectively. It is seen from Fig. 4(a,b,c) that the dependence of the T_{20} for momentum q is weak. For all reactions there are regions where we can see different behaviors of T_{20} depending on the RDWF structure in the core region. These very regions are more important for the experimental investigation of the deuteron structure in the region of the dynamic D-wave enhancement.

5. ELASTIC e-D SCATTERING

Experimental data on the structure function $B(Q^2)$ [4] and the tensor analyzing power T_{20} [7,22,23] in elastic electron-deuteron scattering stimulates the development of both the deuteron theory itself and reaction mechanisms (meson exchange current, etc.)

Here the results of calculation of $B(Q^2)$ and $T_{20}(Q)$ in the framework of the approach put forward in Refs.[8-10] on the basis of the RDWF [10] in the IA will be presented.

It is known that the cross section for elastic e-D scattering for unpolarized particles in one photon exchange approximation is defined by two structure functions $A(Q^2)$ and $B(Q^2)$

$$A(Q^2) = G_e^2(Q^2) + \frac{2}{3}\cdot\eta\cdot G_m^2(Q^2) + \frac{8}{9}\cdot\eta^2\cdot G_Q^2(Q^2) \qquad (8)$$

$$B(Q^2) = \frac{4}{3}\cdot\eta\cdot(1+\eta)\cdot G_m^2(Q^2), \qquad \eta = Q^2/4\cdot M_D^2 . \qquad (9)$$

They are expressed via the electric - G_e, magnetic - G_m and quadrupole - G_Q deuteron form-factors.

Tensor analyzing power T_{20} of the elastic e-D scattering for tensor polarized deuteron was measured [7,22,23]. Under this approximation T_{20} is also expressed by electromagnetic deuteron form-factors.

$$T_{20} = -\frac{\eta}{3\sqrt{2}}\,\frac{8\cdot G_e G_Q + 8\cdot\eta\cdot G_Q^2/3 + (1+2(1+\eta)\,tg^2(\theta/2))\cdot G_m^2}{A + B\cdot tg^2(\theta/2)} . \qquad (10)$$

The calculated results of $B(Q^2)$ and $T_{20}(Q)$ in the relativistic IA using the RDWF [10] are presented in Fig. 5(a,b). We also investigate the sensitivity of $B(Q^2)$ and $T_{20}(Q)$ to different electric neutron form-factor $F_e^n(Q^2)$. The follow parameterization is used to described this form-factor:

$$F_e^n(Q^2) = -F_m^n(Q^2)\,\frac{\tau}{1+p\tau} , \qquad (11)$$

where $\tau = Q^2/4\cdot m^2$, p - a numerical parameter. For another nucleon form-factors dipole formulas and the scaling law are used.

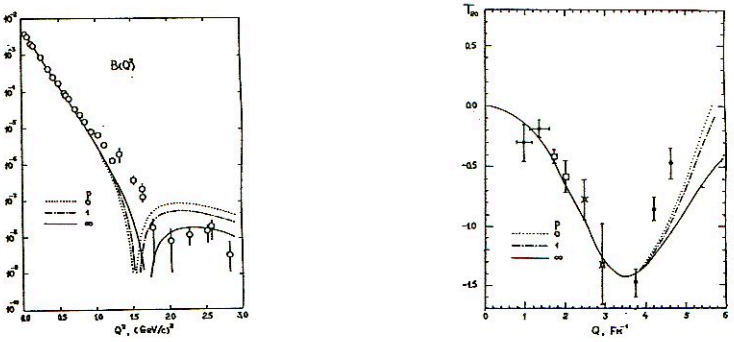

a) b)

Fig.5. Structure function $B(Q^2)$ (a) and tensor analyzing power $T_{20}(Q)$ (b) of the elastic e - D scattering for the RDWF [10] in the IA for various devices of $F_e^n(Q^2)$.
The data is taken from Ref.[4] (a) and Ref.[7,22,23] (b).

From Fig. 5(a) we can see that the agreement of the calculated curves with the experimental data for momentum transfer in the region $Q^2 < 1.0$ $(GeV/c)^2$ is good. For momentum transfer $Q^2 > 1.0$ $(GeV/c)^2$ the theoretical curves lie lower than the experimental points. With increasing parameter p both the shift of the second dip and the decrease of the second maximum of $B(Q^2)$ to higher momentum transfer are observed. The experimental data has a second dip at $Q^2 \simeq 1.9$ $(GeV/c)^2$ and that lies on the right from the theoretical dips.

Fig. 5(b) shows the calculated results of $T_{20}(Q)$ vs Q for the different parameter p. For $Q < 4.0$ (Fm^{-1}) the agreement with the existing experiments for all curves is good. For the higher momentum $Q > 4.0$ (Fm^{-1}) a discrepancy between theoretical curves $(p=0,1,\infty)$ becomes larger and they lie lower than the experimental points.

Thus the obtained results for $B(Q^2)$ and $T_{20}(Q)$ show that even different realistic parameterizations of electric neutron form-factor in the region $Q > 4.0$ (Fm^{-1}) does not allow us to described both characteristics simultaneously. However good qualitative agreement with experimental data is found.

6. CONCLUSION

The presented results on characteristic of processes involving the relativistic deuteron and their comparison with existing experimental data as well as predictions for some processes indicate that the research of qualitative effects predicted by the deuteron theory is of importance. In our opinion such effects may be at most manifested in the region of the dynamic D-wave enhancement. Therefore the calculations with different RDWFs which are distinguished by the deuteron structure in the core region are of great interest. They will allow us to understand more exactly the role of different mechanisms in the description of these processes as well as a test of developed relativistic approaches.

REFERENCES

[1]. Ableev V.G. et al.- Nucl. Phys., 1983, v.A393, p.491.
Zaporozhets S.A. et al.- In: Proc. VIII Inter. Seminar on High Energy Physics Problems. JINR, D1,2-86-668,Dubna, 1986, v.1, p.341.

[2]. Anderson L. et al.- Phys. Rev., 1983, v.28C, p.1224.

[3]. Perdrisat C.F. et al.- Phys. Rev. Lett., 1987, v.59, p.2840.

[4]. Auffret S. et al.- Phys. Rev. Lett., 1985, v.54, p.649.
Arnold R.G. et al.- Phys. Rev. Lett., 1987, v.58, p.1723.

[5]. Ableev V.G. et al.- Pisma Zh. Exsp. Theor. Fiz., 1988, v.47, p.558.
Ableev V.G. et al.- In: JINR Rapid Communication, N4[43]-90, Dubna, 1990, p.5.

[6]. Ableev V.G. et al.- In: Proc. VII Intern. Conf. Polar. Phenomena in Nucl. Phys., Paris 90. Abstract of Contr. Papers, 40F.

[7]. Garson M.- In: Proc. VII Intern. Conf. on Polariz. Phen. in Nucl. Phys., Paris., 1990.

[8]. Braun M.A., Tokarev M.V.- Vestnic LGU, 1983, v.22, p.6.
[9]. Braun M.A.- Yad.Fiz., 1985, v.42, p.818.
[10]. Braun M.A., Tokarev M.V.- Vestnic LGU, 1986, v.4, p.7.
[11]. Braun M.A.- Yad.Fiz., 1980, v.32, p.1283.
[12]. Lacombe M. et al.- Phys.Lett., 1981, v.101B, p.139.
[13]. Gourdin M. et al.- Nuovo Cimento, 1965, v.37, p.524.
[14]. Mc Gee I.J.- Phys.Rev., 1966, v.151, p.772.
[15]. Tokarev M.V.- Few Body Systems, 1988, v.4, p.133.
[16]. Braun M.A., Tokarev M.V.- In: Proc. III Intern. Symposium "Nucleon-nucleon and hardron-nucleus interactions at the intermediate energies", Leningrad, LINR, 1986, p.311.
[17]. Braun M.A., Tokarev M.V.- In: Proc. III Intern. Symposium "Pion-nucleon and nucleon-nucleon interactions", Leningrad, LINR, 1989, p.398.
[18]. Dolidze M.G., Lykasov G.I.- Z.Phys.A.- Atomic Nuclei, 1990, v.336, p.339.
[19]. Tokarev M.V.- Ph.D. Thesis, Tashkent State Univ., 1987, 172p.
[20]. Baldin A.M. et al.- Preprint JINR E1-82-472, Dubna, 1982, 28p.
[21]. Taylor E.E. et al.- Phys. Rev., 1976, v.14D, p.1217.
[22]. Schulze M.E. et al.- Phys. Rev. Lett., 1984, v.52, p.597.
[23]. Vesnovsky D.K. et al.- Preprint INP 86-75, Novosibirsk, 1986, 17 p.

RELATIVISTIC MODELS AND DEUTERON

V.E.Troitsky, N.P.Yudin

Nuclear Physics Institute,
Moscow State University,
Moscow 119 899, Russia

1. We shall discuss the problem of relativistic composite systems. The relativistic aspects of composite systems are of principal importance in both cases - when the momentum distribution of the constituents is analyzed in the rest frame in the range of relativistic values of momentum and in the frame of reference where the composite particle is moving fastly.

The problem of the description of relativistic composite systems became even more important in connection with the developement of quark physics [1] when the relativistic features of the quarks are of great importance and, at the same time, the quark wave function cannot be obtained because to-day it is impossible to take into account the nonperturbative effects. The arising problems can be illustrated by the importance of analyzing the hadrons structure in the reference frame where the hadron momentum is infinite [2] (unnatural from the point of view of common sence). In this connection the well-known ancient Dirac paper [3] attracts the attention once again. In the paper [3] different dynamics were considered - the different methods of description of the physical system evolution; shortly, after there was established [4] that the standard field theory in the reference frame with infinite momentum and the theory with field quantization on the light front hyperplane

$$t + x^3 = 0$$

are equivalent.

During the last decade the importance of having the well developed methods of description of relativistic composite systems has increased. The cause is twofold. First, now one can investigate the re-

lativistic part of the nucleons momenta distribution in a nuclei, e.g., can measure the deuteron form factors at large Q^2 /5/($Q^2 = -q^2$, q is the momentum transfer from the electron to the deuteron). Second, the number of experimental data on nuclear reactions caused by relativistic deuterons and α-particles/6/ are accumulated and are waiting for correct analysis.

In the relativistic theory of composite systems one can recognize two main different approaches. The first one is based on the summation of a class of perturbation theory diagrams and the solution of the equations of Bethe-Salpeter type and different dispersion approaches/7/. The other method is of phenomenological kind and is based on the immediate realization of the Poincaré group (PG) algebra or, in other words, the relativistic invariance condition in the few particles Hilbert space. This second method is usually named the direct interactions theory or relativistic quantum mechanics. Because of the phenomenological character of this approach one is not guided by the fundamental quantum field theory (standard model). This causes automatically the number of principal ambiguities to be resolved only through the comparison of model calculations with the data. To illustrate the problem one can consider the question whether the relativistic nucleon system wave function depends on the total momentum or not. We shall see later that both approaches are realized. In this report we shall restrict ourselves by the two-particle relativistic mechanics keeping in mind the relativistic deuteron. The report contains, first, the general discussion of the problem of relativistic invariant description of nucleon systems, of the methods of interaction inclusion and, cosequently, of different dynamics. In this part we use mainly the known results. The second part contains some original results.

2. To construct the relativistic model with a finite number of degrees of freedom one usually acts as follows. First of all the basis of free relativistic states for one, two, etc., particles is constructed. Then the interaction is added in some way. Before using this standard method we will try to include intuitively the interaction in the system of relativistic particles utilising our non-relativistic quantum mechanical experience.

As is well known, in the case of non-relativistic quantum mechanics the separation of variables takes place. In the case of two particles this means

$$\hat{H}_0 = \frac{\vec{p}_1^{\,2}}{2m_1} + \frac{\vec{p}_2^{\,2}}{2m_2} = \frac{\vec{\mathcal{P}}^{\,2}}{2(m_1+m_2)} + \frac{\vec{k}^{\,2}}{2\mu}, \qquad (1)$$

where

$$\vec{\mathcal{P}} = \vec{p}_1 + \vec{p}_2 \;; \quad \vec{k} = \frac{m_2\vec{p}_1 - m_1\vec{p}_2}{m_1+m_2} \;; \quad \mu = \frac{m_1 m_2}{m_1+m_2} .$$

The interaction is usually included by the following replacement

$$\frac{\vec{k}^{\,2}}{2\mu} = \frac{\vec{k}^{\,2}}{2m_1} + \frac{\vec{k}^{\,2}}{2m_2} \longrightarrow \frac{\vec{k}^{\,2}}{2\mu} + \hat{V}, \qquad (2)$$

- one adds the interaction to the particles kinetic energy in the center-of-mass reference frame.

It seems obvious that this experience "for pedestrian" gives the method for including the interaction in the case of relativistic system:

$$\frac{\vec{k}^{\,2}}{2\mu} \longrightarrow \sqrt{m_1^2 + \vec{k}^{\,2}} + \sqrt{m_2^2 + \vec{k}^{\,2}} \longrightarrow$$
$$\longrightarrow \sqrt{m_1^2 + \vec{k}^{\,2}} + \sqrt{m_2^2 + \vec{k}^{\,2}} + \hat{V} . \qquad (3)$$

This method occurs to be correct as we will see later. However the question arises (unimportant in the non-relativistic quantum mechanics case) what form this interaction has in the other reference frame or, in other words, how the Lorentz boost changes the interaction:

$$U(\Lambda)\left[\sqrt{m_1^2 + \vec{k}^{\,2}} + \sqrt{m_2^2 + \vec{k}^{\,2}} + V\right] U^{-1}(\Lambda) =$$
$$= \sqrt{M_0^2(k) + \vec{\mathcal{P}}^{\,2}} + ? \qquad (4)$$

Here $M_0^2(k) = \left[\sqrt{m_1^2 + \vec{k}^{\,2}} + \sqrt{m_2^2 + \vec{k}^{\,2}}\right]^2$ is the square of the mass operator; $\vec{\mathcal{P}}$, the momentum of the system after boost

$$\mathcal{P}'^{\mu} = \Lambda(M_0, 0, 0, 0) = \left(\sqrt{M_0^2 + \vec{\mathcal{P}}^{\,2}}, \vec{\mathcal{P}}\right) \qquad (5)$$

and $U(\Lambda)$ is the unitary transformation of wave functions (state vectors). One can see from eq.(4) that the common sense does not work while formulating the Lorentz invariant model, so that one needs the tutorial help of the relativistic theory.

3. By convention a quantum theory is relativistic invariant (RI) if it is possible to costruct the unitary representation of PG from the state vectors $|\Psi\rangle$ [8]. Let us use for the elements of this representation the usual notation (a', Λ), where $a' = (t, \vec{x})$ is an arbitrary four-vector of space-time shift and Λ is general

Lorentz transformation with $\det \Lambda = 1$. Let us note by $U(a,\Lambda)$ the unitary operator corresponding to the PG element (a,Λ) in the state vectors $|\Psi\rangle$ space. Now the RI means that the transformation

$$|\Psi\rangle \xrightarrow{(a,\Lambda)} |\Psi'\rangle = U(a,\Lambda)|\Psi\rangle \tag{6}$$

leaves the scalar products

$$\langle\Psi_2|\Psi_1\rangle \xrightarrow{(a,\Lambda)} \langle\Psi_2'|\Psi_1'\rangle = \langle\Psi_2|U^{+}(a,\Lambda)U(a,\Lambda)|\Psi_1\rangle = \tag{7}$$

$$= \langle\Psi_2|\Psi_1\rangle$$

unchanged. We can formulate the RI property in differential form. The problem of the PG representation obtaining is equivalent to construction of its generators $M^{\mu\nu}$, P^{μ} in terms of the given quantum system dynamical variables.

It is well known[8] that the generators $P^{\mu}, M^{\mu\nu}$ are defined by the equation

$$U(\delta a, 1+\delta\Lambda) = 1 - \frac{i}{2} M^{\mu\nu}\delta\omega_{\mu\nu} + i P^{\mu}\delta a_{\mu} \tag{8}$$

and satisfy the system of 45 commutation relations:

$$[M^{\mu\nu}, P^{\sigma}] = -i\,(g^{\mu\sigma}P^{\nu} - g^{\nu\sigma}P^{\mu}), \tag{9a}$$

$$[M^{\mu\nu}, M^{\sigma\rho}] = -i\,(g^{\mu\sigma}M^{\nu\rho} - g^{\nu\sigma}M^{\mu\rho}) - i\,(\sigma \leftrightarrow \rho). \tag{9b}$$

Here $\delta\omega^{\mu\nu}$, δa_{μ} are infinitesimal transformations (Lorentz ones and rotations) in the $\mu\nu$ plane and the space-time translation.

To construct a RI theory means to obtain the operators $M^{\mu\nu}$, P^{μ} (ten operators) which act in the state vector space and obey the commutation relations (9).

4. To advance in the construction of the two interacting particles dynamics let us describe briefly the free particle states[9]. The state vectors of the free structureless particles are transforming according to the PG irreducible representations. The PG irreducible representations are given by two invariants. Usually one chooses for them the mass M and the Pauli-Lubanski vector square[10]:

$$M^2 = P^{\mu}P_{\mu} = H^2 - \vec{P}^2, \qquad H = P_0, \tag{10}$$

$$W^{\mu} = -\frac{1}{2M}\,\varepsilon^{\mu\nu\sigma\rho}\,M_{\nu\sigma}\,P_{\rho} \qquad (11)$$

($\varepsilon^{\mu\nu\sigma\rho}$ is the completely antisymmetric tensor in four dimensional spacetime with $\varepsilon^{0123} = 1$). The irreducible representation vectors are labeled by four quantum numbers. Usually one chooses three projections of the momentum and the spin projection μ on the quantization axis in the rest reference frame. Thus, for the free particle state vectors $|\Psi\rangle$ we have:

$$|\Psi\rangle = |\vec{p}\,\mu\rangle . \qquad (12)$$

However given $\vec{p}$ and μ do not determine the state vector: one must fix"the path" following which the momentum is obtained from its rest reference frame value. Here we approach the problem of different dynamics on the free particles level. We shall restrict ourselves by two of them: instant form dynamics and light front dynamics. The general discussion will be given in p.6. The so-called canonical basis $|\vec{p}\,\mu\rangle_c$ (the instant form dynamics) is obtained with the use of Lorentz transformation $L_c^{-1}(p)$ without rotation:

$$|\vec{p}\,\mu\rangle_c = U\left(L_c^{-1}(p)\right)|0\,\mu\rangle, \qquad (13)$$

where

$$L_c(p)\cdot p^{\mu} = \tilde{p}^{\mu} = (M, 0, 0, 0) \qquad (14)$$

and $U(L_c(p))$ is the PG unitary representation matrix defined before. The canonical operator of spin is defined as follows

$$\vec{S}_c(p) = L_c(p)\,\vec{W}, \qquad (15)$$

where $\vec{W}$ is the space part of Pauli-Lubanski vector (11). The canonical spin operator acts on the state vectors in the standard way:

$$\vec{S}_c(p)\,|\vec{p}\,\mu\rangle_c = \sum_{\mu'} \langle\mu'|\vec{S}|\mu\rangle\,|\vec{p}\,\mu'\rangle_c , \qquad (16)$$

$\langle\mu'|\vec{S}|\mu\rangle$ are the non-relativistic spin operator matrix elements. The important feature of canonical basis is the Wigner (spin) rotation associated with the Lorentz transformation Λ acting on the vector $|\vec{p}\,\mu\rangle_c$:

$$U(\Lambda)\,|\vec{p}\,\mu\rangle_c = \sum |\Lambda p\,\mu'\rangle\, D^{s}_{\mu'\mu}(R^{W}), \qquad (17)$$

with

$$R^{W} = L_c^{-1}(p')\,\Lambda\,L_c(p), \qquad p' = \Lambda p . \qquad (18)$$

The explicit form of PG generators can be obtained if one considers the infinitesimal transformations. One has:

$$J^i = \frac{1}{2}\varepsilon^{ikl} M^{kl} = -i\left[\vec{P}\frac{\partial}{\partial \vec{P}}\right]_i + S_c^i(P),$$

$$N^i = M^{oi} = i P_o \frac{\partial}{\partial P^i} - \frac{[\vec{P}\,\vec{S}_c]_i}{P_o + M}, \qquad (19)$$

$$P_o = \sqrt{M^2 + \vec{P}^2}$$

The light front basis $|\vec{P}\,\mu\rangle_F$ /11-13/ is defined as follows. Among the Lorentz transformations let us choose the subgroup Λ_f leaving the light front surface

$$t + x^3 = 0 \qquad (20)$$

invariant. Let us introduce the single Lorentz boost $L_f^{-1}(P)$ belonging to this subgroup such that

$$L_f(P)\,P^\mu = \tilde{P}^\mu = (M, 0, 0, 0). \qquad (21)$$

Now the light front basis is given by

$$|\vec{P}\,\mu\rangle_F = U\left(L_f^{-1}(P)\right)|0\mu\rangle, \qquad (22)$$

$$\vec{S}_F(P) = L_f(P)\,\vec{W}. \qquad (23)$$

The important feature of this basis is the absence of Wigner rotation in the action of Lorentz transformation Λ_f on $|P\mu\rangle_F$,

$$U(\Lambda_f)\,|\vec{P}\,\mu\rangle_F = |\Lambda_f P\,\mu\rangle_F. \qquad (24)$$

This is the consequence of the fact that the elements $L_f(P)$ form a group (contrary to the case of the elements $L_c(P)$). Let us note that the Wigner rotation, which is absent in the case of Lorentz boost at the light front, "returns" when the usual rotations act on the states $|\vec{P}\,\mu\rangle_F$:

$$U(R)\,|\vec{P}\,\mu\rangle_F = \sum |R\vec{P}\,\mu'\rangle\, D^s_{\mu'\mu}\left(L_f^{-1}(RP)\,R\,L_f(P)\right) \qquad (25)$$

It is covenient to choose (as will be seen later) for the generators in the light front basis the following combinations of the quantities H , $\vec{P}$, $\vec{J}$, $\vec{N}$:

$$P^- = \frac{1}{\sqrt{2}}(P^0 - P^3) = \frac{M^2 + \vec{P}_T^2}{2P^+},$$

$$P^+ = \frac{1}{\sqrt{2}}(P^0 + P^3),$$

$$N^3 = i P^+ \frac{\partial}{\partial P^+},$$

$$E^i = \frac{1}{\sqrt{2}}(N^i + \varepsilon^{is} J^s) = i P^+ \frac{\partial}{\partial P^i}, \qquad (26)$$

$$F^i = \frac{1}{\sqrt{2}}(N^i - \varepsilon^{is} J^s) =$$

$$= \frac{1}{P^+}\left\{P^i N^3 + P^- E^i - \varepsilon^{i\ell}(M S^\ell_f + P^\ell S^3_f)\right\},$$

$$\vec{P}_T = (P^1, P^2).$$

Here $\varepsilon^{i\ell}$ is the completely antisymmetric tensor in the 1,2 - space ($\varepsilon^{12} = -\varepsilon^{21} = 1$). These two bases are connected in the obvious way

$$|\vec{P}\mu\rangle_c = U(L_c^{-1}(P))\,|0\mu\rangle = \qquad (27)$$

$$= U(L_c^{-1}(P))\,U(L_f(P))\,|\vec{P}\mu\rangle_F = U^+(R_M)\,|\vec{P}\mu\rangle_F,$$

where the rotation

$$R_M = L_f^{-1}(P)\,L_c(P) \qquad (28)$$

is called a Melosh rotation[14]. In the case of spin s=1/2 the matrix has the form

$$U(R_M) = D^{1/2}_{\mu'\mu}(R_M) = \left(\frac{m + p_0 + p_3 + i\sigma\cdot\varepsilon\cdot p_T}{\sqrt{(m+\epsilon_1+p_3)^2 + \vec{p}_T^{\,2}}}\right)_{\mu'\mu}, \qquad (29)$$

$$\epsilon_1 = \sqrt{m_1^2 + \vec{P}^2}.$$

5. Now let us consider the structure of basis states of the system **containing two free** particles with spins S_1 and S_2. The state vector $|\vec{P}_1\mu_1;\vec{P}_2\mu_2\rangle$ is the direct product of the vectors $|\vec{P}_1\mu_1\rangle$, $|\vec{P}_2\mu_2\rangle$:

$$|\vec{P}_1\mu_1;\vec{P}_2\mu_2\rangle = |\vec{P}_1\mu_1\rangle \otimes |\vec{P}_2\mu_2\rangle \qquad (30)$$

and is transformed in the following way

$$U(\Lambda)\ |\vec{p}_1\mu_1;\ \vec{p}_2\mu_2> = \tag{31}$$

$$= \sum_{\mu_1'\mu_2'} |\Lambda\vec{p}_1\mu_1';\ \Lambda\vec{p}_2\mu_2'> D^{s_1}_{\mu_1'\mu_1}(R_1^W)\, D^{s_2}_{\mu_2'\mu_2}(R_2^W),$$

where $R^W_{1,2}$ are Wigner rotations for the particles 1 and 2 in the case of Lorentz transformation Λ.

It seems obvious that one can go from the states vectors $|\vec{p}_1\mu_1;\vec{p}_2\mu_2>$ to the vectors $|\vec{\mathcal{P}},\vec{k}\,\mu_1\mu_2>$ with total momentum $\vec{\mathcal{P}}$ and the first particle momentum $\vec{k}$ in their centre of inertia reference frame. These state vectors $|\vec{\mathcal{P}},\vec{k}\,\mu_1\mu_2>$ have the property

$$|\vec{\mathcal{P}},\vec{k}\,\mu_1\mu_2> = U(L^{-1}(\mathcal{P}))\,|\vec{\mathcal{P}}=0,\vec{k}\,\mu_1\mu_2>, \tag{32}$$

$$U(\Lambda)\ |\vec{\mathcal{P}},\vec{k}\,\mu_1\mu_2> = \tag{33}$$

$$= \sum |\Lambda\vec{\mathcal{P}},\vec{k}'\mu_1'\mu_2'> D^{s_1}_{\mu_1'\mu_1}(R^W)\, D^{s_2}_{\mu_2'\mu_2}(R^W),$$

where $\vec{k}' = R^W\vec{k}$ and the Wigner rotation is

$$R^W = L^{-1}(\Lambda\mathcal{P})\,\Lambda\,L(\mathcal{P}). \tag{34}$$

The formal derivation of (32,34) can be found in Ref.[15]. The transformation low (34) for the vectors $|\vec{\mathcal{P}},\vec{k}\,\mu_1\mu_2>$ enables us to obtain the corresponding PG generators

$$\vec{J} = -i\left[\vec{\mathcal{P}}\,\frac{\partial}{\partial\vec{\mathcal{P}}}\right] + \vec{S}(\vec{\mathcal{P}}), \tag{35}$$

$$\vec{N} = i\,\mathcal{P}_0\,\frac{\partial}{\partial\vec{\mathcal{P}}} - \frac{[\vec{\mathcal{P}}\ \vec{S}(\vec{\mathcal{P}})]}{\mathcal{P}_0 + M}, \tag{36}$$

where $\mathcal{P}_0 = \sqrt{M^2+\vec{\mathcal{P}}^2}$; M is the mass operator and $\vec{S}(\vec{\mathcal{P}})$ is the two-particle system spin. This operator acts only on the "internal" variables $\vec{k}\,\mu_1\mu_2$:

$$\vec{S}(\vec{\mathcal{P}}) = -i\left[\vec{k}\,\frac{\partial}{\partial\vec{k}}\right] + \vec{S}_1(\vec{k}) + \vec{S}_2(-\vec{k}). \tag{37}$$

Expanding "the function" $|\vec{\mathcal{P}}, \vec{k}\,\mu_1\mu_2\rangle$ in spherical harmonics $Y_{\ell m}(\hat{k})$ it is easy to obtain the vectors $|\vec{\mathcal{P}}, \ell S J \mathcal{M}\rangle$ with total momentum $\vec{\mathcal{P}}$, orbital angular momentum ℓ, spin S and the total angular momentum J in the rest frame

$$|\vec{\mathcal{P}}, \ell S J \mathcal{M}\rangle = U(L^{-1}(\mathcal{P}))\,|\vec{\mathcal{P}}=0, \ell S J \mathcal{M}\rangle =$$

$$= \sum |\vec{p}_1\mu_1'\,\vec{p}_2\mu_2'\rangle\, Y_{\ell m}(\hat{k}) \cdot \tag{38}$$

$$\cdot \langle S_1\mu_1 S_2\mu_2 | S M_S\rangle \langle \ell m S M_S | J\mathcal{M}\rangle\, D^{S_1}_{\mu_1'\mu_1}(R_1^W)\, D^{S_2}_{\mu_2'\mu_2}(R_2^W).$$

Consequently, the Clebsh-Gordan coefficients which one needs in the calculation take the form:

$$\langle \vec{p}_1\mu_1\,\vec{p}_2\mu_2 | \vec{\mathcal{P}}\,\ell S J \mathcal{M}\rangle =$$

$$= N \sum Y_{\ell m}(\hat{k}) \langle S_1\mu_1 S_2\mu_2 | S M_S\rangle \langle \ell m S M_S | J\mathcal{M}\rangle. \tag{39}$$

$$\cdot D^{S_1}_{\mu_1'\mu_1}(R_1^W)\, D^{S_2}_{\mu_2'\mu_2}(R_2^W).$$

Here $\langle S_1\mu_1 S_2\mu_2 | S M_S\rangle$, $\langle \ell m S M_S | J\mathcal{M}\rangle$ are the rotation group Clebsh-Gordan coefficients, $\hat{k} = \vec{k}/|\vec{k}|$, N - the state normalization coefficient. The Clebsh-Gordan coefficients for PG were derived by Shirokov /16/.

Up to now we have been supposing tacitly that we are dealing with the canonical basis states. It is easy to see, however, that the main result (39) can be generalized directly for light front basis states. In fact, as can be seen from the definition (22) in the rest reference frame the canonical basis states coincide with those of light front, so that

$$|\vec{\mathcal{P}}=0,\ \ell S J \mathcal{M}\rangle_F = |\vec{\mathcal{P}}=0, \ell S J \mathcal{M}\rangle_C \tag{40}$$

and then

$$\langle \vec{p}_1\mu_1\,\vec{p}_2\mu_2 | \vec{\mathcal{P}}, \ell S J \mathcal{M}\rangle_F = {}_F\langle \vec{k}\,\mu_1\mu_2 | \ell S J \mathcal{M}\rangle =$$

$$= \sum D^{S_1 *}_{\mu_1'\mu_1}(R_{M1}^{-1})\, D^{S_2 *}_{\mu_2'\mu_2}(R_{M2}^{-1})\, {}_C\langle \vec{k}\,\mu_1'\mu_2' | \ell S J \mathcal{M}\rangle =$$

$$= \sum D^{S_1 *}_{\mu_1'\mu_1} (R^{-1}_{M1}) D^{S_2 *}_{\mu_2'\mu_2} (R^{-1}_{M2}) D^{S_1 *}_{\mu_1''\mu_1'} (R^{W}_{1}) D^{S_2 *}_{\mu_2''\mu_2'} (R^{W}_{2}) \cdot$$

$$\cdot {}_c\langle \vec{p}_1 \mu_1'' \vec{p}_2 \mu_2'' | \vec{\mathcal{P}} \ell S J \mathcal{M} \rangle_c = \tag{41}$$

$$= \sum D^{S_1 *}_{\mu_1''\mu_1} (R^{W}_{1} R^{-1}_{M1}) D^{S_2 *}_{\mu_2''\mu_2} (R^{W}_{2} R^{-1}_{M2}) \cdot$$

$$\cdot {}_c\langle \vec{p}_1 \mu_1'' \vec{p}_2 \mu_2'' | \vec{\mathcal{P}} \ell S J \mathcal{M} \rangle_c$$

Here we have used the unitarity of Lorentz transformation operators $U^+(\Lambda) U(\Lambda) = 1$; R_{M1}, R_{M2} are Melosh rotations for the particles with momenta $\vec{k}$ and $-\vec{k}$; R^W_1, R^W_2, the Wigner rotations. In the reference system with $|\vec{\mathcal{P}}| \to \infty$ one has $R^W_1 = R_{M1}$; $R^W_2 = R_{M2}$ and

$${}_F\langle \vec{p}_1 \mu_1 \vec{p}_2 \mu_2 | \vec{\mathcal{P}} \ell S J \mathcal{M} \rangle_F \overset{\vec{\mathcal{P}} \to \infty}{=} {}_c\langle \vec{p}_1 \mu_1 \vec{p}_2 \mu_2 | \vec{\mathcal{P}} \ell S J \mathcal{M} \rangle_c \tag{42}$$

6. Now let us discuss the important problem of the including of the interaction between particles. In the relativistic quantum theory the interaction including is a much more difficult problem than in the non-relativistic case. To illustrate the problem let us consider one of the commutators for the PG generators:

$$[\hat{P}^\kappa, \hat{N}^\kappa] = i \hat{H} . \tag{43}$$

If we include the interaction in $\hat{H}$, that is if we change

$$H_0 \to \hat{H} = \hat{H}_0 + \hat{V} , \tag{44}$$

then one can see from (43) that the interaction is to be included in P^κ or in N^κ or in both of them.

The self consistent method of including the interaction in 45 commutation relations for PG is just the main problem in the construction of relativistic quantum theory. The first one who considered the problem of interaction including in the PG algebra was Dirac[13]. Dirac had connected the interaction inclusion with the type of dynamics, that is with the method of the system evolution description.

The non-relativistic quantum theory dynamics can be cosidered in the following way. The initial system state is given on the hyper-

surface $t = 0$ of 4-dimensional space and the evolution is defined by this hypersurface shift in the t-direction.(The Minkowsky space is not adequate to non-relativistic theory but is important for what follows). The interaction (in the case of non-relativistic theory) enters the energy operator which shifts the hypersurface. The momentum and angular momentum operators do not depend on the interaction. These well-known properties of non-relativistic theory reflect the following group theory features. Galilei group is the group of symmetry of relativistic theory. This group generators $\vec{P}$ (momentum), $\vec{J}$ (angular momentum), $\vec{G}$ (Galilei boost) leave the hypersurface $t = 0$ unchanged; the generator $\hat{H}$ (energy) changes the surface position. By generalizing this property of non-relativistic theory we obtain the rule for including of the interaction in relativistic theory: the interaction enters only the generators changing the position of the hypersurface $t = \text{const}$. It is easy to see that the PG generators $\vec{P}$, $\vec{J}$ leave the hypersurface unchanged while the generators $\vec{N}$ and $\hat{H}$ do change its position in the Minkowski space. Consequently, in the case of instant form dynamics when one chooses for evolution the hypersurface $t = \text{const.}$, the operators $\vec{P}$ (momentum) and $\vec{J}$ (angular momentum) do not depend on the interaction while $\vec{N}$ (Lorentz boost) and $\hat{H}$ (energy) do depend. Dirac gave to the operators depending on the interaction the name of Hamiltonians. So the instant form of dynamics (with the evolution of the hypersurface $t = \text{const.}$) is characterized by six kinematical (interaction independent) operators and four Hamiltonians. In non-relativistic physics there is only one possibility: to choose the hypersurface $t = \text{const.}$ as the hypersurface of evolution. In the relativism the situation is changed badly and one can choose for the surface of evolution any surface characterized by one intersection with world lines in the inside of the light cone. It seems natural to choose such evolution surfaces for which the number of kinematic operators is to be maximal. Dirac has considered (besides the hypersurface $t = \text{const.}$) two other surfaces: the light front surface $t + x^3 = \text{const.}$ and

$$x^2 = a^2 > 0 \quad , \quad t > 0 . \tag{45}$$

In these cases one is dealing with the light front dynamics and point dynamics, respectively. In the case of the hypersurface of evolution $t + x^3 = \text{const.}$ the operators (26) $P^+, \vec{P}_T, E^t, J^3, N^3$ are the kinematic generators and P^-, F^t are the Hamiltonians. Note that one cannot say that the dynamics of ligt front with three Hamiltonians is simplier than the instant form dynamics with four Hamiltonians.

Let us discuss briefly the problem of equivalence of different dynamics. Naturally one should expect that the instant form dynamics and light front dynamics are equivalent because the respective hypersurfaces of evolution can be obtained one from another by the Lorentz transformation (more strictly speeking, the light front surface is obtained as a result of limiting procedure $v \to 1$). The equivalence of the light front dynamics and the instant form one in the infinite moment reference frame was shown in [4]. The case of the point form dynamics is more complicated because the hypersurface (45) cannot be obtained by Lorentz transformation of the hypersurface t = const. However its equivalence to two other forms can be established [17] if one takes into account the possibility of PG nonlinear parametrization.

7. Now we have understood in what generators the interaction enters but how does it enters is not clear. The first attempt to solve this problem has been made by Yu. M. Shirokov [18]. He based his approach on the natural requiring that the interaction inclusion in the generator $\hat{H}$ must leave the two-particle scattering amplitude to be Lorentz invariant. Shirokov considered the transformation properties of the pair interaction matrix elements in Born approximation and has obtained (up to the order $(v/c)^2$) the dependence of interaction on the total two-particles moment $\vec{\mathcal{P}} = \vec{p}_1 + \vec{p}_2$. The non-trivial part ΔV of the relativistic corrections to the interaction has the form

$$\Delta V = -\frac{\vec{\mathcal{P}}^2 V_{nr}}{(m_1+m_2)^2} - \frac{(\vec{k}\vec{\mathcal{P}})\left(\vec{\mathcal{P}}\frac{\partial}{\partial \vec{k}}\right) + (\vec{k}'\vec{\mathcal{P}})\left(\vec{\mathcal{P}}\frac{\partial}{\partial \vec{k}'}\right)}{2(m_1+m_2)^2}$$

$$- \frac{(m_2-m_1)(\vec{k}+\vec{k}')\vec{\mathcal{P}}\, V_{nr}}{2m_1m_2(m_1+m_2)} + \tag{46}$$

$$+ i\frac{1}{2m_1m_2}\left\{V_{nr}\left[\vec{\mathcal{P}}\vec{k}'\right]\left(\frac{\vec{S}_1}{m_1}-\frac{\vec{S}_2}{m_2}\right) - \left[\vec{\mathcal{P}}\vec{k}\right]\left(\frac{\vec{S}_1}{m_1}-\frac{\vec{S}_2}{m_2}\right)V_{nr}\right\},$$

where V_{nr} is non-relativistic potential; $\vec{k}$, $\vec{k}'$, the relative momenta. This Shirokov result is of fundamental importance. It shows that method of interaction including can bring us to the two-particles system dynamics depending essentially on the total momentum. In this

case the inseparability of variables in relativistic quantum theory manifests itself. In this situation the method developed by Karmanov[19] begins to work effectively. During the following few years it became clear that in the case of light front dynamics one can include the interaction in such a way that the internal variables are separated from the variables describing the composite system motion as a whole[11]. It became also clear[13-17] that in the frame of usual dynamics one can separate the motion of the system as a whole from the internal variables too. So there exists a more economical method of interaction including than that discussed by Shirokov[18]. This is the method of interaction including into the mass operator $\hat{M}$:

$$\hat{M}_0 \longrightarrow \hat{M} = \hat{M}_0 + \hat{V}, \tag{47}$$

where

$$M_0 = \epsilon_a(\vec{k}) + \epsilon_b(\vec{k}),$$

and the operator $\hat{V}$ satisfies the following commutation relations:

$$[\hat{V}, \vec{\mathcal{J}}] = [\hat{V}, \vec{S}_c] = [\hat{V}, \frac{\partial}{\partial \vec{\mathcal{J}}}] = 0; \tag{48a}$$

(the instant form dynamics)

$$[\hat{V}, \hat{P}^+] = [\hat{V}, \hat{P}_\tau] = [\vec{S}_\perp, \hat{V}] = [E^z, \hat{V}] = [N^3, \hat{V}] = 0 \tag{48b}$$

(the light front dynamics).

Taking into account eq.(48) it is easy to show that the substitution $M_0 \to M_0 + V$ in (19) and (26) left tge PG algebra unchanged.

8. Let us consider now the properties of the state vectors for the two-particle system with the interaction (48a,b). In the rest reference frame the state vectors are to satisfy the equation

$$\hat{M} |\Psi\rangle = \lambda |\Psi\rangle, \tag{49}$$

where λ is the mass of the system and the operator $\hat{M}$ has the form

$$\hat{M} = \hat{M}_0 + \hat{V} = \sqrt{m_1^2 + \vec{k}^2} + \sqrt{m_2^2 + \vec{k}^2} + \hat{V} \tag{50}$$

Other equations (equivalent to (49)) are often used

$$\hat{M}^2 |\Psi\rangle = \lambda^2 |\Psi\rangle. \tag{51}$$

Here the mass operator square is

$$\hat{M}^2 = \hat{M}_0^2 + U, \tag{52}$$

$$U = \hat{M}^2 - \hat{M}_0^2 = \hat{V}^2 + \{\hat{M}_0, \hat{V}\}, \tag{53}$$

$$\{\hat{M}_0, \hat{V}\} = \hat{M}_0\hat{V} + \hat{V}\hat{M}_0$$

and

$$(\kappa^2 + \hat{W})|\Psi\rangle = \eta|\Psi\rangle. \tag{54}$$

The eigenvalue η is connected with the mass eigenvalue by the equation

$$\lambda^2 = 2\eta + m_1^2 + m_2^2 + 2\sqrt{\eta(\eta + m_1^2 + m_2^2) + m_1^2 + m_2^2} \tag{55}$$

and the interaction $\hat{W}$ is given by

$$\hat{W} = \frac{1}{4}\hat{M}^2 + \frac{(m_1^2 - m_2^2)^2}{4M^2} - \frac{1}{4}\hat{M}_0^2 - \frac{(m_1^2 - m_2^2)^2}{4M_0^2}. \tag{56}$$

The operators W and V are connected by the equation

$$V = \sqrt{m_1^2 + \vec{K}^2 + W} + \sqrt{m_2^2 + \vec{K}^2 + W} - \tag{56a}$$
$$- \sqrt{m_1^2 + \vec{K}^2} - \sqrt{m_2^2 + \vec{K}^2}.$$

While the eqs. (49), (51) contain the obviously relativistic forms (the relativistic energies $\sqrt{m^2 + \vec{K}^2}$), the relativistic equation (54) has the form of non-relativistic Schrödinger equation. This fact shows the possibility of phenomenological definition of relativistic potential from the scattering data and two-nucleon binding energy:

$$W = 2\frac{m_1 m_2}{m_1 + m_2} V_{n\ell}, \tag{57}$$

where $V_{n\ell}$ is a phenomenological nucleon-nucleon potential. In general case there is a difficulty: η in (54) is not equal to the deuteron binding energy multiplied by the reduced mass. However in the small energy limit one has

$$\eta = M\varepsilon + \frac{1}{4}\varepsilon^2 \simeq M\varepsilon. \tag{58}$$

Now we can put any N-N-potential, known from non-relativistic physics (e.g., the Paris one), into the relativistic equation (54). However its "Paris" behaviour in the range of relativistic $\vec{k}$ values must be considered specially.

Let us show now that the two-particle wave function does not depend on the total momentum. Acting on the eq.(49) by the Lorentz boost Λ operator $U(\Lambda)$ we obtain the equation

$$\hat{M} \, |\vec{\mathcal{P}}, \Psi> \; = \; \lambda \; |\vec{\mathcal{P}}, \Psi> \; . \qquad (59)$$

Let us multiply this equation by the free particle state vector $|\vec{\mathcal{P}}, \kappa \ell s J>$ from the left. Then the eq.(59) takes the form

$$\hat{M}_0(\kappa) <\vec{\mathcal{P}}, \kappa \ell s J \mathcal{M} \; | \; \vec{\mathcal{P}}, \Psi> \; +$$

$$+ \sum_{\kappa' \ell' s'} <\vec{\mathcal{P}}, \kappa \ell s J \mathcal{M} \, | V | \vec{\mathcal{P}}, \kappa' \ell' s' J \mathcal{M}> <\vec{\mathcal{P}}, \kappa' \ell' s' J \mathcal{M} \, | \vec{\mathcal{P}}, \Psi> = \qquad (60)$$

$$= \; \lambda \; <\vec{\mathcal{P}}, \kappa \ell s J \mathcal{M} \; | \; \vec{\mathcal{P}}, \Psi>$$

The function $<\vec{\mathcal{P}}, \kappa \ell s J \mathcal{M} \, | \, \vec{\mathcal{P}}, \Psi>$ differs from the scalar product $<\vec{\mathcal{P}}', \kappa \ell s J \mathcal{M} \; | \; \vec{\mathcal{P}}, \Psi>$ by the presence of $\delta(\vec{\mathcal{P}}' - \vec{\mathcal{P}})$. Because of the commutation relations (48) the interaction does not depend on $\vec{\mathcal{P}}$, so that now we have from (60) and (49):

$$<\vec{\mathcal{P}}, \kappa \ell s J \mathcal{M} \, | \vec{\mathcal{P}}, \Psi> \; = \; <\kappa \ell s J \mathcal{M} \, | \Psi> \; = \; \Psi_{\ell s J}(\kappa), \qquad (61)$$

Here $\Psi_{\ell s J}(\kappa)$ is the ℓs -component of the wave function at rest. Now it follows from (61) that

$$<\vec{p}_1 \mu_1 \vec{p}_2 \mu_2 \, | \vec{\mathcal{P}}, \Psi> \; = \sum_{\ell s J} <\vec{p}_1 \mu_1 \vec{p}_2 \mu_2 \, | \vec{\mathcal{P}}, \kappa \ell s J \mathcal{M}> \Psi_{\ell s J}(\kappa), \qquad (62)$$

where $<\vec{p}_1 \mu_1 \vec{p}_2 \mu_2 \, | \, \vec{\mathcal{P}}, \kappa \ell s J \mathcal{M}>$ are the PG Clebsh-Gordan coefficients discussed earlier.

Let us emphasize that the result (62) is valid for both of dynamics under consideration (instant form and light front dynamics). The only difference is in the specific PG Clebsh-Gordan coefficients to be put in eq.(62) in these two cases.

9. We have demonstrated how to construct the relativistic invariant model in the case of two particles having the following specific features:

(1) Dynamics independence of the wave function on the system total momentum. This fact is caused by the interaction including in

the mass operator. The including of the interaction in the energy operator in a way analogous to the non-relativistic case leads (as was shown by Shirokov[18]) to the dynamical dependence of the wave functions on the total momentum.

(2) Unitary equivalence of different dynamics types, in particular of light front and instant form dynamics.

(3) "Schrödinger equation" for the wave function in any of the equivalent forms of non-relativistic Schrödinger equation type. This enables one to use phenomenological potential (e.g., Paris) in relativistic case. Note, that the possibility of using the potential in the relativistic momenta range is to be investigated specially.

As we have pointed out in p.96 when constructing the two-particle relativistic model we are not guided by the fundamental standard model (because of the difficulties in taking into account of nonperturbative effects). That is why the considered model presents only one of possibilities and its validity must be checked by the comparison with experimental data.

During recent years a number of calculations were made pretending the correct taking into account of the relativistic effects in processes including the deuteron. We shall discuss here only the results obtained on the base of the method described in this paper, that is on the use of relativistic quantum mechanics. Let us consider some aspects of these calculations. The deuteron form factors were investigated in great detail [21-25]. As is known, the deuteron form factors are defined (up to kinematic factor) by the matrix elements of the deuteron current operator $J^{\mu}(0)$. One of the parametrizations (see, e.g.,[26]) has the form

$$\langle \vec{\mathcal{P}}' m \mid J^{\mu}(0) \mid \vec{\mathcal{P}} m \rangle = - \sqrt{2\mathcal{P}_0' 2\mathcal{P}_0}\; e \cdot$$

$$\cdot \Big\{ G_1(Q^2)(\xi'^{*}\xi)\, d^{\mu} + \tag{63}$$

$$+ G_2(Q^2)\left[\xi^{\mu}(\xi'^{*}q) - \xi'^{*\mu}(\xi q)\right] -$$

$$- G_3(Q^2)\, \frac{(\xi q)(\xi'^{*}q)}{2M_d^2}\, d^{\mu} \Big\} .$$

Here $G_{1,2,3}$ are the deuteron form factors; ξ^μ, ξ'^μ, the four-vectors of the deuteron polarization, $d^\mu = \mathcal{P}'^\mu + \mathcal{P}^\mu$, $q^\mu = \mathcal{P}'^\mu - \mathcal{P}^\mu$; M_d, the deuteron mass, $Q^2 = -q^2$; e, proton charge, m, deuteron spin projection. G_C, G_Q, G_M - charge, quadrupole and magnetic dipole form factors and the standard structure functions - $A(Q^2)$, $B(Q^2)$ - entering ed-scattering cross section, can be found in[21,22]. The main difficulty is naturally the form of the deuteron current operator $J^\mu(0)$. In the papers[23,24] using the instant form dynamics two points were postulated from the very beginning: first, the deuteron current is the sum of the one-particle currents; second, in the one-particle current matrix elements one can neglect off-mass-shell effects for the intermediate nucleons

$$\langle \vec{\mathcal{P}}' m' | J^\mu(0) | \vec{\mathcal{P}} m \rangle =$$

$$= \sum_{\mu_1 \mu_2 \mu_1' \mu_2'} \int d\vec{p}_1' \, d\vec{p}_2' \, d\vec{p}_1 \, d\vec{p}_2 \; \langle \vec{\mathcal{P}}' m' | \vec{p}_1' \mu_1' \vec{p}_2' \mu_2' \rangle \cdot \tag{64}$$

$$\cdot \Big\{ \langle \vec{p}_1' \mu_1' \vec{p}_2' \mu_2' | J_p^\mu(0) | \vec{p}_1 \mu_1 \vec{p}_2 \mu_2 \rangle +$$

$$+ \langle \vec{p}_1' \mu_1' \vec{p}_2' \mu_2' | J_n^\mu(0) | \vec{p}_1 \mu_1 \vec{p}_2 \mu_2 \rangle \Big\} \langle \vec{p}_1 \mu_1 \vec{p}_2 \mu_2 | \vec{\mathcal{P}} m \rangle .$$

How the deuteron form factors depend on the one-particle matrix elements, that is on nucleon form factors and on the deuteron wave function. In the mentioned papers the deuteron wave function was supposed to be independent of the total deuteron momentum. This means that in fact the calculation is made in the frame of the impulse approximation for the potential relativistic model cosidered earlier (not in the Karmanov[19] model, e.g., where the wave function depends essentially on the total momentum). The results for the functions $A(Q^2)$ and $B(Q^2)$ for dipole parametrization of nucleon form factors and Paris deuteron function are given on fig.1,2. In fig.3 the value $\left(\left(A/A_{NR}\right)-1\right)$ is shown; this value characterizes the relativistic corrections for the function $A(Q^2)$. The papers[21,22,25] follow the light front dynamics. In these papers the deuteron current matrix element is written in the form (64) but all the functions of the canonical basis are changed for the light front wave functions. The matrix elements of J^+ current components are calculated too. Because of the fact that the wave functions in the case of different

dynamics are connected by (27) we must expect that the results[23,24] are to coincide with that of Ref.[21,22,25]. However the values of the functions $A(Q^2)$ and $B(Q^2)$ from different papers are slightly different. Let us note two points. First, as can be seen from the figures, the relativistic calculations in the light front dynamics usually give the decreased values of structure functions (this fact takes place in the number of papers on field theory or quasipotential approach) in contrast to the result[24] based on instant form dynamics. The results of Ref.[24] are in better agreement with experiment for $A(Q^2)$. Second, the meson exchange currents must necessarily be taken into account for $B(Q^2)$ as was established earlier. The results of[24] with meson exchange currents are in good agreement with experiment too. One must not prescribe too much importance to the quantitative agreement with the experiment because in the case of deuteron there are too much problems which look very much like the problem of solving the Gordian knot[27]. The main of them are - besides the relativization - the correct account of meson currents(depending crucially on the choice of parameter), nucleon form factors which are not well defined and influence much the final result and, finally, the problem of choosing of nucleon-nucleon potential.

The important point of the cited papers on the deuteron form factors is the supposed equality of the deuteron current to the sum of the nucleon currents. It is not clear a priori in the frame of what dynamics and to what extend the deuteron current does really have such a property. From general point of view here the light front dynamics is more attractive. Really, in the infinite momentum reference frame, which is equivalent to the light front dynamics, the impulse approximation is more justified, the antinucleons role is suppressed and one can demonstrate some serious arguments supporting the fact that in the case when the momentum transfers are not too large the deuteron current J^+ - component can be considered as a sum of nucleons currents J^+-components. However, all these facts are not crucial for the choosing of the light front dynamics, particularly if one keeps in mind the mentioned equivalence of the dynamics. So the calculations based on the instant form dynamics seem to be quite reasonable.[28]

The relativistic form factors calculated in the frame of both of mentioned relativistic models are in agreement with the experimental data. This ensures us in a certain way that some kind of relativistic quantum mechanics is really valid with no dependence of the two-particle wave function on the total momentum. The other sup-

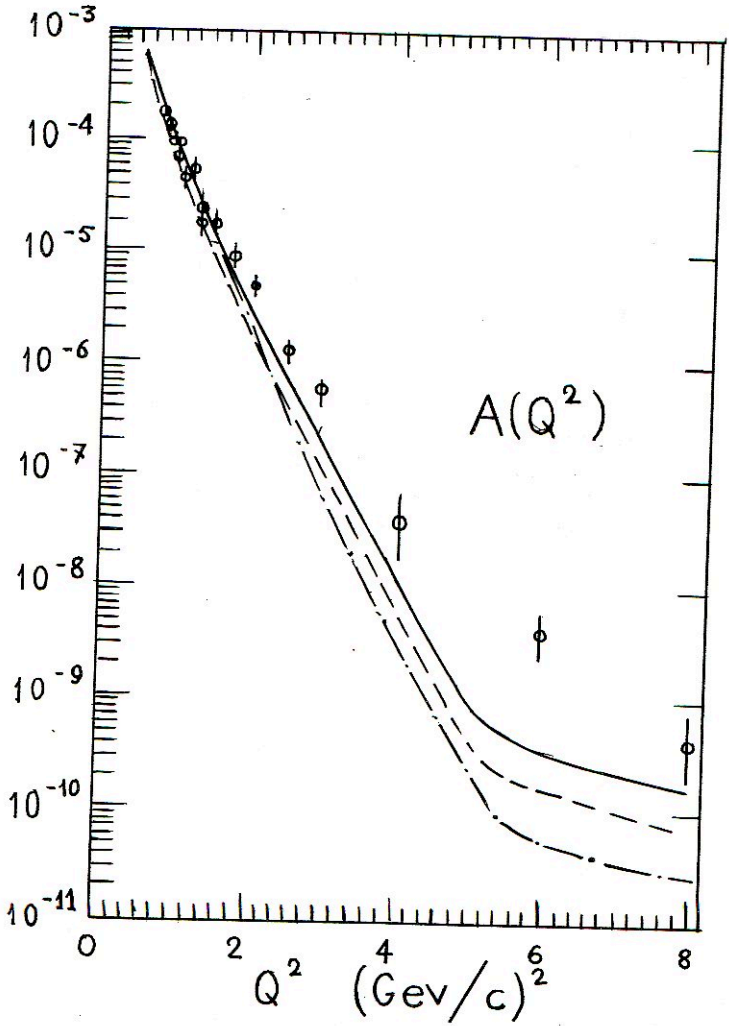

FIG.1. Deuteron structure function $A(Q^2)$.

Dashed curve - the standard nonrelativistic approximation; dash-dotted curve - the relativistic light-front dynamics /21/; solid curve - the relativistic instant form dynamics /24/. Paris wave functions /20/ and dipole nucleon form factors were used.

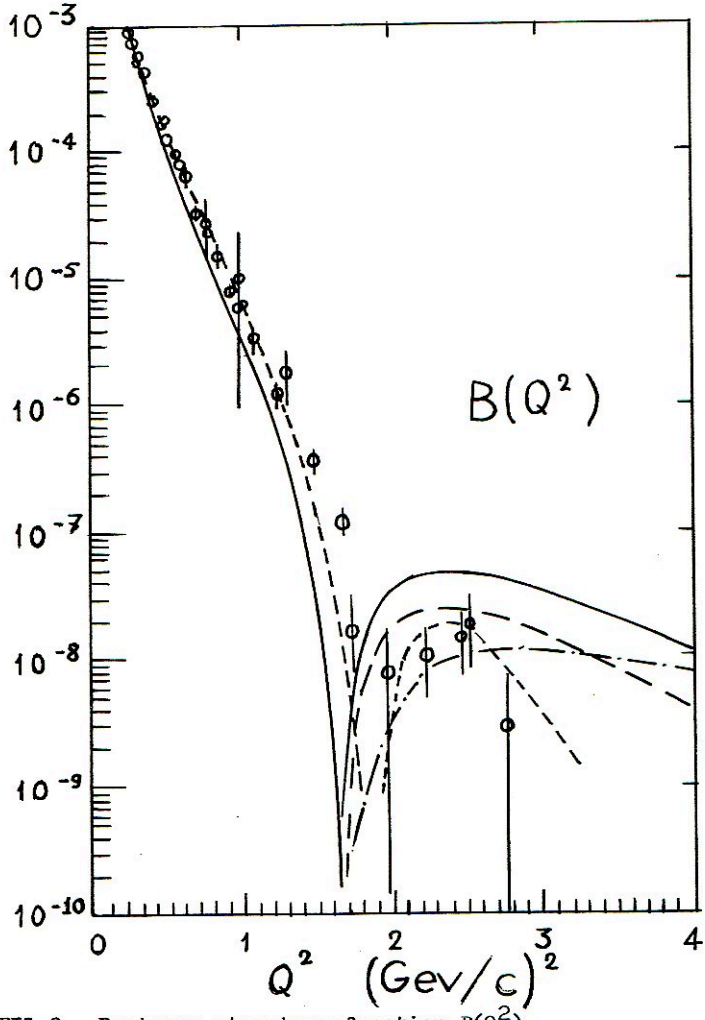

FIG.2. Deuteron structure function $B(Q^2)$.

Long-dashed curve - the standard nonrelativistic approximation; dash-dotted curve - the relativistic light-front dynamics [25]; solid curve - relativistic instant form dynamics [24]; dashed curve - the relativistic instant form dynamics with the meson exchange currents [24]. Paris wave functions [20] and dipole nucleon form factors were used.

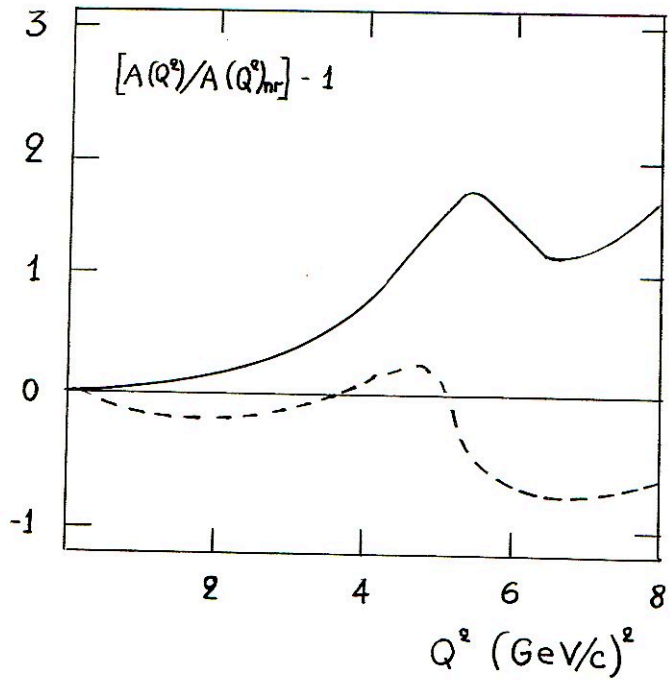

FIG.3. The relativistic effects in the deuteron structure function $A(Q^2)$.

Dashed curve - $R(Q^2) = A(Q^2)/A_{nr}(Q^2) - 1$ in the light-front dynamics /21/; solid curve - $R(Q^2)$ in the instant form dynamics /24/. Paris wave functions /20/ and dipole nucleon form factors were used.

porting arguments are given by the well description /6/ of the proton momentumspectra in the reaction of fragmentation of relativistic deuterons on hydrogen (FIG.4). This description was based essentially on one of the equivalent models (48). The elastic electron-deuteron scattering and deuteron fragmentation data show the validity of the supposition that the nucleon degrees of freedom are dominant in deuteron up to the range of 0,4 fm.

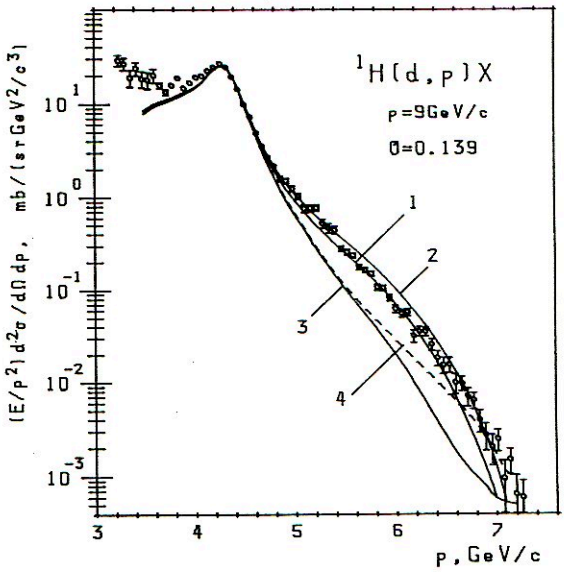

FIG.4. The proton momentum spectrum in the deuteron fragmentation reaction at 9 GeV/c ; emitted angle of protons is 0.139 rad. The curves present the result of calculation with the deuteron wave functions for different NN potentials: 1 - Paris potential /20/; 2 - Reid soft core potential /29/; 3 - Bonn potential, the full model /30/; 4 - Bonn potential, relativistic momentum space.

References

1. F.E.Close, An Introduction to Quarks and Partons, Academic Press, 1979.
2. J.Kogut, L.Susskind, Phys.Rep., 1973, v.8, p.75.
   I.A.Schmidt, R.Blankenbecler, Phys.Rev., 1977, v. D15, p.3321.
3. P.A.M.Dirac, Rev.Mod.Phys., 1949, v.21, p.392.
4. J.B.Kogut, D.E.Soper, Phys.Rev., 1979, v.D1, p.2901.
   J.D.Bjorken, J.B.Kogut, D.E.Soper, Phys.Rev., 1971, v.D3, p.1382.
   S.J.Brodsky, R.Rosvies, R.Suaya, Phys.Rev., 1979, v.D8, p.4574.
   G.P.Lepage, S.J.Brodsky, Phys.Rev., 1980, v.D22, p.2157.
5. R.G.Arnold et al., Phys.Rev.Lett., 1985, v.54, p.649.
   S.Platchkov et al., Nucl.Phys., 1990, v.A510, p.740.
   R.G.Arnold et al., Phys.Rev.Lett., 1987, v.58, p.1723.
   P.E.Boosted et al., Phys.Rev., 1990, v.C42, p.38.
   I.The et al., Phys.Rev.Lett., 1991, v.67, p.173.

6. L.S.Azhgirey et al., Nucl.Phys., 1991, v.A528, p.621.
V.G.Ableev et al., Nucl.Phys., v.A393, p.491.
L.Anderson et al., Phys.Rev., v.C28, p.1224.
7. V.M.Musafarov, V.E.Troitsky, S.V.Trubnikov, Fiz.Elem.Chastits Atom.Yadra, 1983, v.14, p.1112.
V.E.Troitsky, Yu.M.Shirokov, Theor.Mat.Fiz., 1969, v.1, p.213.
A.I.Kirillov, V.E.Troitsky, S.V.Trubnikov, Yu.M.Shirokov, Fiz.Elem.Chastits Atom.Yadra, 1975, v.5, p.3.
V.V.Anisovich, A.V.Sarantsev, preprint Bonn Univ. TK-90-10.
8. Yu.V.Novozhilov, An Introduction to the Particle Theory, Nauka, 1971.
9. E.P.Wigner, Ann.Math., 1939, v.40, p.1949.
Yu.M.Shirokov, ZhETF, 1957, v.33, p.861, p.1196, p.1208; ZhETF,1958, v.34, p. 717; ZhETF, 1959, v.36, p.879.
10. K.Lubanski, Physica, 1942, v.9, p.310.
11. V.B.Berestetsky, M.V.Terent'ev, Yad.Fiz., 1976, v.24, p.1044.
12. L.A.Kondratyuk, M.V.Terent'ev, Yad.Fiz., 1980, v.31, p.1087.
13. W.N.Polysou, Ann. of Phys., 1989, v.193, p.367.
14. H.T.Melosh, Phys.Rev., 1974, v.D9, p.1095.
15. A.Macfarlane, Rev.Mod.Phys., 1962, v.34, p.41.
16. Yu.M.Shirokov, ZhETF, 1958, v.35, p.1005.
17. S.N.Sokolov, A.N.Shatnii, Theor.Mat.Fiz, 1978, v.37, p.291.
18. Yu.M.Shirokov, ZhETF, 1959, v.36, p.474.
19. V.A.Karmanov, Fiz. Elem. Chastits Atom. Yadra, 1988, v.19, p.529.
20. M.Lacomb et al., Phys.Rev., 1980, v.21, p.861.
21. I.L.Grach, L.A.Kondratyuk, Yad.Fiz., 1984, v.39, p.316.
22. P.L.Chung, F.Coester, B.D.Keister, W.N.Polyzou, Phys.Rev., 1988, v.37, p.2000.
23. A.F.Krutov, V.E.Troitsky, Yad.Fiz., 1986, v.43, p.1327.
24. A.F.Krutov, V.E.Troitsky, preprint NPI MSU, 1988, 88-40/61.
25. L.L.Frankfurt, I.L.Grach, L.A.Kondratyuk, M.I.Strikman, Phys.Rev.Lett., 1989, v.62, p.387.
26. F.Gross, Phys.Rev., 1965, v.B140, p.410.
27. M.Gari, H.Hyuga, Nucl.Phys., 1976, v.A264, p.409.
28. L.Heller, A.W.Tomas, Phys.Rev., 1990, v.C41, p.2756.
29. R.V.Jr.Reid, Ann. of Phys., 1968, v.50, p.411.
30. R.Machleid et al., Phys.Rev., 1987, v.149, p.1.

DEUTERON FRAGMENTATION - THE ROLE OF THE TARGET NUCLEUS AND OF PARTICLE PRODUCTION PROCESSES

H. Müller

Zentralinstitut für Kernforschung Rossendorf, Postfach 19,

O-8051 Rossendorf/Dresden Federal Republic of Germany

The deuteron as the lightest nucleus is of particular importance for the understanding of nuclear phenomena. Proton spectra arising from the fragmentation of deuterons were measured [1-6] and interpreted [7-15] mainly with the aim of investigating the deuteron wave function (DWF) at small distances.

In the following the modified phase space (MOPS) model [15] will be used to analyze the proton spectra from the interaction of 9 GeV/c deuterons with hydrogen, deuterium and carbon. It will be shown that particle production processes and the properties of the target nucleus must be taken into account for an accurate description of the deuteron break up.

A nucleus-nucleus reaction is considered as a superposition of nucleon-nucleon (*NN*) collisions. Using the well-known spectator-participant picture the events are classified by the number of projectile nucleons k and target nucleons l involved in the reaction, and the corresponding cross sections σ_{kl} are calculated [16] in the Glauber approximation. The interaction of k projectile with l target nucleons is described by a two-step picture, where the two participating nucleon groups are treated as single entities called clusters. In the first step translational energy is converted into internal excitation energy of the clusters. An excited cluster is pictured as consisting of the valence quarks of the initial nucleons and additional quark-antiquark pairs created during the collision. In the second stage of the reaction the available quarks recombine into baryons and mesons according to the rules of quark statistics [17] populating in this way the channels $\alpha_{kl} = (\alpha_k, \alpha_l)$ defined by the numbers n_k, n_l and types of particles in the final states of the two decaying nucleon groups. By introducing the relative probability $dW_{kl}(s,\alpha_{kl})$ of populating the channel α_{kl} the differential cross section is calculated as an incoherent sum

$$d\sigma(s) = \sum_{k=1}^{A} \sum_{l=1}^{B} \sigma_{kl} \sum_{\alpha_{kl}} dW_{kl}(s;\alpha_{kl}) \qquad (1)$$

with the mass numbers A and B of the interacting nuclei. Here, s denotes the square of the centre of mass (c.m.) energy of the projectile-target interaction. The cross sections σ_{kl} depend on the nucleon densities of the interacting nuclei, while the quantities $dW_{kl}(s;\alpha_{kl})$ reflect the collision dynamics and determine the relative probabilities of the various channels and the distribution of the final particles in the phase space.

For calculating the σ_{kl} a slightly modified version of the Monte-Carlo code DIAGEN [16] is used. In order to evaluate the relative probabilities the interacting nuclei are assumed to dissociate into spectators and participants with their relative momenta described by the internal Fermi-motion of the nucleons. For the deuteron the momentum distribution is described by the square of the Paris DWF [18]. In the case of the carbon target the momentum distribution of a cluster consisting of k nucleons is taken as a Gaussian with the width s_k defined by

$$s_k^2 = \frac{k\ (A - k)}{5\ (A - 1)}\ p_F^2 \ . \qquad (2)$$

Here, A = 12 denotes the mass number, and for the Fermi-momentum a value of p_F = 230 MeV/c is used.

The probability of populating a definite channel α_{kl} is given by the Lorentz-invariant phase space factor times the square of a phenomenological matrix element. This matrix element is split into factors describing the deflection, excitation and statistical properties of the clusters. For a more detailed discussion of the MOPS model we refer to [15].

In Figs.1-6 MOPS model calculations are compared with inclusive proton spectra measured at 0^o and 8^o. The 0^o spectrum from dp interactions (Fig. 1) is dominated by participants from quasi-free inelastic "11*" collisions at momenta below 3.5 GeV/c and by spectators at higher momenta. Thus, the 0^o spectrum reflects the behaviour of the deuteron single-nucleon momentum distribution for spectator momenta far enough from the kinematical limit. Near the limit the phase-space factor sharply decreases and determines the momentum dependence of the cross section. The maximal spectator momentum is related to the minimal c.m. energy of the NN subprocess,

which is given by the sum of the rest masses in the final state of the *NN* interaction. The onset of "phase-space dominance" occurs for each channel at different spectator momenta, depending on the masses of the particles produced, and the spectator reaches the largest momentum in the quasi-elastic "$\bar{1}\bar{1}$" channel. Thus, the calculated cross section is a superposition of functions, whose momentum dependences differ from channel to channel. As can be seen from Fig.1, the different momentum dependences of the quasi-elastic "$\bar{1}\bar{1}$" and quasi-free inelastic "11*" contributions reproduce the shoulder in the spectrum around 6 GeV/c.

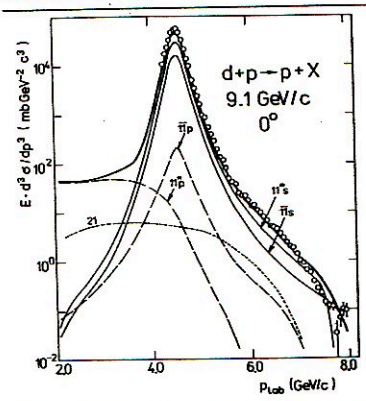

Fig. 1.
Invariant cross section versus laboratory momentum. The partial spectra are labelled by the numbers of projectile and target nucleons participating in the interaction. Quasi-free "11" reactions are divided into quasi-elastic "$\bar{1}\bar{1}$" and quasi-free inelastic "11" collisions. Contributions from participants and spectators are denoted by the lettes p and s. The thick curve represents the sum of the partial spectra. Data from [3].

In the 8° spectrum (Fig. 2), the quasi-elastic peak around 4.3 GeV/c is followed by a region, in which the "21" interaction of the deuteron as a single unit dominates, while at the highest momenta the main contributions to the cross section arise again from the spectators. This typical pattern is also observed, although with modifications depending on the target mass number, in the more complicated *dd* and *dC* interactions.

In Fig. 3 the calculated 0° proton spectrum from *dd* interactions is shown. It is quite similar to the spectrum from *dp* reactions, because the contributions of the additional "12" (the interaction of one projectile nucleon with two target nucleons) and "22" (the interaction of two projectiles with two target nucleons) processes to the 0° spectrum are negligible. As in the case of the *dp* reaction, the low-momentum part of the spectrum is due to participants from quasi-free inelastic "11*p" processes, while the peak and the high-momentum region is governed by the spectators from quasi-elastic "$\bar{1}\bar{1}$s" and quasi-free inelastic "11*s" processes.

At 8° (Fig.4) the momentum region below 4 GeV/c arises again from quasi-free inelastic "11*" reactions. The quasi-elastic peak around 4.3 GeV/c is much broader than in the case of *dp* interactions, because

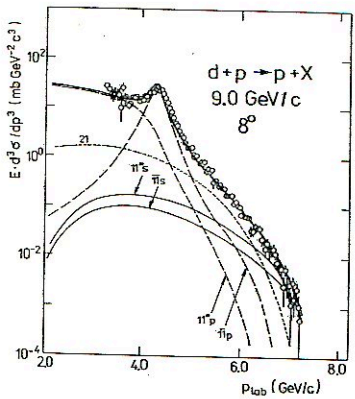

Fig.2.
Invariant cross section versus laboratory momentum. Curves are labelled as in Fig.1. Data from [6].

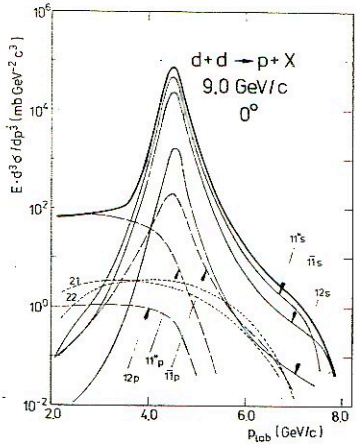

Fig.3.
Invariant cross section versus laboratory momentum. Curves are labelled as in Fig.1.

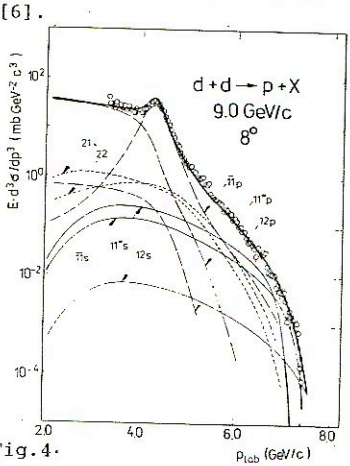

Fig.4.
Invariant cross section versus laboratory momentum. Curves are labelled as in Fig.1. Data from [6].

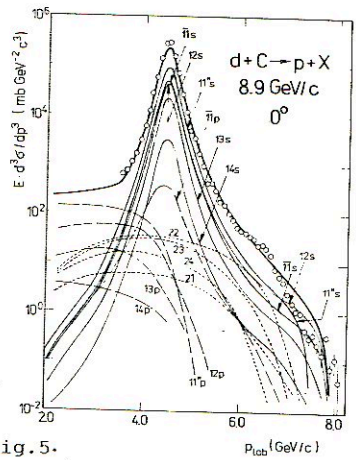

Fig.5.
Invariant cross section versus laboratory momentum. Curves are labelled as in Fig.1. Data from [1].

the Fermi-motion of both the projectile and the target nucleons contributes to the broadening. At high-momenta around 7 GeV/c the spectrum is clearly dominated by spectator contributions.

Especially interesting is the momentum region between the peak

and the high-momentum tail, because around 6 GeV/c altogether five partial spectra essentially contribute to the cross section, namely the participants and spectators from quasi-elastic "$\bar{1}\bar{1}$" scattering, the spectators from quasi-free inelastic "11^{*}s" reactions as well as the processes "21" and "22". The sum of the partial spectra reproduces the data also in this part of the spectrum remarkably well.

The shape of the 0^{o} spectrum from the *dC* reaction (Fig. 5) is similar to that of the 0^{o} spectra from *dp* and *dd* interactions, although there are details worth discussing. With the exception of the region below 4 GeV/c the cross section is again mainly due to the spectator contributions from quasi-free "11" interactions and, this is new compared to *dp* and *dd* interactions, also from the "12" process. Around 6 GeV/c even the "22" interaction considerably contributes to the cross section. This is exactly the region of the conspicious shoulder in the spectrum, the origin of which was controversely discussed in the literature [1,8,9,15]. Here we claimed that in the case of the *dp* reaction the shoulder is caused by particle production processes, which lead to different momentum dependences of the spectator contributions from the quasi elastic "$\bar{1}\bar{1}$s" and the quasi-free inelastic "11^{*}s" contributions. For a carbon target two further processes related to the structure of the target become relevant. These are the above mentioned "12s" and "22" contributions with spectrum shapes different from each other and from the "$\bar{1}\bar{1}$s" and "11^{*}s" contributions. Thus, the presence of the target nucleus makes an unambiguous explanation of the shoulder more difficult.

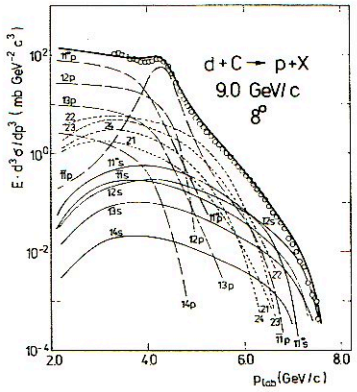

Fig.6. Invariant cross section versus laboratory momentum. Curves are labelled as in Fig.1. Data from [6].

Also the shape of the 8^{o} spectrum (Fig.6) is similar to that of the 8^{o} spectra from *dp* and *dd* interactions with the region below 4 GeV/c dominated by the quasi-free inelastic contributions. Compared to the *dp* and *pp* reactions, the quasi-elastic peak around 4.3 GeV/c is less pronounced. This is caused by the increasing relative yields from all the other processes with smooth momentum dependences in the peak region. The

high-momentum part above the quasi-elastic peak is not dominated by a single process but rather by a superposition of contributions comparable in magnitude.

As demonstrated in Fig.7, the applicability of the MOPS model is not restricted to inclusive measurements. Also the exclusive spectrum from the reaction $d(p,pp)n$ at 1 GeV is reproduced by the calculations. In this case particle production processes are excluded and the spectrum is dominated by quasi-elastic scattering.

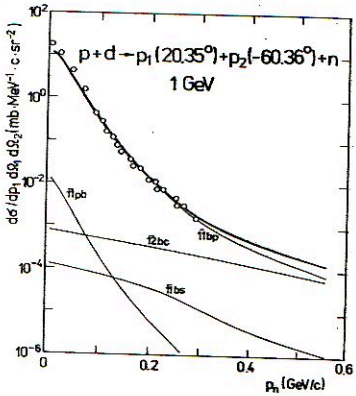

Fig.7.
Cross section versus laboratory momentum of the neutron. Curves are labelled as in Fig.1. Additionally, the letters b and c refer to the scattered beam particle and a particle arising from cluster decay, respectively. Data from [19].

The application of the model to dp, dd, and dC interactions shows that the overall features of inclusive and exclusive spectra are satisfactorily described by using conventional wave functions and taking particle production processes into account. With increasing target mass the properties of the target nucleus become more and more important for the correct description of the spectra. That means that, compared to deuteron-nucleus reactions, the investigation of dp interactions is the more convenient tool for extracting information on the DWF.

References

1. Ableev, V.G. et al.: Nucl. Phys. A393,491(1983)
2. Anderson, L. et al.: Phys. Rev. C28,1224(1983).
3. Zaporozhets, S.A. et al.: Proceedings of the 8the International Seminar on High Energy Physics Problems, Dubna 1986, JINR report D1,2-86-668,Vol.I,p.341
4. Perdrisat, C.F. et al: Phys. Rev.Lett. 59,2840(1987)
5. Punjabi, V. et al.: Phys.Rev. C39,608(1989)
6. Azhgirey, L.S. et al.: Yad.Fiz. 46,1134(1987)
7. Kobushkin, A.P., Vizireva, L.: J.Phys. G8,893(1982)
8. Braun, M.A., Vechernin, V.V.: Yad.Fiz. 43,1579(1986)

9. Ignatenko, M.A., Lykasov, G.I.: Yad.Fiz. 46,1080(1987)
10. Azhgirey, L.S. et al.: Yad.Fiz.: 46,1657(1987)
11. Azhgirey, L.S. et al.: Yad.Fiz. 48,87(1988)
12. Dolidze, M.G. et al.: Z.Phys.A-Atomic Nuclei 335,95(1990)
13. Dakhno, L.G., Nikonov, V.A.: Nucl.Phys. A491,652(1989)
14. Dakhno, L.G., Nikonov, V.A.: Yad.Fiz. 50,1757(1989)
15. Müller, H.: Z.Phys.A 336,103(1990)
Müller, H.: Z.Phys.A to be published
16. Shmakov, S.Yu. et al.: Comp. Phys. Commun. 54,125(1989)
17. Anisovich, V.V., Shekhter, V.M.: Nucl.Phys. B55,455(1973)
18. Lacombe, M. et al.: Phys.Lett. 101B,139(1981)
19. Aleshin, N.P. et al.: Phys.Lett. B237,29(1990)

ANALYSIS OF SPECTRA OF PROTONS EMITTED WITH LARGE TRANSVERSE MOMENTA IN FRAGMENTATION OF 9 GeV/c DEUTERONS ON PROTONS

L.S.Azhgirey, M.A.Ignatenko, S.V.Razin, G.D.Stoletov, I.K.Vzorov and N.P.Yudin*)

Joint Institute for Nuclear Research, Dubna
*) Moscow State University, Moscow

To obtain the information on the high-momentum components of the deuteron wave function, we made measurements of the momentum spectra of protons emitted at angles of 103, 139 and 157 mrad in fragmentation of 9 GeV/c-deuterons on hydrogen, deuterium and carbon nuclei. The measurements were made in Dubna at the JINR synchrophasotron by using a magnetic spectrometer. Experimental details and data analysis procedures have been previously reported [1]. The momentum spectra of protons produced by the deuteron fragmentation on the hydrogen nuclei are shown in figs. 1 - 3.

The protons detected at angles of 103, 139 and 157 mrad have the transverce momenta in the intervals of 0.45 - 0.78 , 0.60 - 1.01 and 0.66 - 1.12 GeV/c, respectively. Since the transverse momenta are invariant under Lorentz boosts along the beam direction, one can expect that the spectra measured contain the information on the deuteron wave function at distances characteristic of the transverse momenta achieved, i.e. 0.2 - 0.4 fm.

The diagrams of the impulse approximation, which describe the process of fragmentation of a deuteron on a nucleus, are displayed in fig. 4. Here B is an incident deuteron, A is a target nucleus, C is a detected proton, h and β include undetected nucleons and, possibly, pions; the letter labels also denote the corresponding four-momenta of particles taking part in the reaction. The diagram (a) describes the direct fragmentation process (stripping), and the diagrams (b) and (c) describe the hard scattering [2-4]. The stripping predominates in the

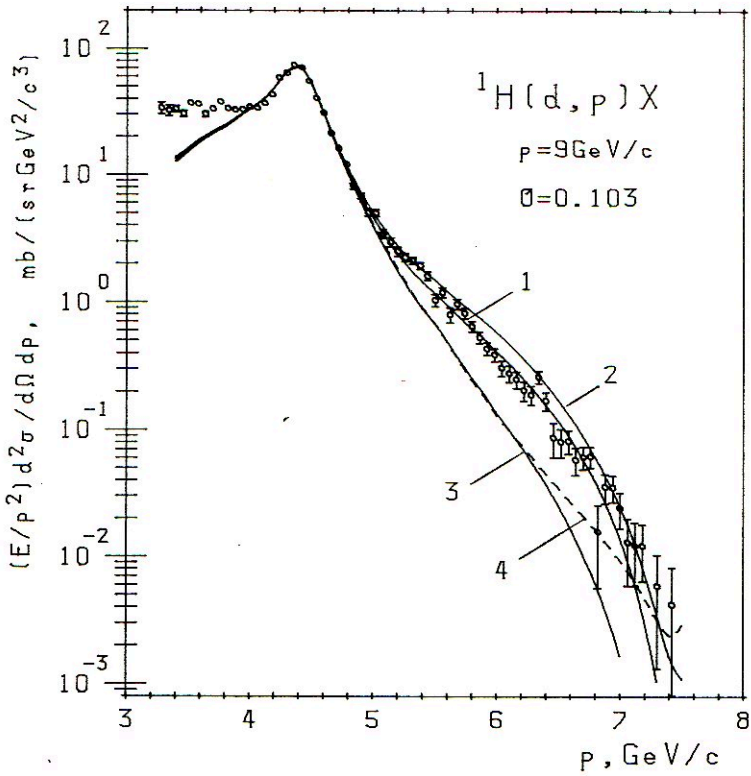

Fig.1. Momentum spectrum of protons detected at an angle of 103 mrad in the interactions of deuterons with the ^1H nuclei. The curves correspond to the calculation results with the following deuteron structure functions: 1 - for the Paris potential, 2 - for the Reid soft-core potential, 3 - for full model of the Bonn potential, 4 - for the relativistic momentum space of the Bonn potential.

region of very small angles of detection of fragmentation products, while the hard scattering manifest itself as these angles increase. For the channels with the identical final states (e.g., if A and h are protons and β is neutron) the interference of both mechanisms is also possible.

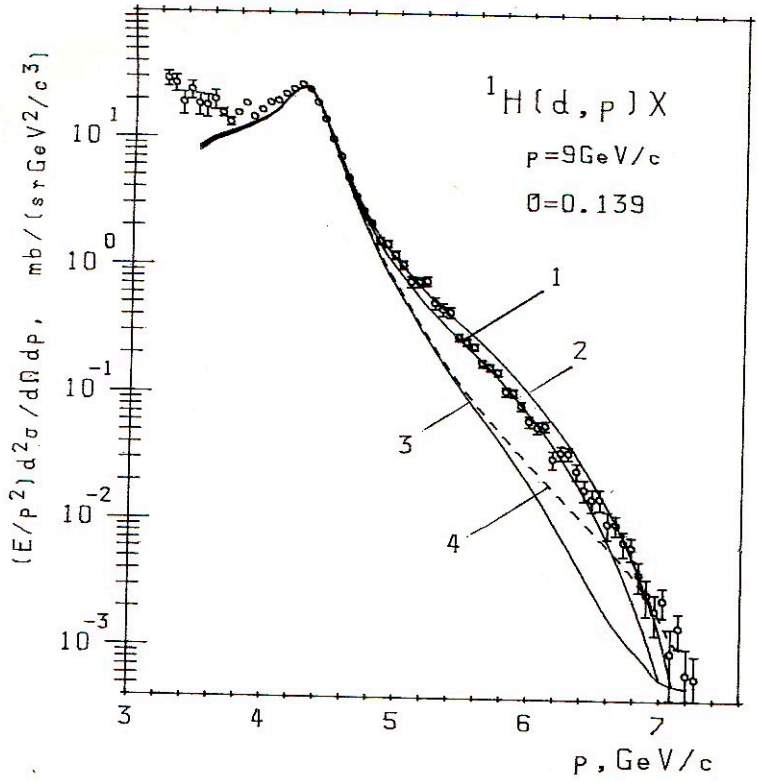

Fig.2. Same as in fig. 1, but for an angle of 139 mrad

It is convenient to describe the fragmentation of relativistic deuterons in the reference frame where the deuteron momentum is infinite (IMF). In favour of this the following reasons can be given. First, it is advisable to take account of the hadron structure and the nuclear structure in the hadron processes in equal measure. In the cases when the effects of the nucleon and nuclear structures are overlapping such a description is necessary. Secondly, in IMF because of the absence of Z-diagrams the effects of the structure of a relativistic system are naturally described by means of a wave function having a probabilistic meaning [5]. Thirdly, the ever increasing number of

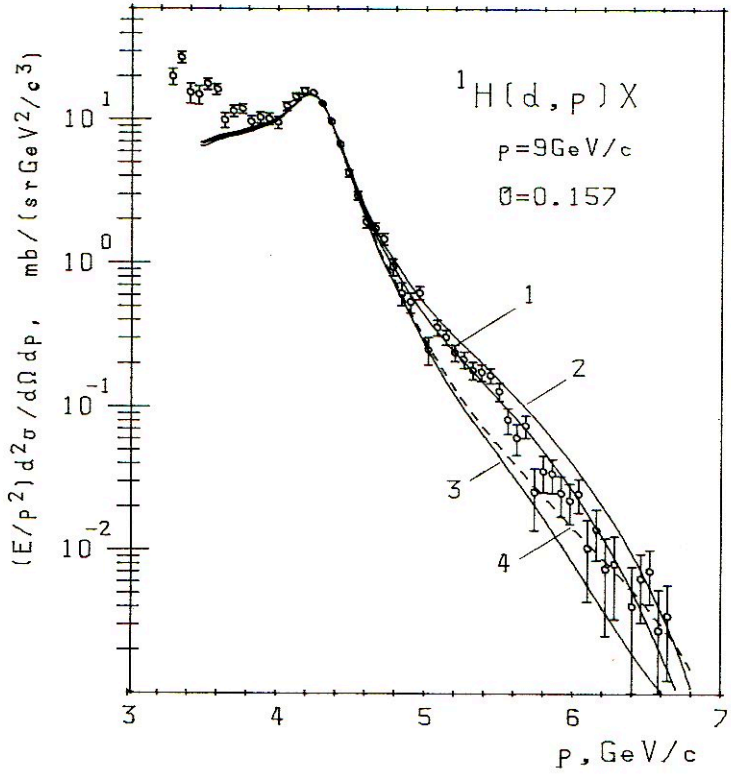

Fig.3. Same as in fig. 1, but for an angle of 157 mrad.

experiments with relativistic nuclear beams and the ambiguity of the transformation of the parameters characterizing the structure of a nucleus when going over from its rest frame to the laboratory one make the analysis of experimental data in IMF very desirable.

As it was previously shown [2-4], in IMF the invariant cross sections have the form

$$C_0\frac{d\sigma}{dC} = \frac{|\psi(y,l_T)|^2}{2(2\pi)^3 y}\,\frac{I(b_1,A)}{yI(B,A)}\,\sigma(b_1A\to h\beta), \qquad (1)$$

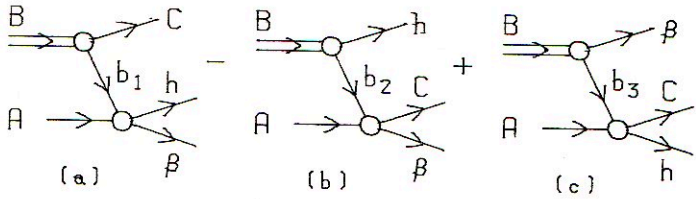

Fig.4. Diagrams of the impulse approximation describing the fragmentation of deuterons on nuclei. The notations are explained in the text

if the spectator particle is detected (the diagram (*a*) of fig. 4), and

$$C_0 \frac{d\sigma}{dC} = \frac{1}{(2\pi)^3} \int |\psi(y,l_T)|^2 \frac{I(b,A)}{yI(B,A)} \frac{dy dl_T}{2y(1-y)} \frac{C_0 d\sigma}{dC}(bA \to CX), \qquad (2)$$

if the particle experienced the hard scattering is detected (the diagrams (*b*) and (*c*) of fig. 4). Here $I(b,A)$, $I(B,A)$ are the invariant fluxes of the colliding particles, and arguments of the wave function $\psi(y,l_T)$ are the momentum fraction y of the fragment b in the nucleus B given by

$$y = (b_0 + b_3)/(B_0 + B_3), \qquad (3)$$

and the fragment transverse momentum l_T.

Occasionally, in place of the wave function $\psi(y,l_T)$ the structure function is introduced,

$$G_{b/B}(y,l_T) = \frac{1}{2(2\pi)^3} \frac{|\psi(y,l_T)|^2}{y(1-y)}, \qquad (4)$$

that signifies the probability of finding a constituent of type b in the nucleus B with a fractional momentum y and a transverse momentum l_T.

The form of a wave function $\psi(y,l_T)$ depends essentially on the type of dynamics, i.e. on the way the 10 generators $P^\mu = (P^0, \mathbf{P})$,

$M^{\mu\nu}$ = (**J**, **K**) of the Poincaré group are split into kinematical and dynamical generators, or Hamiltonians [6]. An action of the kinematical generators on state vectors does not depend on an interaction, on the contrary, an action of Hamiltonians depends essentially on an interaction.

In the most familiar time instant dynamics (usual dynamics) the kinematical generators are the momentum operator **P** and the angular momentum operator **J**, and Hamiltonians are the energy operator P^0 and the Lorentz boost operator **K**. A special feature of the time instant dynamics is the inseparability of the variables that characterize the motion of a nucleus globally from the inner variables that describe the motion of constituents. In consequence of this the transformation of the wave function when going over from one reference frame to another, e.g., from the nucleus rest frame to IMF, is nontrivial. Therefore, it is advisable to construct the wave function $\psi(y,l_T)$ in the time instant dynamics independently of their form in the deuteron rest frame.

It was shown in ref. [7] that $\psi(y,l_T)$ should in general depend on six invariant functions (and on two functions defining *S*- and *D*-waves in the nonrelativistic case). Such the rather complicated parameterization of a wave function in ref. [7] is connected directly with the fact that in the time instant dynamics the direction of the Lorentz boost in IMF has to be taken into account when the wave function is transformed to IMF.

A considerably simpler form has a wave function in the light front dynamics. Here the kinematical generators of the Poincaré group are the following operators (or their combinations):

$$P_+ = P_0 + P_3 \ , \ P_1 \ , \ P_2 \ , \ E_r = \frac{1}{2}\,(K_r + \varepsilon_{rs}J_s) \ , \ K_3 \ , \ J_3 \ . \qquad (5)$$

Accordingly, Hamiltonians are

$$P_- = P_0 - P_3 \ , \quad F_r = K_r - \varepsilon_{rs}J_s \ . \qquad (5a)$$

Here $r,s = 1,2$, ε_{rs} is the antisymmetric tensor: $\varepsilon_{12} = -\varepsilon_{21} = 1$. The kinematical operators form the subgroup of the Poincaré group and leave the hyperplane $t - z = 0$ invariant. A remarkable feature of this

dynamics for the composite system with a finite number of constituents is that the variables ξ, $\mathbf{k}_T$ describing the inner motion uncoupled from the motion of the system as a whole. In the nonrelativistic approximation the light front dynamics coincides with the usual one, and this enables us in describing the deuteron to make use of the usual non-relativistic potentials, assuming that these potentials also correspond to the reality in the region of relativistic momenta.

Within the framework of the light front dynamics [8-11] there is the following relationship between the structure function $G_{b/B}(y,\mathbf{l}_T)$ and the wave function $\phi(\mathbf{k})$ of the deuteron in its rest frame:

$$G_{b/B}(y,\mathbf{l}_T) = k_0|\phi(\mathbf{k})|^2/[2y(1-y)] \ , \qquad (6)$$

where

$$k_0^2 = (m^2 + \mathbf{l}_T^2)/[4y(1-y)], \quad \mathbf{k}_T = \mathbf{l}_T, \quad k_0^2 = m^2 + \mathbf{k}^2,$$

and m is the nucleon mass.

With unpolarized deuteron beams and in case the polarization of nucleons produced is not of interest, the equations for differential cross sections are expected to be of the form similar to that for spinless particles. The more detailed account of particle spins shows [12-14] that the structure function in a first approximation can be written in the form

$$G(y,\mathbf{l}_T) = G_S(y,\mathbf{l}_T) + G_D(y,\mathbf{l}_T) \ , \qquad (7)$$

where $G_{S,D}$ are the "partial" structure functions connected with the wave functions of S- and D-states of deuteron by eq. (4).

The mechanism presented in fig. 4 implies a possibility of the interference of the channels with the identical final states. This possibility is realized if at the low vertex of diagrams (*a*), (*b*) and (*c*) elastic np, charge exchange np and elastic pp scatterings take place, respectively. For example, for the diagrams (*a*) and (*b*) the interference term reads

$$C_0\frac{d\sigma}{dC} = -\frac{2}{\pi}\int \left[y_1/(1-y_1)\right]^{1/2}\left\{ G_S^{1/2}(y_1,l_{1T})\ G_S^{1/2}(y_2,l_{2T}) \right. \qquad (8)$$

$$\left. + \zeta\ G_D^{1/2}(y_1,l_{1T})\ G_D^{1/2}(y_2,l_{2T}) \right\} \left[y_2/(1-y_2)\right]^{1/2}$$

$$* \frac{I(b_1,A)\ I(b_2,A)}{I(B,A)} \left(\frac{d\sigma}{dt_1'}\right)^{1/2} \left(\frac{d\sigma}{dt_2'}\right)^{1/2} \frac{d\beta\ dC}{\beta_0 C_0}\ \delta^4(B+A-\beta-C-h),$$

where y_1,l_{1T} and y_2,l_{2T} are the above defined variables y,l_T relating to the diagrams (a) and (b), and

$$\zeta = P_2\left(\mathbf{k}_1\cdot\mathbf{k}_2\ /\ |\mathbf{k}_1|\cdot|\mathbf{k}_2| \right), \qquad (9)$$

P_2 is the Legendre polynomial, t' is the squared four-momentum transferred in the low vertexes of these diagrams. Similar formulae also take place for the interference terms of the diagrams (*a*) and (*c*), (*b*) and (*c*).

In the process of relativistic deuteron fragmentation under consideration, independently of the form of the dynamics used, off-mass-shell effects take place. In IMF and in the case of the time instant dynamics these effects manifest themselves as the necessity of introducing "spurions" [7], and, in consequence, of introducing vertexes to describe their production and absorption. In the light front dynamics the off-mass-shell effects have to manifest themselves in such a manner that the operator P_- for a virtual particle should differ from the "physical" one describing a free particle.

To take the off-shell nature of the particle b into account the analytic continuations of $d\sigma(s',t')/dt'$ parameterizations to values s', t' defined at $l^2 \neq m^2$ have been used in our calculations.

The contributions of processes $pp \rightarrow pp$, $np \rightarrow pn$, $Np \rightarrow p\Delta$, $Np \rightarrow pN\pi$ (up to values of the invariant mass of the $N\pi$ system of 1.5 GeV/c^2) in the low vertex of the hard scattering diagram have been taken into account when calculating the differential cross section of the reaction $^1H(d,p)X$. The parameterizations of the differential cross sections for the above processes are given in ref. [15].

A procedure of the evaluation of the contributions of diagrams

with the excitation of the virtual pions [16-18] is described in detail in ref. [19].

The analysis of the experimental data on the reaction $^1H(d,p)X$ at 9 GeV/c has been carried out within the framework of the light front dynamics making use of the deuteron structure functions which correspond to the Paris [20], Reid soft-core [21], and two versions of Bonn [22] potentials of the *NN* interaction.

The contributions of various mechanisms at 157 mrad are shown in fig. 5. They have been calculated with the deuteron structure function for the Paris potential (the explicit form of a structure function does not matter for a qualitative comparison of different contributions). A comparison of these results with the ones for 103 mrad, where they behave qualitatively similarly, reduces to the following. At first, the major contribution to the spectra is made by the elastic *pp* scattering process; for the spectrum parts shown it amounts to about 60%. The contributions of the inelastic scatterings concentrate at smaller momenta, on the left of the spectrum maxima; and on the whole they amount to approximately 20% and 30% for 103 and 157 mrad, respectively. The contributions of the diagrams with the production of the virtual pions are distributed more uniformly over spectra, and on the whole they amount to roughly 15% and 5% for 103 and 157 mrad, respectively. The remaining - 5% areas of the spectra are accounted for by the stripping mechanism and its interference with the elastic and inelastic scatterings, the interference being about 15% of the stripping.

A comparatively small summed contribution of the stripping is due to the emission of the protons at the angles considered requiring large transverse momenta ($\geq$ 0.5 GeV/c). The probability of finding nucleons with such large momenta in the deuteron is small, and decreases sharply as the momenta grow. Thus the spectrum maxima are conditioned by the hard scattering mechanism. As the upper bounds of the spectra are approached, the contributions of the stripping and hard scattering mechanisms became comparable owing to a more steep momentum dependence of the hard scattering mechanism.

Although the summed contribution of the spectator protons is relatively small, its influence on the shape of the spectra is quite appreciable, because from the momenta close to 5.3 GeV/c it becomes comparable with the elastic scattering contribution. The relative

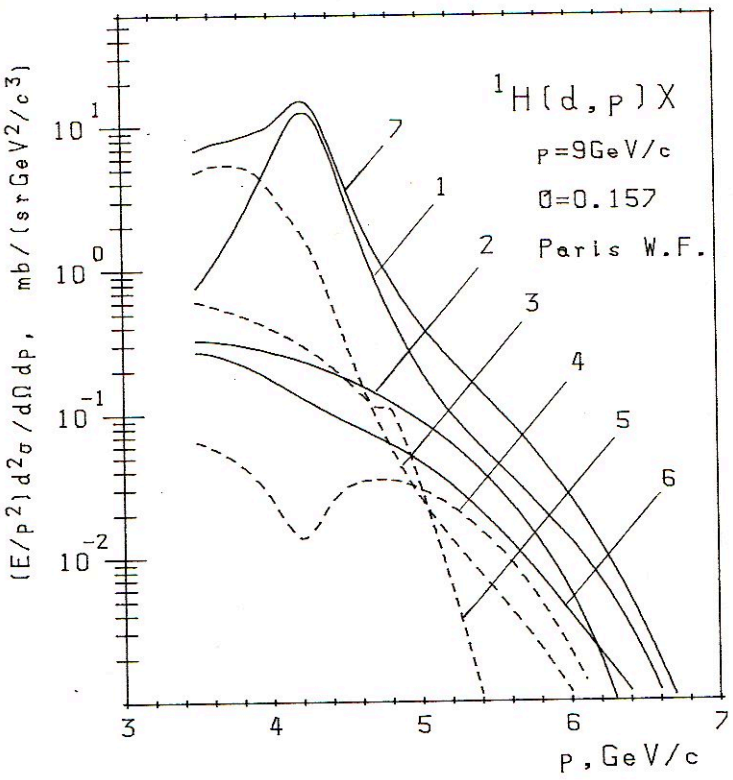

Fig.5. Contributions of various mechanisms to the invariant differential cross section of the $^1H(d,p)X$ reaction at 9 GeV/c and a detection angle of 157 mrad, calculated with the deuteron structure function for the Paris potential. The curves correspond to the following mechanisms: 1 - diagram (*c*) of fig. 4 with the elastic *pp* scattering at low vertex, 2 - stripping, 3 - diagram (*c*) of fig. 4 with inelastic interactions at low vertex, 4 - interference of the amplitudes of diagrams of fig. 4, 5 - diagram with the excitation and absorption of a virtual pion [19], 6 - diagram with the excitation and rescattering of a virtual pion, 7 - sum of all the contributions.

contribution of the spectator mechanism is more at the smaller angle.

The comparability of the contributions of both mechanisms in certain parts of the spectra of protons emitted with large transverse momenta provides an additional opportunity to explore the short-distance behaviour of the deuteron wave function, since the spectator contribution is directly proportional to the deuteron single-nucleon momentum density.

The calculated momentum spectra of protons emitted at 103, 139, and 157 mrad in the reaction $^1H(d,p)X$ at 9 GeV/c are compared with the experimental data in figs. 1 - 3. The calculations have been carried out, taking account of all the above mechanisms - the elastic and inelastic interactions of deuteron nucleons with the target proton, the stripping, the interference effects, the production of the virtual pions - for the deuteron structure functions corresponding to the Paris [20] (curves 1 in figs. 1 - 3), Reid soft-core [21] (curves 2), and Bonn [22] potentials. In the last case we have used both the wave function of the full model (table 11 of ref. [22], the results are shown with curves 3 in figs. 1 - 3) and the wave function of the relativistic momentum space (table 13 of ref. [22], curves 4).

First of all it should be noted that the spectra of protons emitted with large transverse momenta have proved to be rather sensitive to the high-momentum behaviour of the deuteron wave function. We conceive that the information which can be extracted from the deuteron-nucleus collisions in combination with the results of probing deuterons by electrons allows a more complete picture of the deuteron structure to be obtained.

In the present analysis, to our mind, all the most significant mechanisms of the $^1H(d,p)X$ reaction have been taken into account. The results of calculations with the different deuteron wave functions coincide practically in the region of the proton spectrum maxima, and differ appreciably in the high-momentum parts of these spectra where the short range behavior of the wave function is important. In this region, however, the deuteron wave function is the least explored, and its application for describing the deuteron structure, as a matter of fact, seems to be problematic. Our data speak in favour of the wave function of the Paris potential. If this result is no mere chance it can be regarded as a suggestion that nucleons in deuteron appear to keep their individuality up to relative momenta ~ 1 GeV/c.

The authors are most grateful to Prof. M.G.Mescheryakov for valuable discussions.

References

1. Azhgirey L.S., Vzorov I.K., Zhmyrov V.N., Ivanov V.V., Ignatenko M.A., Kuznetsov A.S., Kozhevnikov Yu.A., Mulas E., Razin S.V., Stoletov G.D. and Yudin N.P. Yad.Fiz., 1987, v.46, p.1134.
2. Schmidt I.A. and Blankenbecler R. Phys.Rev.D, 1977, v.15, p.3321.
3. Chemtob M. Nucl.Phys., 1979, v.A314, p.387.
4. Wong Ch.-Y. and Blankenbecler R. Phys.Rev.C, 1980, v.22, p.2433.
5. Weinberg S., Phys.Rev., 1966, v.150, p.1313.
6. Dirak P.A.M. Rev.Mod.Phys., 1949, v.21, p.392.
7. Karmanov V.A., Particles and Nuclei, 1988, v.19, p.525.
8. Terent'ev M.V. Yad.Fiz., 1976, v.24, p.207.
9. Berestetski V.B. and Terent'ev M.V. Yad.Fiz., 1976, v.24, p.1044.
10. Leutwyler H. and Stern J. Ann.Phys., 1978, v.112, p.94.
11. Frankfurt L.L. and Strikman M.I. Phys.Rep., 1981, v.76, p.215.
12. Melosh J. Phys.Rev.D, 1974, v.9, p.1095.
13. Kondratyuk L.A. and Terent'ev M.V. Yad.Fiz., 1980, v.31, p.1087.
14. Chung P.L., Coester F., Keister B.D. and Polyzou W.N. Phys.Rev.C, 1988, v.37, p.2000.
15. Azhgirey L.S., Razin S.V. and Yudin N.P. Yad.Fiz., 1987, v.46, p.1657.
16. Braun M.A. and Vechernin V.V. Yad.Fiz., 1986, v.43, p.1579.
17. Amelin N.S. and Lykasov G.I. Yad.Fiz., 1978, v.28, p.1466.
18. Ignatenko M.A. and Lykasov G.I. Yad.Fiz., 1987, v.46, p.1080.
19. Azhgirey L.S., Ignatenko M.A., Razin S.V. and Yudin N.P. Yad.Fiz., 1988, v.48, p.87.
20. Lacombe M., Loiseau B., Vinh Mau R, Cote J., Pires P. and de Tourreil, R. Phys.Rev.C, 1980, v.21, p.861; Phys.Lett., 1981, v.101B, p.139.
21. Reid R.V., Jr. Ann. of Phys., 1968, v. 50, p.411; Alberi G., Rosa L.P. and Thome Z.D. Phys.Rev.Lett., 1975, v.34, p.503.
22. Machleidt R., Holinde K. and Elster Ch. Phys.Reports, 1987, v.149, p.1.

STUDY OF THE DEUTERON STRUCTURE AT SMALL DISTANCES BY FRAGMENTATION OF UNPOLARIZED AND POLARIZED DEUTERONS

B.Kuehn
Joint Institute for Nuclear Research
Laboratory of High Energies, Dubna 141980

1. Introduction

In this talk we deal with the question what information on the deuteron structure can be obtained by the study of the fragmentation of unpolarized and polarized deuterons at relativistic energies. Special attention will be paid to the structure at small distances or at large internal momenta. This is the region, where the nucleons overlapp and where we can hope that quark degrees of freedom will reveal themselves. At the energies of the Dubna Synchrophasotron we are able to reach internal momenta of $k = 0.88$ GeV/c measured in light cone variables.

A typical fragmentation experiment is the measurement of the spectrum of spectator protons emitted at angles near zero degrees. If one assumes that the impuls approximation is valid the measured spectrum directly can be related to the momentum distribution inside the deuteron, i.e. to the deuteron wave function in momentum representation. If the incoming deuterons are unpolarized the result of such an experiment is the probability density $\Psi^2(k) = v^2(k) + w^2(k)$, that means the sum of the S- and D-state densities. The measurement of polarization observables allows one to obtain the D/S-state ratio at any internal momentum. In this way the existing uncertainties concerning the D-state contribution at distances smaller than 1.5 fm and especially inside the core can be overcome (see for instance Fig.1). Moreover it should be possible to achieve concrete information on the spin structure in the region of overlapping bags or in other words of the assumed 6-quark state.

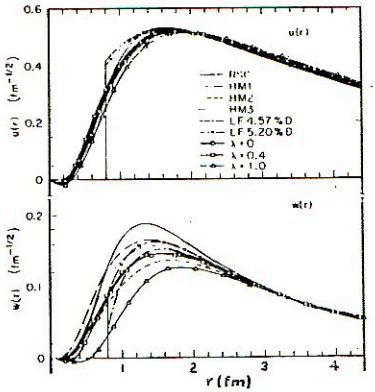

Fig.1. Uncertainties in the deuteron wave function connected with the choice of different potential models. Figure is taken from /1/.

In this talk the results of the fragmentation measurements with unpolarized deuterons will be shortly quoted. Then it will be shown how the tensor analysing power T_{20} and the polatization transfer coefficient $\bar{\alpha}$ are related to the deuteron wave function and especially to its S- and D-state contribution. After the description of the experimental methods the results of the T_{20} and measurements will be shown and described. The crucial question of this investigations is, whether the impulse approximation without restrictions can be applied to the fragmentation process. Therefore it is necessary to discuss the role of different reaction mechanisms. From this it follows that additional experiments are to be performed, which exclude mechanisms beside the quasielastic scattering or at least determine their contribution. Proposals for such experiments will be presented.

This talk intends to give a review of the work which was done in this field at Dubna. The following contributions will present and discuss the different experiments and theoretical investigations in more detail.

2. Fragmentation of Unpolarized Deuterons

Inclusive measurements of proton spectra from the fragmentation of unpolarized deuterons were performed at the magnetic spectrometers ALPHA and MASPIC /2,3/ at the Dubna Synchrophasotron. The angles were 0° and 8° respectively. The incident deuteron momentum was 9 GeV/c. Both groups succeeded to measure the spectra almost up to the kinematic limit at $k = 0.88$ GeV/c (Fig. 8a). The most interesting feature of these spectra is the enhancement of the cross section in the region $0.3<k<0.6$ GeV/c in comparison to the predictions from the conventional phenomenological potentials. This enhancement was interpreted as a peculiarity of the deuteron wave function caused may be by a 6-quark state /4/. But nowadays it seems more likely to be a consequence of contributions to the reaction mechanism apart from the quasifree scattering which are not described by the impulse approximation. This problem will be discussed later in this talk.

3. Fragmentation of Polarized Deuterons

For a more detailed analysis of the reaction mechanism and for more complete information on the wave function polarization experiments are suitable. At the Dubna Synchrophasotron such experiments are possible using the tensor and vector polarized deuteron beams with momenta up to 9 GeV/c.

The polarization observables, which could be measured up to now, are the tensor analysing power T_{20} and the polarization transfer κ from vector polarized deuterons to the spectator protons. Both quantities were measured as a function of internal momentum k. Formulae for these observables were derived by several authors in different approaches /5/. The author of the present review tried to make the connection between the wave function and the polarization effects as anschaulich as possible.

3.1. The Deuteron Wave Function and the Deformation of the Deuteron

The observed polarization effects are caused by the splitting of the wave function into the different magnetic substates of the deuteron. The following functions of the magnetic substates with $M_J = \pm 1$ and $M_J = 0$ (J spin of the deuteron) were derived from the Schroedinger equation with a potential including tensor forces (see for instance /6/).

$$\Psi_{deut} = \Phi_S + \Phi_D \tag{1}$$

$M_J = \pm 1$

$$\Phi_S = \frac{v(r)}{r} Y_0^0 \mathcal{S}_1^1 = \frac{v(r)}{\sqrt{4\pi}\, r} \mathcal{S}_1^1 \tag{2}$$

$$\Phi_D = \frac{w(r)}{r}\left[\sqrt{\frac{6}{10}} Y_2^{\pm 2} \mathcal{S}_1^{\mp 1} - \sqrt{\frac{3}{10}} Y_2^{\pm 1} \mathcal{S}_1^0 + \sqrt{\frac{1}{10}} Y_2^0 \mathcal{S}_1^{\pm 1}\right] \tag{3}$$

$M_J = 0$

$$\Phi_S = \frac{v(r)}{r} Y_0^0 \mathcal{S}_1^0 = \frac{v(r)}{\sqrt{4\pi}\, r} \mathcal{S}_1^0 \tag{4}$$

$$\Phi_D = \frac{w(r)}{r}\left[-\sqrt{\frac{3}{10}} Y_2^{-1} \mathcal{S}_1^1 - \sqrt{\frac{4}{10}} Y_2^0 \mathcal{S}_1^0 - \sqrt{\frac{3}{10}} Y_2^1 \mathcal{S}_1^{-1}\right] \tag{5}$$

Here v(r) and w(r) are the radial wave functions for the S- and D-state respectively, determined by the NN-potential for which the Schroedinger equation is solved. The $Y_L^{M_L}$ are the spherical harmonics and the $\mathcal{S}_S^{M_S}$ the spin functions of the two-nucleon system in the triplet state with S=1 and $M_S = \pm 1, 0$. The numerical factors are Clebsch-Gordon coefficients. The combination of the spin and orbital momentum vectors for the different substates are shown in Fig.2.

The probability density of the deuteron as function of the internal coordinates r and θ (θ polarcoordinate measured from the z-axis is defined by the product

$$\Psi^* \Psi = (\Phi_S^* + \Phi_D^*)(\Phi_S + \Phi_D). \tag{6}$$

Due to the relation $\mathcal{S}_s^{m_{si}^*} \mathcal{S}_s^{m_{sj}} = \delta_{ij}$, following from the definition of the spin functions beside the squares of the $Y_L^{M_L}$ only one interference term survives: the term with $v(r)w(r)Y_2^0 Y_0^0$.

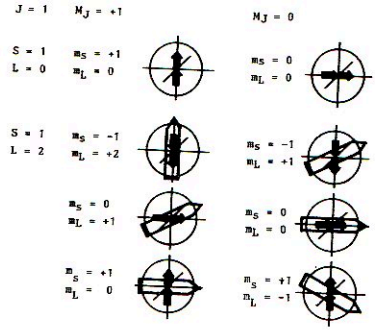

Fig.2. Magnetic substates in the deuteron for $M_y = +1$ and $M_y = 0$.

But this term is essential for the deformation of the deuteron and for the polarization effects.

Using the explicit expressions for the $Y_L^{M_L}(r,\theta)$ we obtain the following probability densities for the pole ($\theta = 0$) and the equator ($\theta = \pi/2$) of the deuteron:

$$M_J=+1 \quad \theta = 0 \qquad \Psi^*\Psi = \frac{1}{4\pi r^2}\left[v^2(r) + w^2(r)(0+0+0.5) + \sqrt{2}\,v(r)w(r)\right] \tag{7}$$

$$\theta = \frac{\pi}{2} \qquad \Psi^*\Psi = \frac{1}{4\pi r^2}\left[v^2(r) + w^2(r)(1.125+0+0.125) - \sqrt{\frac{1}{2}}\,v(r)w(r)\right]. \tag{8}$$

As w^2 can be assumed to be small in comparison to v^2 it follows from equations (7) and (8) that the density of the deuteron in the considered state with $M_J = +1$ in the axial direction is larger than in the equatorial. That means in this state the deformation of the deuteron is prolate (Fig.3a).

For the other substate we obtain the following probability densities:

$$M_J = 0 \quad \theta = 0 \qquad \Psi^*\Psi = \frac{1}{4\pi r^2}\left[v^2(r) + w^2(r)(2+0) - 2\sqrt{2}\,v(r)w(r)\right] \tag{9}$$

$$\theta = \frac{\pi}{2} \qquad \Psi^*\Psi = \frac{1}{4\pi r^2}\left[v^2(r) + w^2(r)(0.5+0) + \sqrt{2}\,v(r)w(r)\right]. \tag{10}$$

Due to the same considerations as above, these formulae indicate that in the state $M_J = 0$ the deuteron has an oblate shape (Fig.3b).

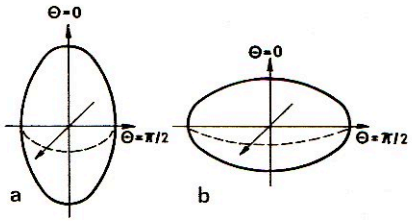

Fig.3. Deformation of the deuteron in the magnetic substates a) $M_y = \pm 1$ and b) $M_y = 0$.

3.2. Deuteron Wave Function and Tensor Analysing Power

The tensor analysing power T_{20} of the fragmentation process is defined by

$$T_{20} = \sqrt{2}\,\frac{\sigma\uparrow - \sigma_0}{\sigma_0} \quad . \tag{11}$$

Here $\sigma\uparrow$ is the cross section for the tensor polarized deuteron, for instance in the $M_J = 0$ state; and σ_0, the cross section for the unpolarized deuteron. Figure 4 demonstrates the situation. The cross sections are given by the radial density distributions for the two polarization states. σ_0 is proportional to the average of the probability density in the scattering plane ($\theta = \pi/2$) for the three possible orientations of the deuteron spin $M_J = \pm 1, 0$. This gives according to the equations (8) and (10)

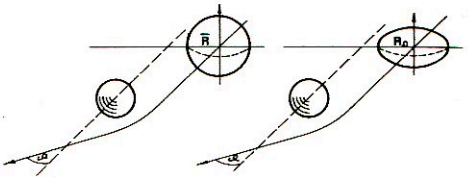

Fig.4. Fragmentation of unpolarized and tensor polarized deuterons.

(The contributions from $M_J = +1$ and -1 are equal. Therefore the value from (8) has to be taken twice.)

$$\sigma_0 = \frac{1}{3\cdot 4\pi r^2}\left[3v^2(r) + w^2(r)(1.25 + 1.25 + 0.5) + v(r)w(r)(\sqrt{2} - 2\sqrt{\tfrac{1}{2}})\right]$$

$$= \frac{1}{4\pi r^2}\left[v^2(r) + w^2(r)\right]. \qquad (12)$$

For the cross section of the tensorpolarized deuteron ($M_J = 0$) one has to take the expression (10). (10) and (12) inserted into equation (11) give the formula for T_{20}

$$T_{20} = \frac{1}{\sqrt{2}} \frac{2\sqrt{2}\,v(r)w(r) - w^2(r)}{v^2(r) + w^2(r)} . \qquad (13)$$

This equation can be expressed also in the form

$$T_{20} = \frac{1}{\sqrt{2}} \frac{2\sqrt{2}\,x - x^2}{1 + x^2}, \qquad (14)$$

where $x = w(r) / v(r)$ is the D- to S-state ratio, taken at the radius r. By these means one obtains from the measurement of T_{20} the D/S state ratio for each distance r. T_{20} reaches for some special x the following values:

node of w(r)	$x = 0$	$T_{20} = 0$
node of v(r)	$x = \infty$	$T_{20} = -1/\sqrt{2}$
for	$x = -\sqrt{2}$	$T_{20} = -\sqrt{2}$. (15)

The last value is the minimum which can be reached. Note, that this minimum is not connected with a node but with a certain w/v-ratio. This ratio can occur in the wave function derived from any potential. Therefore the minimum value doesn't depend on the potential model. But the radius, where it appears, depends on the potential.

3.3. Deuteron Wave Function and the Polarization Transfer Coefficient

The process of the fragmentation of a vector polarized deuteron is sketched in Fig.5. The spins of the protons emerging from this process are oriented according to their orientation inside the deuteron (spectator mechanism assumed). The polarization of them is

$$P_{zprot} = \frac{N_+ - N_-}{N_+ + N_-} , \qquad (16)$$

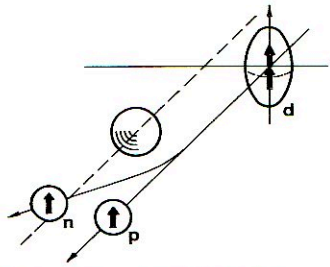

Fig.5. Fragmentation of a vectorpolarized deuteron.

where $N_{+(-)}$ are the probabilities with which the protons of the different orientations appear. These probabilities are proportional to the weight of the substate with the given proton orientation and to the probability of fragmentation of these substates (according to their probability density in the scattering plane). In the numerator of p_{zprot} N_+ and N_- have to be taken with the signs + or - according to the spins up and down in the given substate. In the denominator we have to sum up all contributions with positive sign.

We assume a beam with aligned deuterons, that means all particles are oriented according to $M_J = +1$. For this case the signs and probabilities of the proton orientations are shown in (17).

Substate		Wave function	Contribution to Proton Orientation
$J = 1$ $M_J = +1$ $S = 1$ $m_S = +1$ $L = 0$ $m_L = 0$		$w^2 Y_0^{02}$	+1
$S = 1$ $m_S = -1$ $L = 2$ $m_L = +2$		$\frac{6}{10} w^2 Y_2^{2\ 2}$	-1
$m_S = 0$ $m_L = +1$		$\frac{3}{10} w^2 Y_2^{12}$	0
$m_S = +1$ $m_L = 0$		$\frac{1}{10} w^2 Y_2^{02}$	+1
$m_S = +1$, $m_S = +1$ $m_L = 0$, $m_L = 0$		$\frac{2}{\sqrt{10}} vw\ Y_0^0\ Y_2^0$	+1

(17)

Derivation of the polarization transfer coefficient κ, contribution of the substates to the proton polarization.

Using the spherical functions in their explicit form for $\theta = \pi/2$ and taking into account the different signs of the contributions we obtain similar as in the case of equ.(8)

$$N_+ - N_- = \frac{1}{4\pi r^2}\left[v^2(r) - w^2(r) - \frac{1}{\sqrt{2}} v(r)w(r)\right]. \qquad (18)$$

The denominator in (16) is simply the probability density in the scattering plane of the $M_J = +1$ state, already given in equ.(8).

Expressing p_{zprot} by (18) and (8) we arrive at the formula for the polarization transfer

$$\alpha_{norm} = p_{zprot} = \frac{v^2(r) - w^2(r) - 1/\sqrt{2}\, vw}{v^2(r) + \frac{5}{4}w^2(r) - \frac{1}{\sqrt{2}} vw} =$$

$$= \frac{v^2(r) - w^2(r) - 1/\sqrt{2}\, vw}{(v^2(r) + w^2(r))\left[1 - \frac{1}{2\sqrt{2}} T_{20}\right]}. \qquad (19)$$

The transfer coefficient was denoted here as α_{norm} because it is normalized to a beam with vector polarization $p_{zdeut} = +1$ and with a tensor polarization $p_{zz} = +1$. The second version of (19) is obtained from the first one by inserting equ.(13) into (19).

If the beam has arbitrary contributions of vector and tensor polarization another formula for α must be derived:

$$\alpha_{exp} = \frac{p_{zdeut}(v^2(r) - w^2(r) - 1/\sqrt{2}\, v(r)w(r))}{(v^2(r) + w^2(r))\left[1 - \frac{1}{2}\rho_{20}T_{20}\right]}. \qquad (20)$$

Here p_{zdeut} is the vector and $\rho_{20} = 1/\sqrt{2}\, p_{zz}$ the tensor polarization of the beam. α_{exp} and α_{norm} are related by the equation

$$\alpha_{norm} = \frac{\alpha_{exp}}{p_{zdeut}} \cdot \frac{1 - 1/2\, \rho_{20} T_{20}}{1 - \frac{1}{2\sqrt{2}} T_{20}}. \qquad (21)$$

In the actual talk at the workshop another version of the formula for α was presented. This version was based on the special assumption of $\rho_{20} = 0$. In this case the second braket in the denominator of (19) reduces to unity.

Equation (19) is that relation one wants to have for comparison with theoretical models and equ. (20) and (21) take into account the real situation in experiment. In the report of C.F.Perdrisat on the α measurement at Saclay formula (19) was used[7]. The discrepancy between the "Dubna" and the "Saclay" formulae has drawn the attention of the author to the necessity to take into account the tensor polarization of the beam.*) Indeed, the fully aligned deute-

*) The author thankfully acknowledges discussions with C.F.Perdrisat which helped to recognize these problems.

ron has

$$p_z = \frac{M_+ - M_-}{M_+ + M_- + M_o} = 1 \quad \text{and} \quad p_{zz} = \frac{M_+ + M_- - 2M_o}{M_+ + M_- + M_o} = 1 \qquad (22)$$

with $M_- = M_o = 0$. This is the most advantageous condition for measuring $\mathcal{A}$. Earlier at Dubna and at Saclay[8] it was assumed that one should work with a pure vector polarized beam. In this case $p_{zz} = 0$ or $M_+ + M_- - 2M_o = 0$. Is $M_- = 0$ we have $M_+ = 2M_o$. This inserted into (22) gives $p_z = 2/3$ as maximum value of p_z. And the beam contains a considerable population of the $M_J = 0$ state. This must be taken into account in calculating the denominator of equ.(16), as is demonstrated in Fig.6.

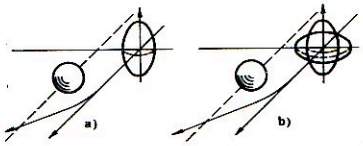

Fig. 6.Fragmentation cross section for deuterons
a) in pure $M_y=+1$ state(aligned deuterons)
b) in mixed state $M_y=+1$, $M_y=0$ according to $p_{zz}=0$.

For the discussion we need only equ.(19). In terms of $x = w/v$ it reads

$$\mathcal{A}_{norm} = \frac{1 - x^2 - 1/\sqrt{2}\, x}{1 + \frac{5}{4} x^2 - 1/\sqrt{2}\, x} \quad . \qquad (23)$$

$\mathcal{A}_{norm}$ reaches values for

node of $w(r)$ $\quad x = 0 \quad \mathcal{A} = +1$
node of $v(r)$ $\quad x = \infty \quad \mathcal{A} = -4/5$. $\qquad (24)$

For the sake of Anschaulichkeit the formulæ for T_{20} and $\mathcal{A}$ were derived in configuration space. It can be shown that their structures are not changed by the transition to momentum space. That is quite naturally because these equations arose from the contributions of the substates in the deuteron expressed by the spherical harmonics and the Clebsch-Gordon coefficients. The radial or momentum dependence of the wave function is not essen-

tial in this context. The expressions for v and w of course change by the transitions from one presentation to the other.

At relativistic energies one has to prefer a relativistic presentation of the wave function. This can be done by the transition from the variable q, the internal momentum in the deuteron c.m. frame, to the variable k measured in the infinite momentum frame, called the light cone variable (see for instance /9/ and the contribution of V.A.Karmanov to this workshop). By this transition the formulae for T_{20} and $\mathcal{A}$ are also not changed.

4. Measurement of T_{20} and $\mathcal{A}$ in the Fragmentation of Polarized Relativistic Deuterons

The experimental setups for these measurements are shown in Fig.7 /10/. The fragmentation of the incoming deuterons was performed at the cross over F3 at the beam line VP1. The fragmentation target consisted of carbon or polyethylen. As the cross sections for increasing internal momenta are rapidly decreasing, the thickness of the target had to be chosen up to 30 cm.

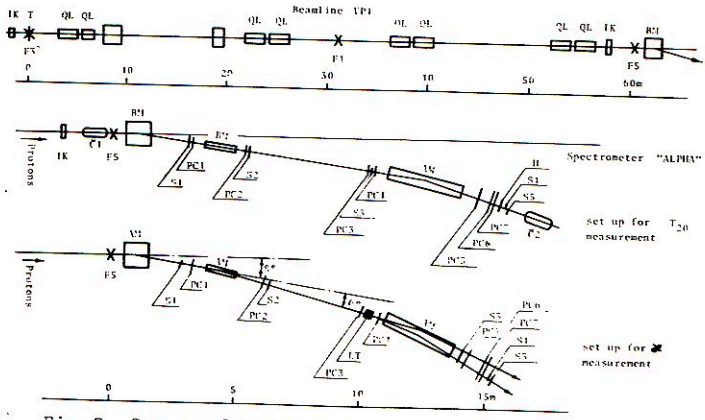

Fig.7. Set up for the measurement of T_{20} and $\mathcal{A}$.

IK Ionisation chamber as beam monitor
FS... Cross overs
T Fragmentation target
QL Quadrupole lenses
BM Bending magnets
AM Analysing magnets
Sn Scintillation counters
PCn Proportional chambers
LT "Living" target (plastic scintillator)
H Scintillation hodoscope
čn Cherenkov threshold counters

The spectator protons emerging from the target at 0° were guided by the beam line over about 60 m to the cross over F5. The magnetic elements of the beam line were adjusted to the proton momentum to be measured. In the case of the T_{20} measurement the protons were finally analysed by the spectrometer ALPHA. The analysing power was obtained by changing the sign of the polarization of the beam after each accelerator cycle. The tensor polarization of the deuteron beam was characterized by the value $p^{+}_{20} + p^{-}_{20} = 0.95 \pm 0.08$. Two Cherenkov threshold counters suppressed the inelastically scattered deuterons with the same momentum as the protons. The data obtained up to $k = 0.875$ GeV/c

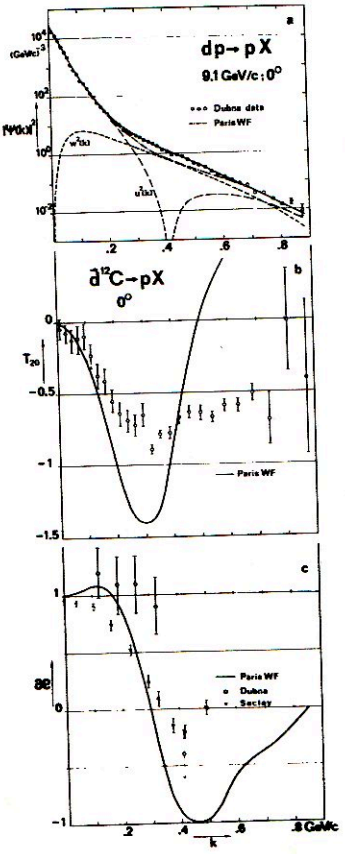

Fig.8. Results of the fragmentation measurements:
a) Deuteron wave function extracted from the cross section measurement for $p_d = 9.1$ GeV/c and 0°,
b) Tensor analysing power T_{20} from $d^{\uparrow}\,{}^{12}C \rightarrow pX$ at 0° (data from /10/),
c) Preliminary data of two measurements of the polarization transfer coefficient $\mathscr{K}_{exp}$ at Dubna and at Saclay /7/.
Both data sets need to be normalized to $\mathscr{K}_{norm}$.

are shown in Fig.8b together with the theoretical prediction according to the Paris wave function /11/. Data measured at SATURNE up to $k = 0.64$ GeV/c /12/ agree very well with the Dubna results.

There is even qualitatively no agreement with the simple impulse approximation. The minimum at 0.3 GeV/c with $T_{20} = -\sqrt{2}$ and the zero crossing at about 0.45 GeV/c are not confirmed by the experiment. This result will be discussed later in this talk and in further contributions to this workshop[13].

The experimental setup for the α-measurement is also shown in Fig.7. The fragmentation target again was placed in F3 and the protons tranported to F5 by the beam line VP1. The analysing magnet AM2 of the spectrometer ALPHA was used to define the momentum of the spectator protons. The polarization of the protons was analysed by a second scattering in the living target LT. By the analysing magnet AM3 the elastically scattered protons were selected. This system accepted scattering events with transferred four momentum around $-t = 0.2$ GeV^2, where the analysing power of the proton-proton scattering has its maximum. The assymmetry measurement was performed by changing the sign of the vector polarization of the beam after each cycle. The beam polarization in the two modes was $p_z^+ = 0.441 \pm 0.021$, $p_{zz} = +0.020 \pm 0.028$ and $p_z^- = -0.307 \pm 0.022$, $p_{zz} = +0.144 \pm 0.028$. Scattering events were triggered by the living target and the scintillation counters behind the analysing magnet AM3 and identified more accurately by the proportional chambers PC3 to PC7. In the first run of the experiment (in 1989) the measurement covered the region of internal momentum k up to 0.32 GeV/c (Fig.8c).

In 1990 a second run was performed using the spectrometer ANOMALON. The setup used in this run is shown in Fig.9.

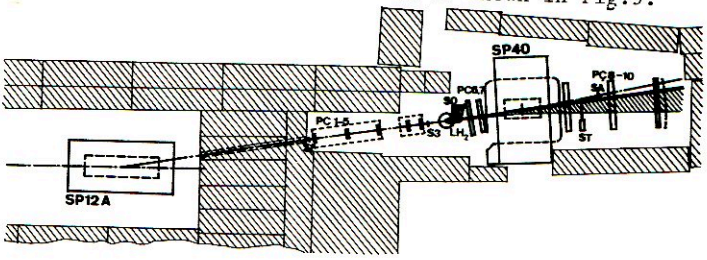

Fig.9. Scheme of the spectrometer ANOMALON used as polarization analyser in the α measurements.

SP12A Analyzer of proton momenta
SP40 Analyzer of proton momenta of the second scattering
S1,S3 Scintillation counters defining the beam
PC1-5 Proportional chambers for beam tracking
LH_2 Liquid hydrogen target, 30 cm long
SO Detector of recoil protons
PC6-10 Proportional chamber identifying the tracks of scattered protons
S4 Veto counter
ST Trigger counter
Hatched region: region of acceptance of scattering events

Here the momentum analysis of the protons was performed by the bending magnet SP12 at the end of the beam line VP1. The polarization analyser in this case was a liquid hydrogen target. The scattering events were triggered by means of the scintillation counters SO registering the recoil protons and by the scintillation counters ST behind the spectrometer magnet SP40. The final selection of the events was performed using the data from the set of proportional chambers PC 1-10 (see Fig.9). The result of this run is one point at $k = 0.425$ GeV/c. Control measurements at small k have shown that the measurements with the two spectrometers are consistent each with the other.

In equations (14) and (23) T_{20} and $\varkappa$ were expressed in terms of x. Eliminating x out of these equations one obtaines a relation between T_{20} and $\varkappa_{norm}$

$$\varkappa_{norm}(T_{20}) = 1 - \frac{9}{2\left[\frac{9}{4} + \left(\frac{1}{2} - \frac{1+\sqrt{2}\,T_{20}}{\tau}\right)^2\right]} ,$$

with

$$\tau = 1 \pm \sqrt{1 - \sqrt{\frac{7}{2}}\,T_{20} - T_{20}^2} . \qquad (25)$$

This relation is shown in Fig.10. It has two solutions with opposite signs. In the region of T_{20} covered by the data in the whole region of internal momenta the values of $\varkappa$ should be near +1 or -1. For the asymptotic experimental value $T_{20} = -0.55$ reached at large internal momenta $\varkappa$ should be ± 0.873. From the two values by means of equation (19) one obtains two possible D/S-state ratios.

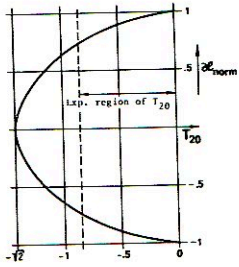

Fig.10. $\varkappa_{norm}$ as function of T_{20}.

For the positive value follows $w(k)/v(k) = -0.27$. This result looks plausible as one usually expects the D-state amplitude to be smaller than the S-state one.

From the negative value $w(k)/v(k) = 13.0$ is yielded. That means the D-state amplitude becomes much larger than the S-state one. The S-state dies out at large internal momenta. From equations (7) and (8) it follows that the deuteron becomes oblate in the $M_J = +1$ state and from (9) and (10) that it becomes prolate for $M_J = 0$, the most probable substate will be in this case that with $M_L = +2$ and $M_S = -1$.

It arises the question, which of the two solutions is physical. At small internal momenta α should be near +1. If the S-wave has a node, α should become negative near it (see (24)). So a transition from the region with $\alpha = +1$ to the region with $\alpha = -1$ becomes likely. The last point was measured just at the node of the Paris wave function. α decreases here already to negative values. The large value of $x = 13.0$ in the asymptotic region would indicate, that the S-state is not continued through the node to higher momenta. The transition to negative values would be a strong evidence for the existence of a node in the S-state and the momentum where it appears could be determined. The continuation of the measurements to larger internal momenta is necessary for a conclusive answer to these questions. In any way these considerations show how the polarization experiments may help to explore the innermost structure of the deuteron.

Unfortunately the above derived rather clear conclusions must be relativated, if other reaction mechanisms beside the quasi-free scattering are playing a significant role. This problem will be discussed in the next section.

5. Is the Present Information on the Deuteron Wave Function Reliable?

Up to now we have assumed that the fragmentation process is pure quasielastic. In this case it can be described by the impuls approximation which delivers directly the deuteron wave function. This assumption seems to be supported by additional experimental data.

The characteristic deviation of the fragmentation cross sections at $0.3 < k < 0.6$ GeV/c from the Paris wave function predictions does not depend on the angle and the incident energy. This follows from the comparison of the data measured at 8° by the MASPIC group (Fig.11)[3] and at 0° by the ALPHA group [2] at 9.1 GeV/c and from data obtained at 5.75 GeV/c and 3.49 GeV/c[14].

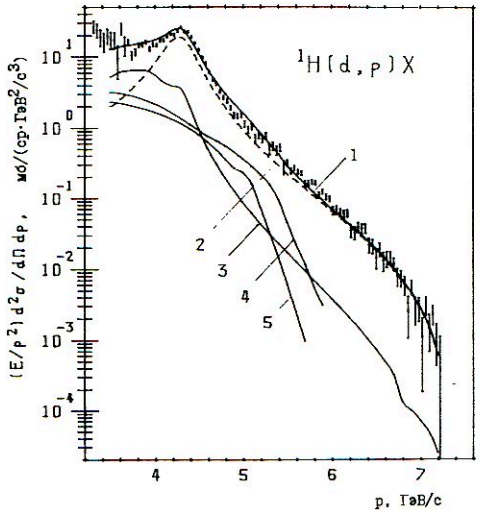

Fig.11. Data of the deuteron fragmentation at 9.1 GeV/c and 8° /3/.

The wave function was derived also from inelastic electron scattering in inclusive and exclusive measurements[15]. It fully agrees within the experimental errors with that from the fragmentation on protons or nuclei (Fig.12). This concerns especially the enhancement between $0.3 < k < 0.6$ GeV/c.

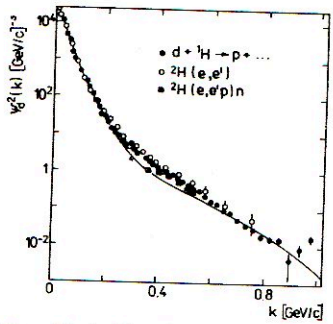

Fig.12. Momentum distribution inside the deuteron derived from deuteron fragmentation by protons /2/ and by means of electrons /15/.

The cross sections of the dp-elastic scattering in backward direction (180°) predicted by the wave function obtained from the fragmentation studies agree within the experimental errors with the data (fig.13) /16/. The same is true for T_{20} data for this process.

The form of the fragmentation spectra measured at different target nuclei between hydrogen and copper is the same. This follows from the cross section ratios as function of the internal momentum (Fig.14) /17/. That means the k dependence of the cross sections is mainly a property of the deuteron.

Further more: in the fragmentation spectra of other light nuclei as ^{3}He and ^{4}He similar enhancements at intermediate internal momenta in comparison to predictions from usual wave functions were observed (Fig.15) /18/.

It was argued, that this set of observations made for rather different processes most naturally can be understood as a consequence of a special feature of the deuteron (^{3}He, ^{4}He) structure.

On the other hand it cannot be ignored that certain contributions to the reaction mechanism considerably may deform the spectra of spectator particles. This was shown by different authors in different approaches.

Mueller investigated the fragmentation process in terms of a phase space model in a statistical approach /19/. Beside the

quasielastic scattering (diagram a) in Fig.16) the process of particle production from highly excited nucleons or a collectively excited deuteron was considered (diagram b) in Fig.16).

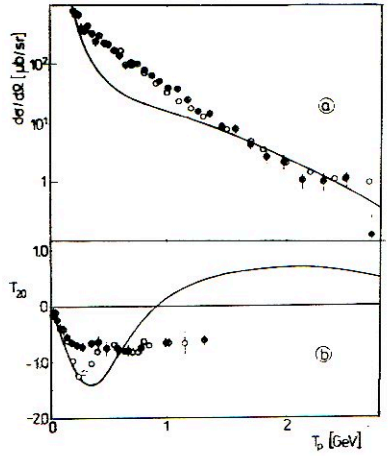

Fig.13. Comparison of the 180° differential cross sections and T_{20} as function of energy for the dp elastic backward-scattering[16] with calculation based on the Paris-wave function (solid line) and the "wave function" following from the Dubna fragmentation data [2] (full points).

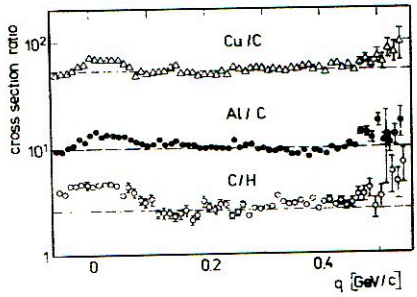

Fig.14. Cross section ratio for the deuteron fragmentation on different nuclei as indicated in the figure as function of internal momentum [17].

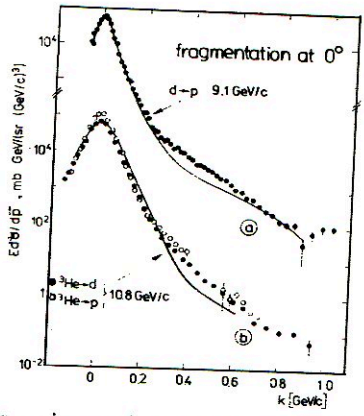

Fig.15. Comparison of fragmentation cross section of deuteron (a) and ^{3}He (b) on carbon as function of internal momentum k. Solid lines: calculations with Paris wave function (a) and with d-momentum distributions in ^{3}He /24/.

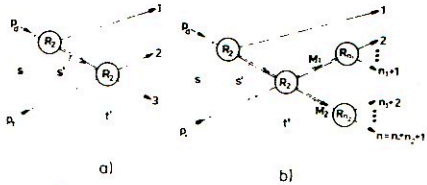

a) b)

Fig.16.Diagrams for the deuteron fragmentation in a quasifree process (a) and in a quasifree inelastic process (b) with highly excited nucleons.

The particle production was assumed as a statistical process in a gas of quarks constrained by phase space conditions. This model was tested by calculating the particle production in nucleon--nucleon collisions and found in full agreement with the data. It was also taken into account that the registered "spectator" particle also can be a "participant". This is especially important for the fragmentation at larger angles (e.g. for the measurement at the MASPIC spectrometer at 8°). Figure 17 shows the results of this model in comparison with the data. In the calculations the deuteron structure was taken into account in the usual form of the Paris wave function. The agreement with the data is almost perfect.

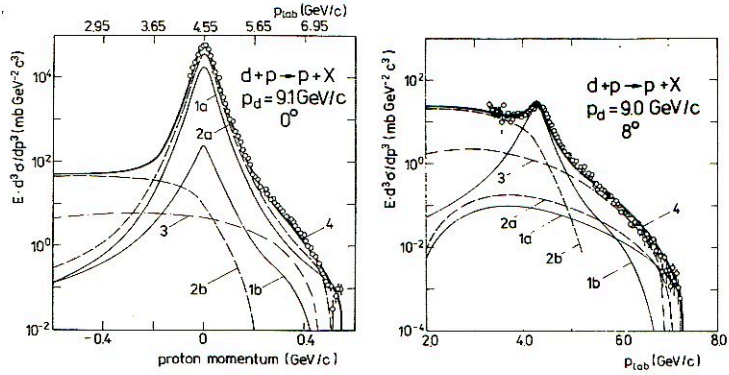

Fig. 17. Comparison of the fragmentation cross section at 0°/2/ and at 8°/3/ with calculations on the basis of the phase space model/19/. Curves for 1 quasi-elastic, 2 quasifree inelastic, 3 cluster excitation process, a) contributions from spectator, b) from participants. 4 sum of all contributions.

The second approach takes competing reaction mechanism in the form of the diagrams shown in Fig.18 detailed into account. This will be discussed extensively by the G.I.Lykasov later on this meeting /20/. The contributions of the quasifree scattering, the rescattering and particle production via rescattering are shown in Fig.19.

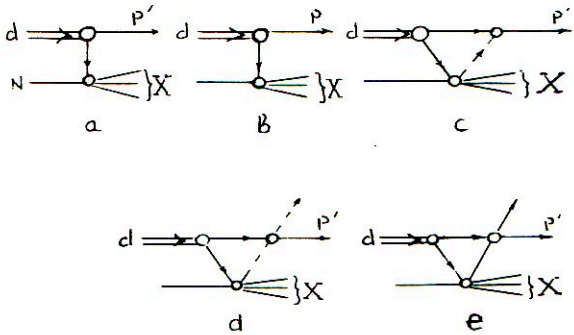

Fig.18. Diagrams of the fragmentation process taken into account in ref./20/.

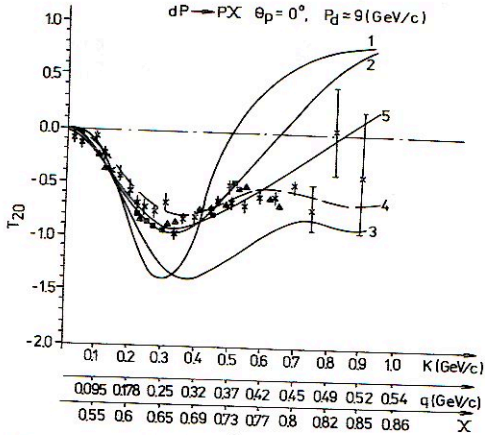

Fig.19. Experimental data and calculations of T_{20}
Data: ■ ▲ -Perdrisat et al./12/; × -Ableev et al./10/;
Curves: 1 - spectator mechanism Fig.18a; 2 - diagrams Fig.18a-c; 3 - calculation of Garsevanishvili V.R./25/;
4 - deuteron wave function with complex 6q-contribution/20/;
5 - all diagrams Fig.18a-e/20/.
q - internal momentum of the deuteron in its c.m.system;
x - contribution of the spectator in the momentum of the deuteron.

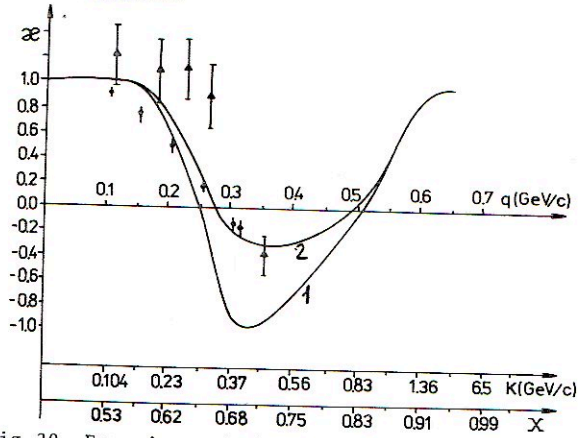

Fig.20. Experimental data and calculation of the polarization transfer æ. Data: ● - Perdrisat C. et al./7/; ▲ - Ableev V.G. et al. this paper;
Curves: 1 - spectator mechanism; 2 - all diagrams Fig.18a-e/20/.

By means of this approach it was also possible to calculate the polarization observables T_{20} and $\mathcal{A}$ (Fig.20). This theory succeeds to reproduce the data in the region of the minima in the curves for T_{20} and $\mathcal{A}$. But it does not describe the data at larger internal momenta behind the minima. These calculations are based on the Reid deuteron wave function.

The asymptotic behaviour of the cross sections and the tensor analysing power at large internal momenta could be understood by the approach of A.Kobushkin presented in his talk in this meeting /21/. He assumed that large internal momenta are due to an exchange of a hard gluon between two nucleons, each consisting of three quarks, occupying a colour octett state (state of hidden colour (Fig.21)). The results of this calculation are shown in Fig.22. If this is right, then this would be a first result concerning quark-gluon degrees of freedom in the deuteron. Obviously

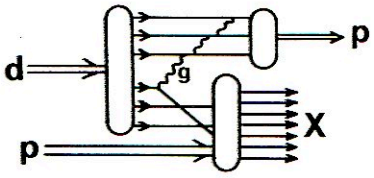

Fig.21. Production of a high momentum spectator proton by exchange of a hard gluon between the nucleons of the deuteron, forming a state of hidden colour.

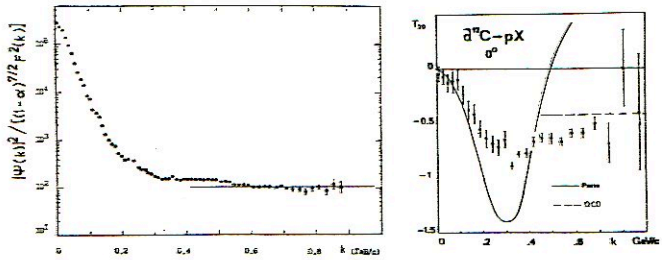

Fig.22. Asymptotic value of the reduced wave function and of T_{20} derived from the mechanism of hard gluon exchange.

such effects reveal themselves only at very large internal momenta corresponding to distances where the nucleons are strongly overlapping.

6. Study of the Reaction Mechanism

The preceding section has demonstrated that there are still alternative interpretations of the experiments possible and further information is necessary to arrive at final conclusions concerning the deuteron wave function. First of all the role of non-quasielastic contributions to the reaction has to be studied. This can be done either by exclusive experiments which allow to analyse the mechanism or by other experiments in such conditions, which exclude nonquasifree processes.

The fragmentation of deuterons in 4π geometry was studied in the 1m hydrogen bubble chamber of LHE[22]. In these experiments the following contributions to the reaction mechanism were studied: quasifree scattering, fragmentation with charge transfer, final state interaction, excitation of isobars, pion production, etc.

In connection with the discussed enhancement in the cross sections it is interesting, that already almost 20 years ago such an effect was found in the bubble chamber at the same internal momentum. It was observed in the pure dp -> ppn reaction, integrated over all angles. It appears most strongly for the fragmentation process with charge exchange (Fig.23).

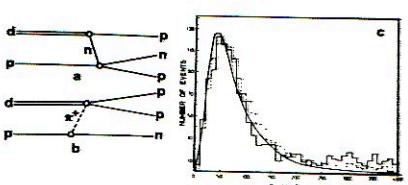

Fig.23. Deuteron breakup in a quasifree (a) and a charge exchange (b) process. (c) - experimental distributions of the spectator nucleon momentum, dashed histogram corresponds to mechanism a, full histogram to b. The curve was calculated from the Gartenhaus-Moravcsik wave function [22].

Another interesting effect seen in the bubble chamber also should be mentioned very shortly. The chamber was irradiated with vector polarized deuterons and the azimuthal distribution of the recoil protons was measured. As it is presented in Fig.24a, it shows the expected left-right assymmetry. On the other hand the corresponding distribution of the recoil neutrons from the charge exchange process dramatically disagrees with the theoretical predictions (Fig.24b). This unexpected effect was not explained up to now.

In one of the next talks[/23/] some aspects of the investigations by means of the bubble chamber will be presented in more detail. Obviously the results of these experiments up to now were not sufficiently taken into account in the discussion of the problems connected with the deuteron structure.

The existing two-arm spectrometers ALPHA, MASPIC and DISK allow to perform exclusive experiments. The quasifree fragmentation of the deuteron has three particles in the final state. Therefore the measurement of the momentum and the direction of two particles allows to reconstruct the full kinematics of the event. By this means at any case all inelastic processes (particle production) can be excluded. By proper choice of the kinematic conditions distinct mechanisms can be either enhanced or suppressed. Figure 25 shows the kinematical locus for a certain kinematic situation characterized by the momentum of the incoming particle and the angles of the two detector systems.

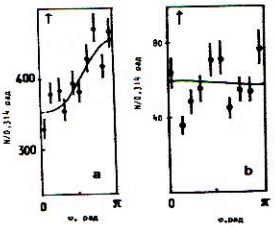

Fig.24. Azimuthal distributions of recoil protons from the quasifree process (a) and of recoil neutrons from the charge exchange process (b) (see diagrams a and b in Fig.23)[/23/].

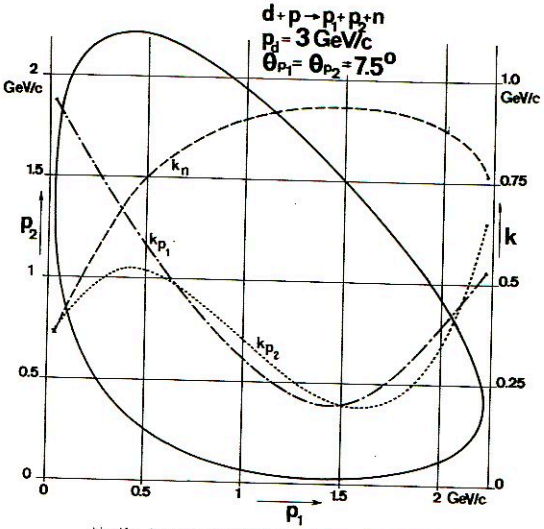

Fig. 25. Internal momentum **k** of a deuteron in an kinematically complete measurement of its fragmentation.
full line: kinematical locus of the two registered protons with momenta p_1 and p_2
broken lines: internal momentum **k** for the case that the indicated particle is spectator.

Kinematics allows to assigne a certain internal momentum of the deuteron to each point of the locus. This means that the measurement of the differential cross sections along the kinematical locus already provide the information on the deuteron wave function in a certain region. At the above-mentioned two arm spectrometers of the Laboratory of High Energies it is possible to perform such experiments with unpolarized and polarized deuterons as incoming particles. Using tensorpolarized deuterons one at once obtains the tensor analysing power along the kinematic locus. Furthermore it will be possible to perform these experiments with a polarized proton target. Such experiments are under preparation at LHE.

Another way to exclude disturbing reaction mechanisms is the following. At the kinematic limit of the spectator spectrum, i.e., at the largest internal momenta which can be reached with certain input momentum only the quasifree scattering survives. All other mechanisms die out, because under these conditions no momentum is left over to be shared in another way between the particles in the final state. Unfortunately the measurement at the kinematic limit is difficult because of the very small cross sections and the large background of inelastical scattered deuterons. Therefore a very effective particle identification is necessary. The internal momentum reached at the kinematic limit can be varied by the choice of the bombarding momentum.

By means of these methods it seems to be possible to overcome the uncertainties concerning the reaction mechanism. Then it will be possible to establish the wave function and the spin structure up to the region of overlapping nucleons and to draw conclusions on the structure and dynamics of the 6q state.

6. Conclusions

From the present status of experimental information provided by the investigation of the fragmentation of unpolarized and polarized deuterons on hadronic targets one can draw the following conclusions:

- the cross sections and the polarization observables T_{20} and $\mathcal{R}$ of the deuteron fragmentation deviate considerably from predictions based on conventional wave functions, if the validity of the impulse approximation is assumed;
- cross sections and polarization observables in part can be described by usual wave functions taking into account additional contributions to the reaction mechanism beside the quasifree scattering;
- the asymptotic behaviour of the cross sections and T_{20} can be understood in terms of quark degrees of freedom;
- quark effects reveal themselves, if at all, only at the largest internal momenta reached up to now;
- exclusive fragmentation measurements with unpolarized and polarized deuterons are necessary to clarify the role of different reaction mechanisms;

- T_{20} and $\mathcal{A}$ measurements at the largest internal momenta will provide reliable information on the spin structure of 6q states;
- the question of quark degrees of freedom remains a challenge for further experimental and theoretical research.

Acknowledgements

The author is indepted to many coworkers of the different experimental and theoretical groups at Dubna for providing him with useful information. Especially fruitful discussions with V.V.Glagolev, G.I.Lykasov and E.A.Strokovsky are thankfully acknowledged.

References

1. Arnold R.G. et al. Phys.Rev. C21(1980) 1426.
2. Ableev V.G. et al. Nucl.Phys. A393(1983)491; A411(1983)541; Pisma ZhETF 37(1983)196.
3. Azhgirej L.S. et al. Preprint JINR P1-86-728(1986); Azhgirej L.S. et al. Preprint JINR P2-87-417(1987).
4. Kobushkin A.P., Vizireva L. J.Phys.G: Nucl.Phys.8(1982)893.
5. Vasan S.S. Phys.Rev.D 8(1973)4092; Karmanov V.A. YaF 34(1981)1020; Belostotsky S.L. Preprint Leningrad Inst. of Nucl.Phys. N°1534(1989); Dolidze M.G., Lykasov G.I. Z.Phys.A: Atomic Nuclei 336(1990)339; Proceedings of XXV Winter School LIYaF 1990, p.187, Leningrad,1990 Strokovsky E.A. unpublished.
6. Hulthen L., Sugawara M. Encyclopedia of Physics ed. S.Flugge vol.XXXIX Structure of Atomic Nuclei, Berlin 1957.
7. Perdrisat C.F. Contribution to this Workshop.
8. Perdrisat C.F. Private Communication.
9. Karmanov V.A. ECHAYA 19(1988)525
10. Ableev V.G. et al. Nucl.Instr.a.Meth. A306(1991)73. Ableev V.G. et al. Pisma ZhETF 47(1988)558. Ableev V.G. JINR Rapid Communications N°4-90(1990)5. Ableev V.G. et al. Preprint ZfK Rossendorf 666(1990).

11. Lacombe M. et al. Phys.Rev.C21(1980)861; Phys.Lett.101B(1981)139; Phys.Rev.C23(1981)2405.
12. Perdrisat C.F. et al. Phys.Rev.Lett.59(1987)2840; Punjabi G.I. Phys.Rev.C39(1989)608
13. Lykasov G.I. Contribution to this Workshop.
14. Anderson L. et al. Phys.Rev.C28(1983)1224.
15. Bosted D. et al. Phys.Rev.Lett.49(1982)1380.
16. Berthed P. et al. J.Phys.G: Nucl.Phys.8(1982)L111.
17. Ableev V.G. et al. Proc.Few Body and Quark-Hadronic Systems, JINR Publ. D4-87-692(1987), Dubna, p.341.
18. Ableev V.G. et al. Loc.cit.
19. Müller H. Z.Phys.A: Atomic Nuclei 336(1990)103.
20. Dolidze M.G., Lykasov G.I. Z.Phys.A: Atomic Nuclei 336(1990)339; Proceedings of the XXV Winter School LIYAF 1990, p.187, Leningrad. Contribution to this Workshop.
21. Kobushkin A.P. Proc. of the 9th Int.Symp. on High Energy Spin Physics, Bonn, September 6-15, 1990. Ed.K.H. Althoff, W.Meyer, vol.1, p.542, Berlin 1991.
22. Aladashvili B.S. et al. Preprint JINR E1-8092(1974).
23. Glagolev V.V. et al. Preprint JINR R1-88-6(1988).
24. Schiavilla R. et al. Nucl.Phys.A449(1986)219.
25. Garzevanishvili V.R. XIII Winter School of Theoretical Physics in Karpacz 1976, v.1, p.313.

NONNUCLEON EFFECTS IN COLLISIONS OF RELATIVISTIC NUCLEI WITH PROTONS

Dubna-Kosice-Moscow-Strasbourg-Tbilisi-Warsaw Collaboration

Presented by Victor Glagolev

Joint Institute for Nuclear Research, Dubna

Until recently there have been explanations of results on hadron-nucleus and nucleus-nucleus interactions which use the representation of the nucleus as the sum of nucleons. For example, the cascade models and some of their modifications describe many results qualitatively. It is important to take into consideration secondary effects with the excitation of nonnucleon (mesons, quark) degrees of freedom for improving the description. We have made an investigation of the interactions of the lightest ($^{2}H, ^{4}He$) nuclei with protons /1-3/ (p_d= 3.35 Gev/c, p_{He}= 8.6 Gev/c) in order to study such a kind of effects. The hydrogen bubble chamber was used as a target and as a detector at the same time.

The used methodics made it prossible to distinguish certain reactions and to separate the reactions without pions from those with pions.

Figure 1 demonstrates the invariant differential cross section for protons flying backward (cos0 [-1., -0.66]) from the **dp → pX** reaction. A shoulder above 0.2 Gev/c is clearly seen. The distribution does not show such an effect for the reactions with pions. It falls down smoothly.

The ratio of the differential cross sections of inclusive protons and protons from the reaction **dp → ppn** (see Fig.2) /1/ approaches one in the region above 0.2 Gev/c. Therefore, the effects in this region are conditioned by the only reaction without pions in inelastic **dp** interactions.

At the same time the emission of protons is amplified relative to the emission of neutrons in the **dp → ppn** reaction at an angie of 180, especially for events with large momentum transfer (X = T/T 0.5), (see Fig.3 /3/).

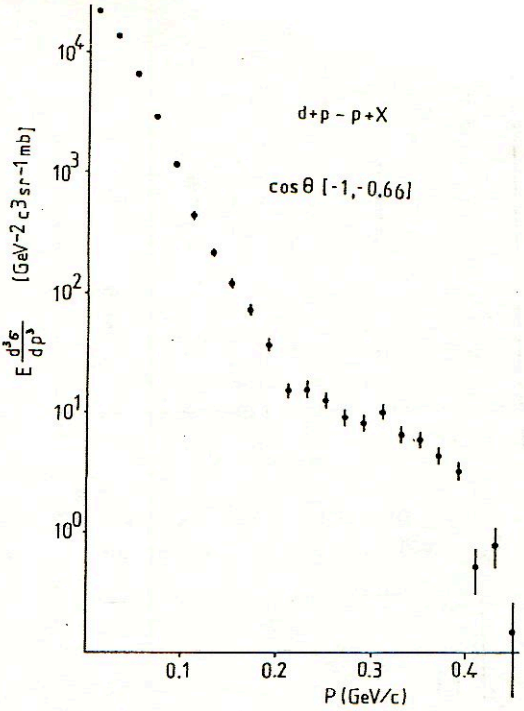

Figure 1. Invariant differential cross section for protons from the reaction dp → pX (cosθ [-1.,-0.66]).

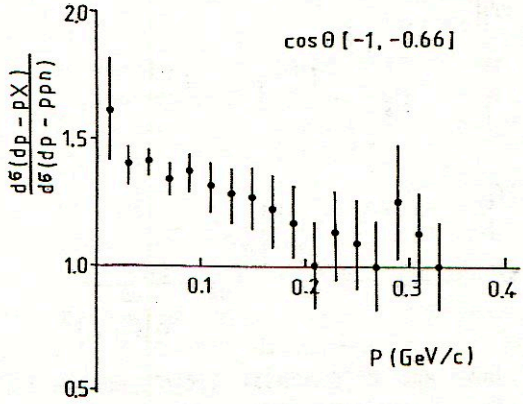

Figure 2. Ratio of the differential cross sections of the reactions dp → pX and dp → ppn (cosθ [-1., 0.66]).

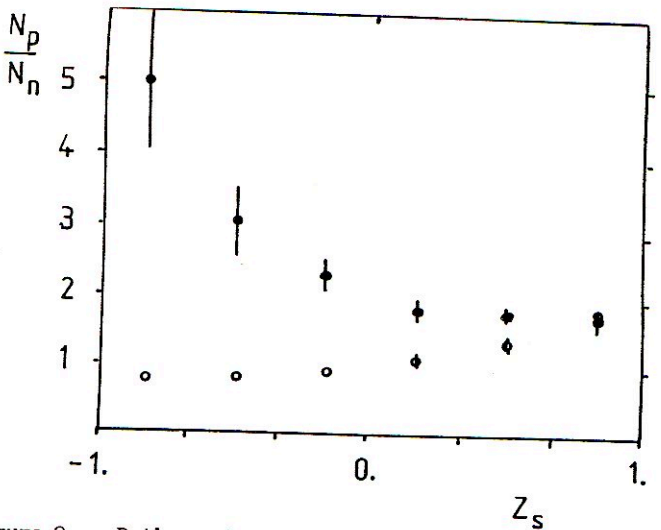

Figure 3. Ratio of proton and neutron emission versus $Z_s = \cos\theta_s$ for $X < 1/2$ (○) and $X > 1/2$ (●).

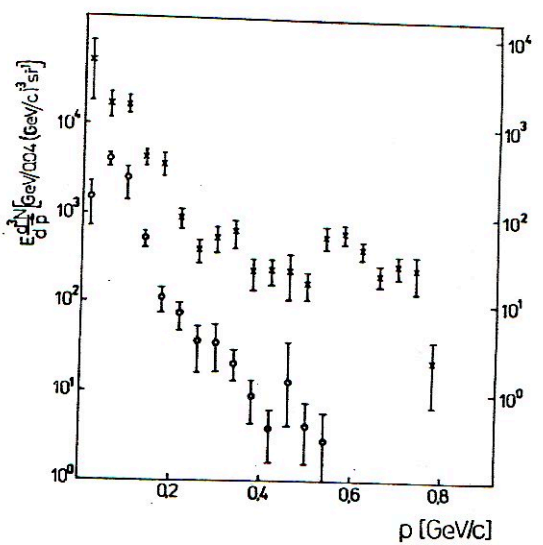

Figure 4. Invariant differential cross sections for protons from reaction ^{4}Hep → pX (cosθ [-1.,-0.66]) for the channels without (æ) and with (○) pions.

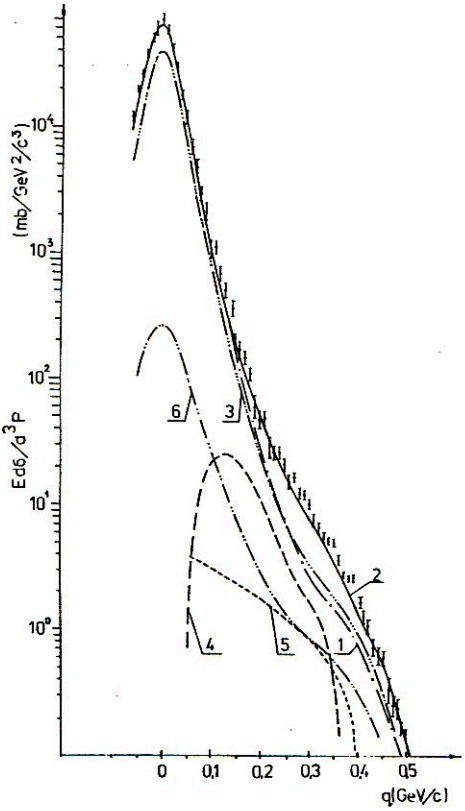

Figure 5. Defendence of the inclusive proton spectrum in the reaction **dp → pX** on the final proton momentum in the deuteron restt frame. Curve 2 - summed contribution of the graphs of Fig.6a.

This excess is easily explained by charge exchange reactions going througn the excitation of the virtual isobaric state Δ. Similar effect can be also seen in the interactions of the ^{4}He nucleus with protons. It particular, there is a qualitative difference in the behaviour of the invariant differential cross sections of the reactions without and with pions (see Fig. 4) /2/. Some shoulder can be observed in the inclusive spectrum of protons at 0 from the reaction **dp → pX** /4/ for higner energy (9 Gev/c). The results are presented in Fig 5., the calculated curves /5/ have been obtai-

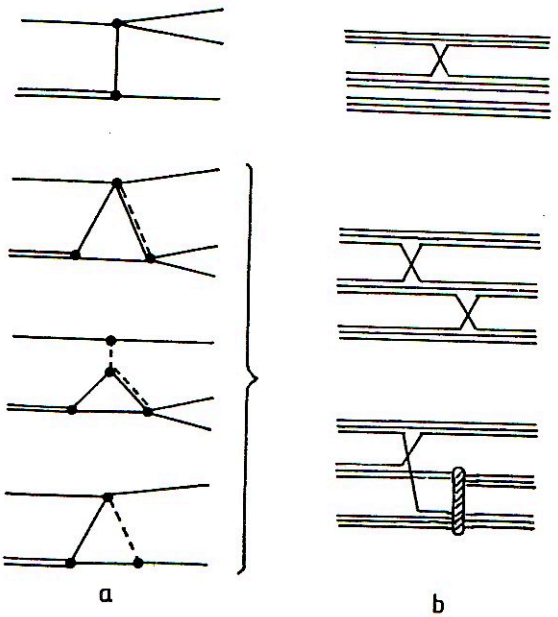

Figure 6. Graphs corresponding to the process $dp \to pX$ /5/(a) and quark graphs (b).

ned for the grsphs of Fig.6a. The fact is of interest that the well-known dibaryon enchancements manifest themselves most clearly in the charge-exchange processes for the regions close to the sum of masses $NN\pi$, $N\Delta$ /6/. For example, it is possible to compare the diagrams of Fig. 6a with the quark diagrams of Fig.6b. The process of the first diagrams goes through the excitation of the Δ-isobar with following ΔN-integration and transition to two relatively fast nucleons. The system is formed in the second diagrams,(4q + 2q) has a hidden colour. This system possessed rotation levels in the Mac-Gregor shceme /7/ showing themselves as narrow resonances when going to two nucleons.

Therefore the appearance of the dibaryon enchancements is justified within the frame of quark models in the region of mesons and isobaric degrees of freedom. It should be noted that all the considered effects are related to collective interactions that should manifest themselves in NA and AA collisions over a very wide range of energies.

REFERENCES

1. B.S.Aiadashvili, A.M.Baldin, V.V.Glagolev, et al. Sov. Journ. of Nuclear Physics, 27, 1978, p.704; S.S.Shimansky et al. JINR, P1-88-443, Dubna, 1988.

2. T.Sobczak et al. ,JINR, P1-88-393, Dubna, 1988.

3. V.V.Glagolev et al., JINR, P1-12907, Dubna, 1979.

4. V.G.Ableev et al.,JETP Lett, v.45, p.596 (1987)

5. M.G.Dolidze, G.I.Lukasov, JINR, E2-89-666, Dubna, 1989.

6. L.Santi et al., Phys. Rev.C., 1988,38, p.2466;
V.V.Glagolev et al., JINR, E1-89-246, Dubna, 1989.
H.Shimizu, E174 Coll.

7. M.N.Mac-Gregor, Phys. Rev., 1979, D20, p.1616;
L.A.Kondratyuk, XIth European Conference on Few-Body Physiks Fontevraud, Suppl.2,242, France,1987.

SPECULATION AROUND DEUTERON DISINTEGRATION DATA

Sitnik I.M. and Penchev L.
Joint Institute for Nuclear Research
Dubna

This report is devoted to the analysis of data on the A(d,p) reaction performed on polarized and unpolarized deuteron beams.

The anomaly in the cross-section data (enhancement over the relativistic impulse approximation[1] (RIA) prediction) mentioned long ago, stimulates measurements of polarization characteristics of the reaction which are more sensitive to the deuteron wave function (DWF) and to the reaction mechanisms. Analysing the tensor polarization (T_{20}) data[2,3], two peculiarities should be mentioned: 1) the experimental minimum value is larger than the RIA prediction $-\sqrt{2}$; 2) the values of the T_{20} data are negative at large values of q (deuteron rest frame momentum).

If the RIA mechanism predominates in the whole q region, the first peculiarity means that the deuteron s-wave does not cross zero. This result is evident when extracting[4] the DWF by the RIA fit of both cross section[5] and T_{20}[2]. Such a DWF predicts that the d->p polarization transfer coefficient (κ) is close to 1 in the whole region which does not contradict the data presented in PARIS-90[6,7] and BON-90. However, new data points[8,9] at larger values of q cross zero which is an indication that the RIA mechanism is not valid in this region (0.2-0.35 GeV/c). The discrepancy between the T_{20} data and the RIA prediction at a minimum can be explained, for example, by an essential admixture of mechanisms described in ref.[10]. For this case we carried out another fit[4] including data only out of a region of 0.2-0.35 GeV/c. Over a momentum region of q>0.35 GeV/c, where such mechanisms become negligible, the second peculiarity ($T_{20} \simeq -0.6$ at large q) means dominance of the d-wave. The fit[4] (with initial

parameters of the Reid soft core DWF[11]) demonstrates this point. In this case the polarization transfer coefficient is predicted to be -1 for sufficiently large momenta.

Although such a procedure of extracting the DWF "directly" from the data is quite rough, it was made before the first measurement of polarization transfer[6,7] and aimed at working out the strategy of measurements. Some of the deuteron static parameters extracted from these DWF's have an appreciable difference from the parameters known from experiment.

Recently we have analysed 28 DWF's presented in ref.[12], which, of course, reproduce well the standard set of data including static parameters. For some of them the d-wave dominates at large momenta. One of them (ψ^{8A}_{LS}) with slightly changed parameters after fitting, but practically without changing the radius, quadrupole momentum and percentage of the d-wave (see tables 1,2), gives a good agreement with the cross-section data over the whole momentum range and with the T_{20} data out of 0.2-0.35 GeV/c (fig.1). It is interesting to note a good agreement of this DWF with the cross-section data in the region of the enhancement (0.2-0.35 GeV/c) despite of the fact these points were excluded from the fit. The prediction for ∞ presented in fig.2 qualitatively agrees with the one based on our previous fit[4] in which a region of 0.2-0.35 GeV/c was excluded.

Table 1. Parameters of ψ^{8A}_{LS}[12] after fitting

M_i (not changed)	C_i	D_i
0.23162	0.88807	0.022795
1.2000	-1.3593	-0.99380
1.6000	-1.2712	0.016015
2.0000	22.208	13.293
2.5000	-65.153	-48.270
3.0000	-25.939	58.544
3.5000	0.022795	-22.611

Table 2. Static parameters of the deuteron

	Percentage of d-wave	Radius fm	Quadr. mom. fm^2
ψ^{8A}_{LS} initial	8.00	1.937	0.2777
ψ^{8A}_{LS} after fit	7.90	1.940	0.2779
experiment (from[14])		1.956	0.2860

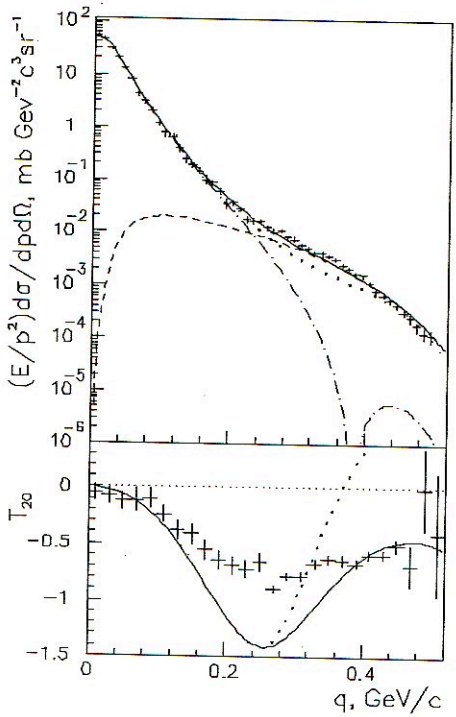

Fig.1. Invariant cross-section data[5] of the H(d,p) reaction (**up**) and the T_{20} data[2] of the ^{12}C(d,p) reaction (**down**) compared with the RIA calculation: dotted curves - Paris potential[15]; full curves - ψ^{8A}_{LS} parameterization[12] after fitting the data excluding a region of 0.2 - 0.35 GeV/c; dash-dotted and dashed curves - s- and d-waves of this parameterization, respectively.

So, it is very important to measure the polarization transfer at large momenta. Our colleagues and we have a proposal for such measurements (experiment "ALPHA") increasing luminosity by a factor of about 20 in comparison with the first measurements[6,7]. The proposal and the one discussed in report[8] are alternative.

If the validity of the RIA mechanism for the A(d,p) reaction in the region of q>0.4 GeV/c is confirmed, the discrepancy, seen from fig.3, between the T_{20} data of the (d,p) reaction and the ed-elastic scattering will become the subject of great interest. If nonnucleon components in the deuteron such as (Δ,Δ), (N,N^*), (N^*,N^*) are essential (see,

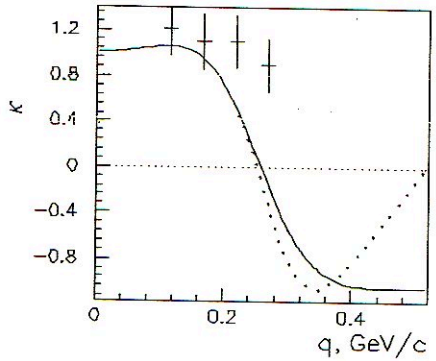

Fig.2. Polarization transfer coefficient data[6,7] and RIA calculations using: dotted curve - Paris potential[15]; full curve - $\psi 8A_{LS}$ parameterization[12] after fitting the data in fig.1.

for example, report[13]), we have not to expect an agreement between the A(d,p) and d(e,e′) data. There is no difference for the electron which configuration (N,N) or (Δ,Δ) creates the s- and d-waves (in case without destroying the deuteron), so such configurations are significant for the d(e,e′)d reaction. On the contrary,when the proton is observed at a zero angle, the contribution of the (Δ,Δ)-configuration in the deuteron fragmentation reaction is suppressed. For example, we expect a significant production of Δ-spectators from this configuration, but the probability to register the proton from the Δ-spectator is sufficiently small.

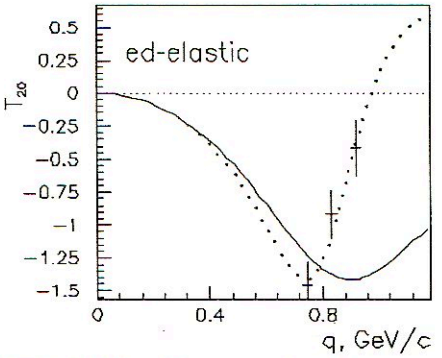

Fig.3. Tensor polarization in elastic e-d scattering $\tilde{t}_{20}$ (neglecting a magnetic contribution) versus four-momentum transfer: Bates data[7] in comparison with the IA calculation using the RSC potential (dotted curve) and the $\psi 8A_{LS}$ parameterization[12] (full curve) after fitting the (d,p) data in fig.1.

If the contradiction between the descriptions of the A(d,p) and d(e,e´) processes is confirmed, that will be a good stimulus to look for (Δ,Δ) and other nonnucleon configurations in the deuteron. The possibility of observing Δ- and N^*-spectators by the spectrometer "ALPHA" is being studied now.

REFERENCES

1. Ableev V.G. et al.- Nucl.Phys., 1983, A393, p.491; A411, p.541(E).
2. Ableev V.G. et al.- JINR RAPID COMMUNICATIONS, 1990, 4(43)-90, p.5; Ableev V.G. et al.- Pis´ma Zh.Eksp.Teor.Fiz., 1988, 47, p.558.
3. Perdrisat C.F. et al.-Phys.Rev.Lett., 1987, 59, p.2840.
4. Penchev L., Strokovsky E.A. and Sitnik I.M. - JINR RAPID COMMUNICATIONS, 1990, 4(43)-90, p.10.
5. Zaporozhets S.A. et al. - In: Proceedings of the VIIIth International Seminar on High-Energy Physics, D1,2-86-668, Vol.1, p.341. Dubna:JINR 1986; Ableev V.G. et al. - Pis´ma Zh.Eksp.Teor.Fiz., 1987, 45, p.467.
6. Ableev V.G. et al - In: 7th International Conference on Polarization Phenomena in Nuclear Physics (abstracts of contributed papers), Paris, July 9-13 1990, p.40F.
7. Garcon M. - In: 7th International Conference on Polarization Phenomena in Nuclear Physics, Paris, July 9-13 1990, p. C6-61.
8. Strunov L.N. et al. - "Polarization transfer in relativistic deuteron fragmentation for high internal proton momenta measured at synchrophasotron", report at this workshop.
9. Perdrisat C.F. and Punjabi V. - "Deuteron structure information obtained from breakup data", report at this workshop.
10. Dolidze M.G. and Lykasov G.I. - Z.Phys., 1990, A336, p.339.
11. Reid R.V. - Ann. Phys., 1969, 50, p.411.
12. Certov A., Mathelitsch L., Moravcsik M.J. - Phys.Rev., 1987, C36, p.2040.
13. Obukhovsky I.T. et al. - "Nonnucleon components in the deuteron and methods for its experimental discovery", report at this workshop.
14. Krasnopolsky V.M. et al.- Phys.Lett., 1985, B165, p.7.
15. Lacombe M. et al. - Phys. Lett., 1981, 101B, p.139.

A POSSIBILITY OF POLARIZATION TRANSFER MEASURING FOR RELATIVISTIC DEUTERON FRAGMENTATION WITH ANOMALON SETUP AT JINR SYNCHROPHASOTRON

A.I.Chernenko, T.Dzikowski, L.B.Golovanov, V.M.Golovin, A.D.Kirillov, A.Korejwo, V.V.Perelygin, D.A.Smolin, L.S.Strunov, A.Yu.Sukhanov, V.A.Sviridov, A.V.Zarubin, L.S.Zolin

Joint Institute for Nuclear Research, Dubna

Introduction

Sensitive probe for the deuteron wave function[1,3] is a coefficient of the vector polarization transfer, æ, vs. internal nucleon momenta, k, in the deutron. For deuteron fragmentation at 0°

$$æ(k)=P_{xp}(k)/P_{xd},$$

where: P_{xd} - deuteron polarization, P_{xp} - spectator proton polarization. Such an experiment[1] was realized by ALPHA team at JINR synchrophasotron. Authors reached internal momentum k of 320 MeV/c. According to this data the transfer coefficient æ within the experimental errors can be assumed to be constant-like vs. k. It is the range of internal momentum higher than 300 MeV/c that is the most interesting one because at the small internucleon distances the differences between theoretical model predictions become more significant[3]. But at the same time this range is the least available for experimental test because fragmentation cross-section decreases by the order of magnitude when k increase is 100 MeV/c[2]. Further advance to high internal momenta of the proton in the deuteron is limited by trigger rate and requires: to increase intensity of the stripping protons that is limited by polarized deuteron beam intensity of 10^9 per burst at the synchrophasotron; or to increase polarimeter efficiency that is limited, for instance, by setup aperture[1].

In this paper we discuss a possibility of the second way to realize such an experiment using the magnetic spectrometer ANOMALON as proton polarimeter in configuration of 1990. An experiment on stripping proton production for deutron fragmentation process and its transportation to the polarimeter has been performed to estimate the secondary beam parameters and trigger rate of the "good" events for internal momentum range up to 600 MeV/c.

Secondary proton beam parameters for deuteron fragmentation.

The general lay-out of double scattering experiment is shown in fig.1. Polarized deuteron beam $d^{\uparrow}$ is focusing by the head part of the VP-1 channel on the carbon target T_1 at beam focus F_3. The stripping protons $p^{\uparrow}$ from the projectile deutron fragmentation at 0^{o} are transported 100 m down stream by VP-1 channel to the polarimeter - magnetic spectrometer ANOMALON (beam focus F_7). The proton polarization can be measured from the angle distribution asymmetry of the proton elastic scattering on the liquid hydrogen target T_2.

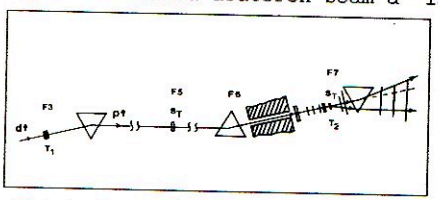

Fig.1. Lay-out of experiment.

For estimations of secondury beam parameters we used unpolarized deuteron beam with momentum 9 GeV/c. The beam line after the carbon target T_1 down stream from focus F_3 to F_7 was tuned for the defined momentum of secondary protons. The operating regime of magnets and quadrupole lenses was chosen experimentally for deuteron momentum 9 GeV/c and proton momentum 4.5 Gev/c using the beam wire profilometer system. For intermediate values of the proton momentum this regime was chosen by linear interpolation. The proton momenta were measured by magnetic spectrometer ANOMALON.

The beam channel transparency is shown in fig.1. It decreases from 98% at focus F_5 to 65% at F_7. Only 15% of the total beam is focusing on the liquid hydrogen target with diameter 6 cm. At the same time the proton momentum interval is constant for the full momenta range and is equal to $\delta p/p=1.3\%$. Fig.2 shows relative beam intensity per one primary deuteron per burst in focus F_7 vs. proton momentum. The data are taken from ref.[1,2]. Closed triangles show our measurements. One can see that with proton momentum increase stripping proton intensity decreases to 5 order of magnitude. Moreover d/p ratio reaches the values 10-100 at the high proton momenta. High *d* back-ground and low proton flux requires careful *d/p* separation for transfer polarization measurement at high secondary proton momenta.

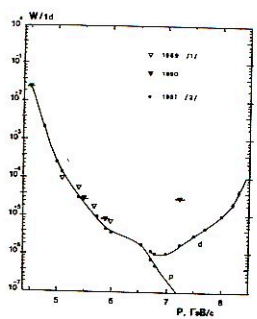

Fig.2. Secondary proton beam intensity in F_7 per d vs. p momentum.

Conclusion

We considered a possibility of the ANOMALON setup application for polarization transfer measurements at high internal nucleon momenta. As a conclusion we can make few remarks. The negative point: advantage of the wide magnetic spectrometer aperture is compensated in great degree by poor beam line transportation from focus F_6 to F_7. Positive points: large flying base and precision TOF system allows to separate high deuteron back-ground up to kinematical limit; liquid hydrogen target provides a high analyzing power for p–p elastic scattering; small beam channel momentum interval $\sigma p/p = 1.3\%$ admitts to make an experiment without projectile proton momentum measurement for elastic event selection. The estimations for transfer polarization measurement at deuteron momentum 9 GeV/c are represented in fig.5. For deutron beam intensity 10^9 it shows fluxes per burst for: p+d– secondary unseparated beam, p–proton and d–deutron beams; T-trigger rate of the "good" event; $1/\varepsilon$ – inverted polarimeter efficiency and A_{pp}– analyzing power as function of the internal momentum k. Fig.5 shows that with present polarimeter configuration at the internal momentum $k \simeq 500$ MeV/c trigger rate is $\simeq 0.2$ event per burst or 1500 event per day.

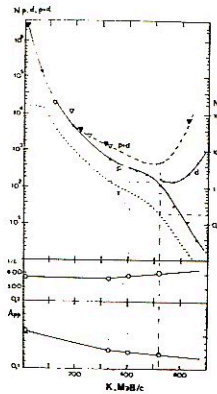

Fig.5. Secondary beam fluxes N_{p+d}, N_p, N_d; N_T -trigger rate at deuteron intensity 10^9 per burst; $1/\varepsilon$-inverted polarimeter efficiency and A_{pp}-analyzing power vs. k at the deuteron momentum 9 GeV/c.

We would like to thank Alpha team members for helpful discussions.

References

1. V.G.Ableev et al in: Proc. of 7-th Int. Conf. on Polarization Phenomena in Nucl. Phis., 9-13 July,Paris 1990, p. 40 F.

2. V.G.Ableev et al JINR Preprint,13-81-782, Dubna,1981. & Eq. and Tech. of Exp. N 1,1983, p. 266-274 (in Russian).

3. S.L.Belostotsky, in: Proc.of Symp. on Nucleon-nucleus & Hadron-nuclear Int. at Intermediate Energies 21-23.04.1986, Leningrad, 1986, p.266-274.

4. O.Benary, L.R.Price and G.Alexander Preprint UCRL-20000 NN, Berkeley, August, 1970.

5. H.Spinka et al Nucl.Inst.& Meth. 211 (1983) 239-261.

VECTOR-POLARIZATION TRANSFER MEASURING AT SYNCHROPHASOTRON FOR DEUTERON FRAGMENTATION AT MOMENTUM 6 GeV/C AND INTERNAL PROTON MOMENTUM 410 MeV/C

T.Dzikowski, I.A.Golutvin, V.S.Khabarov, A.Korejwo, V.V.Perelygin, B.Yu.Semenov, D.A.Smolin, V.A.Sviridov, A.V.Zarubin

Laboratory of Superhigh Energies, JINR, Dubna

V.G.Ableev, Yu.T.Borsunov, S.V.Dzhemukhadze, L.B.Golovanov, A.D.Kirillov, B.Kuehn, V.P.Ladygin, A.A.Nomofilov, L.Penchev, N.M.Piskunov, V.I.Sharov, I.M.Sitnik, E.A.Strokovsky, L.N.Strunov, A.Yu.Sukhanov, A.P.Tsvinev, S.A.Zaporozhets, L.S.Zolin

Laboratory of High Energies, JINR, Dubna

B.Naumann, L.Naumann, S.Tesh

ZfK Rossendorf, Dresden, Federal Republic of Germany

L. Vizireva

HCTI, Sofia, Bulgaria

We have measured vector polarization of deuteron P_{xd} and proton P_{xp} and analyzed vector polarization transfer coefficient $\varkappa = P_{xp}/P_{xd}$ in the fragmentation process $d^{\uparrow} + {}^{12}C \to p^{\uparrow}$ at 0^{o}. We have used double-scattering method with elastic p-p scattering as an analyzer of the proton polarization. The general lay-out of double-scattering experiment for polarization transfer measuring is shown in fig.1.

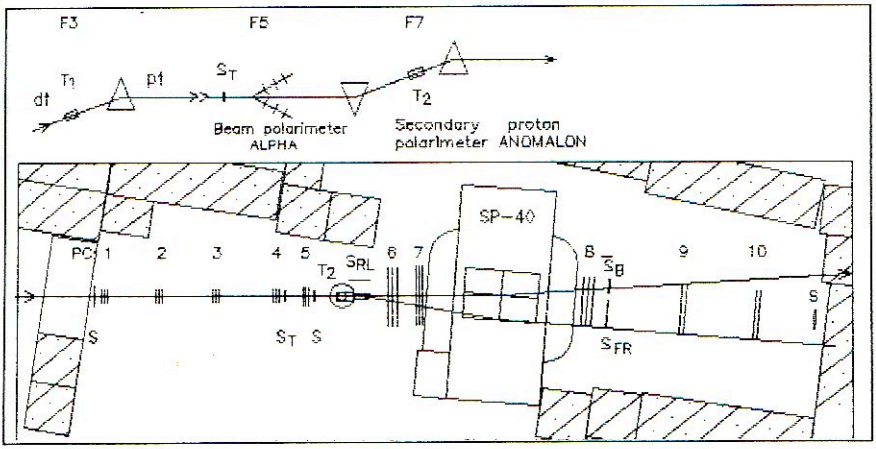

Fig.1. Lay-out of experiment and proton polarimeter ANOMALON

SP-40- analyzing magnet (gap 20cm)
PC - 2- and 3-dimensional MWPC
S - scintillation counters
S_{RL} *- left recoil hodoscope*
S_{FR} *- right forward hodoscope*
$\overline{S_B}$ *- anti-beam counter*
S_T *- time-of-flight counters*
T_1 *- first carbon target*
T_2 *- liquid hydrogen target.*

Polarization measurement

Two magnetic spectrometers were used: polarimeter ALPHA [1] in focus F_5 for vector-polarized deuteron beam tuning, monitoring and periodical check-up of deuteron polarization during the run and proton polarimeter ANOMALON in focus F_7 for data taking. The application of ANOMALON set-up for proton polarimetry was discussed in the previous paper[2].

Deuteron momentum was chosen 6 GeV/c to increase analyzing power of p-p elastic scattering. Deuteron polarization for different mode operation was $P_x^+=0.40$ and $P_x^-=0.36$ and remained stable during data taking time.

We have taken only two stripping proton momentum because of the beam time lack. The momentum of 3 GeV/c corresponds to the internal momentum $k=0$ and $\alpha=1$. Therefore it was taken for calibration and estimation of systematic errors. The momentum of 4.25 GeV/c ($k=410$ MeV/c) is the most interesting because α should reach the minimal value of -1 near this point according to standard Paris deuteron wave function (see fig.5).

At the latter momentum the admixture of deuteron in secondary beam was 30% and was separated by TOF. Taking into account polarimeter aperture, the effective analyzing power was 0.16. We used soft forward trigger when proton was scattered at polar angle $\vartheta_1 > 30$ mrad while recoil information was used as a mark for further off-line analysis. The trigger rate reached 4 "raw" events per burst at the highest polarized deuteron beam intensity of 10^9 per burst. The polarimeter measured scattering angle ϑ_1 and scattered proton momentum P_{1M}. The projectile proton momentum P_0 was known[2] with accuracy 1.3%. For secondary proton beam line tuning we used half momentum stripping protons produced in 9 GeV/c deuteron fragmentation.

Fig.2 demonstrates quality of the elastic event selection. It shows a distribution of the difference between the measured and kinematically expected momenta, P_{1M} and $P_{1\vartheta}$. The left tail of the raw data spectrum points out a background of inelastic event. The final spectrum is the result of the event selection with the recoil mark. Fig.3 shows polarimeter inverted efficiency $1/\varepsilon$ - number of projectile protons per one detected elastic event corrected for the event reconstruction efficiency as a function of cutoff scattering angle ϑ_{1m}. One can find a good agreement between the measured $1/\varepsilon$ for the forward trigger events and the estimated one.

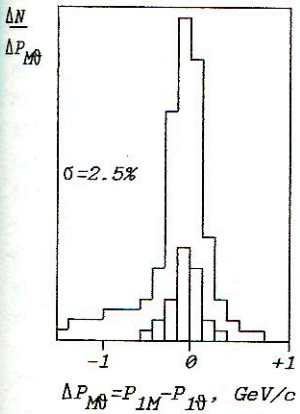

Fig.2.Raw and selected momentum spectrum for p-p elastic events.

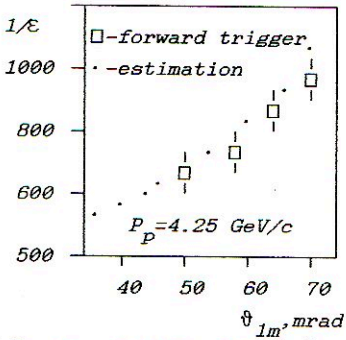

Fig.3. 1/ε vs. cutoff angle ϑ_{1m} ε- corrected polarimeter efficiency.

Stability of measured proton polarization P_x as a cut criterion function is illustrated by fig.4a. One can see that within the experimental errors P_x is independent of the cutoff scattered angle or four-momentum transfer for both the types of selection: recoil and forward triggers. It could be considered as reliability of the result.

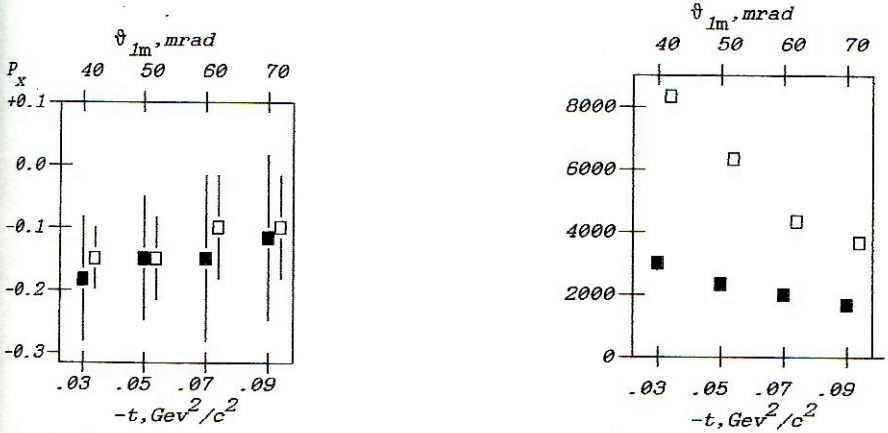

Fig.4. Proton polarization P_x (a) and event number N (b) vs. cutoff scattering angle ϑ_{1m} or four-momentum transfer -t at P_p=4.25 GeV/c and P_d=6 GeV/c for event selections types: □-forward and ■-recoil triggers.

Furthermore, as it follows from fig.4 b, in the case of our set-up configuration the forward trigger increases statistics by several times and allows one to operate with small scattering angles.

Results and conclusion

We have measured the vector-polarization transfer for deuteron fragmentation at momentum 6 GeV/c with ANOMALON set-up at the JINR synchrophasotron. The deuteron polarization was measured with ALPHA polarimeter[1]. For stripping protons with momentum 3 GeV/c and internal momentum k=0 we have obtained $æ$=1.00±0.07. High internal nucleon momentum k=410 MeV/c corresponding to the stripping proton momentum 4.25 GeV/c has been reached. It has been found that $æ$ changes the sign and equals $æ$=-0.4±0.20 at this k. Our data are shown in fig.5 together with data from ref[3] and some theoretical predictions. The curves correspond to: 1 - standard Paris deuteron wave function, 2 - final state interactions were taken into account[4], 3 - relativistic DWF with core[5] and 4 - without core[6]. From fig.5 we can conclude that it is very important to advance to nucleon internal momenta of 600- 650 MeV/c to have a reason to choose between different theoretical predictions based on experimental data. High luminosity polarimeter for this purpose is described in ref [7].

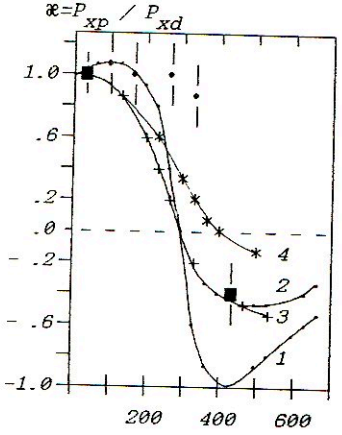

Fig.5. Transfer polarization æ vs. internal momentum k • - P_d=9 GeV/c from ref[3] ■ - P_d=6 GeV/c this data.

We are grateful to accelerator and beam control staff for the support.

References

1. V.G.Ableev et al Nucl. Instr. and Meth. A306(1991) 73-82
2. A.I.Chernenko et al in: Proc.of Workshop on Deuteron,June,Dubna,1991
3. V.G.Ableev et al in: Proc. of 7-th Int. Conf. on Polarization Phenomena in Nucl. Phis., 9-13 July, Paris 1990,p 40 F.
4. M.G.Dolidze and G.I.Lykasov in: Proc. of LINP XXY Winter School, v.3 p.187-215, 1990. & in: Proc.[2]
5. M.A.Braun and M.V.Tokarev Vestnik LGU,1988,v.4,p.7. & in: Proc.[2]
6. M.A.Braun and M.V.Tokarev Vestnik LGU,1983,v.4,p.22. & in: Proc.[2]
7. Yu.T.Borsunov et al "Anomalon setup modernization... " in: Proc.[2]

ANOMALON SETUP MODERNIZATION INTO HIGH LUMINOSITY POLARIMETER FOR POLARIZATION TRANSFER MEASURING FOR RELATIVISTIC DEUTERON FRAGMENTATION WITH HIGH INTERNAL PROTON MOMENTA AT SYNCHROPHASOTRON

Yu.T.Borsunov, L.B.Golovanov, A.D.Kirillov, V.V.Perelygin, V.F.Peresedov, P.A.Rukoyatkin, B.Yu.Semenov, L.N.Strunov, A.Yu.Sukhanov A.L.Svetov, V.A.Sviridov, A.P.Tsvinev, A.V.Zarubin, L.S.Zolin
Joint Institute for Nuclear Research, Dubna

S.L.Belostotsky, A.A.Izotov, V.V.Sulimov
Leningrad Institute of Nuclear Physics, Gatchina, Russia

Measurements of vector polarization transfer coefficient κ for deuteron fragmentation at Dubna [1] and Saclay[2] reached internal proton momentum k=410 MeV/c. Further advance to higher internal momenta is available at JINR synchrophasotron in nearlest future. It requires to increase accelerator polarized beam intensity by 5 - 10 times up to 10^{10} per burst, to increase spill-out time and to create high luminosity polarimeters. In this paper we describe the modernization of ANOMALON set-up into a high luminosity proton polarimeter realized in 1991 . The points of the modernization were as follows: beam line, target and polarimeter.

Hardware modernization

In ref[3] poor beam line VP-1 transparency and low transportation ability from focus F_6 to F_7 was noted. 35% of the beam has been lost at bending and collimation. And just 15% of the beam was focusing on the target because last pair of quadrupole lenses was installed over 20 m up stream the beam . The new beam line and set-up lay-out are shown in fig. We increased diameter of collimator and beam pipe to 190 mm and installed new pair of quadrupole lenses 20 K100. By this way we believe to increase the luminosity by 5 times.

The special 1 meter length liquid hydrogen target was designed, constructed and installed. It gives 3 times increase of luminosity. Furthermore new target has low dense walls in both forward and recoil directions that makes possible to decrease the detection threshold for recoil protons.

In ref[2] was shown a possibility to detect elastic scattered proton at a small polar angle with a small systematic errors. That is why we increased the forward spectrometer aperture to 200 mrad in symmetrical left-right configuration taking into account threshold angle of 40 mrad. It gives 1.6 times increase of luminosity. To increase the azimuthal aperture of the forward spectrometer we widened analyzing magnet gap by 2 times. Furthermore we created two complementary left and right scintillation recoil systems. One of it is suitable for recoil proton energy measurement.

Polarimeter parameters

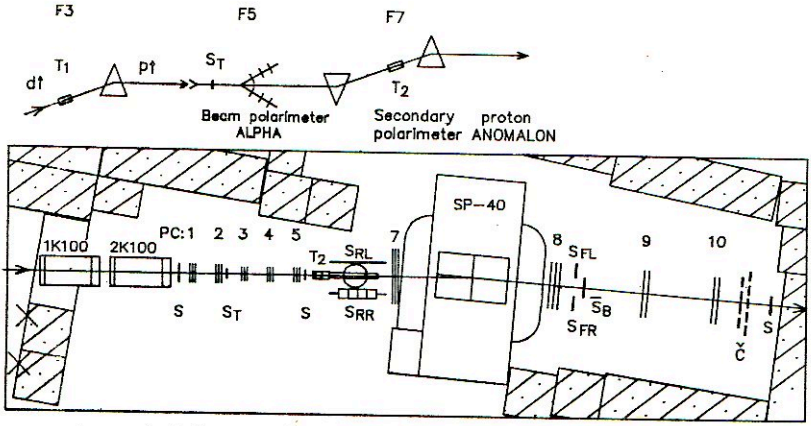

Lay-out of the magnetic spectrometer ANOMALON for relativistic nuclear fragmentation and polarization experiments

K 100 – quadrupole lenses
SP-40 – analysing magnet
PC – three- and two-dimensional MWPC
S – scintillation counters
SRL,SRR – left and right recoil scintillation E-counter walls

SFL,SFR – forward scintillation hodoscopes
SB – antibeam counter
ST – TOF counters
C – cherenkov Z^2 hodoscopes
T1 – first target
T2 – liquid hydrogen target

Magnetic spectrometer as a high luminosity polarimeter is shown in fig. Polarimeter consists of:

-coordinate detector for the track tracing based on MWPC with sensitive area from 64 mm to 1280 mm composed into 8 three-dimensional and 2 two-dimensional blocks with 5000 readout LRS channels;

-precision TOF system with extremely large flying base 40 - 100 m for p-d identification up to kinematical limit;

-flexible triggering system with scintillation counters;

-left and right recoil systems with full absorption scintillation counters;

-profilometer for the beam position check-up and control;

-special 100 cm liquid hydrogen target;

-analyzing magnet SP-40 with the pole gap of 40 cm.

Spectrometer forward angle acceptance: polar is ±100 mrad, azimuthal is ±35 deg.; recoil angle acceptance: polar is 60-90 deg., azimuthal ±45 deg.

Conclusions

As a result of the modernization we expect 40-50 times increase of luminosity of our experiment. Polarimeter can measure three kinematical parameters of the p-p elastic scattering that is very important for reliability of results. For such a polarimeter the value of æ within statistical errors ±20% at internal momentum 600 - 650 MeV/c can be obtained during one week data taking time. And for 15 day run full internal momenta range within the errors from 10 to 20% can be scanned.

We are grateful to Chief Engineer Services, Work-Shops and the Cryogenic Division for the support of our experiments.

References

1. T.Dzikowski et al "Transfer vector-polarization measuring at synchrophasotron..." in: Proc. of Workshop on Deuteron, Dubna, June, 1991
2. C.F.Perdrisat in: Proc./1/.
3. A.I.Chernenko et al "A possibility of transfer polarization measuring..." in: Proc./1/.

STUDY OF RESIDUAL INTERACTIONS IN PROTON INDUCED DEUTERON DISINTEGRATION AT MEDIUM ENERGIES

Imrich Zborovsky
Nuclear Physics Inst., Czechoslovak Acad. Sci., Řež
CSFR

I. Introduction

The deuteron breakup on nucleon at medium and high energies is in a first approximation a relatively simple process in which one of the nucleons of the deuteron interacts with a probe (e.g., a proton) and the other one proceeds largely undisturbed. This simple picture presented by a plane-wave impulse approximation (PWIA) needs to be corrected for the effects such as multiple scattering, final-state interaction (FSI) and also for other possible contributions. In this paper we study the process $p\vec{D} \rightarrow ppn$ for incoming momenta $\cong 1 - 2$ GeV/c with a proton detected at 180^0. This reaction canal dominates in deuteron breakup processes induced on the proton probe especially in the region when one approaches the corresponding kinematic limit. The aim of our study is to estimate here the final-state interaction (FSI) and the Glauber double-scattering (GDS) effects. The calculation results are compared with the measured inclusive cross sections and the tensor asymmetry T_{20} for deuteron breakup at 1.25 and 2.1 GeV /1/.

II. Outlook of the Formulation

We outline here the used formalism for the calculation of the inelastic scattering of a proton from a deuteron target

$$P_1 + \vec{D} \rightarrow P'_3 + N'_1 + N'_2 \qquad (1)$$

incorporating the multiple-scattering expansion in addition to the single-scattering contribution of the PWIA. The calculation is performed in the rest frame of the deuteron using non-relativistic wave functions. The transformation of the NN amplitudes to this frame and kinematics are treated relativistically.

Assuming that nuclear interaction is mainly mediated by

two-body forces and following an earlier work of Faddeev /2/ and Wallace /3/, for the three nucleon T matrix elements we write /1/:

$$\langle \mathcal{A}(f)|\,\overline{\mathbb{T}}\,|\mathcal{A}(i)\rangle = \langle \mathcal{A}(f)|T_a G_o T_c|\varphi_1\rangle + \langle \mathcal{A}(f)|T_a T_o T_b|\varphi_1\rangle$$

$$+\langle \mathcal{A}(f)|T_b|\varphi_1\rangle + \langle \mathcal{A}(f)|T_b T_o T_c|\varphi_1\rangle \qquad (2)$$

$$+\langle \mathcal{A}(f)|T_c|\varphi_1\rangle + \langle \mathcal{A}(f)|T_c T_o T_b|\varphi_1\rangle .$$

In the approximation used here we neglect the third- and higher-order scattering terms. G_o is a free propagator and free-particle two-body transition matrices T_i satisfy the Lippmann-Schwinger equations. The initial state $|\varphi_1\rangle$ is the product of the free nucleon state $|p_1\rangle$ and the deuteron wave function $|D_{23}\rangle$ which is antisymmetrized and normalized to unity. The state $\langle f|$ describes a free motion of the three nucleons after reaction. When evaluating amplitudes (2), the approximation /1,3/ is often used which includes only impulse terms and the energy-conserving parts of double-scattering terms connected with decomposition:

$$G_o = P[1/(E-H_o)] - i\pi\delta(E-H_o). \qquad (3)$$

It is hoped that in the deuteron breakup the principal-value part cancels the higher-order scattering terms similar to the case of elastic pD scattering. We proceed here in a different way exploring the method of evaluating the nucleon-nucleon wave functions in energy continuum. So we include the whole propagator G_o and expansion (2) up to its first order. Using the decomposition

$$(1 + G_o^- T_x^-)\, f = \psi_x^- = f + \phi_x^- \qquad (4)$$

expression (2) can be rewritten to:

$$\langle \mathcal{A}(f)|\,\overline{\mathbb{T}}\,|\mathcal{A}(i)\rangle = \langle \mathcal{A}(f)|T_b|\varphi_1\rangle + \langle \mathcal{A}(f)|T_c|\varphi_1\rangle$$

$$+\langle \mathcal{A}(\phi_a^-)|T_b|\varphi_1\rangle + \langle \mathcal{A}(\phi_a^-)|T_c|\varphi_1\rangle \qquad (5)$$

$$+\langle \mathcal{A}(\phi_c^-)|T_b|\varphi_1\rangle + \langle \mathcal{A}(\phi_b^-)|T_c|\varphi_1\rangle .$$

In a more explicit form we divide it into three parts which describe the PWIA, final state interaction contribution and Glauber double-scattering corrections of our approximation. For the particle with momentum $\vec{k}'_3$ detected as a proton we have:

$$\overline{T}_{A(f,i)} = \overline{T}_0 + \overline{T}_{FSI} + \overline{T}_{GDS} \qquad (6)$$

$$\overline{T}_0 = 2\cdot {}_a\langle p'_1|_{bc}\langle \Phi_o(n'_2p'_3)|T_{ab}|\varphi_1\rangle + 2\cdot {}_a\langle p'_2|_{bc}\langle \Phi_o(p'_3n'_1)|T_{ab}|\varphi_1\rangle$$

$$\overline{T}_{FSI} = 2\cdot {}_a\langle p'_1|_{bc}\langle \Phi^-(n'_2p'_3)|T_{ab}|\varphi_1\rangle$$

$$\overline{T}_{GDS} = 2\cdot {}_a\langle p'_1|_{ca}\langle \Phi^-(n'_2p'_3)|T_{ab}|\varphi_1\rangle + 2\cdot {}_b\langle n'_1|_{ca}\langle \Phi^-(p'_2p'_3)|T_{ab}|\varphi_1\rangle$$

The residual interactions with the forward fast moving particle were neglected here. The NN wave functions $\langle \Phi_o(N'_iN'_j)+\Phi^-(N'_iN'_j)|$ /4/ were found as solutions of the Schrödinger equation with a potential and with appropriate asymptotic.

The PWIA terms make a main contribution to our amplitudes. For its dominant part, the spectator mechanism, we write:

$$\overline{T}_0 = -\sum_{\mu_2} \mu'_1\mu'_2 \overline{T}_{\mu_1\mu_2}(N'_1N'_2, pn; \vec{k}_1-\vec{k}'_1)\ \Phi^M_{\mu_2\mu_3}(\vec{k}'_3)\,. \qquad (7)$$

Here Φ denotes the deuteron wave function with the spin projection M and with the nucleon spin projections μ_2, μ_3. The NN amplitudes $\overline{T}$ were evaluated at energy ε which corresponds to the collision of the projectile with the nucleon from the deuteron at rest. For the FSI and GDS terms in (6) we write:

$$\overline{T}_{FSI} = -\sum_{\bar{\mu}_j\mu_2} \bar{\mu}'_1\bar{\mu}_j \mathbf{T}_{\mu_2\mu_2}(\vec{k}_d)\cdot \mu_j \mathbf{R}^M_{\mu_2}(\vec{k}_d, \vec{k}_f, \mu'_2, \mu'_3, T'=0)$$

$$\overline{T}_{GDS} = \sum_{\bar{\mu}_k\mu_2} \bar{\mu}'_k\mu_1 \mathbf{T}_{\mu_1\mu_2}(\vec{k}'_1)\cdot$$

$$\frac{1}{2}\left[\ \bar{\mu}_k \mathbf{R}^M_{\mu_2}(\vec{k}_d, \vec{k}_f, \mu'_2, \mu'_3, T'=0) + \bar{\mu}_k \mathbf{R}^M_{\mu_2}(\vec{k}_d, \vec{k}_f, \mu'_2, \mu'_3, T'=1)\ \right]$$

The quantity R used here corrects the deuteron wave function in (7) and represents the overlap integral of the deuteron WF and the

part of the NN wave functions responsible for residual interactions.

$$\bar{\mu}_j^R{}^M_{\mu_2}(\vec{k}_d,\vec{k}_f,\mu_2',\mu_3',T') = \int d\vec{r} e^{-i\vec{k}_d\vec{r}/2} \Phi^-_{\bar{\mu}_j\mu_k}{}^*(\vec{r};\vec{k}_f,\mu_2',\mu_3',T') \Phi^M_{\mu_2\mu_k}(\vec{r}).$$

The function Φ^- describes the residual interaction of the NN pair with isospin T', relative momentum $\vec{k}_f$ and the total momentum $\vec{k}_d$. The magnetic quantum numbers $\bar{\mu}_j,\mu_k$ and μ_2',μ_3' are nucleon spin projections before and after interaction.

III. Concluding Remarks

We have plotted the results of our calculations together with the experimental $\vec{d}p$-breakup data /1/ at a deuteron energy of 1.25 and 2.1 GeV. Paris deuteron wave function /6/, the NN amplitudes /5/ and the potentials for the lowest orbital NN canals /7,8/ with proper description of NN phases were used as an input.

To conclude our results, we find that in the investigated region FSI plays more significant role than GDS and especially that in canals $^1P_1, ^3S_1-^3D_1, ^3D_2$, has at medium energy a certain influence on cross section and corrects considerably the behavior of T_{20}. We note here that similar conclusions have been made for the inclusive deuteron breakup at higher energies /9/, for the $\vec{d}p$ disintegration at medium energy /1/ and also for the processes of the deuteron electro-disintegration /10/. The insufficiency in cross section at 2.1 GeV energy for low proton detected momenta can be connected with π-production not included in the calculation.

I would like to thank prof. B.Tecoult for valuable ideas stimulating this work, Yu.Panebratsev, A.Litvinenko for many helpful discussions and M.Sumbera for technical support in the calculations.

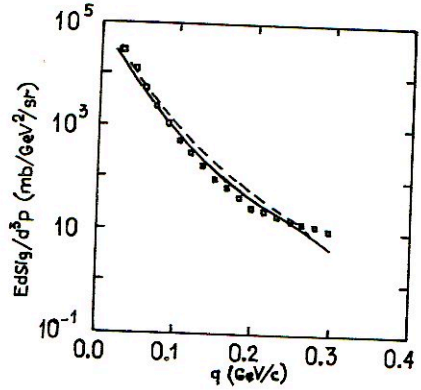

Fig. 1. The inclusive H(d,p)X invariant cross section of ref. 1 at a deuteron energy of 1.25 GeV. plotted versus the proton momentum in the deuteron frame compared with the PWIA and the full calculation results.

°°°° experimental data
- - PWIA
——— PWIA + FSI + GDS (S,P,D waves)

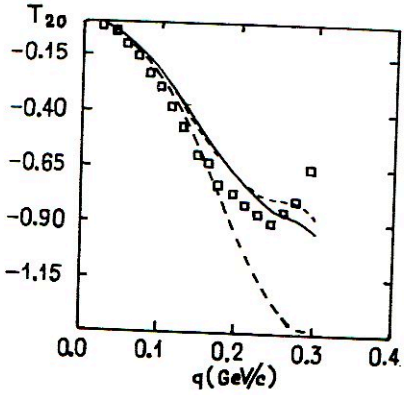

Fig. 2. The T_{20} data of ref. 1 of 1.25 GeV compared with the PWIA and with the complete calculation.

□□□□ experimental data
- - PWIA
——— PWIA + FSI + GDS (S,P,D waves)
---- PWIA + FSI

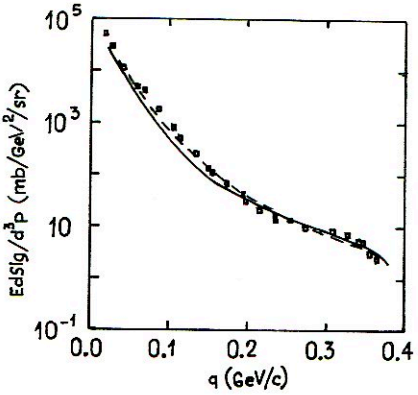

Fig. 3. The inclusive H(d,p)X invariant cross section of ref. 1 at a deuteron energy of 2.1 GeV. plotted versus the proton momentum in the deuteron frame compared with the PWIA and the full calculation results.

∘∘∘∘ experimental data
- - PWIA
—— PWIA + FSI + GDS (S,P,D waves)

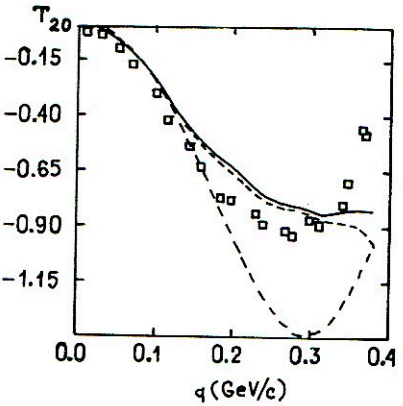

Fig. 4. The T_{20} data of ref. 1 of 2.1 GeV compared with the PWIA and with the complete calculation.

□□□□ experimental data
- - PWIA
—— PWIA + FSI + GDS (S,P,D waves)
---- PWIA + FSI

REFERENCES

1. V.Punjabi et al., *Phys.Rev.* **C39**(1989),608.
   C.F.Perdrisat et al., *Phys.Rev.* **C42**(1990),1899.
2. L.D.Faddeev, *Zh.Eksperim.i.Teor.Fiz.* **39**(1960),1459.
3. J.M.Wallace, *Phys.Rev.* **C5**(1971),609.
4. M.L.Goldberger and K.M.Watson, *Collision theory. NEW YORK--LONDON-SYDNEY.* 1964.
5. R.A.Arndt et al., *Phys.Rev.* **D28**(1983),97.
6. M.Lacombe et al., *Phys.Lett.* **B101**(1981),139.
7. R.V.Reid, *Ann.Phys.* **50**(1968),411.
8. B.D.Day, *Phys.Rev.* **C24**(1981) 1203.
9. M.G.Dolidze, G.I.Lykasov, Preprint JINR, E2-89-666, Dubna (1989)
10. E.L.Bratkovskaya, A.I.Titov, A.A.Goy, B.L.Reznik, Preprint JINR, E2-90-524, Dubna 1990.

DEUTERON STRUCTURE INFORMATION OBTAINED FROM BREAKUP DATA

C. F. Perdrisat

College of William and Mary,
Williamsburg, VA 23185, USA

and

V. Punjabi

Norfolk State University
Norfolk, VA 23504, USA

INTRODUCTION

There is now a considerable amount of data concerning deuteron breakup, both from the exclusive (p,2p) and (d,2p), and the inclusive (d,p) reactions, for energies ranging from a few hundreds of MeV to almost 10 GeV. The question of whether these data present us with sensitive tests of the deuteron wave function, has not received a definite answer so far. There are still many unanswered questions: (i) the complete description of the reaction, (ii) the choice of the scaling variables, (iii) the construction, of a relativistically invariant wave function, and of a covariant NN->NN, or NN->NX amplitudes.

The prime motivation for experimental studies of deuteron breakup is the hope that ultimately the deuteron wave function will be determined experimentally, including all non-nucleonic components. The relationship between observables and the deuteron wave function has been discussed many times[1]. Does the rather detailed experimental information we now have actually allow us to "see" the deuteron structure, or, as suggested for example by Kuehn & Nissan-Meyer[2], does one merely "see" the nature of the target boundary on which the deuteron breaks up? Newer developments to describe the data include the use of Light Cone Variables (LCV) or of the Infinite Momentum Frame (IMF), pioneered by Frankfurt and Strickman[3], with work by many others, including but not exclusively, Azhgirei et al[4]., Kobushkin et al.[5], Dolitze et al.[6]

The importance in deuteron breakup, of processes other than the IA has been pointed out before. A direct extraction of a deuteron wave function from either invariant cross section (ICS) or T_{20} data is not meaningful, unless the impulse approximation (IA) process is dominant. Neither the empirical evidence, nor our Feynman graph calculation limited to NN interaction, indicate that processes beyond the IA are negligible.

The static properties of the deuteron, like binding energy, quadrupole moment, magnetic moment and asymptotic D/S ratio, are well reproduced by all NN interaction potential models (Paris[7], Bonn[8], Reid[9], Moscow[10], Amsterdam[11]....) because they are imposed

"ad origine". Yet great difficulties are encountered in measuring non-static properties of the deuterons, which these models predict: particularly the nucleon wave function in momentum space and the amount of D-state; or the amount of non-nucleonic components like NN*, ΔΔ..., or the importance of a 6-quark component which are discussed in the literature, but for which there is scant experimental evidence.

Inclusive experiments have been conducted at 0°, where the detected proton is undoubtedly the spectator, at least for small internal momenta (along the $q_{\parallel}$ axis), as well as at angles large enough for the detected proton to be almost certainly not the spectator (along the $q_{\perp}$ axis). In both cases the inclusive ICS data can be fairly well understood in terms of removal of the unobserved neutron by elastic and inelastic process, including pion exchange followed by rescattering or absorption. Agreement with some of the data can be achieved with a non-relativistic deuteron-wave function in the lab frame, provided all rescattering graphs are included. Comparable agreement can also be obtained with several forms of relativistic wave function in the IMF approach. However, some of these calculations use spin-averaged amplitudes for NN->NN, NX, or πX, and therefore cannot be trusted for the evaluation of spin observables like T_{20} and P_y. The calculation we have made at William and Mary, is non-relativistic and takes into account only the elastic part of the NN interaction, but contain the full spin structure as contained in phase-shift amplitudes. We have the advantage of having phase shift amplitudes available both for pp and np up to 1300 MeV (VPI, R. Arndt et al.[12], also Saclay-Geneva[13] up to 800 MeV), which is just high enough for a deuteron energy of 2.1 GeV when the fermi momentum is taken into account. However, both pp and np amplitudes are not precise above 800 MeV, due to the scarcity of experimental data; this is particularly true for the np amplitudes. In this presentation, aspects of the Saclay inclusive data[14], chosen from the recent results of a series of experiments at 0° and 2.1 GeV deuteron energy, will be described in some details. We will also report <u>new results of the polarization transfer measurements</u> in the <u>inclusive</u> channel made last year at Saclay (experiment 202), and the <u>new study of exclusive</u> $^1H(d,pp)n$ reaction at 2.0 GeV by Belostotsky[15] and collaboration. These data include ICS, the analyzing powers A_y, A_{yy} (exclusive data) and T_{20}, polarization transfer P_y, as well as a systematics of energy and target dependence for ICS and T_{20}. There are aspect of the data which are close enough to the IA prediction for one to be led to conclude, that the inclusive and exclusive data we now have are giving us an image, probably quite distorted, but never-the-less an image of the deuteron wave function.

INCLUSIVE REACTION AT 2.1 AND 1.25 GeV

First the energy and target dependence of all measured observables of the <u>inclusive</u> channel (d,p) are examined; cross section (ICS) and T_{20} data exist at 1.25 GeV (hydrogen only,

Saclay), 2.1 GeV (hydrogen, ^{4}He, C, Ti and Sn, Saclay), 4.2 GeV (C only, Berkeley[16]) and 7.2 GeV (hydrogen and C, Dubna[17,18]).

In figure 1 the Saclay ICS data at 2.1 GeV, for the 5 targets ^{1}H, ^{4}He, C, Ti and Sn are shown versus the momentum of the proton, q, in the deuteron frame, obtained by Lorentz transforming the laboratory proton momentum:

$$q\ (\equiv q_l) = \gamma(p_l - \beta E_p), \text{ with } \gamma = E_d/m_d \text{ and } \gamma\beta = p_d/m_d, \quad (1)$$

where $p_l = p\cos\theta_p$, p and E_p, and p_d and E_d are the momenta and energies of the detected proton and beam deuteron, respectively; θ_p is the proton detection angle. In the IA with breakup by np interaction, q is the spectator momentum; the inclusive invariant cross section is then given by:

$$E_p d\sigma/d^3p d\Omega = E_p\ \sigma^{tot}_{NA}\ (\sigma^{inel}_{dA}/\sigma^{tot}_{dA})\ \cdot\ \phi^2(q)\,. \quad (2)$$

For all targets there is the indication of a shoulder in the ICS around q=300 MeV/c; this anomaly is most noticeable for the ^{1}H target. Except the shoulder, the data indicate a simple A^n-behavior, with n=0.43±0.03.

In figure 2 the corresponding T_{20} data for the same targets are shown versus q. The target dependence is quite small; the largest tensor analyzing power is observed for ^{1}H, the smallest for Ti. Note for all targets T_{20} is minimum near q=280 MeV/c, and appears to be heading for a zero near q=450-500 MeV/c. In the IA for (d,p) and when the observed proton is a "spectator", T_{20} is entirely defined by the deuteron wave function:

$$T_{20} = (2\sqrt{2}\phi_D\phi_S - \phi_D^2)/\sqrt{2}(\phi_S^2 + \phi_D^2)\,. \quad (3)$$

This expression reaches a minimum value of $-\sqrt{2}$ when $\phi_D/\phi_S = -\sqrt{2}$.

In figure 3 ICS data for C at 2.1 GeV are shown together with the 4.2 and 7.2 GeV C-data versus the same variable q, the proton momentum in the deuteron frame.

In figure 4a we show that for ^{1}H, T_{20} is the same at 1.25 and 2.1 GeV when plotted versus q for 0<q<250 MeV/c. Additional evidence for energy independence comes from the comparison of the T_{20} data for C at 2.1 and 7.2 GeV as in figure 4b: here again there is little evidence for an energy dependence, and this up to 400 MeV/c in this case.

The data discussed thus far suggest the following relatively simple picture:

a) the data is sensitive to the deuteron structure,

b) the variable q effectively acts as a scaling variable; but q can be a scaling variable only in the extreme case where the proton is a spectator: the data suggest dominance of the spectator regime.

c) the cross sections follow a simple A^n law over the range of targets A's investigated at Saclay, 4<A<110, indicating that the structure of the target, in particular its boundary, is not very important (contrary to ref. 2),

d) The invariant cross sections show no energy dependence when plotted versus q up to q≈200 MeV/c, which is of course the Impulse Approximation prediction.

f) The cross section data show an anomalous shoulder around q=300 MeV/c, as first discovered in Dubna, noticed in Berkeley and confirmed in Saclay. This anomaly is not explained in a spectator model without pion exchange, even when rescattering is included. A number of calculations suggest that meson effects might explain the shoulder, at least qualitatively.

The LCV internal momentum k_F has been proposed as the proper relativistic scaling variable, leading to several ways of writing down a relativistic form for the deuteron wave function. The definition of k_F is interesting; it is a function of α_p, the fraction of the projectile deuteron carried by the proton, as seen from an Infinite Momentum Frame moving towards the deuteron; then $\beta=1$ (and $\gamma=\infty$), and:

$$\alpha_p = (p_l+E_p)/(p_d+E_d) \equiv (q_l+E_q)/m_d ; \qquad (4)$$

with values between 0 and 1, and a corresponding α_n for the neutron with values between 1 and 0: $\alpha_p+\alpha_n=1$. Here again p and E_p, p_d and E_d are the momenta and energy of the detected proton and beam deuteron, respectively; q is defined from (1) and $E_q = \sqrt{(q^2+m^2)}$.

The definition of k_F in terms of α is (ref. 3):

$$k_F = m(1-2\alpha)/2\sqrt{\alpha/(1-\alpha)}. \qquad (5)$$

It is obvious from (4) that α_p is a relativistic invariant. Therefore the relation between q from equation (1), and k_F from equation (5) is independent of the beam energy; it is also independent of the target mass.

In figure 5 are the Saclay C data (at 2.1 GeV) and the Dubna C data (7.2 GeV) versus the LCV k_F; As in fig. 2 the C-data agree in absolute value and shape at least up to 200 MeV/c. No drastic difference is seen when k_F replaces q. Because of the one to one relation between q and k_F nothing new can be learned by changing from one variable to the other. One of several possible forms for a relativistic deuteron wave function is (see ref. 5):

$$\psi^2_{rel} = (k_F/2(1-\alpha)(1-2\alpha))\ \phi^2_{nr}(k_F), \qquad (6)$$

where ϕ_{nr} is the non-relativistic wave function.

Interestingly, the quantity k_F of the IMF approach is closely related to the recoil variable discussed by Gugelot[19], who proposed a model for particle removal reactions in general, in which the projectile is required to bring energy and momentum to the target so as to have all reaction participants on the energy shell, and energy and momentum conserved at all vertices. This model has met with a number of successes for various inclusive and exclusive processes. Such a four-momentum transfer can be visualized as due to the projectile entering the potential well of the target and

imparting an momentum-energy transfer ($\Delta\vec{p}$,ΔE) to it. The kinematics of the problem is entirely defined; because of the energy-momentum communicated to the target, the target moves with a velocity $\beta=\Delta\vec{p}/(m_2+\Delta E)$ and the recoil momentum $\vec{p}_S$ is not the internal momentum; the latter is then defined in the frame where both nucleons have zero momentum, $\vec{q}'+\vec{q}_B=0$. The quantity q_B is closely related to k_F; indeed both are defined by the requirement that the constituents of the targets be on their mass shell. Energy is conserved in the definition of q_B, which explains the small numerical differences between q_B and k_F visible in figure 6. As the deuteron beam energy increases, or the mass of the target increases, q_B tends towards k_F. We have used k_F here, but it is obvious from figure 6 that the two internal momenta k_F and q_B are practically the same numerically, and have very similar physical meanings.

MULTIPLE SCATTERING CALCULATION

We will now compare the inclusive Saclay data with our calculation[20], which includes NN->NN vertices only, and evaluates all first and second order Feynman graphs shown in figure 7 for the breakup process. The physics inputs to the calculation are the phase shift analysis amplitudes of Arndt et al (VPI) (and also Lechanoine et al, Saclay-Geneva for the 1.25 GeV hydrogen data), and 5 modern wave functions for the deuteron shown in momentum space in figure 8: Paris, Bonn, Amsterdam, Moscow and Reid soft-core. The calculations require an on-shell approximation for all 2-body amplitudes. The 3-body amplitudes of all diagrams are added. Antisymmetrization is enforced by including the amplitudes for each diagram with the two proton interchanged.
We point out the following:

a) as seen in figures 9 and 10, the calculation reproduces the ^{1}H inclusive cross section data at 1.25 and 2.1 GeV deuteron energy up to the anomaly without problem; the sensitivity to the wave function is small;

b) for the tensor analyzing powers T_{20}, the calculation is partially successful at 1.25 GeV (fig. 11), but quite unstable at 2.1 GeV (fig. 12), that is it depends critically upon the large q behavior of the wave function, which affects the rescattering correction drastically.

c) in the only case where the spin dependence can be tested (T_{20} at 1.25 GeV, seen in figure 13, where the Saclay-Geneva phase shift are available), it is seen that T_{20} depends upon the spin structure of the NN amplitudes through the double scattering terms.

d) the polarization transfer data results from experiment 202 at 2.1 GeV (preliminary[21]) are seen in figure 14; they are in good agreement with the Impulse Approximation up to q≈300 MeV/c. The correction from the double scattering diagrams appears to be too large. Again, in the simplest IA the proton polarization is that of a proton in a fully polarized deuteron, and entirely defined by the deuteron wave function:

$$P_y = (\phi_S^2 - \phi_D^2 - \phi_D\phi_S/\sqrt{2})/(\phi_S^2 + 5\phi_D^2/4 - \phi_D\phi_S/\sqrt{2}). \quad (7)$$

This value of P_y passes through zero when $\phi_D/\phi_S = -\sqrt{2}$, i.e. at the same q-value for which T_{20} goes through a minimum. The P_y data in figure 14 do indeed go through zero at q=280 MeV/c, i.e. precisely where T_{20} is minimum; however the experimental minimum value of T_{20} is not the predicted $-\sqrt{2}$, but ≈ -0.9.

Although neither the data, nor the results of our calculation justify such a procedure, we have extracted the ration ϕ_D/ϕ_S from the inclusive 2.1 GeV T_{20} and P_y data using the inverted formulas of (3) and (7). The results are seen in figure 15, where they are compared with the same ratio for the Paris wave function. The two entirely independent experiments give results which are surprising close to each other; the rather large difference at large q, can only be understood to mean that distortions affect T_{20} much more than P_y, in agreement with the results of the calculation. Figure 14 also tells that the calculation does not reproduce P_y!

EXCLUSIVE BREAKUP, DATA AND CALCULATION

Experiment 145 (ref. 10) at Saclay measured the analyzing powers A_y and A_{yy} in a kinematics selecting the unobserved neutron as spectator, and detecting one proton (scattered) at 18° in the spectrometer SPES 4, and the other (recoil proton) in a proportional chamber-plastic scintillator telescope between 57 and 65° in the lab; the out-of-plane acceptance of the recoil telescope was ±5°; the momentum of the forward proton was increased in steps of 0.1 GeV from 1.6 to 2.0 GeV/c, with one additional point at 2.05 GeV/c; the kinematics is entirely defined by the forward momentum vector and the angle of the recoil. There are two kinematical solutions for each angle pair up to the kinematical limit; these are distinguished by the time-of-flight differences between the 2 protons, and also by the energy of the recoil proton. As seen in figures 16 for A_y, the data are in fair agreement with our calculation with Paris wave function (left); the sensitivity to the wave function is shown by comparing the data with the Bonn wave function (right). In these figures only those events with near coplanarity have been kept, as the calculation is limited to coplanar kinematics. The Tensor analyzing power A_{yy} are shown in figure 17a, and compared to the calculation with paris and Bonn wave function. The corresponding ratios ϕ_D/ϕ_S are in figure 17b; they are strikingly similar to the ratios in figure 15.

The exclusive polarization transfer results shown in figure 18 with calculation for Paris wave function; the small number of events requires that all data point for one value of the forward proton momentum be combined into one data point for each of the kinematical solutions.

Δ EXCITATION AND EXCLUSIVE BREAKUP

It has been suggested that a few diagrams including Δ-

excitation at one of the vertices should be added to the NN diagrams retained in our calculation. We point out that in a calculation of the impulse approximation diagrams based on empirical NN amplitudes which are phenomenological fits to the NN data base, virtual, single and double Δ excitation at the NN vertices is included.

When the rescattering diagrams are added, more complex diagrams involving one or two Δ-excitation lead to a whole family of diagrams with virtual pion exchange. Still missing would be some of which are typical 3-body diagrams. Adding explicit Δ-excitation graphs to the NN rescattering ones would lead to some double counting.

We have experimental evidence, based on the TRIUMF 500 MeV exclusive ^{2}H(p,2p)n data showing that, empirically, there may be no need to add explicit Δ-excitation graphs. In several entirely different kinematic regions, all presumed to lead to Δ-excitation on the basis of the pair wise NN invariant masses (which is $\approx m_N+m_\Delta$), we find that the 6 diagrams are sufficient to explain most of the deviations from the IA (here it is pp). In one region, (Perdrisat et al.[22]) symmetric kinematics, a single Δ-excitation diagram has been evaluated by Yano[24]; see figure 19a. Our calculation, seen in figure 19b taken from Epstein et al.[23] gives comparable results without explicit Δ-excitation.

The same calculation indicates that in the region of very small recoils, where the TRIUMF (p,2p) experiment (Punjabi et al.[25]) was calibrated on the elastic pp cross section and suffered from uncertainties no larger than 1%, the data seen in figure 20 are below calculation by about $(9.4\pm0.8(\text{stat})\pm2.5(\text{syst})^*)\times10^{-2}$. Such a missing strength could indicate that the wave function is depleted at small q, for example by an anomalous D-state distribution as in the Moscow University wave function (Kukulin et al[14]). However this wave function gives incorrect predictions for the T_{20} and polarization transfer of the inclusive Saclay data.

The situation is likely to be entirely different in the inclusive channel, where no constrain on the presence of pions exists. Yet the Saclay anomaly occurs below pion threshold, and would have to indicate virtual Δ-excitation or pion exchange; it could come from the 3-body, double pion exchange diagrams (without external pion lines) which are not included in our calculation.

CONCLUSION

The new data from Saclay, including both inclusive (d,p) and exclusive ^{1}H(d,pp)n, show interesting features; some of these can be explained in impulse approximation, some not. The William and Mary calculation of Feynman graphs succeeds in explaining a good part of the data, but fails most notoriously for the polarization transfer P_y. The ratios ϕ_D/ϕ_S we deduce from T_{20}, A_{yy} and P_y are in good agreement with each other; we are "seeing" the deuteron structure in a q-window around 100 to 200 MeV/c, and it looks similar to the Paris wave function. Universality of the data - target and energy independence - indicates that q (or k_F, or q_B)

are scaling variables, although the theoretical background for this behavior is unclear. The Dubna ICS anomaly, although well established experimentally, has yet to be explained in a consistent manner, that is including all polarization data available, at least for the Saclay and the Dubna energies.

REFERENCES

1. R. Serber Phys. Rev. 72, 1008 (1947)
   R. G. Glauber, Phys. Rev. 99, 1515 (1955)
   A.I. Akhiezer and A.G. Sitenko, Phys. Rev. 106, 1236 (1957)
   L. Bertocchi and D. Treleani, Nuov. Cim. 36A, 1 (1976)
2. J. Kuehn and S.A. Nissan-Meyer, Nucl. Phys. A312, 409 (1978)
3. L.L. Frankfurt and M.I. Strickman, Nucl. Phys. B148, 107 (1979)
4. L.S. Azhgirei et al. Sov. J. Nucl. Phys. 46, 988 (1987)
5. A.B. Kobushkin and L. Vizireva, J. Phys. G8, 893 (1982)
6. Dolitze et al. Dubna preprint, 1990
7. M. Lacombe et al. Phys. Lett. 101B, 139 (1981)
8. R. Machleidt, Adv. Nucl. Phys. 19, 189 (1989)
9. R. V. Reid. Ann. Phys. (N.Y.) 50, 411 (1969)
10. V.M. Krasnopol'sky et al. Phys. Lett. 165B, 7 (1985), and V. I. Kukulin, private communication (1991)
11. H. Dijk and B.L.G. Bakker, Nucl. Phys. A494, 438 (1989)
12. R. Arndt et al. Phys. Rev. D35, 128 (1988)
13. J. Bistricky et al. J. Phys. (Paris) 48, 199 (1987)
14. C.F. Perdrisat et al. Phys. Rev. Lett. 59, 2840 (1987)
    V. Punjabi et al. Phys. Rev. 39, 608 (1989)
15. S. Belostotsky et al. Spin Conf. Paris 1990
16. L. Anderson et al. Phys. Rev. C28,1224 (1983)
17. V.G. Ableev et al. Nucl. Phys. A393, 491 (1983)
18. V. G. Ableev et al. Pism'ma Zh. Eksp. Teor. Fiz. 49, 558 (1988)
19. P.C. Gugelot, Phys. Rev. C30, 654 (1984)
20. C.F. Perdrisat and V. Punjabi, Phys. Rev. C42, 1899 (1990)
21. E. Cheung et al. Bull. Am. Phys. Soc. Washington Spring (1991)
22. C.F. Perdrisat et al. Phys. Rev. 156B, 38 (1985).
23. V. Punjabi et al. Phys. Rev. C38, 2728 (1988), and
    M. Epstein et al. Phys. Rev. C42, 510 (1990)
24. A.F. Yano, Phys. Lett. 156B, 33 (1985).
25. V. Punjabi et al. Phys. Letters B179, 207 (1986).

FIGURE CAPTION

1. Invariant cross section for A(d,p)X at 2.1 GeV deuteron energy and 0° proton detection angle, for several targets; the dotted curved is the Paris deuteron density normalized to the ^{1}H-data. The variable is q, the Lorentz transform to the deuteron frame, of the proton momentum. Note the anomalous hump near q=300 MeV/c.

2. Tensor analyzing power T_{20} versus q, for the same energy, detection angle and targets as fig. 1

3. The ICS for (d,p) at 0° for C at 2.1 Gev (open square), 4.2 GeV (black square) and 7.2 GeV (X), versus q.

4a) Comparison of T_{20} for ^1H at 1.25 GeV (open circle) and 2.1 GeV (black circles). b) Comparison of T_{20} for C at 2.1 GeV (black triangles) and 7.2 GeV (open circles).

5. ICS for C at 0° and 2.1 GeV (open square) and 7.2 GeV (X), versus k_F, the light cone variable.

6. The relation between q and k_F, the light cone variable, and q_R, the recoil variable of ref. 19.

7. The two impulse approximation (IA) and 4 rescattering graphs calculated in ref. 20.

8. The deuteron density distributions for the 5 wave functions discussed, including the latest version of ref. 14.

9a) and b), IA and MS results for $^1H(d,p)$ ICS at 1.25 GeV and 0°, 5 wave functions, VPI NN amplitudes; data of ref. 7.

10a) and b), same as 9a and b, but for 2.1 Gev.

11a) and b), IA and MS results for $^1H(d,p)$ T_{20} at 1.25 GeV and 0°, data of ref. 7.

12a) and b), same as 11a and b, but for 2.1 GeV

13 T_{20} at 1.25 GeV, Paris and Bonn wave function, with VPI and Paris-Geneva phase shift NN amplitudes.

14. Preliminary 0° proton polarization for vector polarized 2.1 GeV deuteron; shown is the ratio $\kappa = P_y/P_d$. The expected value at q=0 is 0.985±0.005 for all 5 wave functions considered. Part a show the IA prediction, part b) the full calculation for the 5 wave functions.

15. The ratios ϕ_D/ϕ_S extracted from the Saclay inclusive $^1H(d,p)X$ data at 1.25 and 2.1 GeV assuming the IA, and using formulas (3) for T_{20} and (6) for P_y.

16. Vector analyzing power A_y at 18° for 2.0 GeV deuterons in the $(\vec{d},pp)$ reaction (ref. 10), compared to the calculation for the Paris (left) and Bonn (right) wave functions. Data for both the low (full circle) and high (open circle) recoil proton energy solutions defined.

17a. Same as 16 but for the tensor analyzing power A_{yy}.

17b. Ratio ϕ_D/ϕ_S derived from A_{yy} in fig. 17a, 1.6 to 1.8 GeV/c only.

18. Polarization of the forward proton for deuteron with spin up (P_{up}) and spin down (P_{down}); again, it is the ratio P_y over P_d. Each kinematics characterized by the forward proton momentum has been reduced to one data point statistically averaged over the acceptance of the experiment.

19a) Data from ref. 22 for equal angle and equal energy $^2H(p,2p)$ kinematics at 508 MeV, versus proton angle and compared with the estimate of the Δ contribution by Yano in ref. 24. b) Same data (but including unequal energies) shown versus the neutron recoil momentum, and compared to the MS calculation (from ref. 23). Paris wave function.

20. Comparison of data from ref. 25 with the MS calculation in the q<55 MeV/c region. The missing strength in this region is discussed in the text.

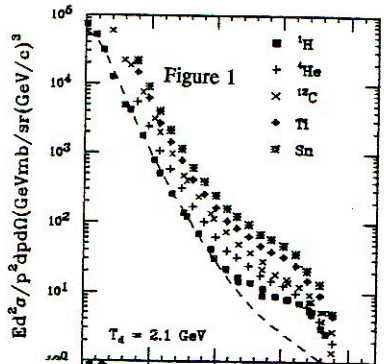
Figure 1
$Ed^2\sigma/p^2dpd\Omega$(GeVmb/sr(GeV/c)^3
^{1}H
^{4}He
^{12}C
Ti
Sn
T_d = 2.1 GeV

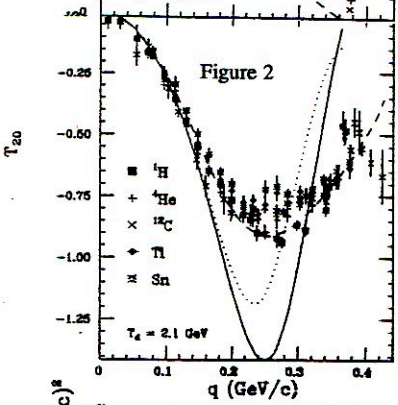
Figure 2
T_{20}
^{1}H
^{4}He
^{12}C
Ti
Sn
T_d = 2.1 GeV
q (GeV/c)

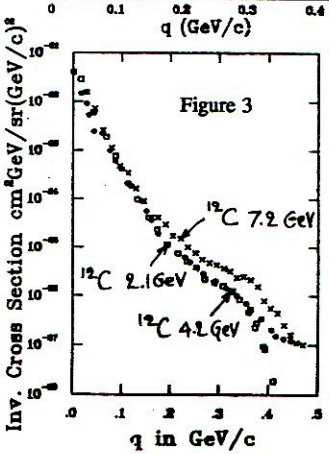
Figure 3
Inv. Cross Section cm^{2}GeV/sr(GeV/c)^3
^{12}C 7.2 GeV
^{12}C 2.1GeV
^{12}C 4.2 GeV
q in GeV/c

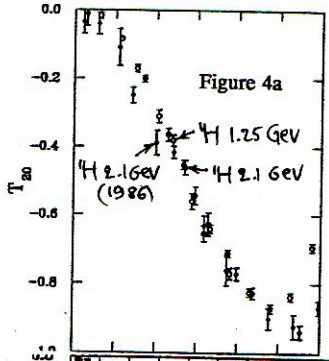
Figure 4a
T_{20}
^{1}H 1.25 GeV
^{1}H 2.1GeV (1986)
^{1}H 2.1 GeV

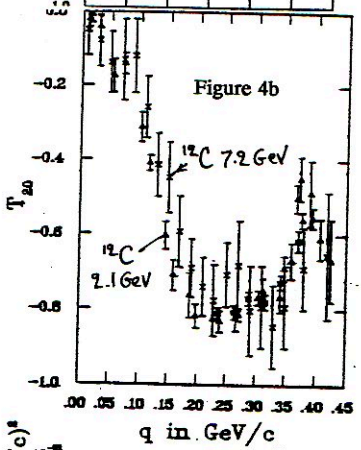
Figure 4b
T_{20}
^{12}C 7.2 GeV
^{12}C 2.1 GeV
q in GeV/c

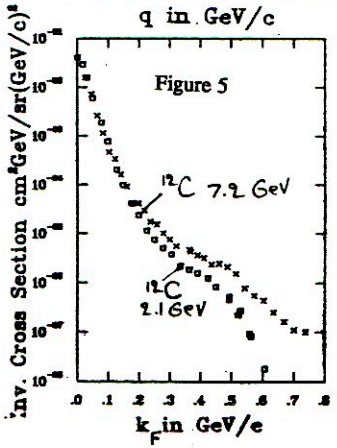
Figure 5
Inv. Cross Section cm^{2}GeV/sr(GeV/c)^3
^{12}C 7.2 GeV
^{12}C 2.1GeV
k_F in GeV/c

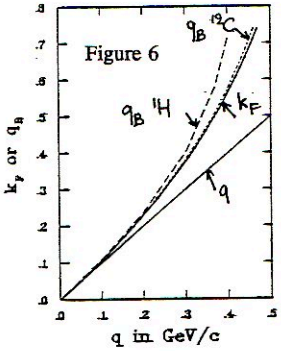
Figure 6
q_B ^{12}C
q_B ^{1}H
k_F
q
k_F or q_B
q in GeV/c

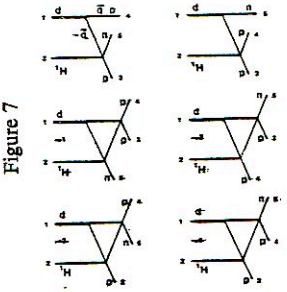
Figure 7

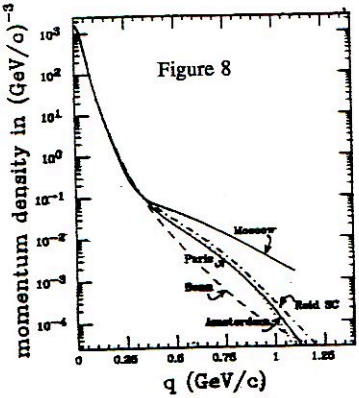
Figure 8
momentum density in (GeV/c)$^{-3}$
Moscow
Paris
Saclay
Rutgers SC
Amsterdam
q (GeV/c)

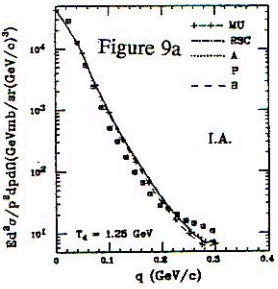
Figure 9a
MU
RSC
A
P
B
I.A.
T_q = 1.25 GeV
q (GeV/c)

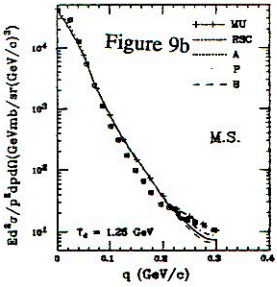
Figure 9b
MU
RSC
A
P
B
M.S.
T_q = 1.25 GeV
q (GeV/c)

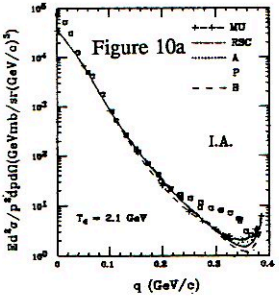
Figure 10a
MU
RSC
A
P
B
I.A.
T_q = 2.1 GeV
q (GeV/c)

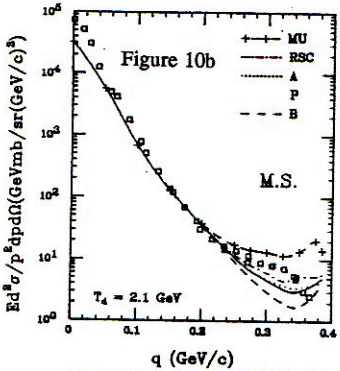
Figure 10b
MU
RSC
A
P
B
M.S.
T_d = 2.1 GeV
$Ed^3\sigma/p^2dpd\Omega$(GeVmb/sr(GeV/c)^3)
q (GeV/c)

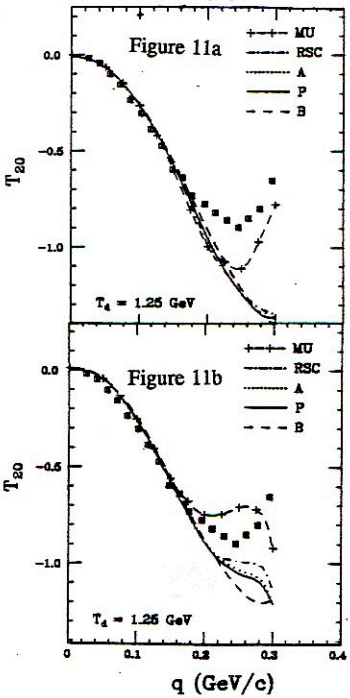
Figure 11a
MU
RSC
A
P
B
T_d = 1.25 GeV
T_{20}
Figure 11b
MU
RSC
A
P
B
T_d = 1.25 GeV
T_{20}
q (GeV/c)

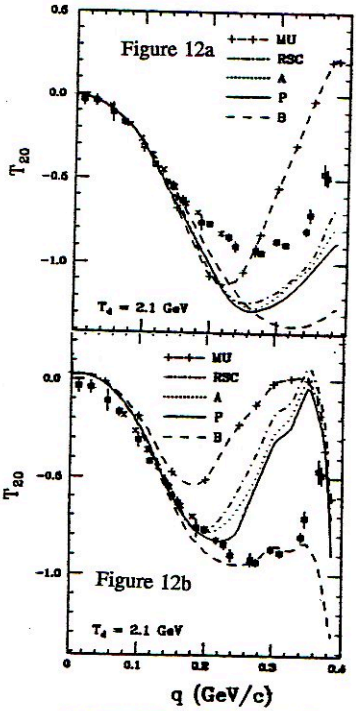
Figure 12a
MU
RSC
A
P
B
T_d = 2.1 GeV
T_{20}
Figure 12b
MU
RSC
A
P
B
T_d = 2.1 GeV
T_{20}
q (GeV/c)

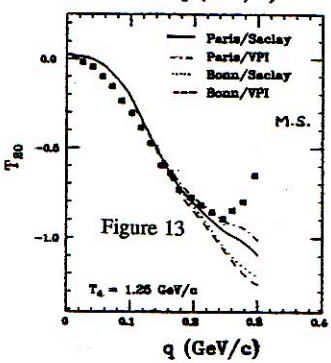
Paris/Saclay
Paris/VPI
Bonn/Saclay
Bonn/VPI
M.S.
Figure 13
T_d = 1.25 GeV/c
T_{20}
q (GeV/c)

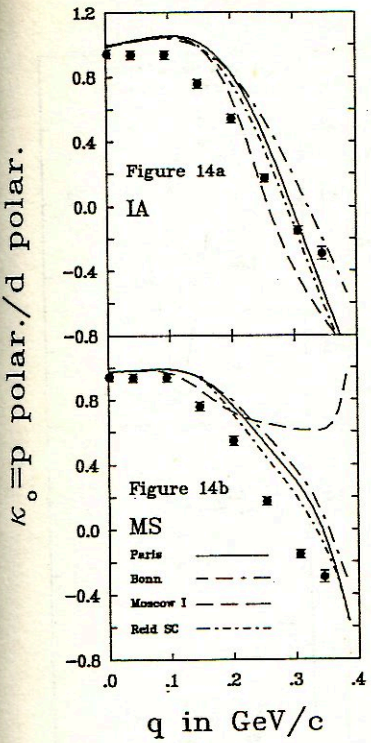

κ_o = p polar./d polar.

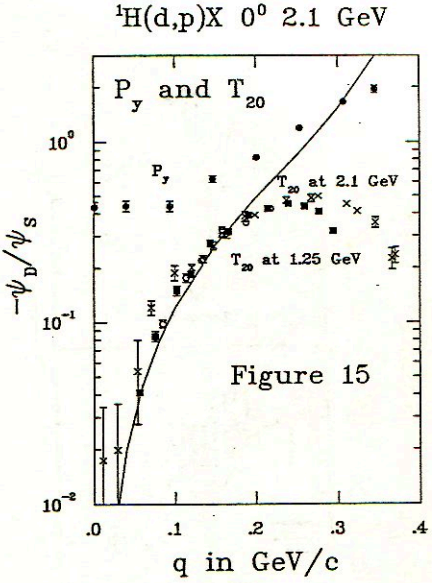

Figure 16

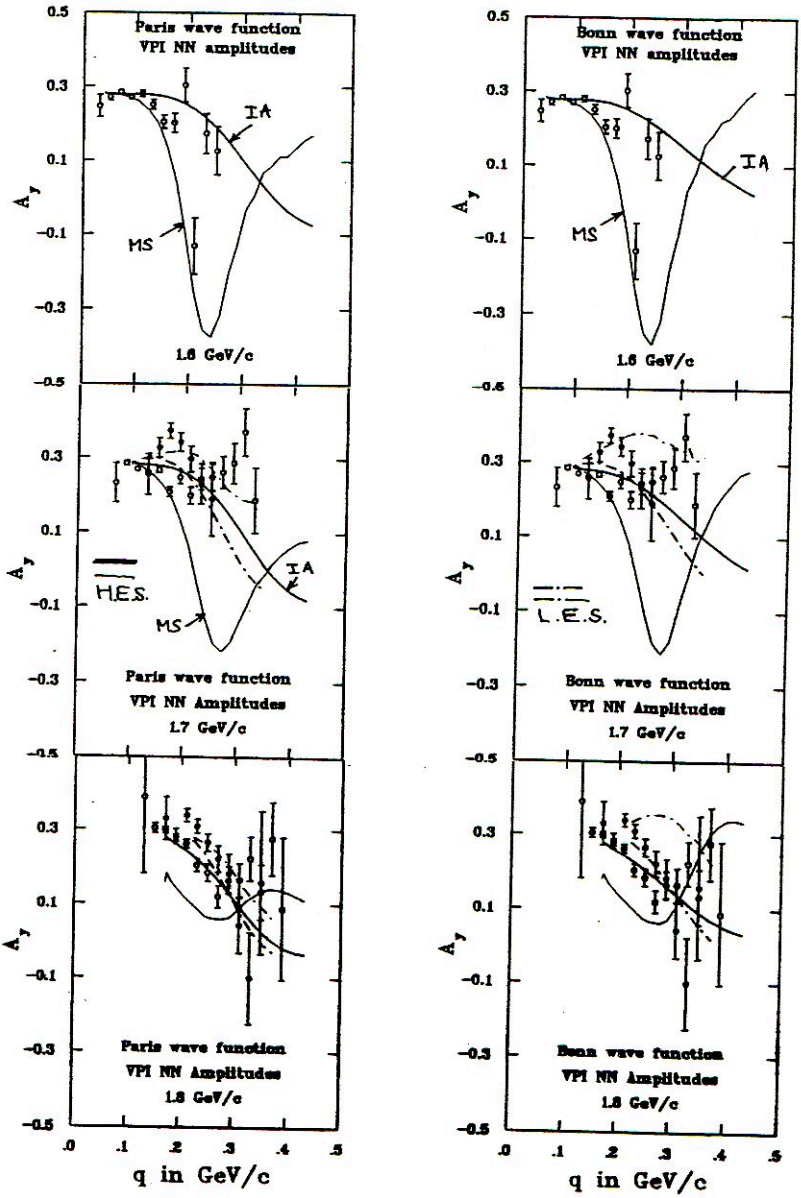
Paris wave function
VPI NN amplitudes
IA
MS
1.6 GeV/c
H.E.S.
IA
MS
Paris wave function
VPI NN Amplitudes
1.7 GeV/c
Paris wave function
VPI NN Amplitudes
1.8 GeV/c
q in GeV/c
Bonn wave function
VPI NN amplitudes
IA
MS
1.6 GeV/c
L.E.S.
Bonn wave function
VPI NN Amplitudes
1.7 GeV/c
Bonn wave function
VPI NN Amplitudes
1.8 GeV/c
q in GeV/c

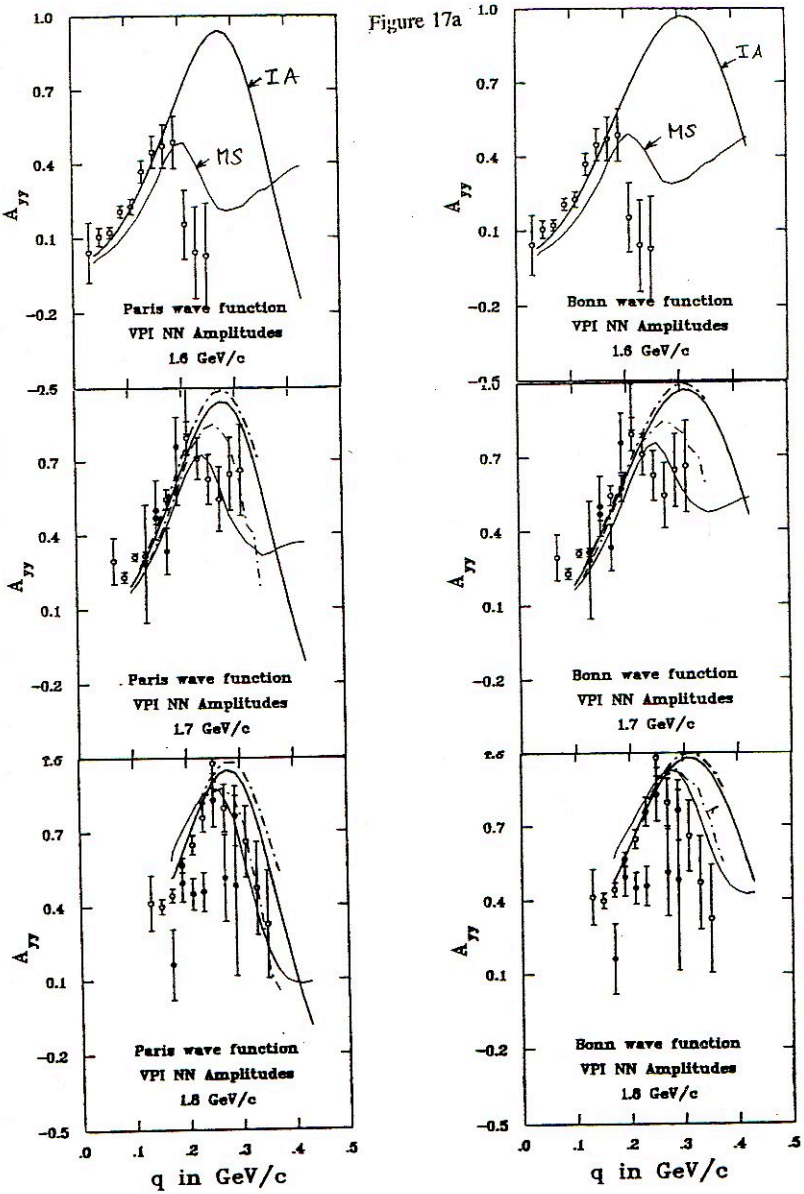
IA
MS
Paris wave function
VPI NN Amplitudes
1.6 GeV/c
Paris wave function
VPI NN Amplitudes
1.7 GeV/c
Paris wave function
VPI NN Amplitudes
1.8 GeV/c
Bonn wave function
VPI NN Amplitudes
1.6 GeV/c
Bonn wave function
VPI NN Amplitudes
1.7 GeV/c
Bonn wave function
VPI NN Amplitudes
1.8 GeV/c
A_yy
q in GeV/c

Figure 17a

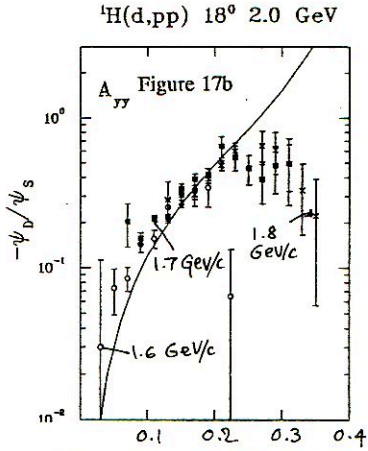
^{1}H(d,pp) 18° 2.0 GeV
A_{yy} Figure 17b
$-\psi_D/\psi_S$
1.6 GeV/c
1.7 GeV/c
1.8 GeV/c

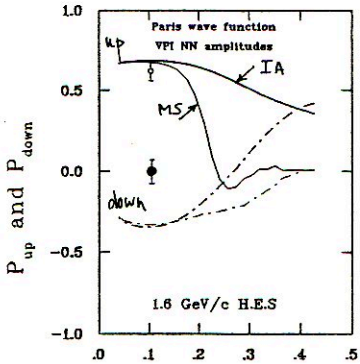
Paris wave function
VPI NN amplitudes
up
IA
MS
down
1.6 GeV/c H.E.S
P_{up} and P_{down}

Figure 18

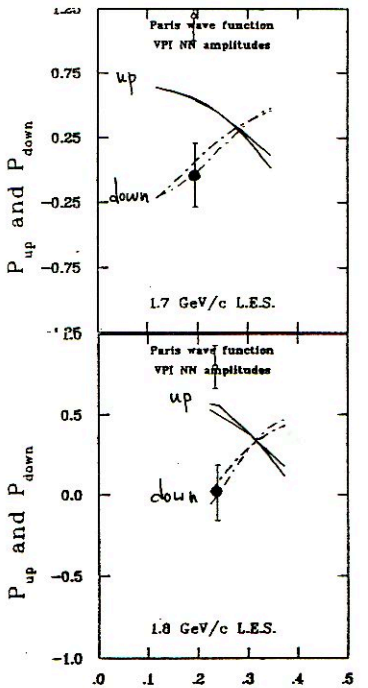
Paris wave function
VPI NN amplitudes
up
down
1.7 GeV/c L.E.S.
1.8 GeV/c L.E.S.
P_{up} and P_{down}
q in GeV/c

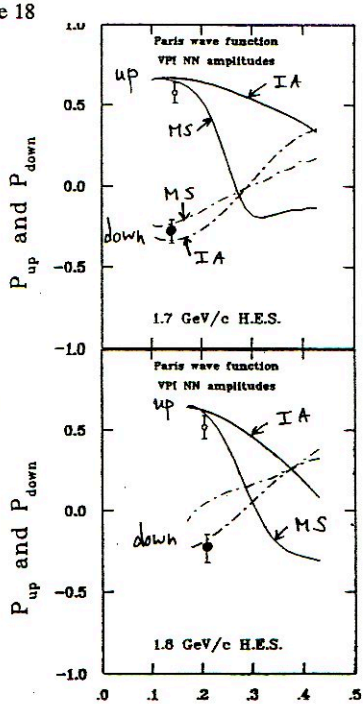
Paris wave function
VPI NN amplitudes
up
IA
MS
down
1.7 GeV/c H.E.S.
1.8 GeV/c H.E.S.
P_{up} and P_{down}
q in GeV/c

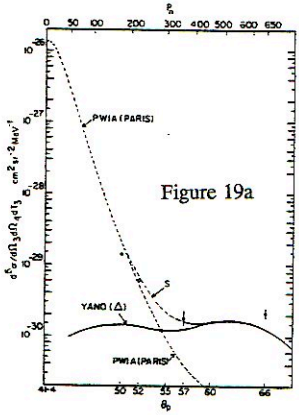

Figure 19a

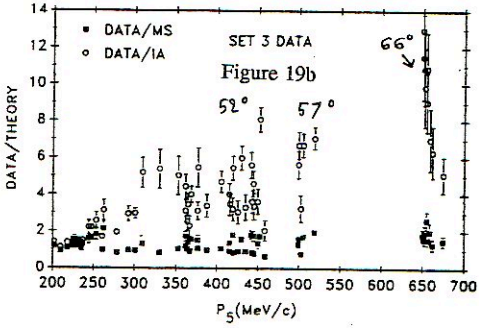

Figure 19b

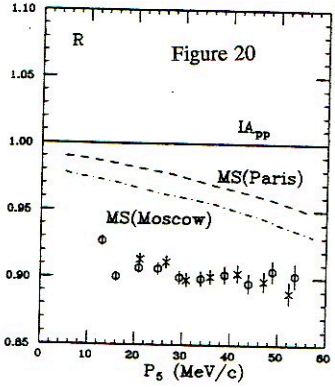

Figure 20

POSSIBILITY OF EXCLUSIVE STUDY OF THE DEUTERON BREAK-UP WITH POLARIZED PROTONS AND DEUTERONS AT COSY

V.I.Komarov, Joint Institute for Nuclear Research, Dubna
O.W.B.Schult, Institut für Kernphysik, Forschungszentrum Jülich, FRG

ABSTRACT

Exclusive study of the deuteron break-up with polarized protons and deuterons in a collinear geometry is discussed. The possibility of performing such experiments using a special magnetic system - 0°Facility at the internal beam of the cooler proton synchrotron COSY is considered.

We discuss here a proposal [1] for exclusive study of the deuteron breakup by protons in conditions which affect high-momentum components of the deuteron wave function (DWF). A novelty of the expected exclusive data is determined by

- a special geometry of the experiment (coincidence of the backward and forward emitted protons),
- an unexplored range of incident proton energies (1-2.5 GeV),
- employment of both initial nucleus polarization.

Advance of the deuteron break-up study is recently possible in the exclusive polarization experiments at high momentum transfers. The conditions of the experiments should conserve a satisfactory sensitivity of the observables to the DWF behavior and the analysis should be accurate enough to determine the contribution by different mechanisms of the process.

A traditional approach of the deuteron break-up study is based on the impulse approximation (IA). It is supposed that backward emission of the fast proton is a good kinematic condition for the IA. The differential cross section of the backward emission decreases rapidly when the momentum of the spectator proton grows up. So the observation of the accompanying scattered projectile proton is preferable in an exclusive experiment at small forward angles where the differential cross section has a maximum. It leads to a collinear geometry (momenta of all the ejectiles are collinear), where the transverse momentum

transfer to the deuteron is reduced to zero. This collinear geometry has not yet been used for the deuteron break-up study in the electronic experiments.

With forward angles in the range $\sim 0^0$-10^0, that is close to the collinear case, the vector and tenzor analyzing power as well as spin-correlation effects can be studied. For the spin-correlation asymmetry measurement two initial particles must be polarized. This kind of experiments is difficult to be carried out at an external beam. An intense proton beam would be needed in this case, causing problems in using a polarized solid state target of the conventional cryogenic type. At the cooler proton synchrotron COSY the necessary luminosity can be reached in the internal polarized proton beam with a polarized deuterium gas target. The measurement of the vector and tenzor analyzing power and spin-correlation asymmetry besides the spin-averaged cross sections at several incident energies will provide redundance of the data necessary for verification of the process mechanism. So the role of nucleon rescattering and pion exchange in the intermediate state of the process can be investigated.

If one restricts itself to the experiments with single scattering and does not measure polarization of the ejectiles, the only useful polarization observable at zero angle of the forward proton emission is the tenzor analyzing power. Nevertheless, the deuteron break-up study in the almost collinear geometry at small forward angles is attractive. Here the process has a character of the inelastic diffraction of the deuteron. The backward proton emission with momenta 0.4-0.5 GeV/c corresponds to the deuteron invariant mass increasing up to 0.3-0.7 Gev during the projectile-deuteron interaction. In this case a longitudinal coherence length is equal to $0.6\sim 0.3$ fm. So one can expect that the process of the deuteron break-up under these conditions becomes similar to the diffractive dissociation of a usual hadron (e.g. $\pi+p\rightarrow 3\pi+p$ dissociation at small angles). A study of such a hadron-like behaviour of few-nucleon systems is of great interest. The maximum energy of protons available at COSY seems to be sufficiently high for such a new approach to the deuteron study.

Deuteron fragmentation can be investigated in an exclusive manner by making sure that the resolution is sufficient to separate p+d→p+p+n processes from p+d→p+p+n+π^0 reactions. This is easier if the projectile energy is not too high. On the other hand, one needs sufficient energy and one must select such a geometry that higher internal momenta of the nucleons composing the deuteron become measurable.

COSY-Jülich with its variable beam energy of 40-2500 MeV for protons is well suited for a study, in particular because of the possibility of choosing the desired beam conditions including cooling at the target position TP2 in the storage ring, where sufficient space can be available for installation of a magnetic system which permits measurements of ejectiles even at 0 and 180 degrees [2]. The internal target geometry not only permits the background from windows or thick targets to be avoided but also allows installation of the most advanced polarized gas targets like the Hermes target*.

A magnetic spectrometer is superior for measuring the proton momenta of interest, especially for obtaining good resolution even in the 2.5 GeV/c region. The planned 0^0-degree facility allows a momentum resolution down to ~ 1% FWHM at 2.5 GeV/c, and a better resolution for ejectiles with lower momenta.

For a working point of COSY Q_x=3.38 and Q_z=3.38 the betatron functions are β_x=1.7m and β_z=5.0m at the TP2. With a ring acceptance of a_x=130π mm mrad and a_z=35π mm mrad, the maximum beam diameters during injection are 31 mm horizontally and 27 mm vertically. The cooled beam emittances are expected to be $\varepsilon_x \sim \varepsilon_z \sim 1\pi$ mm mrad which corresponds to beam diameters of 2.6 mm horizontally, in the direction of dispersion, and 4.5 mm vertically. Such a projectile beam would have ideal overlap with a cluster beam of a gas target and it would provide a well-localized line source if it traverses the polarized gas target cell of the Hermes target. The target at TP2 yields the maximum

luminosity at COSY and the best resolution. At TP2 the required space is available for installations to minimize the gas load of the storage ring.

Furthermore, the COSY telescope which contains TP2 can be operated in the mode which is the best for the particular experiment. This is also possible for other working points of the machine. The fact that the target can be installed at a suitable distance from the spectrometer magnet ensures good imaging by the magnet so that small-angle scattering in detector or chamber has minimal influence on resolution. Monte Carlo simulations including this effect (σ=3 mrad), a position resolution of σ=1mm for multi-wire proportional chambers and a target width of 2 mm horizontally show that a momentum resolution of $\Delta p(FWHM)/p$ of 0.3% can be obtained for ejectiles with a momentum of p=600 MeV/c while a 2.5 GeV proton beam is on the target.

The 0^0-degree facility is depicted in Fig.1. Three dipoles D1, D2 and D3 create a closed orbit bump which is kept constant, since the target is localized. Ejectiles at 180^0 are analyzed by D1 and the forward going particles are measured with the spectrometer magnet D2. A gap height of 20 cm is being considered for D2. There is enough space for the forward detector FD. In cases where both protons go in forward direction the detector SD can detect ejectiles with p~600-1200 MeV/c leaving D2 at the side. Clearly coincidence rates benefit very much from a large gap. The need for running the magnetic field in parallel with the field in the ring magnets and the vicinity of wire chambers restrict the gap height which can be realized. We think that 20 cm is near the optimum.

The variation of the beta functions with distance along the storage ring implies that horizontally at least 31 and 37 mm must be kept free between the axis of the circulating beam and any structural material at the end of D2 and the beginning of D3, respectively. Minimizing detector walls, etc., should measure 0^0-degree ejectiles with momenta up to ~2.7 GeV/c in FD.

*We are very grateful to Prof.Dr.K.Rith for discussion and most valuable hints.

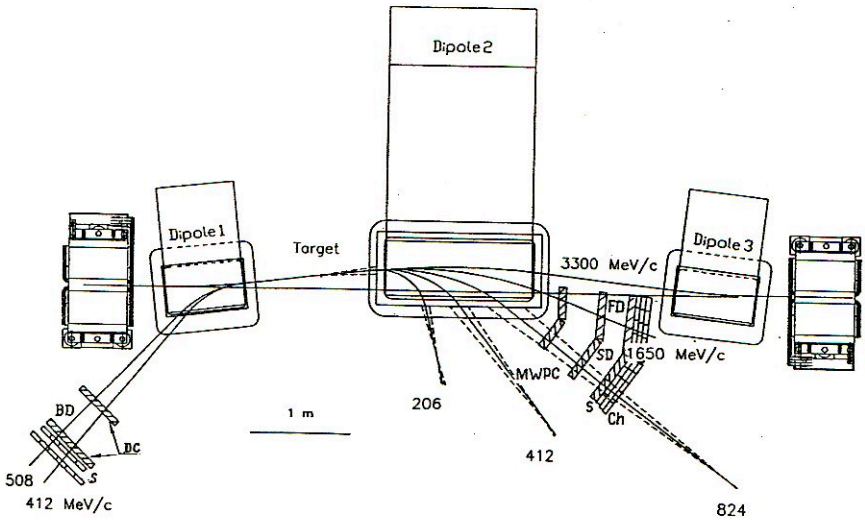

Fig. Schematic drawing of the 0^{o}-facility between quadrupoles of the target telescope of COSY-Jülich. Dipole 1 serves as a 180^{o} spectrometer for protons emitted backward. The C-shape magnet Dipole 2 with a large window serves as a spectrometer for charged particles emitted at and near 0^{o}. FD, SD and BD are forward-, side-, and backward detectors respectively; S - scintillation (Ch-cherenkov) counter hodoscopes; MWPC-multiwire proportional chambers; DC-drift chambers.

We are greatly indebted to coworkers of our collaboration for the joint work and many fruitful discussions of the considered here topic.

REFERENCES

1. Belostotsky S.L.[e], Borgs W.[a], Büsher M.[a], Dakhno L.G.[e], Dienel S.[f], Dombrovski H.[c], Dshemuchadze S.V.[d], Grebenyuk V.G.[e], Grzonka D.[a],

Ivanov M.A.[d], Koch H.R.[a], Komarov V.I.[d], Kurbatov V.S.[d], Leege K.W.[f], Lykasov G.I.[d], Michel P.[f], Müller H.[f], Nikonov V.A.[e], Ohm H.[a], Sabirov B.M.[d], Santo R.[c], Schieck H.P.[b], Schneidereit Chr.[f], Schult O.W.B.[a], Serdyuk V.Z.[d], Seyfarth H.[a], Shelkov V.G.[d], Sistemich K.[a], Zalykhanov B.Zh.[d], Zhuravlev N.I.[d] Proposal for exclusive deuterons break-up study with polarized protons and deuterons at COSY. KFA Jûlich, 1991.

a. Insitut für Kernphysik, Forschungszentrum Jülich, FRG;
b. Institut für Kernphysik, Universität zu Köln, FRG.
c. Institut für Kernphysik, Universität Münster, FRG;
d. Joint Institute for Nuclear Research, Dubna, USSR;
e. Leningrad Nuclear Physics Institute, Gatchina, USSR;
f. Zentralinstitut fûr Kernforschung Rossendorf, Dresden, FRG;

2. Borgs W. et al., Proc. Top. Conf. in Particle production near Threshold, Nashville, IN, USA, October 1990, Particle and Fields Series 41(1991)299, AIP Conference Proceedings 221, New York (H.Nann, E.J.Stephenson eds.)

POLARIZATION PHENOMENA IN DEUTERON FRAGMENTATION PROCESSES

G.I.Lykasov
Joint Institut for Nuclear Research
Dubna

I. Introduction

As known, the investigation of polarization phenomena in hadron and hadron-nuclear interactions gives more detailed information about the dynamic interaction and the structure of colliding particles. The study of the polarization effects in the interaction of particles with deuteron especially in the cumulative region can give new information about the deuteron structure, relativistic and quark effects of deuteron. Investigating the processes like elastic e-d[1] and h-d[2,3] scattering, deuteron break-up by electrons[4,5] and protons[6,7] and also $dA \longrightarrow pX$ reaction [8-12] at intermediate and high energies the authors try to get new information about the deuteron structure from the comparision of theoretical calculations with experimental data.

Note that by the analysis of such processes it is necessary to take into account the reaction mechanism at large and middle N-N distances r_{NN} [6,8-10] and the relaivistic deuteron effects, especially at small r_{NN} [5,9].

There is also an interesting problem related to the polarization phenomena in the reactions discussed : possible

existence of dibaryon states. For example, there are enhancements observed in the two-proton invariant mass distribution in the pionless deuteron break-up,[13] $He^3p \longrightarrow dX$ [14] reaction and so on. Besides, the investigation of polarization effects in hadron and hadron-nuclear reactions can indicate these resonances[15].

This revew is divided into three parts. The investigation of the deuteron tensor component T_{20} in the deuteron fragmentation on nucleons is presented in section II, the role of polarization effects, in particular T_{20}, in the investigation of the dibaryon problem is analyzed in part III . Other possible interesting polarization characteristic of protons in $dp \longrightarrow pX$, when deuteron is vector polarized are considered in section IV.

II. Tensor component polarization of deuteron T_{20} and deuteron structure at small N-N distances

If we consider the inclusive $d+p \longrightarrow p+X$ reaction, then the deuteron tensor component T_{20} can be written in the following general form[16]:

$$T_{20} = \frac{\int Sp(\rho_0 F^+ \Omega_{20} F)\, d\Gamma}{\int Sp(\rho_0 F^+ F)\, d\Gamma}, \qquad (1)$$

where the following notation is introduced :
$\Omega_{20} = \frac{1}{\sqrt{2}}\{\frac{3}{2}(1+\sigma_{pz}\sigma_{nz}) - 2\}$ is the tensor operator corresponding to the deuteron polarization component T_{20}; σ_{pz}, σ_{nz} are the z-components of Pauli's matrices corresponding to the proton and to the neutron ;
$d\Gamma = \frac{d^3p_2 \ldots d^3p_n}{2E_2 \ldots . 2E_n}$ is the phase volume of n-1 final particles ,
$p_2, \ldots, p_n$ and $E_2, \ldots, E_n$ are its momenta and energies; note that p_1 and E_1 are the momentum and the energy of the registered particles.

Consider now the fragmentation type processes of deuteron when it is emitted forward in the l.s. or backward in the rest frame of deuteron. In the general case we must take as the deuteron wave function the relativistic one and the reaction mechanism must be taken into account, i.e., it is necessary to take into account the nonspectator graphs.

We will analyse the discussed processes in the infinite momentum frame (IMF), using Karmanov's relativisation method of d.w.f. Then we will consider our processes in the frame of the old perturbative theory (OPTh) instead of Feynman's covariant formalism, because each Feynman graph of n^{th} order is equivalent to n! time -ordered graphs of OPTh and many of them vanish in IMF. The possible graphs which give the considerable contribution to the observed values of reactions discussed are presented in fig.1. According to refs. of A.Kobushkin,[17] V.Karmanov[5] and others[17-19], w.f.d. $\Psi(x,k_t)$ is related to the nonrelativistic w.f.d. $\Phi_{n.r.}$ depending on the relativistic invariant variable k^2 :

$$\Psi(x,k_t) = \left(\frac{m^2 + k_t^2}{4x(1-x)}\right)^{1/4} \Phi_{n.r.}(\mathbf{k}^2), \qquad (2)$$

where $\mathbf{k}^2 = (m^2 + k_t^2)/(4x(1-x)) - m^2$.

In the spectator mechanism when the pole graph of fig.1a is taken into account, the expression for T_{20} has the following simple form :

$$T_{20} = - \frac{\Psi_0\Psi_2 - \Psi_2^2}{\sqrt{2}\,(\Psi_0^2 + \Psi_2^2)}, \qquad (3)$$

where Ψ_0 , Ψ_2 are the parts of the w.f.d. related to the nonrelativistic S- and D- waves of $\Phi_{n.r.}$.

If all graphs of fig.1 are taken into account, then the expression of T_{20} has a more complex form.

The calculation results of T_{20} are presented in fig.2. Curves in this figure mean the following : 1 is the contribution of the spectator mechanism (fig, 1a); 2 is the contribution of the figs.1(a-c) graphs; 3 is the calculation

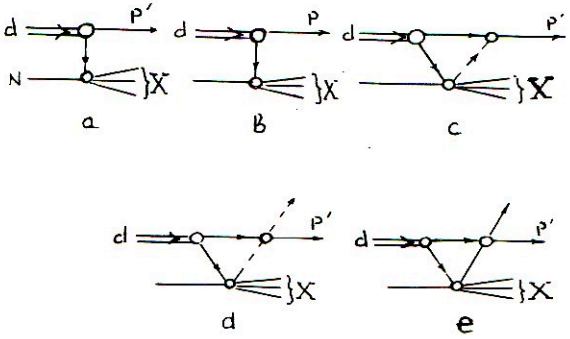

Fig.1. Some graphs of the dp→pX process.

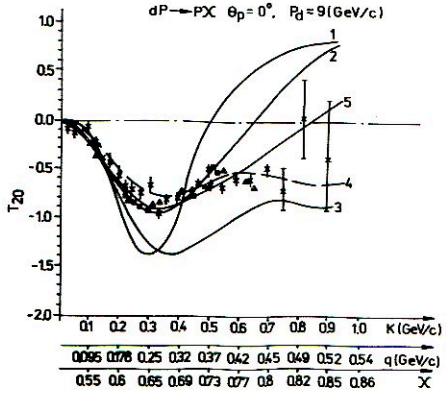

Fig.2. Dependence of T_{20} on k,q,x. Curves: 1– contribution of the spectator mechanism, fig.1a; 2 – contribution of fig.1(a–c) graphs, 3– calculation result from[21]; 4 – T_{20} with the complex 6q–component included in the deuteron (see ref.[9]); 5 – full contribution of fig.1(a–e); experimental data: ▲ , ■ — from[11] ✱ — from [22].

result of M. Braun and M. Tokarev[21] (Gross's relativisation method[20] of d.w.f.) in the spectator mechanism; 4 is the calculation result when the complex six – quark component of deuteron is introduced; experimental data were taken from refs.[11,22].

These results allow us to make the following conclusions. It is just incorrect to use the spectator mechanism, i.e.,fig.1a graph, for the analysis of the deuteron stripping reactions. As very clearly shown in fig.2, it is necessary to take into account the nonspectator type graphs of fig.1 at $0.15 \leq q \leq 0.45$(Gev,/c) or $0.2 \leq k \leq 0.7$ (Gev./c).As shown in fig.2, the deuteron tensor component T_{20} is very sensitive to relativistic effects in deuteron : different relativisation methods yield different T_{20} behaviour at $q \geq 0.45$(Gev./c) or $k \geq 0.7$ (Gev./c). In order to describe the experimental data of T_{20} it is necessary to introduce the complex six-quark (6q) admixture in the d.w.f.: $\Psi_d(x) = \omega_1\Psi(x) + w_2\ \Delta(x)\exp(i\phi)$, where ω_1,ω_2 are parameters related to the probability value of the non–nucleon state existence in the deuteron, $\Delta(x)$ is the non–nucleon admixture of d.w.f. here the 6q–state in deuteron is calculated according to our ref.[23] at $\phi = 110^0$. However according to standard quantum mechanics including only the N-N line in Fok's column, this complexity in d.w.f. results in T–invariance violation. The discrepancy between calculated curve 5 and experimental data at $q > 0.45$(Gev./c) or $k > 0.7$(Gev./c) ($x>0.8$) can't be a direct indication of the 6q–state existence in the deuteron because of its complexity. The theory does not describe the experimental data of T_{20} at $q \geq 0.45$(Gev./c) or $k \geq 0.7$(Gev./c). Therefore the experimental investigation of T_{20} at large k is very interesting because it can help to verify of different theoretical models of relativisation of d.w.f., and this investigation is necessary for the development of our idea about the deuteron structure at small N-N distances.

III. Tensor polarization T_{20} and dibaryon problem

Consider now the relation of polarization phenomena and the problem of the possible existence of dibaryons. Recently new interesting experimental data about the tensor polarization components as functions of the effective mass of two protons produced in dp $\longrightarrow$ ppX were published in ref.[15]. In particular, an interesting phenomenon was observed in this ref.: small oscillations of $T_{20}(m_{pp})$ at m_{pp} = 1.94—1.96 (Gev.). Therefore the question arises, what is a cause of such behaviour of T_{20}. Here we will present the calculation results of T_{20} as the function of m_{pp}.

Consider the process dp$\longrightarrow$ppX when two protons are emitted at $\vartheta = 0^0$, the effective masses $m_{pp} < 2.0$(Gev.) as in the experiment of ref.[15]. Under such kinematic conditions the main mechanism involved is the charge exchange, with X = $(n\pi^0, p\pi^-$, or $\Delta^0)$ [15]. For simplicity we can consider this d-p process when three particles are produced: two protons and a particle with a mass m_X.

If we are interested in the dependence of the observables in dp$\longrightarrow$ppX on the effective mass of two protons m_{pp} then the relation between the m_{pp} — distribution of this value and the amplitude $\mathcal{F}_d$ can be written for example for $d\sigma/dm_{pp}^2$ in the following form :

$$\frac{d\sigma}{d\,m_{pp}^2} = \frac{1}{(2\pi)^5\ I_{dN}} \int \frac{d^3p_1\ d^3p_{23}}{2E_1\ 2E_{23}}\ \delta^{(4)}(p_{in} + p_d - p_1 -$$

$$- p_{23}) \int \frac{d^3p_2 d^3p_3}{2E_2\ 2E_{23}}\ \delta^{(4)}(p_2 + p_3 - p_{23})\ Sp(\rho_0 \mathcal{F}_d^+\ \mathcal{F}_d)\,, \qquad (4)$$

where I_{dN} is the invariant stream of the initial particles, for example in the rest frame of deuteron $I_{dN} = 4m_d|\vec{p}_{in}|$; m_d and $\vec{p}_{in}$ are the deuteron mass and the three-momentum of the initial proton respectively ; p_1 and E_1 are the three-momentum and the energy of a particle X with

the effective mass m_X ; p_2, p_3 and E_2, E_3 are the three-momenta of two protons and their energies respectively, p_{in} , p_1, p_2, p_3 are the four momenta of particles mentioned above , $E_{23}^2 = p_{23}^2 + m_{pp}^2$.

A similar expression for $T_{20} d\sigma/dm_{pp}^2$ can be written :

$$T_{20}\frac{d\sigma}{dm_{pp}^2} = \frac{1}{(2\pi)^5 I_{dN}} \int \frac{d^3p_1 d^3p_{23}}{2E_1 2E_{23}} \delta^{(4)}(p_{in} + p_d - p_1 - p_{23}) *$$

$$\int \frac{d^3p_2 d^3p_3}{2E_2\ 2E_3} \delta^{(4)}(p_2 + p_3 - p_{23}) Sp(\rho_0 \mathcal{F}_d^+ \Omega_{20} \mathcal{F}_d) \qquad (5)$$

After some integrations in (2) and (3) we can get a simpler formula for T_{20}:

$$T_{20} = \frac{\int Sp(\rho_0 \mathcal{F}_d^+ \Omega_{20} \mathcal{F}_d) p_3 du/(E_2 E_{23})}{\int Sp(\rho_0 \mathcal{F}_d^+ \mathcal{F}_d) p_3 du/(E_2 E_{23})} \qquad (6)$$

where $u = (E_{in} - E_1)^2 - (\overrightarrow{p_{in}} - \overrightarrow{p_1})^2$ is the transfer from the initial proton to the particle X (N π).

Consider now the mechanism of the reaction discussed Under the above kinematic conditions ($m_{pp} \leq 2.0$(Gev.)) the values of the final proton momenta are not large, less than 0.2(Gev./c). But, as it was shown above, the spectator mechanism gives the main contribution to T_{20} in the inclusive reaction dp⟶pX at these proton momenta. In our case there is an integral over du or over the momentum of one of the two protons. Therefore we can calculate T_{20} in the frame of the spectator mechanism but taking into account the Pauli's principle and the final state interaction of two protons.

Now we note that the reaction dp⟶(pp)n was considered in detail in ref.[24] when m_{pp} is very small ($m_{pp} < 1.9$(GeV.)) It was shown that the main mechanism in this case is the np⟶pn charge-exchange process. But we will consider the pd⟶ppX reaction at larger m_{pp}, i.e., $m_{pp} > 1.9$(GeV./c); however we will also take into account the Pauli's principle in the triplet state of two protons as in ref.[24], and the

final state interaction of these protons in the $^1S_0$– state. Then the amplitude of our process in the impulse approximation can be of the following form:

$$\mathcal{F}_d^{(1)} = f_{pn}\left(\frac{1}{\sqrt{2}}\,(\Phi(p_3) - \Phi(p_2)P_{np} + \Phi_{FSI}\right), \qquad (7)$$

where f_{pn} is the amplitude of the process $pn \to Xp$; Φ is the deuteron wave function ; $P_{np} = P_T - P_S = (1 - \vec{\sigma}_p\,\vec{\sigma}_n)/2$ is the exchange operator of spins of the proton and the neutron; $P_S = (1 - \vec{\sigma}_p\,\vec{\sigma}_n)/4$ is the singlet projection operator, Φ_{FSI} is the contribution of the final state interaction (FSI) of two protons. Since we have no information about the spin dependence of the amplitude of the $pn \to Xp$ reaction we neglect it and get the following formula for T_{20} :

$$T_{20} = \frac{\int \frac{d\sigma_{pn}}{du}\left(2\sqrt{2}\,\Psi_0\Psi_2 - \Psi_2^2 + F_{1FSI}\right)\frac{p_3\,du}{E_2 + E_3}}{\int \frac{d\sigma_{pn}}{du}\left(\Psi_0^2 + \Psi_2^2 + F_{2FSI}\right)\frac{p_3\,du}{E_2 + E_3}}, \qquad (8)$$

where $d\sigma_{pn}/du$ is the differential cross section of the processes $pn \to Xp$ $(X = N\ \pi)$; $\Psi_0 = (\Phi_0(p_3) - \Phi_0(p_2))/\sqrt{2}$ and $\Psi_2 = (\Phi_2(p_3) - \Phi_2(p_3))/\sqrt{2}$; Φ_0, Φ_2 are the S– and D–wave of the deuteron wave function Φ; F_{1FSI}, F_{2FSI} are some expressions taking into account the FSI of two protons in the $^1S_0$ — state, which are presented below. In the calculation of T_{20} using (7) we took the fit of $d\sigma_{pn}/du$ from ref. /25/.

The contribution of FSI was calculated in the approach of the effective radius,the expressions for F_{1FSI} and F_{2FSI} are the following :

$$F_{1FSI} = (2\Phi_2 I_0 - \Phi_2 I_2)\frac{g_s}{g_s^2 + k^2} + \frac{1}{g_s^2 + k^2}\,(2I_0 I_2 - |I_2|^2)\ ,$$

$$F_{2FSI} = ((\Phi_0 I_0 + \Phi_2 I_2) g_s + |I_0|^2 + |I_2|^2)/(g_s^2 + k^2);$$

where $k = (p_2 - p_3)/2$;

$$I_0 = \int \Phi_0(r)(j_0(\vec{p_3}\,\vec{r}) - j_0(\vec{p_2}\,\vec{r}))dr ;$$

$$I_2 = \int_0^\infty \Phi_2(r)(j_2(\vec{p_3}\,\vec{r}) - j_2(\vec{p_2}\,\vec{r}))dr ;$$

here $j_0(\vec{p}\,\vec{r})$ and $j_2(\vec{p}\,\vec{r})$ are the zero order and second order cylindric functions respectively;

$$g_s = -\frac{1}{a_s} + \frac{1}{2} r_s k^2 \; ; \; a_s = -7.822(\text{fm.}); \; r_s = 2.839\text{fm.});$$

the values of a_s and r_s are taken from ref.[26] .

The calculation results of $T_{20}(m_{pp})$ in the frame of the approach mentioned above are presented in fig.3. The solid curve is the calculated T_{20} when the Paris wave function [27] is taken as the deuteron wave function (d.w.f.); the dashed one corresponds to the d.w.f. of type [28]. It is seen from these results that our calculation of T_{20} does not give the oscillations in the behaviour of T_{20} at $m_{pp} = 1.94$—1.96 (GeV.), which were observed in the experiment of ref.[15].

IV. Polarization transfer in dp⟶pX

Consider now another interesting polarization characteristic: the polarization of final protons $\mathcal{P}'$ when the initial deuteron has the vector polarization $\mathcal{P}$ or the so-called polarization transfer $\kappa = \mathcal{P}'/\mathcal{P}$. The general expression for the polarization of final protons produced in the inclusive deuteron fragmentation reaction dp⟶pX has the following form[24]:

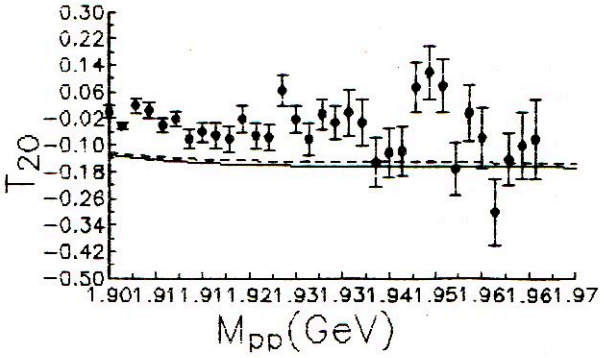

Fig.3. Dependence of T_{20} on m_{pp} in dp⟶ppX reaction. Solid curve is the calculation using Paris d.w.f.[28]. Experimental data – from ref.[15].

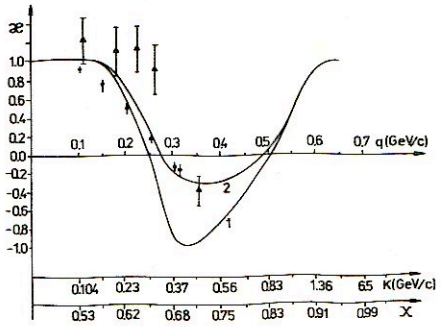

Fig.4. Dependence of the polarization transfer κ in the dp⟶pX reaction on q,k,x. Curves:1– contribution of the spectator mechanism, fig.1a; 2 – full contribution of fig.1(a–e). Experimental data; ▲ – from ref.[30], ◆–from ref.[31].

$$\vec{\mathcal{P}}' \vec{n} = \frac{\int \mathrm{Sp}(\rho_d \mathcal{F}_d^+ \vec{\sigma} \vec{n} \mathcal{F}_d) d\Gamma}{\int \mathrm{Sp}(\rho_d \mathcal{F}_d^+ \mathcal{F}_d) d\Gamma}, \qquad (9)$$

where ρ_d is the density matrix of the polarized deuteron in the rest frame : $\rho_d = 1/3\ P_T(1 + 3/2\ \mathcal{P}\ S - 1/2\rho_{20}(3S_z^2 - 2))$, here $P_T = (3 + \sigma_p\sigma_n)/4$ is the projection operator of the deuteron triplet state , $S = (\sigma_p + \sigma_n)/2$, $S_z = (\sigma_{pz} + \sigma_{nz})/2$, ρ_{20} is the alignment of the initial deuteron.

In the spectator mechanism we have the following simple expression for κ :

$$\kappa = \frac{\Psi_0^2(\mathbf{k}) - \frac{1}{\sqrt{2}}\Psi_0(\mathbf{k})\Psi_2(\mathbf{k}) - \Psi_2^2(\mathbf{k})}{(\Psi_0^2(\mathbf{k}) + \Psi_2^2(\mathbf{k}))(1 - \rho_{20}T_{20})}. \qquad (10)$$

When $\rho_{20} = 0$, as in ref[17,30], we have from (9) :

$$\kappa = 1 - \frac{1}{2\sqrt{2}} T_{20} - \frac{9}{4((\Psi_0/\Psi_2)^2 + 1)}. \qquad (11)$$

This expression has a more complicated form if all graphs of fig.1 are taken into account[29] .

The calculation results of κ and the corresponding experimental data , obtained in Dubna by the group "Alpha" at $p_{in} \simeq 9$(Gev,/c), are presented in fig.4. It is seen from this fig. that the polarization transfer is more sensitive to the reaction mechanism at $0.2 \le q \le 0.5$(Gev./c) or $.2 \le \mathbf{k} \le .8$(Gev./c), i.e., the nonspectator graphs give a larger contribution to κ larger than in the case of T_{20} consideration. We note that our calculation result (see the curve 2 in fig.4) was got obtained before the latest experimental data[30,31]. As seen from fig.4 there is not experimental information about κ at large q ($q > 0.3$(Gev./c)), $\mathbf{k}$ or x. Therefore it is interesting to measure the transfer polarization at large q, $\mathbf{k}$, x, in order to obtain fuller information about the polarization phenomena at small N-N distances.

Conclusion

Now we will make the conclusion about the problem discussed. The investigation of fragmentation processes of deuteron can give really new information about the deuteron structure. However it is necessary to take into account the mechanism of the fragmentation reaction. It is especially important in the kinematic region corresponding to mean N-N distances r_{NN}, as shown in fig.2, at $q \leq .4$(Gev./c) or $r_{NN} \geq 0.5$ (fm.). The relativistic effects in the deuteron are very important at larger q or smaller r_{NN}. That is well seen from the analysis of the tensor polarization deuteron component T_{20} as the function of q,k, or x.

The infestigation of another polarization characteristic, transfer polarization κ, showed that (see fig.4) it is very sensitve (more than T_{20}) to the reaction mechanism especially at $0.3 \leq k \leq 0.8$ (Gev./c) or $0.2 \leq q \leq 0.5$(Gev./c), which corresponds to the middle N-N distances r_{NN}. Joint analysis of T_{20} and κ in the fragmentation deuteron reaction $dN \rightarrow pX$ can give fuller information about the dynamic reaction and the deuteron structure at small N-N distances. Therefore it is very interesting to have the experimental information about κ at large k ($k \geq 0.5$(Gev,/c)) or $q \geq 0.3$(Gev./c).

The investigation of T_{20} in the $dp \rightarrow ppX$ reaction as the function of m_{pp} can give nontrivial information about the possible existence of dibaryon resonances as the fig.3 showes Therefore it is interesting to measure $T_{20}(m_{pp})$ in a large interval of m_{pp} in order to try to find the resonances at $m_{pp} \geq 2.0$(Gev.).

In the conclusion I would like to thank L.Dachno, V.Karmanov, B.Kuhn, C.Perdrisat, E.Strakovsky, L.Strunov, I.Sitnik, V.Sharov. B. Tatischeff, M.Tokarev, A.Zarubin, L.Zolin for usefull advice and discussions and especialy S.Shimanskiy for the help in the calculations.

References

1. Arnold R.G. e.a. Phys.Rev.Lett. 1975,v.35,p.776.
2. Arvieux J.e.a. Nucl.Phys. 1984,v.A431,p.513.
3. Keistler D.I. Phys.Rev.,1981,v.240,p.2528.
4. Rekalo M.P. Proceed. III International Symposium "Pion-Nucleon and Nucleon-Nucleon interactions" Leningrad, 1989, v.2, p.200.
5. Karmanov v.A. EPAN 1988,v.19,p.525.
6. Amelin N.S., Glagolev V.V., Lykasov G.I. EPAN 1982, v.18,p.130.
7. Glagolev V.V. e.a.,Preprint JINR P1-83-566,1983; Jad.Phys. 1984, v.40, p.482.
8. Dolidze M.G. and Lykasov G.I. Z.Phys. 1990, v.A335, p.95.
9. Dolidze M.G. and Lykasov G.I. Z.Phys. 1990, v.A336, p.339.
10. Perdrisat C.F. and Punjubi V. Phys.Rev. 1989,v.C42, p.1899.
11. Perdrisat C.F. e.a. Phys.Rev.Lett. 1987,v.59, p.2840.
12. Ableev V.G. e.a. Pisjma JETP, 1988, v. 47, p. 558.
13. Dolidze M.G., Glagolev V.V. Lykasov G.I. e.a. Z.Phys.1986, v.A325, p.391.
14. Tatisheff B. e.a. Phys.Rev. 1987,v.C36,p.1995.
15. Tatisheff B. e.a. Proceed. of 7^{th} Intern. Conf. on Polarizatioin Phenomena in Nuclear Physics, Paris, 1990, v.2, p. C6-371.
16. Bug D.V. and Wilkin C. Phys.Lett.,1985, v.B152, p. 37.
17. Kobushkin A.P., Vizireva L.J. Journ. Phys. G:Nucl.Phys. 1982,v.8, p.893.
18. Frankfurt L.L., Strikman M.I. Phys.Rep. 1981, v.6, p. 215.
19. Garsevanishvili V.R. XIII Winter School of Theoretical Physics in Kappacz 1976, v.1, p. 313.
20. Franz Gross Phys.Rev. 1974, v. D16, p. 223.
21. Braun M.A., Tokarev M.V. Proc.III Intern. Symp. "Pion-Nucleon and Nucleon-Nucleon Physics", Leningrad 1989, v.2, p.398.

22.Ableev V.G. e.a. Proceed. 7th Intern. Conf. on Polarization Phenomena in Nuclear Physics, Paris, 1990, v.I Abstracts of contributed paper, p. 40F.
23.Efremov A,V.,e.a. Jad.Fiz. 1988,v.47,p.1364; Sovjet Journal of Nucl. Phys. 1988, v.47, p.868.
24.Bugg.D.V., Wilkin C. Nucl.Phys. 1987,v.A467, p.575.
25.Azhgirey L.S. e.a. Jad. Fiz. 1987,v.45, p.1353 and 1657.
26.Sher M. Ann.Phys. 1970,v.58,p.1.
27.Lacombe M. e.a. Phys.Lett.1981, v.151, p.139.
28.Jan J.McGee Phys.Rev. 1966,v.151,p.772.
29.Dolidze M.G., Lykasov G.I. Proceed. XXY Winter Scool LIPh, Leningrad 1990, v.III, p.187.
30.Strunov L.S., Zarubin A., Zolin L.S. Proc. of Dubna-Workshop on Problems of Deuteron Structure at High Energies,Dubna,June-1991.
31.Perdrisat C. e.a. Proc of Dubna-Workshop on Problems of Deuteron Structure at High Energies, Dubna, June-1991.

ELASTIC BACKWARD pD-SCATTERING AND BREAKDOWN OF DEUTERON BY PROTONS IN Δ-RESONANCE REGION

Uzikov Yu.N.
Kazakh State University, Department of Physics, Timiryazev str. 46, Alma-Ata 480121, Kazakhstan

Two attractive physical ideas are connected with the study of $pD \to Dp$ process at $\sim$1 GeV energies, namely, the D.P.Blokhintsev's hypothesis of the nuclear density fluctuations /1/ and a laterassumption of the excitation of three-baryon resonance/2/. Both ideas are quite natural from the standpoint of quark presentations, and their development is continued in nuclear physics. However, as it is shown by further analysis /3,4/, the main contribution to the cross-section of $pD \to Dp$ process at 0.5-1.5 GeV energies is made by less exotic mechanisms, i.e. by double scattering with Δ-isobar exitation and by one-nucleon exchange (ONE) with a very small contribution of single scattering (SS) (See Fig.1.).

The contribution of Δ-mechanism to the coherent sum of ONE+Δ+SS was tested in /4,5/ on the basis of description of the data of $pp \to pn\pi^+$ reaction in the same kinematic Δ-resonance region at T=0.8 GeV energy in the approximation of one-meson exchange. It was found as a result that the parametrizations of $NN \rightleftarrows N\Delta$ amplitudes used earlier /2,3/ in the description of backward pD-scattering, overestimate by a factor of 1.5-2 the contribution of Δ-isobar, and in /2/ it also distorts considerably its energy dependence. A new parametrization of $NN \rightleftarrows N\Delta$ amplitude was built in /5/ and it agrees with the data on $pp \to pn\pi^+$ reaction. Calculations with the revised Δ-parametrization in the ONE+Δ+SS model using the Paris wave function of the deuteron, show that the agreement with the data on $pD \to Dp$ process cross-section becomes better to be compared with the results of /2/ (See Fig.2). In this case the expected con-

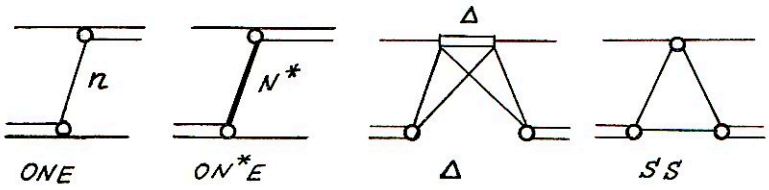

Fig.1. Mechanisms of elastic backward pD-scattering (see, the text).

tribution of exotic mechanisms of three-baryon resonance type sharply decreases. The overall increase of the calculated cross-section at a relative decrease of the Δ -mechanism contribution is delicate by nature and is due to the constructive character of the interference of the renewed Δ -amplitude with ONE amplitude to be compared with /2/. Nevertheless, the discrepancy with the data on differential cross section remains (Fig.2) and its value is more appreciable than it follows from Ref./3/. Thus in the region of T=0.75 GeV initial energy where the prediction of Δ -mechanism is the most reliable due to the fact that Δ -isobar is present on the mass shell, the model underestimates the cross-section by a factor of ~2. There also remains the problem of the description of tenzor polarization T_{20}.

In the present work there has been calculated the contribution of the exchange by $N^*(1/2^+)$ and $N^*(1/2^-)$ isobars to the coherent sum of Δ +ONE+ON*E+SS. The component NN* is present in the deuteron due to the quark S^4P^2 configuration. However, if one assumes that the main nucleon state has S^3 quark configuration, while P-odd and P-even N^x states have S^2P and SP^2 configurations respectively, then, according to /6/ the weight of NN^x component in the deuteron is less than 0.5%. In this case, wave functions of the relative NN* motion have an oscillatory f: m of $\varphi_{os}(k)$ and $\varphi_{1p}(k)$ for $1/2^+$ and $1/2^-$states respectively with the oscillator parameter b=0.55 fm. Our calculations in the relativistic Hamiltonian dynamics show the contribution of N^* exchange to the cross-section of **pD → Dp** process to be 2-3 orders

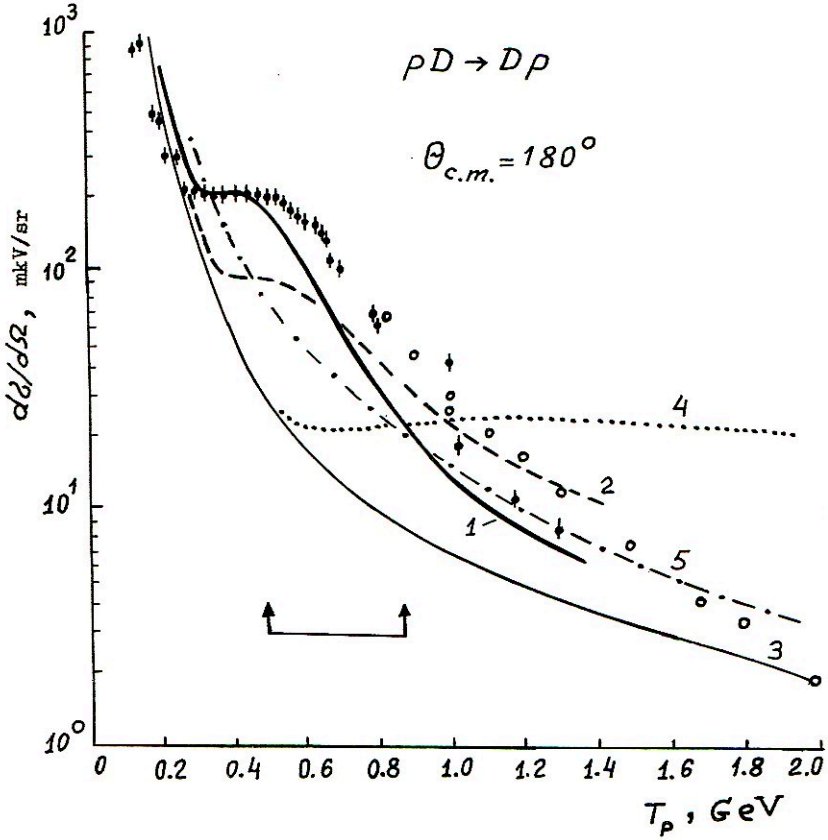

Fig.2. Differential cross-section of the elastic backward pD-scattering at $\theta_{c.m.}$=180° as a function of the initial energy.

Curves: 1 - ONE+ Δ+SS calculation with an account of the off-shell behaviour of Δ -isobar; 2 - the same without an account of Δ -off-shell behaviour /4/; 3 - ONE (Paris); 4 - ONE with MU wave function of deuteron /8/; 5 - ONE, MU+(OS)[6]. Data (● ○) from /11/. Arrows show the energy range where the parametrization of NN-NΔ amplitude was fixed according to data on $pp \to pn\pi^+$ reaction /5/.

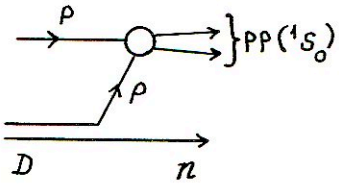

Fig.3. The dominating mechanism of $p+D \to n(180°)+pp(0°)$ reaction at $E_{pp} \lesssim 3$ MeV.

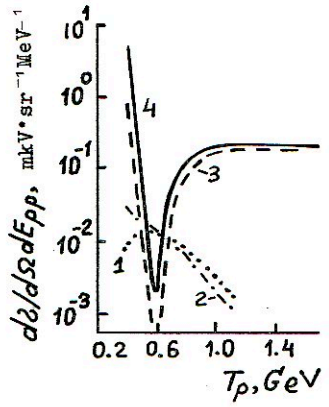

Fig.4. Cross-section for the reaction $p+d \to n+(pp)$ at $\Theta_{cm}=180°$ and $E_{pp}=3$ MeV as a function of the proton initial lab. energy T_p. Curves: 1 - the Δ mechanism; 2 - single scattering (SS); 3 - one-nucleon exchange (ONE); 4 - the coherent sum Δ+ONE+SS.

lower than the contribution of the exchange by a neutron in the energy region under discussion.

This result agrees with that obtained earlier /7/ from the isotopic relations for (p,pD) and (p,nD) reactions on ^{6,7}Li nuclei by the conclusion that in the elastic backward pD-scattering the exchange of a neutron or N^* isobar with T=1/2 is not dominating in $T_0=0.70$GeV energy region. Therefore, the discrepancy between the ONE+Δ+SS model and the experimental data cannot be removed by further modification of the spatial part of the deuteron wave function and is most probably due to the contribution of other mechanisms, the excitation of N* isobars, in the double scattering in particular.

Outside the Δ-resonance region ($T_p > 1.0$ GeV) the contribution of ONE mechanism is considerable. Here we have shown high sensi-

tivity of the process cross-section to the form of the deuteron wave function in the case of the Moscow University potential /8/. According to /9/, NN-potential /8/ with the forbidden state corresponds to the account of only S^4p^2 configuration of deuteron and does not contain the contribution of $(OS)^6$ configuration. The $(OS)^6$ configuration enters the total wave function of deuteron with the weight of 3% and an opposite sign with respect to S^4p^2. As it is seen from Fig.2, the cross-section of pD-Dp process clearly separates S^4p^2 and $S^4p^2+(OS)^6$ approximations in favour of the latter.

On the whole, the ONE+Δ+SS model seems to be rather reliable in the energy range under discussion. Due to a nontrivial effect of Δ+ONE interference, this model provides an independent proof of the validity of the available ideas of both the momentum n-p distribution in the deuteron in $q \lesssim 0.5$ GeV/c region and the "soft" nature of πNN-, ρNN-, πNΔ-, ρNΔ- (with cut-off parameters of 0.5-0.7 GeV/c) form-factors.

The modified variant of ONE+Δ+SS model has been built by us for prediction of characteristics of p+D$\rightarrow$n(180°)+pp(0°) reaction at a low relative energy of pp-pair, $E_{pp} \leq 3$ MeV, in the same region of initial energies /10/. Below we quote main results of this work.

1. Under these kinematic conditions, pp-pair is formed mainly in $^1S_0$-state. The contribution of P-, D-waves to the cross-section are suppressed by factor of 10^{-2}-10^{-3} because of the centrifuginal barrier. (On the contrary, the admixture of $^3D_1$ state in the deuteron is created by tenzor forces).

2. The Δ-contribution is negligible to be compared with the spectator mechanism of ONE (Fig.3) due to isotopic spin relations. The suppression of the Δ-contribution with all the theoretical difficulties of its description makes the reaction more attractive than the backward elastic pD scattering with respect to the investigation of short-range NN-interaction.

3. The spectator mechanism dominates very strongly. As a result, the cross-section of this reaction measures with good accuracy the production

$$(u(q)^2 + W(q)^2) \times |t_{pp}(q, k_{pp})|^2$$

and the tenzor analyzing power T_{20} is determined by the deuteron

structure only

$$T_{20} \frac{\sqrt{8}\, u(q)W(q) - W(q)^2}{\sqrt{2}\, u^2(q)+W^2(q)} .$$

4. The half-off-shell t-matrix $t_{pp}(q,k_{pp})$ is the same value as the S-wave vertex of the deuteron by its mathematical and physical nature: $\Gamma(D\to p+n) = -(\varepsilon+q^2/m)u(q)$. In particular, the $t_{pp}(q, k_{pp})$-matrix has the same node as the u(q) wave function at $q=0.4$ GeV caused by repulsive core in the $^1S_0$-state of the NN-interaction.

5. The above-mentioned node takes place both the cross-section as a deep minimum (SeeFig.4) and in the feature of T_{20}. The Coulomb effects enhance these features in polarization chareacteristics.

6. The channel $p + D \to p(180°) + np(0°)$ at $E_{np} \sim 3$ MeV is not so interesting because of large $^3S_1$-$^3D_1$ state contribution. In the np-pair the singlet $^1S_0$-state dominates over the triplet $^3S_1$-$^3D_1$ state only at lower energies $E_{pn} \lesssim 50$ keV and above-mentioned features (1-5) take place again.

These theoretical predictions for the reaction under discussion have been obtained by apparent modification of the well-established theoretical approach to the description of $pD \to Dp$ process in the same kinematic region and points to a necessity of experimental study of this reaction.

REFERENCES

1. D.I.Blokhintsev, JETF 33(1957)1295.
2. L.A.Kondratyuk, F.M.Lev, L.V.Shevtchenko,Yad.Fiz.33(1981) 1208.
3. A.Boudard, M.Dillig, Phys.Rev. C31(1985)302.
4. O.Imambekov, Yu.N.Uzikov, L.V.Shevtchenko, Z.Phys. A 332 (1989)349.
5. O.Imambekov, Yu.N.Uzikov, Yad.Fiz. 47(1988)1089.
6. L.Ya.Glozman et al.,Phys.Lett. B252(1990)23.
7. O.Imambekov, Yu.N.Uzikov, Izv. AN SSSR, Ser.Fiz. 51(1987) 947.
8. V.M.Krasnopolsky et al., Phys.Lett. B165(1985)7.
9. I.T.Obukhovskyi, A.M.Kusainov, Yad.Fiz.47(1988)494.
10. O.Imambekov, Yu.N.Uzikov. Yad.Fiz.52(1990)1361.
11. J.Arveux et al., Nucl.Phys. A431(1984)613.

INFORMATION ON DEUTERON STRUCTURE FROM $\pi\vec{d}$ INTERACTIONS

E. T. Boschitz
Institut für Experimentelle Kernphysik, Universität Karlsruhe,
7500 Karlsruhe, Federal Republic of Germany

In spite of the fact that during the past twenty years substantial progress has been achieved in the understanding of the πNN system, the interaction of pions with deuterons still presents a real challenge to few-body theorists. There are many open questions regarding the reaction mechanism, and for this reason I believe it is premature to use πd interactions for extracting reliable information on the structure of the deuteron.

In order to justify my pessimism I like to give a brief "historic" account of the theoretical developments which took place (many based on the very active interplay between theory and experiment), and show the problems which still exist. For details, I refer you to the excellent reviews by Garcilazo and Mizutani in a journal article [1] and a monograph [2]. As indicated by the arrow on the d in the title of my talk I shall focus mainly on what we have learnt from polarization measurements.

For the research program of our group, a milestone was set by the rapporteur's talk of Thomas [3] at the International Conference on Few Body Systems and Nuclear Forces in Graz in 1978. I shall explain:

Before 1978, early theoretical approaches based on the Glauber eikonal approximation or Watson multiple scattering series had matured into theories based on the Faddeev approach with the hope of obtaining an exact solution for the πd system. After the pioneering work of Petrov and Peresypkin [4], Thomas and Afnan [5] and Myhrer and Koltun [6], Thomas [7] successfully described the πd elastic cross section data at 48 MeV by including spin and isospin, the deuteron D-state and relativistic kinematics (for the pion) in his three-body calculation. Then, Rinat and Thomas [8] extended this calculation in order to describe early data in the region of the Δ - resonance. At the time of the Conference in Graz effects of different two-body inputs in the scattering theory was investigated by two groups. With considerable effort the Lyon [9] and the Rehovot group [10] included all s and p-wave πN channels in their theories, while before P_{33} dominance was assumed. Actually, in view of the weakness of the πN interaction in all but the P_{33} channel this should not have been necessary. However, large effects were observed for the polarization observable iT_{11}, but only small ones for t_{20}^{lab}, the tensor polarization of the recoil deuteron, when the small πN waves were included.

The interest in the tensor polarization dates back to the suggestion of Gibbs [11] that one might be able to determine P_D, the D-state probability of the deuteron, from a measurement of t_{20}^{lab} at 180°. The new calculations from the Lyon [9] group confirmed the suggestion of Gibbs, however, looking closer at their prediction the situation for measuring P_D was not promising. The curve of $t_{20}^{lab}(180°)$ versus P_D was quite flat beyond 4%, which is the interesting region. Nevertheless, it was suggested that information

about the angle and energy dependence of t_{20}^{lab} would be extremely valuable in sorting out the theory. I will come back to this.

The predictions for polarization observables presented at the Graz conference, triggered our research program on the systematic investigation of the spin dependence in πd elastic scattering, and the πd breakup and absorption reactions, which has lasted until now. Our very first (and very crude) data points on iT_{11}in πd scattering [12] already demonstrated the need for including the small πN waves, invalidating the P_{33} dominance in some calculations. Many more iT_{11} data were taken by our group in the following years with increasingly better precision [13]. The same was done for the differential cross sections in the Δ-region [14]. During these years the relativistic three-body theories were also steadily refined to a high degree of sophistications.

When comparing theoretical predictions with the large body of data accumulated for the differential cross section-and the vector analyzing power systematic discrepancies were observed in comparison to all theories. This persistent failure to reproduce the data was considered to be an indication for important reaction dynamics being missing in the calculations. For a short time there were attempts to explain the discrepancies by contributions from dibaryon resonances [15], however the ad-hoc addition of such amplitudes to the ones from the three-body theories did not solve the problem.

Then, Ferreira et al [16] tried to explain the discrepancies in term of a residual $N\Delta$ interaction which is not contained in the standard three-body description obtained from the relativistic Faddeev theory. They constructed an $N\Delta$ model, the amplitudes of which were added to the Faddeev amplitudes. Since it was not known beforehand which of the parameters of the $N\Delta$ interaction would prove to be relevant, they were treated as free parameters, and were determined from fitting all available data on the total cross section, the differential cross section and the vector analyzing power. From these fits it was shown that only two $N\Delta$ states with lowest angular momentum, $^5S_2$ and $^5P_3$, gave important contributions. With those, remarkable agreement with the data was achieved. From more precise iT_{11} data, taken recently, in fact, an additional contribution from the $^3S_1$ $N\Delta$ interaction was extracted [17], and there was hope to learn something about the $N\Delta$ spin-spin interaction. However, these results from Ferreira et al. were obtained in calculations where the phenomenological NΔ interaction was added in Born term to the background few-body amplitudes. Recently, Alexandrou and Blankleider [18], and Garcilazo [19] (see Fig. 1) investigated the effect of including such an $N\Delta$ interaction to all orders, within a unitary few body calculation of the πNN system. It was found that the higher order $N\Delta$ interaction terms have as much influence on the πd observables as the lowest order term, and, in fact, tend to cancel the effects obtained by adding the $N\Delta$ interaction in Born term. This, unfortunately, invalidates the conclusions of Ferreira et al., and leaves us with the question of the origin of the large discrepancies between theory and experiment.

About the same time when the vector analyzing power iT_{11} was measured at SIN, the tensor polarization t_{20}^{lab} was measured at LAMPF [20]. This observable had a considerable impact on the understanding of the πNN system. Namely, in the course of developing an unified theory of the NN-πNN

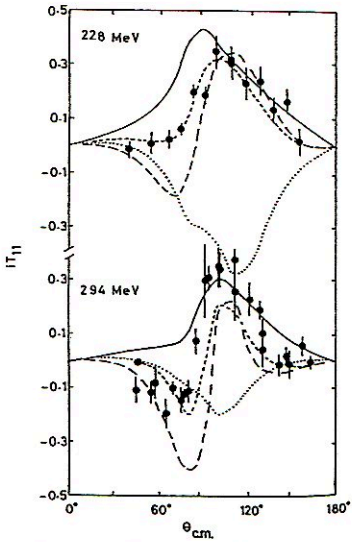

FIG. 1. The effects of the residual NΔ interaction in the πd elastic vector analyzing power iT_{11}. The solid lines are the results without NΔ interaction, the short-dashed lines are the first-order results within the Ferreira et al. model, the long-dashed lines are the first-order results within the separable model, and the dotted lines are the results of including the NΔ interaction to all orders within the separable model. The experimental data are from Ottermann et al. (Ref. 25).

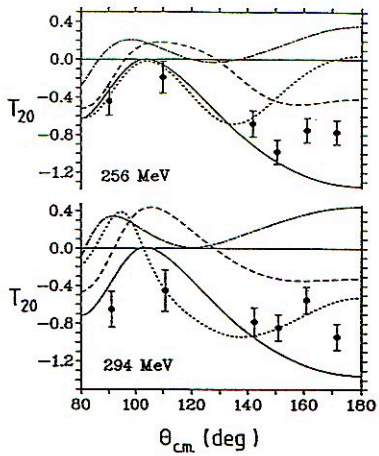

FIG. 2. Experimental results for T_{20} compared with theoretical predictions from Garcilazo (solid line), Hannover (dotted line), Flinders (dashed line), and Lyon (dot-dashed line).

system the pion elastic scattering channel had to be coupled to the pion absorption channel via the P_{11} πN amplitude. Field theoretical considerations [21,22] lead to a model in which this amplitude was split into a "pole" and a "non-pole" part, both of which were large, the sum, however, had to be small because of the on-shell behavior of the P_{11} πN amplitude up to 300 MeV. It now came as a surprise that this new improved version of the Faddeev approach disagreed markedly with the t_{20}^{lab} data while the standard three-body theory which either neglected π absorption at all, or kept the individual "pole" and "non-pole" terms small, agreed quite well. This "P_{11} puzzle" presented an interesting problem. As pointed out by Afnan and McLeod [23] it arises because in πd scattering, in the intermediate state, the pole term is Pauli blocked for certain partial waves and the tensor polarization t_{20} turns out to be very sensitive to the exact way in which the P_{11} πN t-matrix is split.

In order to clarify this problem it was considered interesting to trace this sensitivity to specific helicity amplitudes, and from there to certain partial waves. Unfortunately, the tensor Polarization t_{20}^{lab} is not a very suitable observable because it is a linear combination of the c.m. observables T_{20}, T_{21} and T_{22}, the individual contributions of which vary with scattering angle. Therefore, it is difficult to know exactly which observable is most sensitive to the theoretical treatment of the P_{11} channel.

A few years ago, after considerable effort, tensor polarized deuteron targets suitable for πd scattering became available. This enabled the Karlsruhe-SIN-TRIUMF collaboration to start a program at TRIUMF and at SIN to measure the tensor analyzing power T_{20}, T_{21} and T_{22} at five energies in the region of the (3,3) resonance. The measurements are quite difficult because the target polarization is rather low, and different orientations of the target quantization axis in respect to the direction of the incident pion beam must be applied. From these measurements of T_{20}, T_{21} and T_{22} [24,25], it became clear that T_{20} is the most sensitive observable and the P_{11} effects are most pronounced towards 180° (see Fig. 2). Since the first two of the four helicity amplitudes A, B, C, D (for the notation see Ref. 26) vanish at 180° the tensor observable T_{20} reduces to

$$T_{20}(180°) = \sqrt{2}\,\frac{|C|^2 - |D|^2}{2|C|^2 + |D|^2}\,.$$

The fact that experimentally $T_{20}(180°)$ is close to its theoretical lower limit ($-\sqrt{2}$) at some energies, means that $|C|^2 << |D|^2$. This is also the prediction of theories with small contributions from the pole and non-pole parts of the P_{11} πN amplitude. On the other hand, theories with large contributions have $|C|^2 = |D|^2$. Therefore, at 180°, we trace the P_{11} problem to the helicity amplitude C. The effects of the P_{11} channel modify mainly the J=0 and J=1 partial waves, and, since the J=0 partial wave does not contribute to C (angular momentum selection rules) all the large effects seen at 180° are almost exclusively due to the $J=1^+$ partial wave in C. This result was confirmed by a model dependent amplitude analysis [27].

A possible solution of the P_{11} problem was suggested by Jennings [28]. He observed that, in the impulse part of the πd amplitude, the Pauli exchange term to the contribution coming from the P_{11} pole part appears to be compensated to a large extent by a certain diagram with a four particle intermediate state: the initial pion is absorbed by one nucleon before the second nucleon emits the final pion. Jennings and Rinat [29] then added this contribution to the amplitude from the *NN*-π*NN* model to show that, in fact, this observation was adequate (see Fig. 3). In a more precise calculation including the self-energy of the pion for the propagating two-nucleon state (with no pion) it has been shown by Mizutani et al [30] that the degree of the near cancellation is not as good as claimed by Jennings, and there is an imaginary part which is larger than the reduced real part. but the fact remains that the four-particle process is important and not to be neglected. Therefore, what one apparently has learnt from this P_{11} problem is the incompleteness of the *NN*-π*NN* model once contained within the two- and three- particle states: it should also include four particle $\pi\pi$*NN* states. At this point, I like to quote conclusions drawn by Blankleider in a recent review talk [31]:

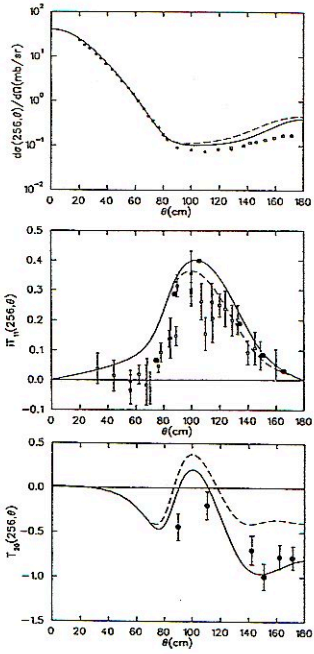

FIG. 3. Effects of the "Jennings corrections". Dashed lines are the predictions from Rinat and Starkand (Ref. 10) without, the solid lines with the Jennings corrections included; according to Jennings and Rinat (Ref. 28). The data are from Ref. 13, 14 and 25.

"There appears to be essentially two possibilities: either we have not yet included "*the*" mechanism, in which case further heroic calculations probably cannot be avoided; or we are simply doing the whole problem using "the wrong expansion" - including progressively more pions in intermediate state may not be the most convergent way to sum the series."

In addition to the $N\Delta$ and T_{20} problems, mentioned, there are many others which so far have hardly been investigated, for example, off-shell effects which are very important in the case of the $\pi d \rightarrow pp$ reaction [32]. Now you understand the pessimism which I expressed at the beginning of my talk.

Nevertheless, forgetting about a detailed comparison between theory and experiment for the time being, one may perform model calculations in order to study the sensitivity of the various πd observables to the properties of the deuteron. I want to show the results of such a study.

By now, a large number of deuteron wave functions exist for calculating various phenomena which include the deuteron. Yet, calculations which use these different wave functions tend to yield inconclusive results, with respect to questions of radial distribution and percentage D-state. This is because the wave functions may originate from different phenomenological or theoretical schemes and

are not designed to differentiate in terms of the two properties mentioned. For this reason, Čertov, Mathelitsch [33] and Moravcsik constructed model wave functions for the deuteron to facilitate the unambiguous exploration of dependencies on the percentage D-state and on the small-, medium-, and large-distance parts of the deuteron wave function. The wave functions were constrained by those deuteron properties which are accurately known experimentally, the S-state normalization A_S, the D to S asymptotic ration η, the quadrupole moment and the charge radius.

These model wave functions were applied by Garcilazo and Mathelitsch [34] to calculate the observables in πd elastic scattering within the Faddeev theory of Garcilazo. In Fig. 4 and 5 some typical results are shown for pion bombarding energy of 256 MeV. The notation of the wave functions for the S and D state are $u^{P_D R}_{R_1 R_2}$ and $w^{P_D R}_{R_1 R_2}$, where P_D indicates the D-state probability in percent; R stands for the range in which the S-state wave function is varied. A means that the wave function is varied within 3 fm, B means that the variation is allowed only within 1,5 fm. The subscripts L, M and S indicate that in the specific regions (R_1 and R_2) the S-state wave function is large, medium, or small. In the case of A R_1

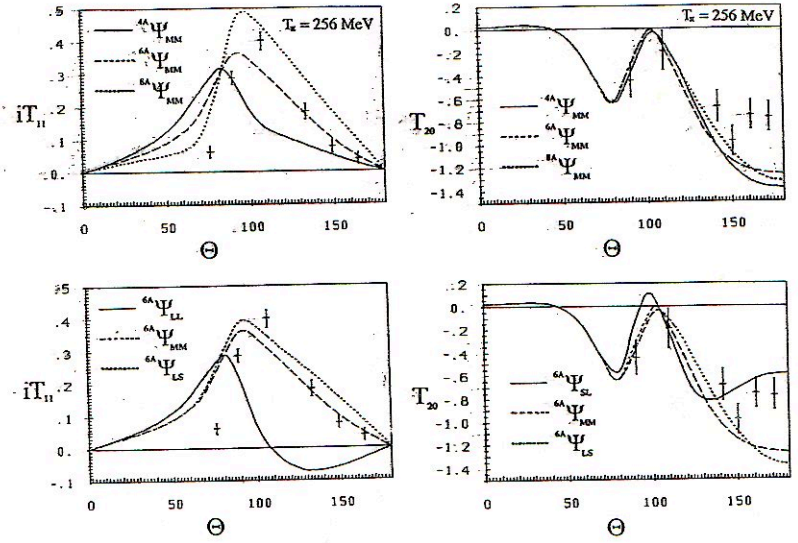

FIG. 4. Sensitivity of the deuteron structure to the πd elastic vector analyzing power iT_{11}. Upper part, sensitivity to the percentage D-state. Lower part, sensitivity to the radial form. The curves are from Garcilazo and Mathelitsch, Ref. 33, the data from Ref. 25.

FIG. 5. Sensitivity of the deuteron structure to the πd elastic tensor analyzing power T_{20}. Upper part, sensitivity to the percentage D-state. Lower part, sensitivity to the radial form. The curves are from Garcilazo and Mathelitsch, Ref. 33, the data from Ref. 25.

covers the region from 0 to 1.5 fm and R_2 from 1.5 to 3 fm. The nomenclature L, M and S is, of course, arbitrary. The guide line has been, to call the Paris S-state wavefunction medium for $P_D = 6\%$.

From this model calculation, it was found that variations within 1.5 fm (case B) show no appreciable sensitivity, i.e. pions of this energy do not explore this region of the wave function. Variations within 3 fm (case A), on the other hand, show that the cross section at large angles is sensitive to both, the D-state probability and the radial form. The same is true for iT_{11} (see Fig. 4). Interesting enough T_{20} is not sensitive to the D-state probability, but sensitive to the radial form (see Fig. 5). The comparison with the data should no be taken serious, according to what has been said before.

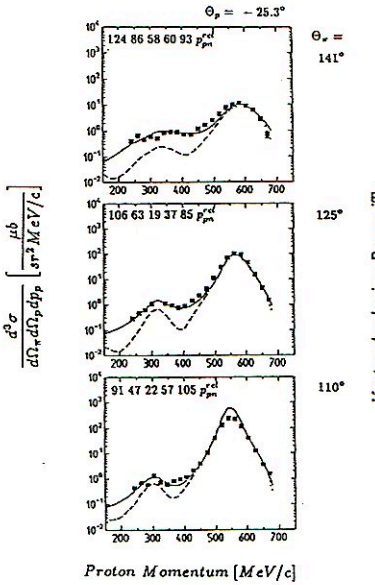

FIG. 6. The effect of the deuteron D state on the πd breakup cross sections. The solid curve represents Garcilazo's prediction with D-state, the dashed curve without D-state. More realistic variations between 4.25% D-state (Bonn potential) and 5.8% (Paris potential) show differences too small to be seen in the figure.

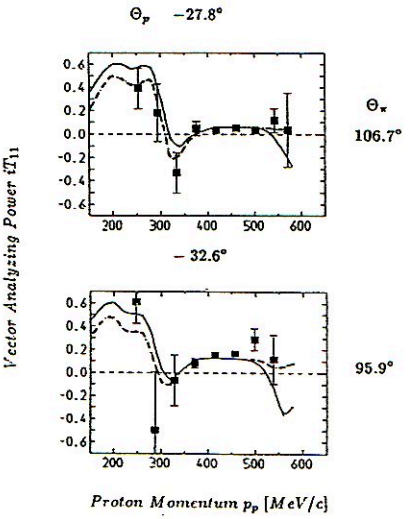

FIG. 7. Effect of the deuteron D-state on iT_{11}. The solid curve corresponds to the calculation with D-state. The dashed curve when the D-state is neglected.

So far, I have only discussed πd elastic scattering. Let me show you some results on the πd breakup reaction. Some years ago, our group has studied the $\pi^+ d \rightarrow \pi^+ pn$ reaction in a kinematically complete experiment, covering a fairly large region of phase space [35]. Since the gross features of the πd breakup reaction are dominated by the deuteron wave function it was interesting to see the effects of the D-state on the cross sections and the vector analyzing power. It Fig. 6 the extreme case is shown when the D-state is completely neglected. The comparison with the calculation when the D-state is included shows that the effect is sizable only in the np final state interaction region. It is smallest when the relative proton-neutron momentum approaches a minimum. A more realistic comparison of the different D-state components was achieved by comparing the Paris potential with the Bonn potential as *NN* input in Garcilazo's calculation. While the D-state component in the Paris potential amounts to 5.8%, it is only 4.25% in the Bonn potential. The theoretical predictions for these two cases show essentially no difference. In Fig. 7 the effects of the D-state on the vector analyzing power is shown. As one would

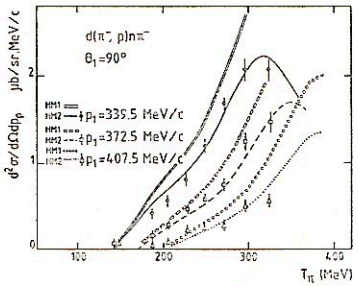

FIG. 8. Comparison of the experimental results for the $\pi^- d \rightarrow pX$ reaction (Ref. 36) with theoretical predictions from Laget (Ref. 37). The curves labeled HM1 correspond to 6.6% D-state, the ones labeled HM2 correspond to 4.5% D-state.

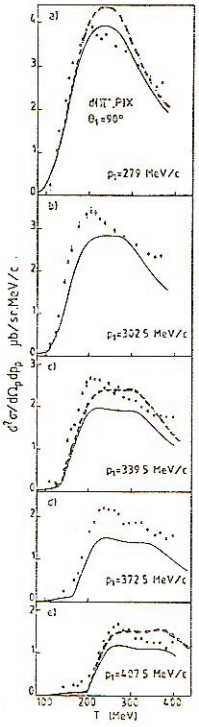

FIG. 9. Comparison of the experimental results for the $\pi^+ d \rightarrow pX$ reaction (Ref. 36) with theoretical predictions from Laget (Ref. 37). The solid curve corresponds to model HM2 (4.5% D-state), the dashed one corresponds to model HM1 (6.6% D-state).

expect there are no differences in the region of quasifree πp scattering which is around 450 Mev/c proton momentum. This kinematical region cannot sample the D-state component. Differences are seen however, in the np final state interaction region and at higher proton momenta. Similar to the cross section the differences between the Paris and the Bonn potential are hardly recognizable.

Some years ago an inclusive measurement of the πd breakup has been performed at SIN [36]. Excitation functions were measured for the reaction $\pi^{\pm} d \rightarrow pX$ for a fixed proton angle (90°), and several fixed proton momenta. The experiment was motivated by the search for a dibaryon resonance of mass 2.23 GeV/c². This was not found, but interesting results were obtained regarding the sensitivity of the data to the D-state component, within the model of Laget [37]. In Fig. 8 and Fig. 9 two Bonn potentials are compared, with 6.6% D-state (HM1) and 4.5% D-state (HM2). The cross section (as a function of the pion energy) has two components depending on the role of the detected proton. The first one, at the lowest incident pion energy, corresponds to a proton resonating with the outgoing pion. The most probable configuration occurs when the undetected spectator neutron has the lowest kinematically allowed momentum, in the range of 150-250 Mev/c for this experiment. There, the wave function is well known. The component gives a small contribution for π^-. The second component, at higher pion energies, is obtained when the detected proton is the spectator, and the two undetected particles are resonating. The momentum envolved is then higher (280-400 MeV/c) and the cross section is sensitive to the large momentum components, expeciallly the D-state admixture. The π^- cross section is strongly dominated by this process. While the π^- induced breakup cross sections clearly prefer the smaller percentage D-state component (HM2), it is not so clear in the case of the π^+ induced breakup.

Like in the case of πd elastic scattering, the πd breakup reaction in principle offers the possibility to investigate the high momentum components of the deuteron wave function (by choosing the proper kinematics), but more refined theoretical models will be required.

Let me conclude with the pion absorption reaction $\pi d \rightarrow pp$, which envolves large momentum transfer. This reaction presents the biggest headache to theorists because many polarization observables are sensitive to practically all ingredients of the theoretical models used. There is presently no hope to extract information on the deuteron structure from this reaction.

References

1) H. Garcilazo and T. Mizutani, Few-Body Systems 5, 127 (1988)
2) H. Garcilazo and T. Mizutani, Monograph, World Scientific Publ. Co., 1990
3) A.W. Thomas, Rapporteur's talk at the 8th Int. Conf. on Few-Body systems and Nuclear Forces, Graz, 1978, publ. in Lecture Notes in Physics 87, p. 247
4) N.M. Petrov and V.V. Peresypkin, Phys. Lett 44B, 321 (1973)
5) A.W. Thomas and I.R. Afnan, Phys. Lett. 45B, 437 (1973)
6) F. Myhrer and D.S. Koltun, Phys. Lett. 46B, 322 (1973)

7) A.W. Thomas, Nucl Phys. A 258, 417 (1976)
8) A.S. Rinat and A.W. Thomas, Nucl. Phys. A282, 265 (1977)
9) N. Giraud, G.H. Lamot and C. Fayard, Phys. Rev. Lett. 40, 438 (1978)
10) A.S. Rinat, Y. Starkand, E. Hammel and A.W. Thomas, Phys. Lett. 80B, 166 (1979)
11) W.R. Gibbs, Phys. Rev. C3, 1127 (1971)
12) J. Bolger et al., Phys. Rev. Lett. 46, 167 (1981), G.F. Pröbstle, Ph. D. thesis, Univ. of Karlsruhe, unpublisched; KfK report 3285 (Nov. 1981)
13) G.R. Smith et al., Phys Rec. C29, 2206 (1984)
14) K. Gabathuler et al., Nucl. Phys. A350, 253 (1980), C.R. Ottermann et al., Phys. Rev. C32, 928 (1985)
15) K. Kubodera et al., J. Phys. G6, L1 (1980), K. Kanai et al., Progr. Theor. Phys. 62, 153 (1979)
16) E. Ferreira, S.C. de Andrade and H.G. Dosch, Phys. Rev. C36, 1916 (1987), and references therein.
17) E. Ferreira and H.G. Dosch, Phys. Rev. C40, 1750 (1989)
18) C. Alexandrou and B. Blankleider, Phys. Rev. C42, 517 (1990)
19) H. Garcilazo, Phys. Rev. C42, 2334 (1990)
20) R.J. Holt et al., Phys. Rev. Lett 43, 1229 (1979), ibid 47, 472 (1981), E. Ungricht et al., Phys. Rev. C31, 934 (1985)
21) B. Blankleider and I.R. Afnan, Phys. Rev. C24, 1572 (1981)
22) T. Mizutani, Phys. Rev. C24, 2633 (1981)
23) I.R. Afnan and R.J. McLeod, Phys. Rev. C31, 1821 (1985)
24) G.R. Smith et al., Phys. Rev. C38, 251 (1988)
25) C.R. Ottermann et al., Phys. Rev. C38, 2296 (1988), ibid C38, 2310 (1988)
26) W. Grein and M.P. Locher, J. Phys. 67, 1355 (1981)
27) H. Garcilazo et al., Phys. Rev. C39, 942 (1989)
28) B.K. Jennings, Phys. Lett. B205, 187 (1988)
29) B.K. Jennings and A.S. Rinat, Nucl Phys. A485, 421 (1988)
30) T. Mizutani et al., Phys. Rev. C40, 2763 (1989)
31) B. Blankleider invited talk at the IUCF Topical Conference "Particle Production near Threshold", 1990, Nashville, Indiana, USA
32) M.P. Locher and A. Svarc, Few Body Systems 5, 59 (1988)
33) A. Certov, L. Mathelitsch and M.J. Moravcsik, Phys. Rev. C36, 2040 (1987)
34) H. Garcilazo and L. Mathelitsch, to be published
35) W. Gyles et al., Phys. Rev. C33, 538 (1986) and ibid C33, 595 (1986), W. List et al., Phys. Rev. C37, 1587 (1988) and ibid C37, 1594 (1988)
36) J. Arvieux et al., Nucl. Phys. A444, 578 (1985)
37) J.M. Laget, Phys. Reports 69, 1 (1981)

EXPERIMENTAL SEARCHES FOR NARROW DIBARYONS

B. TATISCHEFF, M.P. COMETS, Y. LE BORNEC and N. WILLIS

Institut de Physique Nucléaire, BP n° 1, 91406 ORSAY Cedex, France

INTRODUCTION

The studies of narrow structures in Nuclear Physics at excitation energies, typically of several hundreds of MeV, have been actively carried out since the last five to ten years. Such studies correspond to different topics presenting all some common features :

When observed, they correspond to new physics, usually not taken into account in conventional theories of baryons and mesons in interaction.

The signatures, if any, will correspond to narrow and small effects, difficult to extract from a large physical background. It is therefore very important to get as careful and precise experiments as possible, with unquestionable data, and then to answer the question concerning the origin of the observed structures. Among the different topics which predict such manifestations :

a) The physics of dibaryons [1] has been intensively studied, experimentally and theoretically. Such narrow structures have been extracted from many data. But also in many cases, they have not been observed.

b) The small and narrow increase of inclusive pion production with 350 MeV incident protons, observed in some laboratories [2] has been interpreted as being the signature of a $\Delta\Delta$ state in nuclei decaying by two pion emission [3], or through a Δ ball corresponding to a Δ localized inside the nuclei [4].

c) It has been argued [5] that deeply bound π^- states can be produced in heavy nuclei like ^{208}Pb and are expected to have narrow widths due to the repulsive nature of π^- neutron interaction. A reaction like (n,p) or (d,2p) produce a π^- (in a 1 s state) inside the nucleus. In the same way, the possibility to have eta meson nucleus bound states has been estimated [6] theoretically and found possible. Again transfer or knock-out reactions have to be used in order to produce low momenta - eventually recoiless - η inside nuclei [7].

d) Auerbach suggested that narrow anti-nucleonic states should exist in nuclei [8], being a consequence of the Dirac description of p nucleus scattering. There, large energy ($\approx$ 1 GeV) transfers, but low momenta are expected.

Nearly all amongst these topics, have been motivated by theoretical works, and some measurements have been already undertaken. Since the reactions are mainly the same, namely either knock-out or transfer reactions, one should be careful when associating a structure to a specific topic a) $\rightarrow$ d). For exemple, in the reaction A + C $\rightarrow$ pp + X where the two proton missing masses are studied, one has to pay attention to the fact that a structure in Mpp can reflect a resonance in X. Therefore it is advised to have Bx = 0 (meson) or Bx = 1(without narrow structure). It is of course essential to compare results from different experiments.

For these reactions, narrow enhancements may occur for energies corresponding to the opening of a new channel with meson production (threshold effects) and special care must be brought against that. When inclusive experiments are done, special effort has to be also devoted to explain how a narrow structure can be observed when Fermi momenta should spread the momenta and energies inside nuclei.

Among these various topics, the topic of dibaryon physics is particularly interesting since if narrow structures are observed, they can be related to precursor partial quark deconfinement. That possibility stimulated the large number of data corresponding to such studies. We will therefore restrict this review to recent data [1].

ANALYZING POWERS IN NUCLEON-NUCLEON ELASTIC SCATTERING

Very precise measurements of the analyzing power in elastic proton proton scattering, have been recently performed [9] using Saturne polarized proton beams. SPES3 detection was used and a rotating wheel with 16 different thicknesses of an energy degrader, to get data for incident proton energy bins $\approx$ 2.6 MeV.

a) The first measurements have been accomplished for 14 different incident energies ranging from 558 to 725 MeV. The detection of the recoil proton by use of a backward telescope allows to reduce the background to a ratio close to 10^{-3}. The mean value of the extracted proton beam energy shift : 12 MeV, is smaller than the range in energy corresponding to each measurement : 32 MeV. It results in a large overlap allowing relative adjustments between data corresponding to different energies (different beam polarizations). The depolarization resonance $\gamma G = 3$ occurs in the region of Tp = 630 MeV. In that energy domain, the polarization of the beam was reduced up to 15% but thanks to our relative adjustments, this has no consequence on the final data. Due to the different thicknesses of the absorbing wheel, the straggling in energy varied from 1 to 5 MeV. The data which correspond to the forward angle $\theta_{lab} = 19.1°$ (corrected for very small angular variations, are displayed in fig. 1 [9]. There is no room for any structure like those found [10] in the KEK experiment : ($\Gamma_{1/2} \approx 14$ MeV, $\Delta A \approx 2.5\%$). Our limits are lower than 0.2 % for a resonance having about the same width but of course much worse for any broad resonance $\Gamma > 40$ MeV close to Tp $\approx$ 645 MeV (Mpp $\approx$ 2174 MeV) which corresponds to the maximum of the analyzing power (and also $M_N + M\Delta$).

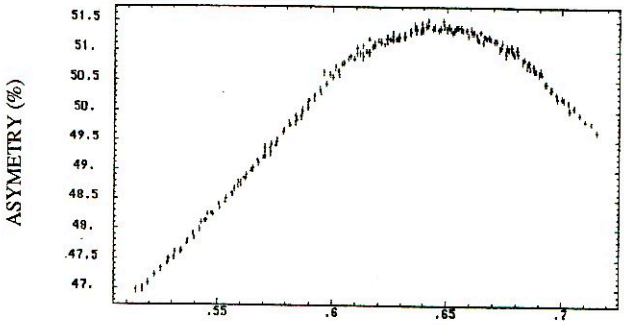

Fig. 1. Asymetry versus incident proton kinetic energy in GeV for elastic pp scattering.

These data contradict the KEK results where structures have been observed at Mpp ($\Gamma_{1/2}$) = 2160 (14) and 2192 (13) MeV. The discrepancy may be induced by the γG=3 depolarization resonance occuring in that region as already mentioned, and perhaps, not completely corrected at KEK. The KEK results have been analyzed recently [39]. Nagata et al. introduced a Breit-Wigner term in order to describe the narrow structure at 2.16 GeV. They performed a PSA of the other data to determine background partial wave amplitudes. They found $^3P_2$, $^3F_3$ and $^3H_5$ as possible candidates for the 2.16 GeV structure. The structure however should be still there for Saturne experimental conditions ($\theta_{CM} \approx 43°5$ for $\sqrt{s}$ = 2.16GeV). Although the angles (and angular acceptances) are somewhat different in both experiments, the differences are too small ($\Delta\theta_L \approx 2.4°$) to explain the discrepancy. We have rather to conclude that up to now no narrow structure has been observed in NN elastic scattering. Notice that analyzing powers can be more precise than cross sections to pick out small effects because of the interference terms, but it is also possible that additionnal amplitudes will give rise to the same analyzing powers than the background alone.

b) A second set of measurements with a thicker wheel, has been performed recently around Tp = 2.1 GeV, where an increase in analyzing power has been predicted by Lehar [11], from a twofold motivation. On one hand the extraction of amplitudes at

three energies predicts a crossing of a phase φa through zero and that annulation should manifest itseft by an increase of the analyzing power. On the other hand a display of the world data, shows a maximum for that energy ($\sqrt{s} \simeq 2.73$ GeV) although it relies really on few data only.

The analyzing power measurements, performed at Saturne, do not show any increase. The data correspond to a fixed backward angle $\theta_{lab.} = 56°$. Each extracted energy allows the measurements in a range $\Delta Tp = 52$ MeV, with 3.25 MeV bins. The total range $2.034 < Tp < 2.321$ GeV corresponds to $2.709 < \sqrt{s} < 2.807$ GeV. The statistical precision obtained is not as precise as it was in the set of measurements around Tp = 630 MeV since the pp → NNπ cross sections dominates here. The data are only preliminary. The limit for a narrow relative increase of the asymetry around Tp = 2.15 GeV, is approximately equal or smaller than 2%.

These data are in conflict with the analysis performed by Lehar and colleagues. It is clear that new measurements on the Saturne NN beam line, will be useful.

THE $\vec{p}(\vec{d},pp)X$ REACTION

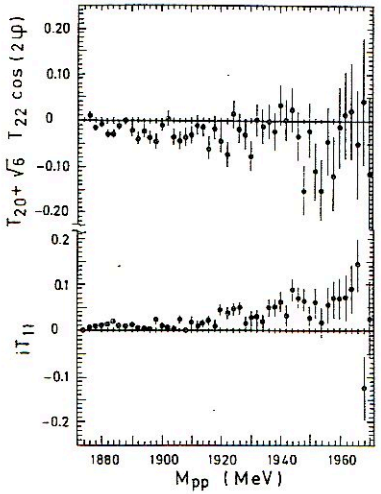

Fig. 2 . Tensor and vector analyzing powers for $\vec{p}(\vec{d},pp)X$ reaction at T_d = 2.1 GeV, θ = 17°.

Using Saturne polarized deuteron beams and SPES3 facility, the analyzing powers of $\vec{p}(\vec{d},pp)X$ reaction have been measured at $T_d = 2.1$ GeV, θ = 17° and $T_d = 1.722$ GeV, θ = 0°. Both protons were detected and identified at the same angle. Since they have each a momentum larger than 600MeV/c, the main mechanism involved is the charge exchange, with X = (nπ°,pπ⁻ or Δ°). The resolution F.W.H.M. is close to 1 MeV. The data presented in fig. 2 and 3 are binned into 2 MeV intervals. Fig. 2 displays the tensor analyzing power $T_{20} + \sqrt{6}.T_{22}\cos(2\varphi)$ and the vector analyzing power iT_{11} at Td = 2.1 GeV. There is a small bump in iT_{11} at M_{pp} = 1945 MeV, very poorly defined since it corresponds to S.D. = 1.15 only. An oscillatory pattern centered around 1.946 GeV is observed in the tensor analyzing power. The tensor analyzing power for the same data, plotted versus the missing mass M_X does not present such an oscillation. To get the corresponding number of standard deviations (S.D.), we define "a background" as a nearly flat curve extrapolating data for smaller Mpp.

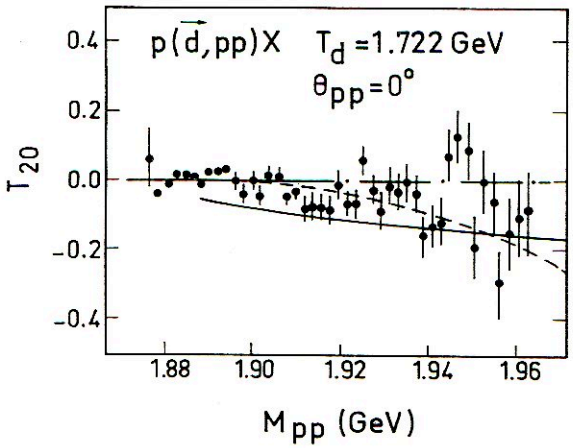

Fig. 3. Tensor analyzing power for p(d⃗,pp)X reaction at Td = 1.722 GeV, θ = 0°. The theoretical curve are from Lykasov [26]. Full (dashed) curve is the result of T_{20} calculation within spectator mechanism, when FSI and Glauber screening effect are (are not) taken into account.

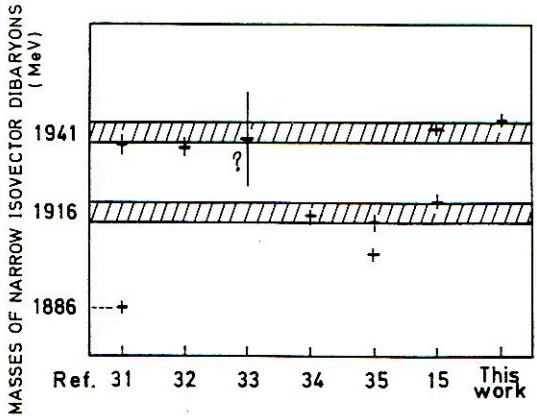

Fig. 4. Masses of isovector narrow structures observed recently, in the range 1876 < M_{pp} < 1955 MeV.

Since the effect is an oscillation, the number of S.D. depenses very little on the assumption concerning "the background", allowing the assumption that the background is obtained without unprecision. We obtain then S.D.= 2.45 for the tensor analyzing power (maximum value).

The measurement has been repeated in new conditions with 1.722 GeV polarized deuterons, the protons being detected at 0° [12]. Fig. 3 displays the results for T_{20} versus Mpp. We observe an oscillation centered at 1945 GeV but with opposite sign. The corresponding number of S.D. is 3.86. In order to strengthen the oscillation versus background, both results have been mixed (with sign inversion). We obtain then S.D. = 4.7. In the Mpp range studied in this experiment, the observation of different narrow dibaryons have been reported [1] - see fig. 4 - although always with poor statistics. They concentrate around 1916 MeV and 1941 MeV. In the data presented here, there is no signal around 1915 MeV. Since the large statistics at small Mpp is mainly due to small transfer momenta, we cannot conclude that our data bring a strong argument against a narrow structure at this mass.

Around 1939 MeV, three different studies reported to have observed narrow dibaryons. Troyan studied $np \rightarrow pp\pi^-$ and $\rightarrow pp\pi^-\pi^\circ$ and reported [31] the existence of a resonance at 1937 MeV with 3.7 S.D. A study of the ratio of elastic to inelastic proton scattering [32] has been done at Dubna and the authors, in spite of a small statistical precision, concluded to the presence of a narrow signal at 1936MeV. Glogolev studied $dp \rightarrow ppn$ and $\rightarrow p\pi^+nn$ and reported [33] the observation of a peak in Mpp at 1939 ± 15 MeV ($\Gamma_{1/2} = 27 \pm 13$ MeV) with 2.2 S.D.

In order to extract an oscillation, the assumption here has been done that the physics of mesons and nucleons in interaction will give rise to a continuous curve. Such calculation has been performed by Lykasov [26].The theoretical results are plotted on fig. 3 where full (dashed) curve corresponds to spectator mechanism with (without) FSI and Glauber screening effect. The Paris deuteron wave function has been used. The calculated values decrease slowly without any oscillation.

THE $^2H(p,n)X^{++}$ REACTION

It has been studied at IUCF using $T_p = 200$ MeV proton beam. Neutrons were detected at 0° with a flight path of ≈ 50m allowing a very good missing mass resolution : $\Delta M_x \approx 0.2$ MeV. The useful experimental range is $20 < T_N < 160$ MeV since for larger neutron energies the spectrum displays peaks from C (CD_2 target was used). This range corresponds to $\approx 2.0 > M_X > 1.91$ GeV. The preliminary data [13] are shown in fig. 5. They do not display any structure and the authors concluded that "for missing masses near 2 GeV/c^2 and particle intrinsic widths $\lesssim$ 500 keV, we expect the 0° $^2H(p,n)X^{++}$ cross section limits to be of order 0.1 - 1 μb/sr".

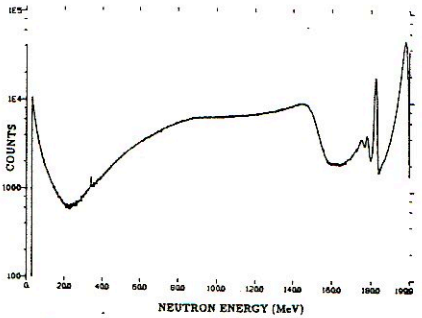

The neutron time spectrum of Fig. 1(a) converted to a neutron energy spectrum. The peak at $E_n \simeq 34$ MeV arises from pulse selection feedthrough. The rise at low E_n corresponds to background events uncorrelated with the cyclotron rf signal.

Fig. 5 . CD_2 $(p,n)X^{++}$, 0°. Data from Indiana [13].

DIBARYON SEARCHES FROM PHOTONUCLEAR REACTIONS

Since the measurements performed at Bonn, where the $\gamma d \rightarrow pp\pi^-$ reactions were studied with observation of a narrow enhancement in two proton mass distribution at Mpp = 2014 ± 2 MeV [14], many works have been devoted to such studies, using γd as input channel. In the range of masses below $2M_N + M_\pi$, deuteron photodesintegration cross sections using // and ⊥ polarized photons from Kharkov electron linear accelerator, have been studied ($1904 < \sqrt{s} < 1973$ MeV). When photons are polarized orthogonally to the scattering plane, the differential cross sections of $\gamma d \rightarrow pn$ exhibit a narrow structure at $\sqrt{s} = 1919.5$ MeV [15].

For masses above $2M_N + M_\pi$, no structure has been observed in cross sections :

- neither at INS (Tokyo), in the total cross section of the $\gamma d \rightarrow \pi^- pp$ reaction studied [16] in the range $2222 < \sqrt{s} < 2582$ MeV,
- nor in $M_{\pi pp}$ mass distribution studied at Bonn [17] in $\gamma d \rightarrow pp\pi^-$ reaction ($2.16 < \sqrt{s} < 2.32$ GeV), and at Saclay [18] $2.19 < \sqrt{s} < 2.293$ GeV).

However many studies have been performed using polarization degrees of freedom, ($\gamma d \rightarrow pn$ reactions) :

- no structure from INS [19] in the target asymmetry $T(\theta)$ studied in the range $2.155 < \sqrt{s} < 2.480$ GeV,
- using linearly polarized photons from Yerevan synchrotron, the polarization of the emitted proton has been measured at center of mass proton angles : 75°, $2.16 < \sqrt{s} < 2.28$ GeV [20] and 65°, $2.15 < \sqrt{s} < 2.25$ GeV [21]. There is a possible narrow structure

close to $\sqrt{s} = 2.24$ GeV in Py (plane orthogonal to the scattering plane) but its definition is not precise enough.

- Polarized deuterons photodisintegration has been studied at Bonn at $T\gamma = 450$, 550 and 650 MeV [22]. The authors concluded that a second minimum of T at 550 ± 50 MeV around 90° could perhaps be an indication for a dibaryon resonance. This speculation is not strong enough.

- A few analysis have been performed in order to improve the agreement between theoretical description and different photonuclear data by introduction of dibaryon resonances as free parameters. Such approach has been used in the analysis of data from Yerevan synchrotron [23], $2.24 < \sqrt{s} < 2.55$ GeV, and especially for analysis of data from Kharkov accelerator [24], $2.11 < \sqrt{s} < 2.40$ GeV ($d\sigma/d\Omega$, Σ, P, T). The agreement is of course improved when additional free parameters are introduced, but this very indirect approach is not convincing enough.

CONCLUSION

Although we have restricted this review to recent data, it is clear that the number of experiments increase continously. The number of precise results increase, which is as a matter of fact more important.

There is no measurement amongst those presented, from where unambiguous dibaryons can be extracted. There is a possible evidence for a dibaryon close to 1940 MeV.

It is specially important that both precise analyzing power measurements in pp elastic scattering, performed at Saturne (SPES3) concluded to the absence of any narrow structure. If we remember that never any dibaryon has been observed in isospin 0 or 2 channels [25], one can been lead to speculate that they simply do not exist. However that would be incorrect since precise data exist in case of isovector channel where narrow dibaryons have been observed [1].

The answer to the first question set in the introduction, namely is there unquestionnable data showing dibaryons, must be no, for the recent data discussed here.

Some years ago, a semi-phenomenological di-quark model [27] has been able - after adjustement of a few free parameters - to get a good agreement between data and calculated masses and widths of some isovector dibaryonic resonances. Recently a work has been presented, within a modified MIT bag model where a di-quark cluster has been assumed [28]. A good agreement has been achieved for approximately half of the masses found in various experiments for isovector dibaryons (fig. 6). However it has been shown that the improvement of calculations, from spherical MIT [29] to cloudy bag model [30], enhanced by a few hundreds of MeV the masses of predicted dibaryons. We have therefore to consider with care the previous agreement between di-quark cluster model and data.

The answer to the second question set in the introduction concerning the origin of the observed structures remains still open.

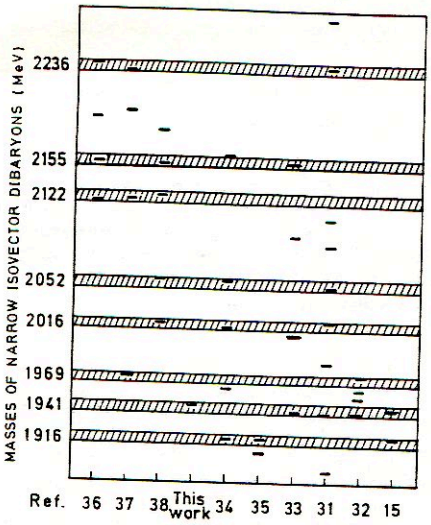

Fig. 6 . Masses of isovector narrow structures.

REFERENCES

[1] Many experimental review talks exist. References can be found in the most recent one : B. Tatischeff et al. Proceedings of the X International Seminar on High Energy Physics Problems, Relativistic Nucl. Phys. and Quantum Chromodynamics, Dubna, Sept. 1990.

[2] V.A. Krasnov et al., Phys. Lett. 108B (1982 11
J. Julien et al., Phys. Lett. 142B (1984) 340

[3] A.B. Kurepin, Nucl. Phys. A519 (1990) 395c

[4] V.A. Khodel, Journal of Nucl. Phys. 52 (1990) 1355, in russian

[5] H. Toki and T. Yamazaki, Phys. Lett. B213 (1988) 129

[6] Q. Haider and L.C. Liu, Phys. Rev. C34 (1986) 1845

[7] R.E. Chrien et al., Phys. Rev. Lett. 60 (1988) 2595
B.J. Lieb, L.C. Liu et al., Lampf Progress Report LA-11670-PR, 1989

[8] N. Auerbach et al., Phys. Lett. B182 (1986) 221

[9] R. Beurtey et al., to be published

[10] H. Shimizu et al., Phys. Rev. C42 (1990) R483

[11] C.D. Lac et al., J. Phys. France 51 (1990) 2689

[12] B. Tatischeff et al., Proceedings of the 7th Intern. Conf. on Polarization Phenomena in Nucl. Phys., Paris, 1990, p. C6-371

[13] L.C. Bland, S.E. Vigdor et al., Indiana University Cyclotron Facility Scientif and Technical Report, May 1989 - April 1990, p.14

[14] B. Boch et al., Nucl. Phys. A459 (1986) 573

[15] V.B. Ganenko et al., JETP Letters 50 (1989) 220, in russian

[16] M. Asai et al., Phys. Rev. C42 (1990) 837

[17] W. Ruhm et al., Nucl. Phys. A459 (1986) 557

[18] G. Audit et al., Phys. Rev. C34 (1986) 2217

[19] Y. Ohashi et al., Phys. Rev. C36 (1987) 2422

[20] R.O. Abakian et al., Journ. of Nucl. Phys. 52 (1990) 312, in russian

[21] R.O. Abakian et al., Journ. of Nucl. Phys. 52 (1990) 618, in russian

[22] K.H. Althoff et al., Preprint, Bonn-Me- 89-01

[23] P.I. Galumian, Preprint YERPHI-1084 (47) - 88, in russian

[24] V.P. Barannik and Yu V. Kulish, Nucl. Phys. A451 (1986) 751
Journ. of Nucl. Phys. 47 (1988) 1580, in russian

[25] M.P. Combes-Comets et al., Phys. Rev. C43 (1991) 973

[26] G.I. Lykasov et al., private communication and contribution to this Worshop

[27] N. Konno et al., Phys. Rev. D35 (1987) 239 ; Phys. Rev. D37 (1988) 154

[28] C. Besliu et al., Proceeding of the X International Seminar on High Energy Physics Problems, Relativistic Nucl. Phys. and Quantum Chromodynamics, Dubna, sept. 1990

[29] A.Th. Aerts et al., Phys. Rev. D17 (1980) 260

[30] P. La France and F.L. Lomon, Phys. Rev. D34 (1986) 1341

[31] Yu.A.Troyan et al., JINR preprint PI-90-78, in russian

[32] V.V. Avdeichikov et al., JINR preprint PI-90-52, in russian
Yu.A.Troyan et al., JINR preprint PI-90-79, in russian

[33] V.V. Glogolev et al., Journal of Nucl. Phys. 51 (1990) 736, in russian

[34] O.B. Abdinov et al., JINR preprint PI-88-102, in russian

[35] N. Angelov et al., JINR preprint PI-88-905 ; S.A. Azimov et al., 60-88 HEP (Tashkent, preprint)

[36] B. Tatischeff et al., Phys. Rev. C36 (1987) 1995

[37] B. Tatischeff et al., Europhysics Letters 4 (1987) 671 ; Zeit. Phys. A-Atomic Nuclei 328 (1987) 147

[38] L. Santi et al., Phys. Rev. C38 (1988) 2466

[39] J. Nagata, M. Matuda, N. Hiroshige and T. Ueda, To be published

NARROW COHERENT EFFECTS IN πNN-DYNAMICS

A.E.Kudrjavtsev

Institute for Theoretical and Experimental Physics,SU-117259 Moscow, Russia

G.Z.Obrant

Leningrad Nuclear Physics Institute, Gatchina,SU-188350 Leningrad, Russia

The problem of narrow dibaryon resonances is one of the most intriguing in the intermediate energy physics.We shall understand the resonances with a mass more than a sum of the pion mass and two nucleon masses $2m+\mu$ and with a width $\Gamma \sim 0.01$GeV as the narrow dibaryon resonances.There are some indications on such effects in the experiments with few-nucleon systems and in the hadron-nucleus scattering[1].The consideration of such processes via πNN-dynamics does not show any narrow peculiarities usually in the energy dependence of the cross-section (see for ex.[2]).There is some indication of the possibility of such effects in[3] where the pole is discussed in the NΔ-amplitude with isospin I=2 and a mass near $2m+\mu$ and a width of some MeV.

It will be shown lower how the narrow effects in the cross-section energy dependence can be produced via πNN-dynamics.As there is the little parameter μ/m in the problem one can try to create the resonance of the pion wave on two heavy scatterers.The condition of this resonance neglecting the elementary amplitude complexness is the divisibility of the distance between scatterers to the half of the wavelength.There are the interference phenomena producing the sharp energy dependence of the cross-section.The width of the peculiarities can be by an order of magnitude less than πN-resonance one.

The main features of the problem are seen in the one-dimension exactly solvable model of the particle scattering by two potential barriers of the rectangular form with the height U_0, thickness a standing on the distance h one after another[4]. The total scattering amplitude on two barriers (the amplitude of the reflection wave) is

$$A = A_1 \frac{1-(1+\eta^2-2i\eta\,\mathrm{Ctg}\,k_2a)/(1+\eta^2+2i\eta\,\mathrm{Ctg}\,k_2a)\exp(2ik_1h)}{1-A_1^2\exp(2ik_1h)} . \qquad (1)$$

(Here $k_1=(2\mu E)^{1/2}$,E-initial energy of the particles, $k_2=(2\mu(E-U_0))^{1/2}$,$\eta=k_2/k_1$). If k_1 is real, it is expressed directly

through the elementary amplitude A_1

$$A = A_1 \frac{1 - A_1/A_1^* \exp(2ik_1h)}{1 - A_1^2 \exp(2ik_1h)} . \qquad (2)$$

This scattering amplitude has poles at the unphysical sheet and goes to zero at real k_1 near the pole positions. The width of the resonance is determined by the value of the elementary amplitude A_1. The condition of vanishing the denominator in (1,2) can be written as

$$Im\, k_1 = \ln|A_1|/h . \qquad (3)$$

At the low value of the initial momentum the amplitude A_1 is near unit and the width of the resonance is very small. This corresponds to the narrow quasibound state of the particle and to the standing wave creation between two barriers with low transparency. The amplitude A_1 decreases as initial momentum increases and the resonance width increases in the correspondence with (3). For all that the character of the resonance changes beginning from the momenta more than k_0. Here a standing wave is not produced. However the resonances continue to be sufficiently narrow. The resonance width becomes large with further momentum increasing and physics is determined by the numerator of (2).

The above consideration shows how in the one-dimension three- body problem the narrow resonances are produced when there is a wide resonance in an elementary amplitude[4], if a mass of the initial particle is much lower than scatterer masses. The generalization of (1,2) for the amplitude of the deuteron breakup process $\pi d \to \pi pn$ in which in the last interaction the particle 3 is the spectator looks as[5]

$$F_3(\vec{k},\vec{p}_3) = \int_0^\infty z^2 dz \, \frac{\sin(p_3 z)/p_3 z + \alpha \int \exp(ikz)/z \cdot \sin(|\vec{k}-\vec{p}_3|z)/|\vec{k}-\vec{p}_3|z)}{(1-\alpha \int \exp(ikz)/z)(1+\alpha \int \exp(ikz)/z)} \Psi(z) \qquad (4)$$

($\vec{p}_3$-nucleon momentum in the deuteron rest-frame). We shall consider only S-wave pion-nucleon interaction neglecting the nucleon spin and isospin. The standard Breit-Wigner form with Δ-resonance parameters is taken for πN-amplitude f(k). The value $\alpha = S^{1/2}/m$ arises after the transition from invariant πN-amplitudes to amplitudes f in the pion-nucleon c.m.frame. In all further calculations Paris deuteron wave-function is used.

The structure of the integrand in (4) is analogous to (1,2) in the one-dimension sample; the resonance states correspond to zeros of the denominator with the fixed distance r between the nucleons. The locations of this zeros on the complex plane k are shown in fig.1 at different

values of r .The amplitude poles create two branches corresponding to two factors in the denominator and joined by the solid lines.The trajectory of the first factor gives poles remote from the real axis . The second trajectory connects zero locations of the second factor in the denominator (4) and besides it is the nearest trajectory to the real axis.It crosses the real axis at $k=k_0=0.285$GeV/c, $r=r_0=6(\text{GeV/c})^{-1}$ and the poles get to the physical sheet of the scattering amplitude.The trajectory does not crosses the axis in the case of infinitely heavy nucleons $\alpha=1$.

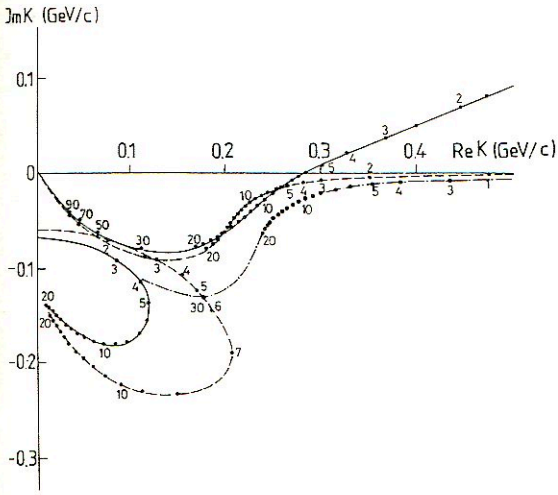

Fig.1. Pole trajectories of the scattering amplitude at the fixed distance between scatterers (shown by digits with dimension $(\text{GeV/c})^{-1}$). The solid curve-the nucleon mass m=0.9383GeV, the dashed curve-the nucleon mass is 50m, the dot-dashed curve -the nucleon recoil effects are calculated.

The further consideration will be carried out for the S-wave amplitude $\Phi_3(W,q_3)$ of the deuteron breakup in the pion-deuteron c.m.frame under the condition that nucleon 3 is in the S-wave relatively to the pion-nucleon subsystem 1,2. (Here W-the total energy in the pion-deuteron c.m.frame, $\vec{q}_3$ -the momentum of nucleon 3) The choice of the S-wave in the πd-interaction allows to increase a contribution of the small nucleon-nucleon range physics in the pion-deuteron scattering.This enhances the above- mentioned resonant mechanism as the pole trajectory approaches near the real axis in fig.1 at the small nucleon-nucleon distances $(r_0=6(\text{GeV/c})^{-1}=1.2\text{fm})$.

One can estimate the pole contribution at $r=r_0$ in eq.(4) using the

nearness of the chosen initial momentum to k_0, i.e., lay out the denominator in the row near zero and thus pick out clear the pole factor.

$$\left(1-\alpha\int \exp(ikz)/z\right)^{-1}\left(1+\alpha\int \exp(ikz)/z\right)^{-1}\approx z\left(2\left(1-ik_0z_0\right)\left(z-z_0+i\varepsilon\right)\right)^{-1}.$$

After the addition of a such pole contribution to the integral over the large distance region the oscillating picture arises in the real part of the amplitude[4]. The oscillation in $Re\Phi_3$ at $k\approx k_0$ is produced from the denominator of (4) and besides it is determined in the main by the region $r\approx r_0$. It has the same physical reason as the coherent phenomena in the one-dimension sample. When pole trajectory fig.1 does not cross the real axis (for ex. dashed line in fig.2) one could speak about certain effective value of the parameter r_0.

One can develop the modification of the Brueckner theory estimating the nucleon recoil effects in the propagator[4](Fig.1). It allows one to avoid the problem of crossing the real axis by the pole trajectory.

The calculation of the deuteron breakup amplitude on the basis of Faddeev equation is the next step on a pass to the real pion- deuteron interaction. It allows first of all to take into account exactly the nucleon recoil effect and the unitarity condition. If three-particle Wick $|\alpha\rangle$ states are chosen as basic states analogously [6] (see in detail[4]) these equations can be written as

$$\Phi_i^{L_iS_i\alpha_i'}(W,q_i') = (1-\delta_{1i})\Phi_i^{(0)L_iS_i\alpha_i'}(W,q_i') + \sum_{j\neq i}\sum_{L_jS_j\alpha_j}\int_0^\infty q_j^2\,dq_j\; K_{L_jS_j\alpha_j}(q_i',q_j)\,\Phi_j^{L_jS_j\alpha_j}(W,q_j) \qquad (5)$$

and the nucleus of the equations is

$$K_{L_jS_j\alpha_j}(q_i',q_j) = \tau_j^{L_iS_ij_j}(w_0(q_j))\int_0^\infty p_j^2\,dp_j\,\frac{p_i}{2w_i}\,I_j(p_j,q_j)\,\frac{W(p_j,q_j)}{W^2(p_j,q_j)-S-i\varepsilon}\cdot$$
$$\cdot\Theta(1-\cos^2\vartheta_j)\sum_{\lambda_j\lambda_k} h^{L_iS_i}(p_i)\langle\alpha_i|\alpha_j^0\rangle h^{L_jS_j}(p_j). \qquad (6)$$

The certain approximations have been made at the calculation of the amplitude $\Phi_3(W,q_3)$ via (5,6) allowing to compare the calculation with the analogous results from static case. At first only equations 2 and 3 are considered from the three equations of the system and the amplitude $\Phi_1(W,q_1)$ is discarded. Secondly the elementary πN-amplitude $\tau_j(w_0(q_j))$ is taken at the energy correspondent to the nucleon at rest in the deuteron rest- frame; the form factors $h^{L_iS_i}$ are discarded too. The calculations are carried out for the spinless nucleons; only S-wave elementary πN-amplitudes are considered and further we shall deal only with S-wave inelastic πd-scattering. The solution of integral equation (5) with

the singular nucleus (6) was carried out by the Pade-approximant method.The convergence of the method has been obtained already for [4,4]Pade-approximant.

The results of the calculation according to (5,6) for the amplitude $\Phi_3(W,q_3)$ show approximately the same effects as in the static case (4). There is the oscillation in $Re\Phi_3(W,q_3)$ at $k \approx k_0$ that can be considered as a trial effect for the coherent fenomena.Their region is moved strongly to the low momentum side relatively to the static case and somewhat weaker comparing with the modified static variant.The approximate calculation of the nucleon recoil effects in the modified static theory qualitatively reflects the tendency of the movement of the oscillation region to low q_3[4].

The amplitude $\Phi_3(W,q_3)$ in the kinematic field of the process $\pi^+ d \to pp$,i.e. $q_3=((W/2)^2-m^2)^{1/2}$ approximately describes the absorption of the scalar pion by deuteron (Fig.2). The double scattering amplitude has the standard resonancelike behaviour with the maximum in the imaginary part at W=2.17GeV connected with the resonance in the elementary amplitude.The resonancelike behaviour of $\Phi_3(W,q_3(W))$ is conserved if one takes into account all multiple rescatterings in (5,6) but the maximum is at lower energy W=2.086GeV and the width is approximately twice smaller.At the same time the real part $Re\Phi_3$ vanished just at the point of the maximum of $Im\Phi_3$.Thus the loop on Argan-diagram is produced with the correct resonancelike direction of movement with the energy increase. The main reasons of the maximum displacement are the sharp decrease of the imaginary part of the double-scattering amplitude at $k \approx k_0$ by virtue of the discussed interference phenomena. The multiscattering amplitude increases with the initial momentum decrease and $Im\Phi_3$ is vanishing at k=0 because of the unitarity condition.

The picture in the modified static theory qualitatively corresponds to the exact calculation right up to W≈2.12GeV,the maximum in the imaginary part is produced too (at W≈2.066GeV) and the real part at the same time goes through zero.The distinction is that due to the nonunitarity of the amplitudes with the multiplicities being more than two in this calculation the imaginary part does not vanish at k=0 and the maximum is rather wide.Thus the discussed coherent effect arises in the modified static theory too and it has sufficiently general character. The principal difference between the exact calculation and

the modified static variant arises at W>2.12GeV ($k^* k_0$). As this theory is nonunitary in considered region the only conclusion of this calculation is the statement that the imaginary part decreases in this field in accordance with the Faddeev equation calculation.

The obtained from (5,6) resonancelike amplitude $\Phi_3(W,q_3(W))$ includes some nonresonant background in $Re\Phi_3$.The interference with this

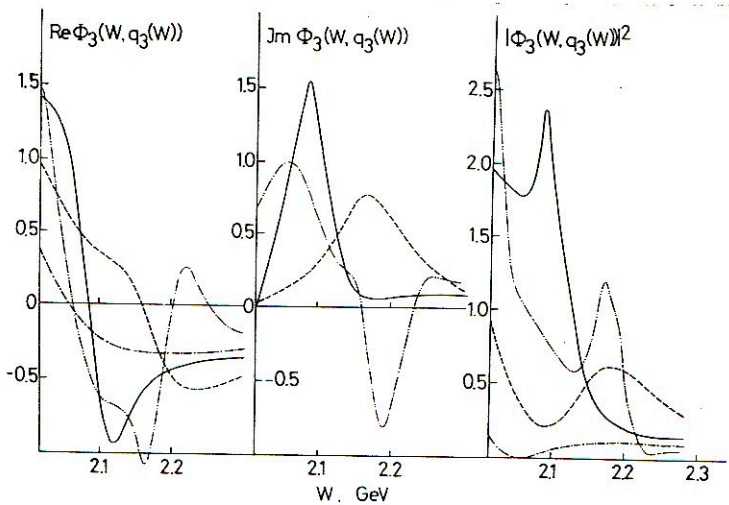

Fig.2.The scattering amplitude $\Phi_3(W,q_3(W))$ at $q_3=((W/2)^2-m^2)^{1/2}$ as a function of W. Solid curves-Faddeev equations;dashed curves-the single and the double scattering from Faddeev equations;dot-dashed curves-the single scattering from Faddeev equations,double-dot-dashed curves-the modified static theory.

background leads to the narrow peak in the cross section (fig.2) and besides the peak width in the energy dependence is very small,almost by the order of magnitude lower than in the elementary interaction. The further more comprehensive investigation,turning off step by step all approximations being done,allow to give unambiguous answer about the value of such effects in the real pion-deuteron scattering.

The most suitable examples for the manifestation of the discussed

effect are $^3P_1$ and $^1D_2$ waves in the real $\pi^+d \to pp$ process (the classification on the final state). The experimental situation is obviously unsatisfactory for the observation of the discussed narrow effects in the energy behaviour at small energies from the threshold to W≈2.08GeV[7].On the other hand it is necessary to consider the possible manifestation of S-wave πN-resonances with the higher masses.The obtained peaks in πd-cross-section move to the low energy relatively the mass of the πN-resonance,and in principle could appear in the region of experimentally observed effects[1].

REFERENCES

1. B.Tatischeff et al.
   Proc.10th International Seminar on High Energy Physics Problems,Relativistic Nuclear Physics and Quantum Chromodinamics,Dubna,24-29 September,1990;IPNO-DRE 90-15.
   Kamal K.Seth. Proc.International Conference on Medium and High Energy Physics,Thaipei,Taiwan May 16-21,1988 (World Scientific,Singapure).
2. M.A.Braun,V.M.Suslov. Nucl.Phys. A496,687(1989).
3. H.Garcilaso,L.Mathelitsch. Phys. Rev. C34,1425(1986).
4. A.E.Kudrjavtsev,G.Z.Obrant. Preprint LNPI-1661,Leningrad,1990.
5. K.A.Brueckner. Phys.Rev. 89,834(1953); 90,715(1953).
   A.E.Kudrjavtsev. Zh.Eksp.Teor.Fiz. 61,490(1971).
   B.M.Kolubasov,A.E.Kudrjavtsev. Yad.Fiz. 17,42(1973).
6. H.Garcilaso. Nucl.Phys. A360,411(1981).
7. N.Hiroshige,W.Watari and M.Yonezawa. Progr.Theor.Phys.72,1146(1984).
   D.V.Bugg,A.Hasan,R.L.Shypit. Nucl.Phys. A477,546(1988).
   I.I.Stracovsky,A.V.Kravtsov,M.G.Ruskin. Yad.Fiz. 40,429(1984).

GENERAL REGULARITIES AND INDIVIDUAL FEATURES OF THE CUMULATIVE PARTICLE PRODUCTION

Agakishiev G.A.[1], Averichev G.S.[1], Bondarev V.K.[2], Borzunov Yu.T.[1], Giordanesku N.[3], Golovanov L.B.[1], Gusejnaliev J.[4], Zborovski I.[5], Efimov L.G.[1], Litvinenko A.G.[1], Minaev Yu.I.[1], Moroz N.S.[1], Panebratsev Yu.A.[1], Pentia M.[6], Sulejmanov M.K.[4], Trofimov V.V.[1], Tsvinev A.P.[1], Shahaliev E.[4], Shimanskiy S.S.[1], Yurevich V.I.[1], Yakovlev R.M.[7]

INTRODUCTION

In our opinion, one of the main tasks of modern nuclear physics is to construct theory of the atomic nucleus based on fundamental components of hadron matter - quarks and gluons.

In recent years a number of experiments have been carried out to search for and investigate non-nucleon and quark degrees of freedom in lepton-nucleus, hadron-nucleus and nucleus-nucleus interactions. Several new phenomena were found in those experiments (cumulative nuclear effect, EMC effect, production of particles on nuclei with large p_T, color screening effects). They cannot be explained within the classical proton-neutron model. Now the available experimental data and their theoretical interpretation led to the conclusion that deuterons and other lightest nuclei can be objects for investigation of quark degrees of freedom already at intermediate energies, help one to solve the problem of taking into account relativistic and off-shell effects and to come closer to the solution of the multinucleon interaction problem.

---

1 JINR, Dubna
2 Leningrad State Univ., Leningrad, Russia
3 Bucharest Univ., Romania
4 NPO Cosmic Research, Baku, Azerbaijan
5 Nucl. Phys. Inst., Řež, ČSFR
6 Inst. for Physics and Nuclear, Bucharest, Romania
7 Radium Inst., Leningrad, Russia

The purpose of this report is to discuss generalities of cumulative effects (locality, asymptotic behaviour, universal character of nuclear structure functions) and their individual specific features related to cumulative production of particles on the lightest nuclei. Following the topic of the workshop, we shall consider the investigations of the deuteron structure in cumulative processes most thoroughly.

It should be mentioned that since discovering the cumulative effect we have regarded it as a signal that in nuclei there are "hadron matter drops" or multiquark configurations, whose structure greatly differs from that of free nucleons [1]. Arguments for this point of view will be presented in the report. It should also be mentioned that the study of cumulative processes is connected with the most important problems of long-range quantum chromodynamics: search for and investigation of multiquark states, study of difference between quark hadronization in vacuum and in a nuclear medium, search for the transition of matter from the hadron phase to the quark one. It is cumulative reactions that allow some unique opportunities which in principle cannot be received in the experiments with "elementary" hadrons.

GENERAL CHARACTERISTICS OF THE PHENOMENON

In this section we shall briefly discuss such important properties of the cumulative nuclear effect as its locality and asymptotic behaviour. The cumulative effect was predicted by A.M.Baldin in 1971 [2]. He supposed that production of particles in the region which is kinematically forbidden for particle production in nucleon-nucleon interactions results from interaction of a primary hadron with a local object of several nucleon masses inside a nucleus. Theoretical estimations [3](weaker correlations at the speed difference $y=2$ of the incident hadron and the target, or later $b_{ik} \geq 5$) showed that the phenomenon comes to the asymptotic behaviour quite early, at the energy of primary protons 3.5-4 GeV. Pioneering proton beam experiments of Dubna [4]on the investigation of cumulative pion production on nuclear targets proved that at the proton energy

over 3.5-4 GeV a) the slope parameter of the pion energy spectrum is no longer dependent on the energy (in the first approximation the production cross section of cumulative particles bears a simple exponential relationship to the kinetic energy), b) the ratio of cross sections for production of positively and negatively charged particles is equal to 1, c) the dependence of cross sections on the atomic weight of the fragmenting nucleus is of type A^1 instead of $A^{2/3}$, which is traditional for nuclear physics.

All these generalities united were called limiting nuclear fragmentation. Note that the general rules of limiting nuclear fragmentation were confirmed both by a series of experiments at Berkeley [5], where the asymptotic behaviour was studied in the interval of primary energy 1-6 GeV, and in a series of experiments at the Serpukhov accelerator [6] (the interval of primary energy form 10 to 70 GeV). In the whole energy interval of the Serpukhov accelerator the slope parameter of the cumulative pion spectrum did not change by more than 2% and the cross section values by more than 20%.

In the experiments on cumulative production of protons in interaction of high-energy particles with nuclei one also found a number of asymptotical rules united into what was called "nuclear scaling". They are a supplement to limiting nuclear fragmentation for cumulative meson production [7].

In this case, at energies higher than several GeV, the slope of the cumulative proton spectrum (the spectrum has an exponential shape depending on the kinetic energy) is practically independent of the incident particle energy and type. It is valid not only for incident hadrons but also for photons [8] and neutrinos [9].

Now let's discuss the experimental data that bear evidence for local character of cumulative processes. First of all, it should be mentioned that the shape of the energy spectrum and angular dependence of cross sections for production of cumulative protons on the helium nucleus and on the lead nucleus is practically the same and does not depend on the energy, starting from the energy of several GeV. It naturally indicates the local

character of the interaction. Indeed, in cascade models the spectrum shape must strongly depend on the atomic weight of the target and the yield of cumulative particles on the initial energy. In the model of multiple intranuclear rescattering the shape of the spectrum and angular dependence must strongly depend on A. It is shown in ref. [10] that for cumulative protons relative variation of T_o with A indicates that it is smaller than the relative variation of the mean coupling energy or the Fermi momentum of nucleons in a nucleus. This fact should also be interpreted as evidence for dominance of local properties of nuclear matter over individual characteristics of particular nuclei in production of cumulative particles.

CUMULATIVE PARTICLE PRODUCTION AND QUARK DISTRIBUTION IN NUCLEI.

This section is to discuss the experimental data which testify in favor of the fact that the distribution of quarks and gluons in nucleons which are embedded in nuclei essentially differs from the free nucleon case. In other words we shall give arguments for the fact that the quark-parton structure functions of nuclei are independent (irreducible to one-nucleon) objects of hadron physics and shall discuss the presently available properties of these functions.

In our studies of hadron-nucleus reactions special attention was paid to the region kinematically forbidden for one-nucleon collisions (cumulative effect) because, according to the suggested ideas, these data show evidence for existence of multiquark configurations and superfast quarks in nuclei.

In 1980 A.M.Baldin [11] introduced a new physical concept, namely the quark-parton structure function of nuclei, which is being intensively studied in hadron and deep inelastic processes. It was assumed that the cross section for fragmentation of nuclei into mesons measured experimentally in the inclusive process h+A→1+... is proportional to the momentum distribution of quarks in the nucleus (quark stripping followed by soft hadronization):

$$E_1 \, d\sigma/dp \propto G_{A/q}(X, P_T^2)$$

The validity of the assumption that the distribution of fast

pions in the fragmentation region is similar to that of fast valence quarks in pp interactions is considered, for example, in papers [12].

When analyzing the data we use the capital X variable [13]. The cumulative number X determines the minimum mass of the target (in nucleon masses) on which the process can occur. The region X > 1 corresponds to the processes forbidden for interaction on free nucleons. It differs from the Bjorken variable X by taking account of mass correction. Note that at high energies the variable X coincides with the light cone variable $\alpha = (E - p_N) / m_0$.

In the experiments at the Dubna synchrophasotron the group led by V.S.Stavinsky [14] obtained the most comprehensive data on cumulative production of mesons in proton-nucleon reactions; on their basis the main properties of nuclear structure functions [15] were formulated. They are discussed below.

First of all it should be mentioned that, as expected, pion spectra on deuterium and hydrogen nuclei are similar up to the kinematic boundary of NN-interactions for pion production in the kinematically allowed region of NN-collisions. Besides, the following relation is valid:

$$E d\sigma/d\vec{p}(D \to \pi^{\pm}) \simeq E d\sigma/d\vec{p}(H \to \pi^{+}) + E d\sigma/dp(H \to \pi^{-}).$$

From the point of view of traditional nuclear physics, a new and nontrivial fact is that the slope parameter of the energy spectrum of pions arising from deuteron fragmentation at $T_\pi > T_\pi^{max}(NN)$ shows only slight changes as compared with its value for the kinematically allowed region. Indeed, when the spectrum is approximated with the function $\exp(-T/T_0)$, the value of the parameter T_0 is (51.0±1.2) MeV in the "soft" part of the spectrum and (35.3±0.9) MeV in the cumulative region (T_π>280 MeV). In other words, there is no noticeable effect of the kinematic boundary of NN-interaction in the region X > 1 up to X ≃ 1.7. It is a surprising experimental fact regarding the deuteron, whose binding energy is very low.

The spectrum of cumulative pions on the deuteron nucleus has an exponential form exp (-X/<X>) depending on the scaling variable X, the value <X> being 0.098 for deuterons. It is known from the

analysis of the data on cumulative production of pions on medium and heavy nuclei that for X > 1 the cross sections depend on X as exp (-X/<X>), the parameter <X>≃0.14 being universal for different nuclei and different secondary particles [Fig.1].

Note that the numerical value of the parameter <X>≃0.14 is close to the value of the mean nuclear density. It seems to be natural because in its physical sense $X*m_N$ is the minimum possible target mass. In Fig.2 there is the ratio of parameters <X> for different nuclei to the parameter <X> for lead nuclei (o). There are also the results obtained in ref. [16,17] for π^+-mesons (o) and for K^+-mesons (*). Besides, there is a curve of the nuclear density ratio. The behaviour of this ratio as a function of A corresponds to nuclear density changes. It was pointed out in ref. [18] that within the flucton models the difference in the spectra of cumulative mesons arising from fragmentation of different nuclei indicated that in heavy nuclei there were relatively more multinucleon fluctons than in light nuclei. On the other hand, if interaction resulting in production of cumulative particles is really local, its characteristics must be independent of such quantities as nuclear radii or masses. One can assume that the above-mentioned difference in spectra results from the effect of the right kinematic boundary of the reaction p + A → h + ... To take it into account, one assumes that $f(X)=f_0(X)(1-X/A)^n$, where $f_0(X)$ is independent of A, n is a parameter. This description appears to be possible with n = 7±1 for π^+-mesons, n = 7.0±1.7 for K^--mesons, n = 10±1.4 for K^+-mesons. The function $f(X) = C_i \exp(-X/X_0^*)$. The values $X_0^* \simeq 0.14$ for different mesons differ only by several per cent. So, we can say that for all mesons there is a scale-invariant, A-independent function $f_0(X)$, which characterizes local properties of hadron matter. It was experimentally shown that at equal momenta cross sections for production of protons on the lightest nuclei are about two orders larger than pion production cross sections.

The inclusive reaction p + D → p + ... is the simplest reaction and a key to understanding nucleon degrees of freedom in hadron-nuclear interactions, to determination of the nonnucleon

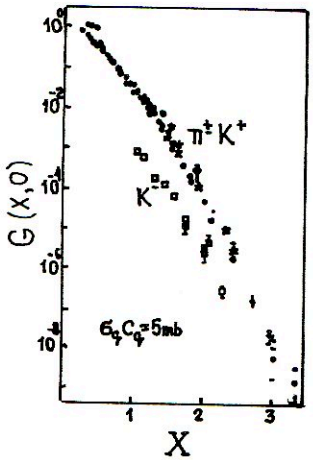

Fig.1

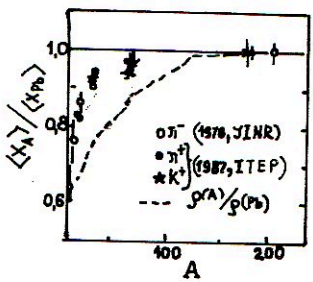

Fig.2

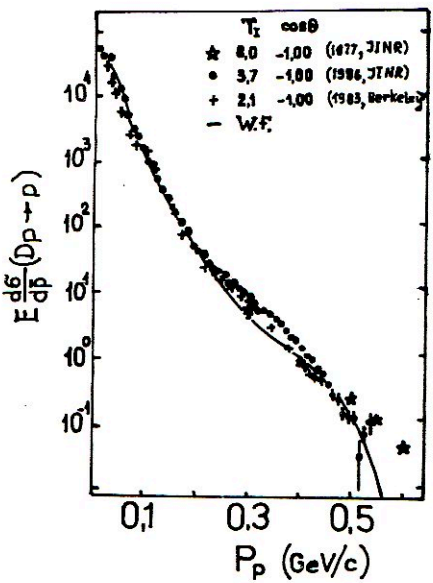

Fig. 3

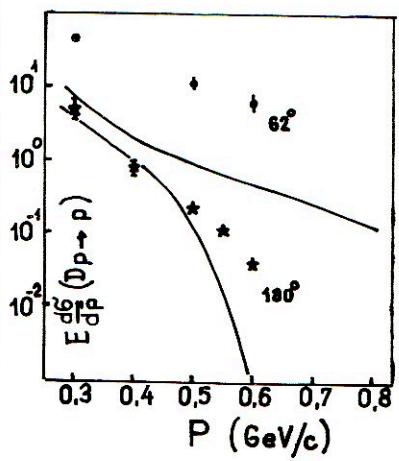

Fig. 4

component in the structure function of a deuteron. Setting up the experiment we assumed that cumulative production of nucleons on nuclei is connected with a high-momentum component of the wave function and thus these processes may help one to study properties of nuclear matter at short internucleon distances and to find out to what relative momenta of nucleons in a deuteron one can describe the experimental results in terms of nucleon degrees of freedom and under what conditions it is impossible without introducing nonnucleon (multiquark) degrees of freedom in the deuteron structure function and allowing for relativistic and off-shell effects.

In Fig.3 there are experimental data on fragmentation of deuterons to nucleons at high energy. Symbols (*) are the experimental data obtained at the installation DISK , symbols (o) are the experimental data obtained at the installation ALFA at primary energy 3.7 GeV/nucleon, symbols (+) are the Berkeley data at energy 2.1 GeV/nucleon. The curve in the figure corresponds to the calculation in the relativistic momentum approach with the "Paris" wave function of the deuteron.

Measured at different energies, the cross sections are in rather good agreement for proton momenta below 450 MeV/c and practically coincide with the calculation. On the other hand, there is sharp difference between calculation and experiment for proton momenta over 500 MeV/c. Fig.4 shows the hard part of the spectrum for convenience. Symbols (*) are the data for the observation angle 180^{o}, symbols (o) are those for the observation angle 62^{o}. These data were obtained at the installation DISK in order to measure the energy spectrum of protons in the deuteron fragmentation reaction, the transverse momentum component being other than zero. One curve in the figure (lower) corresponds to the calculation for the angle of 180^{o}, the other (upper) for the angle of 62^{o}. As seen, the calculation and experiment at 180^{o} differ by more than an order at the spectrum boundary, though there is good agreement at momenta 0.3-0.4 GeV/c. The experimental data for the observation angle 62^{o} differ from calculation approximately by a factor of 10 for the whole momentum interval.

So, at present there is actually no theoretical model which allows unified description of deuteron fragmentation, to say nothing about the energy and angular dependence. Noteworthy are the calculations in ref. [19], which show that it is also impossible to describe the hardpart of the spectrum of cumulative pions produced in deuteron fragmentation without introducing an additional 6q component in the deuteron wave function. Note also other theoretical models where the effect of the relativistic approach are introduced in a specific way. For example, in models of Brown, Tokareva [20] they managed to describe the spectrum of cumulative pions from deuteron fragmentation within covariant formalism based on the relativistic deuteron wave function and with one nucleon on the mass shell [Fig.5].

Investigating the dependence of cross sections (structure functions) on the atomic weight of a fragmenting nucleus, one found that

$$Ed\sigma/dp=\text{const}\ A^{m(X)}\exp(-X/<X>).$$

The index m(X) is 2/3 + X/3 for the region $0.6 \le X \le 1$ and 1 at $X > 1$ and $A \ge 20$. In Fig.6a there is the X dependence of the pion production cross sections (per nucleon) on lead, deuteron and aluminium nuclei. It is found that at X>1 $d\sigma(Pb)/d\sigma(A)<1$ as a result of the above-mentioned dependence of the power index m on X (here $d\sigma(A)$ denotes $\frac{Ed\sigma}{A}/dp$ for nucleus A). At X>1 the ratio of the structure function of the lead nucleus to that of the deuteron is much larger than 1. It is due to the fact that in the deuteron there are no configurations with quarks of more than two nucleons. Yet, for the lead and aluminium nuclei the ratio of cross sections per nucleon is approximately equal to 1 for X>1.

The X>1 data were interpreted as an interesting prediction for deep inelastic experiments of the next generation. The review [21] contains the analysis of the SLAC experiment E133, where S.Rock et al. measured the ratio of eAl/eD cross sections related to one nucleon for X=1.4. This ratio equals 5, which confirms the Dubna hA data [Fig.6b].

It should be stressed that both for deep inelastic scattering and for hadron-nuclear reactions the ratio of cross sections per

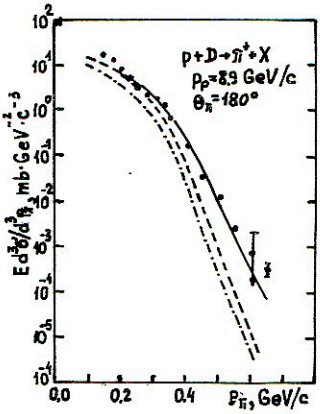

Fig.5

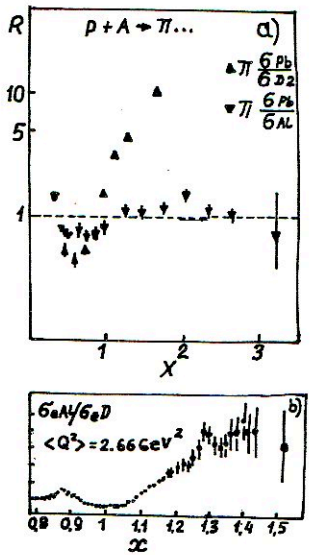

Fig.6

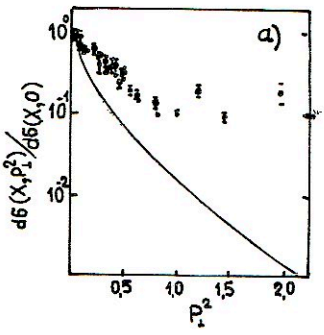

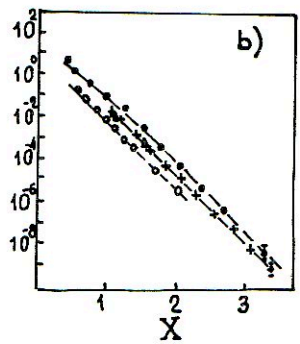

Fig.7

nucleon (structure functions) of a heavy nucleus and a deuteron was experimentally observed to intersept 1 at X = 0.9 and not at X = 0.5, as follows from the calculations based on nuclear models allowing only for nucleon degrees of freedom.

Note that in experiments on cumulative production of particles the dependence of cross sections on the transverse momentum (particle emission angle), which is unusual in hadron physics, is found.

The experimental data on pion production cross sections for emission angles 90^{o}, 119^{o}, 168^{o} [22] allowed one to study the dependence of the cumulative production cross sections on $P_T(\theta)$ [Fig.7a]. Actually, we study a question of additional dependence on the transverse momentum (emission angle) besides the one involved in the variable

$$X=(\sqrt{P_{\parallel}^2+P_T^2+m^2}-P_{\parallel_0})/m \ .$$

The dependence $\Phi(p_T^2)=d\sigma(X,0)/d\sigma(X,p_T^2)$ is found to be quite weak and it differs from the dependence on the transverse momentum for PP-interactions (the line in Fig.7a). An unusual behaviour of the cross sections was observed in the region X > 1; it indicated factorization of the cross sections by the variables X and θ (see Fig.7b).

Thus, we see from the experimental data that this additional dependence on the transverse component of the momentum is no t only rather weak but also practically independent of P_T^2.

In reference [23] it was shown on the basis of the hard scattering model that the shape of the spectrum in X is universal at different registration angles, and dependence of cross sections on the angle is included in the factor $(\sin\theta/2)^8$, i.e. the ratio of cross sections for production of cumulative particles at different angles does not depend on X and is $\simeq$0.06 for angles of 168^{o} and 90^{o}, and $\simeq$0.3 for angles of 168^{o} and 119^{o}, which is quite close to the experimental values $\simeq$0.1 and $\simeq$0.4 respectively.

In reference [24] an attempt is made to describe this result within the framework of the dual string model. Disintegration of a

fast fluctons into its constituent quarks with gaining additional transverse momentum K_T in each disintegration act was considered.

In our opinion, production of strange mesons arouses great interest now. As mentioned above, it was found in our experiments that the shape of spectra of different particles is universal if cross sections are represented as a function of the scale-invariant variable X.

For heavy and medium nuclei the following approximate relation has been observed between the cumulative effect cross sections for identical X [Fig.8]:

$$E_1 d\sigma(\pi^+)/d\bar{p} = E_1 d\sigma(\pi^-)/d\bar{p} = E_1 d\sigma(K^+)/d\bar{p}.$$

Structure function ratios of two different particles obtained for $X < 1$ in PP-interactions (open symbols in Fig.8) are taken from [25]. A considerable difference is seen in the behaviour of kaon and pion cross section ratios, depending on the scaling variable X for PP- and PA-interactions.

Note that in approximation of the dependence of cross sections on the atomic weight of the nucleus by the function A^n for medium and heavy nuclei the behaviour of pion and K^--meson production cross sections is of the same character ($n = 1$), while the A-dependence of production cross sections for K^+-mesons is close to that for protons ($n = 1.3-1.5$).

The approximate equality of production cross sections for cumulative π^+-mesons and K^+-mesons can be qualitatively comprehended within the fragmentation model. Indeed, cumulative π^+-mesons and K^+-mesons result from picking up a $\bar{d}$ or $\bar{s}$ antiquark by a valence u-quark. However, there is no complete theoretical explanation of difference in the character of the A-dependence for pions and K^+-mesons.

Note that the recently obtained [26] A-dependence for production cross sections of cumulative Λ-hyperons coincides with the A-dependence for cumulative protons and thus for K^+-mesons.

Actually, at present there are no completed theoretical calculations to explain specific features of K^+-meson production on medium and heavy nuclei. Measurements and theoretical calculations for the simplest nuclear system, a deuteron, can be

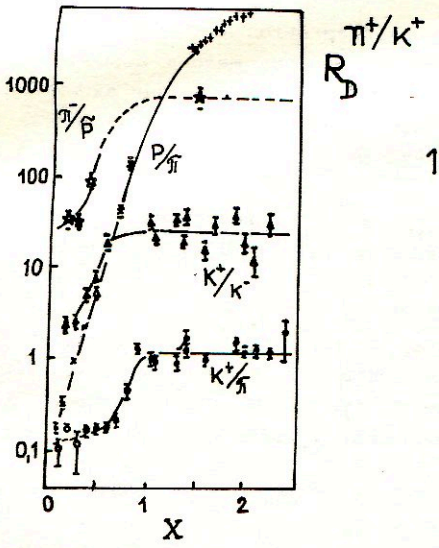

Fig. 8

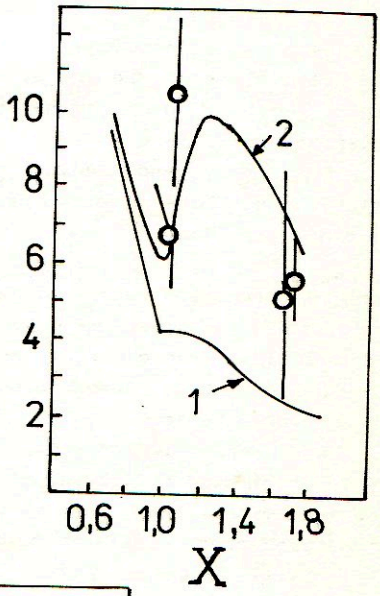

Fig. 9

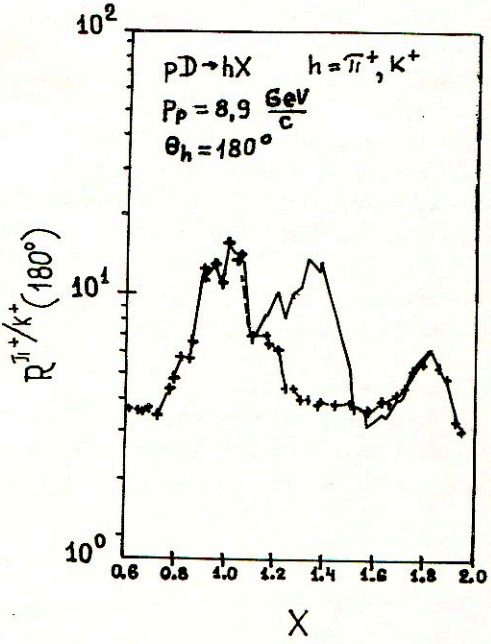

Fig. 10

helpful in solving the problem of production of cumulative strange particles. These calculations have been performed in ref. [27,28]. They are shown in Fig.9,10 . As seen, different assumptions on the deuteron wave function lead to essential quantitative effects, which can be investigated by measuring the ratio of K^+ and π^+ production cross sections as a function of X.

The structure function G(X) for $\bar{K}$ is similar to the G(X) for pions and K^+-mesons, but its absolute value takes into account 5% of the latter. The experimental data on the "K^-/K^+" [Fig.8] do not confirm the generally accepted opinion that the sea quarks have a "smoother" distribution. Thus, we have obtained the first experimental data which give evidence for the presence of the "hard sea" in the structure functions of nuclei in the region of X from 1 to 2.5. The "hard sea" momentum distribution is similar to that of valence quarks in the cumulative region.

CONCLUSIONS AND PROGRAM OF FURTHER INVESTIGATIONS

So we think that already now the available experimental data and their theoretical interpretation allow the nuclear structure functions to be considered independent objects of hadron physics (irreducible to one-nucleon objects). Common properties of these structure functions and their individual specific features related to the lightest deuteron nucleus have been discussed above. However, there are some new experimental setups which allow one to study other properties of structure functions [29]. These experiments are aimed first of all at studying properties of structure functions of the lightest nuclei in detailed inclusive and correlation experiments with a two-arm spectrometer DISK and magnet-free hadron spectrometers for detection of charged hadrons and neutrons.

At first, spectra of cumulative protons and neutrons from deuterium nuclei up to the kinematic boundary of the reaction are supposed to be measured at different registration angles. The reaction of deuteron fragmentation in interaction with protons is is the simplest reaction and a key to understanding nucleon degrees of freedom in hadron-nuclear interactions, to determination of the nonnucleon component in the structure

function of deuterium. The installation DISK allows detailed measurements of proton spectra in the reaction p + D → p + ... in the interval of secondary proton momenta from 250 MeV/c and up to the kinematic boundary of the reaction for the angles from 180^{o} to 60^{o}.

It is clear that with increasing primary energy of incident protons the kinematic limit the reaction becomes higher and thus we get an "increasing" contribution of small internucleon distances (large relative momenta of nucleons in deuteron), where manifestation of the 6q-component can be expected. In the experiments with DISK the region of target fragmentation at the primary proton energy up to 9 GeV is studied. This energy is twice as high as in the experiments on the study of deuteron beam fragmentation (4.5 GeV/nucleon).

So, one can study the deuteron wave function at higher relative momenta of nucleons in deuteron (up to ≃900 MeV/c). In the experiments with DISK one will study the dependence of proton production cross section on the transverse and longitudinal components of the momentum near the kinematic boundary of the reaction, the behaviour of cross sections for production of cumulative protons from the primary energy within one experiment, which will undoubtedly contribute to clarification of the deuterium fragmentation mechanism in the proton. In the report much attention was paid to discussion of results on K^{+}-meson production on nuclei.

In the program of experiments at DISK we are going to investigate cumulative production of K^{+}- and K^{-}-mesons on the lightest nuclei of deuterium and helium.

Difficulty in experimental investigation of cumulative kaon production arises from a small production cross section. The momentum being the same, the cross section for K^{+} production on medium and heavy nuclei is two orders smaller than that for pions, and the cross section for K^{-} production is suppressed by another two orders. Acceptance of DISK is $4.5*10^{-5}$ sr. It could allow investigations high-intensity beams (up to $2*10^{11}$ particles per cycle) with targets of thickness up to 10 g/cm^{3}. Using a

cryogenic target, we have to be restricted to a thickness of ≤ 1 g/cm^3, for investigation of nucleus-nucleus interactions we have beams with intensity up to $5*10^8$ nuclie per cycle. So we connect the prospects of these investigations with high- intensity beams of protons and nuclei. The expected yield of kaons with the momentum 500 MeV/c and angle of emission 180^o from a 1 g/cm^3 deuterium target is ≃6 K^+-mesons (with allowance for additional suppression of cross sections for K^+ production on deuterium by an order or so) and 0.6 K^+-mesons at the intensity $5*10^{11}$ protons/cycle in an hour of accelerator operation.

So far the technique of two-particle correlation measurements has been utilized and results have been obtained in measurement of two-particle pp, πp dp correlations in cumulative production of particles. The correlation investigations are supposed to be continued.

In ref. [30] V.S.Stavinsky developed a unified approach to description of reactions producing particles with large momenta and of cumulative hadron production processes. Underlying the approach is the idea of minimum economic interaction. According to it, the inclusive cross section for particle production in extreme situations, i.e either cumulative production or production of a hadron with a large transverse momentum, depends on the minimum possible total energy of colliding constituents. In this approach existence of kinematic regions with the two-particle correlator R_2 >> 1 is predicted. The search for dynamic correlations is supposed to be carried out at the installation DISK. Besides, predictions of various theoretical models, e.g. the model of few-nucleon correlations, are supposed to be checked in the correlation experiments.

Thus, the experimental investigations to be carried out at the installation DISK will allow new experimental data. These data will be a great help in studying non-nucleon degrees of freedom, constructing the relativistic wave function of deuterium, studying the yield of strange particles and correlation phenomena, which is necessary for construction of a consistent deuteron theory.

REFERENCES

1. Baldin A.M. et al., Proc. Rochester Meeting APS/OPF,N.Y. p.131, 1971.
2. Baldin A.M., Brief Comm. on Phys., p.35, 1971.
3. Baldin A.M., Nucl.Phys., A434, p.695,1985.
4. Baldin A.M. et al.,Yad. Phys., v.20, p.1201,1974.
5. Shroeder L.S. et al. Phys.Rev.Lett., v.43, p.1787,1979.
6. Zolin L.S. et al., Yad. Phys., v.49, p.473,1989.
7. Leksin G.A.. Proc. of XVIII. Int.Conf. on High Energy Physics, Tbilisi, v.1, p.A6-3, 1976.
8. Alanakyn K.V. et al. Yad.Phys., v.26, p.1018,1977.
9. Efremenko V.I. et al. Phys.Rev.D,v.22, p.2581, 1980.
10. Gavrilov V.B. et al., Preprint ITEP-96, Moscow, 1985
11. Baldin A.M. Proc.Conf. on Extreme States in Nucl. Systems, Dresden, v.1, p.1, 1980.
12. Ochs W., Nucl.Phys. B118, p.397,1977.
13. Stavinsky V.S. JINR Communications P2-9528 ,Dubna, 1976
14. Baldin A.M. et al. JINR Communications E1-82-472, Dubna, 1982
15. Baldin A.M., Panebratsev Yu.A., Stavinsky V.S., DAN USSR 279, 1352(1984)
16. Boyarinov S.V. et al., Yad. Phys., v.50, p.1605, 1989.
17. Boyarinov S.V. et al., Yad. Phys., v.47, p.1472, 1987.
18. Boyarinov S.V. et al., Proceedings of the IX International Seminar on High Energy Physics Problems ,v.1,p.219, Dubna,1988.
19. Kaptar L.P., Reznik B.L., Titov A.I., Yad.Phys.,v.42,p.777, 1985.
20. Braun M.A., Tokarev M.V.,Proceedings of the third International Symposium "Pion-Nucleon and Hadron-Nucleus interactions at the intermediate energies",p.311, LINR,Leningrad,1986.
21. Strikman M.I., Frankfurt L.L., Phys.Rep.,v.160,p.235,1988.
22. Baldin A.M. et al.,JINR Communications E1-82-472, Dubna, 1982.

23. Efremov A.V., Particles and Nucleus, v.13, p.613,1982.
24. Kaidalov A.V. et al., Proceedings of the IX International Seminar on High Energy Physics Problems ,v.1,p.271, Dubna,1988.
25. Brenev et al. Phys.Rev. D26, 1497(1982)
26. Vorobjev L.S., Preprint ITEP-126, Moscow, 1987.
27. Baghanski I.I. et al., Yad.Phys.,v.45,p.910,1987.
28. Braun M.A., Tokarev M.V.,Proceedings of the third International Symposium "Pion-Nucleon and Nucleon-Nucleon Physics", p.398,LINR, Gatchina,1989.
29. Averichev G.S. et al.,JINR Rapid Comm.,2-89,p.103,Dubna, 1989.
30. Stavinskij V.S., JINR Rapid Comm., 18-86, p.5, Dubna, 1986.

The Quark Model, Deuteron Properties and Magnetic Moments *

Amand Faessler
Institut für Theoretische Physik
Auf der Morgenstelle 14
Universität Tübingen
D-W7400 Tübingen, Germany

1. INTRODUCTION

The first idea about the nature of the nucleon-nucleon interaction came from Yukawa in 1935. He assumed that the strong interaction between two nucleons is carried by an interaction quantum, which is a particle of a medium heavy mass of about 200 MeV, the meson. After finding the π meson one thought one has found the carrier of the strong nuclear force. But the fifties saw a time where more and more mesons were found which contribute to the nucleon-nucleon interaction. One of the high points of this development was the suggestion of Gregory Breit in 1958 that the short range repulsion should be due to a vector, isoscalar meson, the omega meson (ω) of the order of 800 MeV. It was a big success of the meson exchange theory of the nucleon-nucleon interaction when this ω meson was found also experimentally.

But just the ω meson shows that this cannot be the whole story. Flavor symmetry $SU(3)$ predicts from the ρ-nucleon coupling the ω-nucleon coupling squared $g^2_{\omega NN}/(4\pi) = 4.5$. In reality one needs to reproduce the short repulsion according to the Bonn-potential values between 12 and 24. Normally flavor $SU(3)$ is only violated within 30 % or less. The need to blow up the $\omega - NN$ coupling constant by a factor 3 and more indicates that the ω meson must carry a load for which it is not prepared. After we learned that the nucleon is composed out of three valence quarks, gluons and sea quarks it is natural to look on the quark level for the nature of the short range repulsion. Indeed we will show in the next chapter

* Supported by the Deutsche Forschungsgemeinschaft.

that the short range repulsion of the NN interaction can be understood in the quark model by the symmetry of the 6-valence quarks.

The main purpose of this lecture is to search for quark degrees of freedom in the deuteron properties and in finite nuclei.

In the third chapter we calculate the deuteron wave function in the quark cluster model for the electromagnetic deuteron form factors of the elastic electron deuteron scattering we include the impulse term where the photon is directly interacting with the quarks and exchange currents. These exchange currents can be on the quark level due to quark exchange stemming from the antisymmetrization of the 6-valence quarks in the two nucleons. They can originate also from meson exchange currents. The specific quark degrees of freedom show up in these meson currents if also a quark pair is exchanged due to the antisymmetrization on the quark level between the two nucleons. Without quark exchange the meson exchange currents can be included on the nucleon level by suitably choosing the photon nucleon vertex function. Additional contributions come from gluon exchange currents. These are exchange currents where the photon is absorbed by a quark-antiquark pair and the antiquark is again annihilated with the quark by exchanging a gluon to some other valence quark. Again these terms show up as quark degrees of freedom which cannot be treated on the nucleon level only if at the same time a quark pair is exchanged due to antisymmetrization of the 6-valence quarks.

Finally in chapter 4 we calculate magnetic moments and magnetic form factors in finite nuclei including quark degrees of freedom. On one side we calculate contributions in the impulse approximation where the photon exchanged between the electron and the nucleus or the magnetic moment operator and the nucleus is interacting with a quark. But these terms can be included on the nucleon level by again suitably chosing the photon nucleon vertex function. Quark degrees of freedom which cannot be described effectively on the nucleon level arise by additional quark exchange between two nucleons due to the antisymmetrization of

the valence quarks. In addition one gets also quark degrees of freedom involved if one has meson and gluon exchange currents between quarks of different nucleons. This leads to two body currents in the magnetic moments and the magnetic form factors stemming from quark degrees of freedom.

The quark degrees of freedom are best seen at high momentum transfer above $q = 5 \ fm^{-1}$ for the magnetic dipole form factor of the deuteron. Especially the spin degrees of freedom of the quark exchange currents give here a large contribution. The magnetic form factors for elastic electron scattering in nuclei away by one nucleon from double closed shells are affected by quark exchange currents but even in the maxima this contributions are so small that their effect could not be seen relative to effects coming from configuration mixing (Arima and Horie, ref. 6) and relative to the meson exchange current. A large effect from genuine quark degrees of freedom due to quark exchange currents can be seen in the isovector magnetic moments of the two nuclei with one proton and one neutron more or less as double closed shell nuclei. Specificly for ^{39}K and ^{39}Ca where the Schmidt value is relative small (due to the cancellation of the spin and the orbital part) one obtains a surprisingly large effect of 21% of genuine quark degrees of freedom (quark exchange current) relative to the Schmidt value. The quark degrees of freedom improve here the agreement with the experiment considerably.

The work presented here has been published in a series of papers together with A. Buchmann and Y. Yamauchi (ref.9,10). The magnetic form factors for elastic electron scattering on finite nuclei and the work on the isovector magnetic moments is contained in a paper with Yamauchi, Buchmann and Arima (ref. 11).

2. THE QUARK MODEL AND THE NUCLEON-NUCLEON INTERACTION

At large distances the nucleon-nucleon interaction can be represented quite successfully by exchanging mesons between the centre of mass of nucleon 1 and the centre of mass of nucleon 2. At smaller distances as indicated in fig. 1 it makes no sense to exchange mesons between the centre of mass of nucleon 1 and of nucleon 2 since due to antisymmetrization it is not even known where the centre of masses of the two nucleons are, since the antisymmetrizer attaches the 6-valence quarks in each of the ten terms of the antisymmetrization to other nucleons. The difficulty of the meson exchange model at short distances might be indicated by the too large $\omega - NN$ coupling constant needed to reproduce the data as indicated in the introduction.

At short distances (below $1fm$), where the quark contents of the two nucleons overlap, the quark degrees of freedom should play a major role in describing the nucleon nucleon interaction and especially the short range repulsion.

In the non-relativistic quark model one uses for the quark quark interaction the one gluon exchange potential (OGEP) and a linear or quadratic confinement term. In addition the 6-quark Hamiltonian of the two interacting nucleons contains the rest mass of the quarks and the kinetic energies.

$$\hat{H}_{Quark} = \sum_{i=1}^{6}[m_i + \frac{\mathbf{p}_i^2}{2m}] + \sum_{i<j=1}^{6}[V_{qq}^{OGEP}(i,j) - a\boldsymbol{\lambda}_i \cdot \boldsymbol{\lambda}_j r_{ij}^2] \qquad (1)$$

$\boldsymbol{\lambda}_i$ are the eight color octet matrices acting on quark i. The scalar product between the two color matrices $\boldsymbol{\lambda}_i$ and $\boldsymbol{\lambda}_j$ is to be taken over the eight different color matrices for quark i and quark j.

The last term is the quadratic confinement term which is described microscopicly by the exchange and the interaction of many gluons.

The one gluon exchange potential (OGEP)

$$V_{qq}^{OGEP} = \frac{g^2}{4\pi}\frac{1}{4}\lambda_1\cdot\lambda_2[\frac{1}{r_{12}}+\frac{\pi}{m_q^2}(1+\frac{2}{3}\sigma_1\cdot\sigma_2)\delta(\mathbf{r}_{12}) \; + \; tensor \; + \; \mathbf{l}\cdot(\mathbf{S}_1+\mathbf{S}_2)+\ldots] \tag{2}$$

thus contain in addition to the color Coulomb and the color magnetic interaction, which are written explicitly, tensor and two-body spin orbit contributions and additional momentum dependent terms. We did not write them down explicitly since they are quite lengthy although the tensor term plays an important role for the description of the deuteron.

In addition to the quark Hamiltonian (1) we have to include to describe the nucleon-nucleon interaction at large distances pion exchange between the different quarks and the exchange of a scalar and isoscalar σ meson. The pion-quark coupling constant is adjusted so as to reproduce the known pion nucleon coupling with the quark wave function of the nucleon. The σ-quark and by that the σ-nucleon coupling is the only quantity adjusted to the nucleon-nucleon phase shifts. The other parameters like the mass of the quark m_q, the strong gluon-quark coupling constant $g_s^2/(4\pi)$, the oscillator length b and the confinement parameter a are adjusted to three-quark data like the nucleon mass, the Δ mass the root mean charge radius from electron-proton scattering and the stability condition for the mass of the proton. The last condition says that the derivative of the proton mass as a function of the oscillator length b should have a minimum at the charge root mean square radius including also the charge distribution from the pion cloud which surrounds the nucleon (ref. 4).

As already mentioned above the only quantity directly fitted to two nucleon data is the σ meson-nucleon coupling. $(g_\sigma^2/(4\pi) = 3.34)$. The same parameters which reproduce the nucleon-nucleon phase shifts as shown in fig. 2 and 3 describe also the hyperon nucleon interaction. That means with the same parameters we can describe the world data collection (ref.14 and 15) of the nucleon-lambda and the nucleon-sigma interaction.

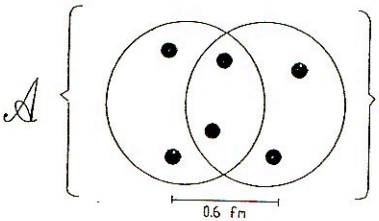

Fig. 1.

Qualitative sketch of the nucleon-nucleon interaction in the meson exchange model at large distance between two nucleons consisting out of three valence quarks and the interaction between two nucleons at smaller distances where the quark contents of the two nucleons overlap. In the last case it makes no sense to describe the nucleon-nucleon interaction by the exchange of mesons between the centre of gravity of nucleon 1 and of nucleon 2. Due to the antisymmetrization it is not even known where these centres of gravitiy are since the antisymmetrizer attributes in all different ten terms different quarks to nucleon 1 and nucleon 2. The short range part of the nucleon-nucleon interaction must be described within the quark model.

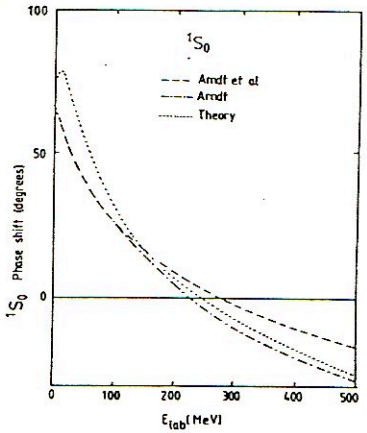

Fig. 2.

Singlet S_0 phase shift from proton-proton scattering (isospin $T = 1$). The dashed curve are the experimental phase shifts by Arndt and Mc Gregor while the short dashed line is the calculation of the quark model (ref.12).

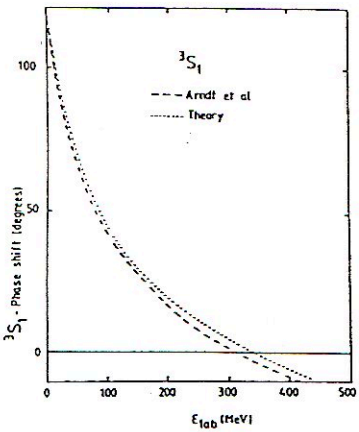

Fig. 3.

The figure shows the $^3S_1$ nucleon-nucleon phase shifts. The long dashed lines are the experimental values of Arndt and Mc Gregor (ref.13), while the short dashed line is the result of the present model calculation (ref.12).

The quark cluster model explains also nicely the short range repulsion of the nucleon-nucleon interaction (ref.1 and 16). Fig. 4 shows the spatial symmetries of the 6-quarks at small distances.

From Fig. 4 one sees that it is more probable by the weight 8/9 to have at short distance the [42] symmetry compared with the completely symmetric orbital wave function [6] which has only the weight 1/9. Fig. 4 indicates also the lowest energy realizations of the orbital symmetries [6] and the mixed orbital symmetry [42]. The last configuration requests at zero distance of the two nucleons ($r = 0$) that two quarks are in the $1p$ state for the lowest energy realization of this configuration. The usual way of representing the two nucleon wave functions by 6 quarks in the $1s$ state is only at most available with the probability 1/9. It is obvious from that the [42] orbital symmetry cannot be neglected. If for a moment we neglect 1/9 compared to 8/9 we have at small distances $r \approx 0$ at least two harmonic

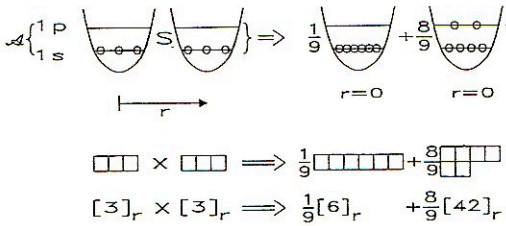

Fig. 4.

The left hand side shows two nucleons in the quark model at distance r. In each of the two nucleons all three valence quarks are in the $1s$ state. Group theory tells us that if the two nucleons are in a relative orbital S-state the permutation symmetry of all 6 valence quarks can either be only completely symmetric [6] or have the [42] symmetry. The square of the Clebsch-Gordan coefficients of the permutation group of 6 objects gives also the probability to find the completely symmetric spatial representation [6] or the [42] symmetry.

oscillator quanta excited. Or in other words at least two quarks have to be not in the $1s$ state. For the lowest configuration they are in the $1p$ state. That means at short distances this configuration with the probability 8/9 has at least two harmonic oscillator quanta excited. If one moves again the two nucleons apart at distance r as on the left hand side of Fig. 4, one sees that inside the two nucleons one has no harmonic oscillator quanta excited. Since one has to conserve the number of harmonic oscillator quanta, the two quanta must be contained in the relative motion. If one expands the relative S wave function of the two nucleons in harmonic oscillators

$$u(r_{12}) = \alpha_1|1s> + \alpha_2|2s> + \alpha_3|3s> + \ldots \quad with: \alpha_1 = 0 \ (Pauli forbidden) \quad (3)$$

one finds that the $1s$ amplitude must be zero since all parts of the wave function have to contain at least two harmonic oscillator quanta if one considers the orbital [42] symmetry. Thus the relative wave function $u(r_{12})$ is dominated at small distances by $|2s>$ and therefore has a node near the so-called hardcore radius ($r = 0.4fm$). This node is seen in the asymptotic phase shift measured by the

differential cross section. To explain the node one requests that the nucleon-nucleon interaction potential has a hard or soft core at this radius. In reality the node in the wave function is enforced by the orbital [42] symmetry.

3. DEUTERON FORM FACTORS

To describe deuteron properties one has first to reproduce the deuteron binding energy of 2.2 MeV. With the σ-nucleon coupling constant $g_\sigma^2/(4\pi) = 3.34$ one obtains a binding energy of 3.3 MeV. This discrepancy between theory and experiment seems at the first moment disappointing, after the big success for the nucleon-nucleon phase shifts and even the hyperon-nucleon scattering data. But one has to keep in mind that in the non-relativistic quark model one is not only calculating the binding energy of the deuteron but the total energy of the order of 1875 MeV. Although one is fitting the nucleon mass one should keep in mind that a discrepancy of 1 MeV is not much for such a number. But the quality of the deuteron wave function has to be better than that to study quark degrees of freedom in the deuteron form factors. Thus we readjust the σ-nucleon coupling constant and obtain $g_\sigma^2/(4\pi) = 2.68$. To calculate the deuteron we include the same diagrams as for the nucleon-nucleon interaction. A typical selection from these diagrams is shown in fig. 5. The results (ref.10,17) are shown in table 1.
The elastic electron deuteron cross section is described by a longitudinal and a transversal form factor.

$$\begin{aligned}\left(\frac{d\sigma}{d\Omega}\right)_{eD} &= \left(\frac{d\sigma}{d\Omega}\right)_{Mott}[A(q) + B(q)tg^2\frac{\theta}{2}] \\ A(q) &= F_c^2(q) + \alpha_1 q^2 F_Q^2(q) + \alpha_2 q^2 F_M^2(q) \\ B(q) &= \beta q^2(1+q^2)F_M^2(q^2)\end{aligned} \qquad (4)$$

q is the momentum transfer and $F_C F_Q$ and F_M indicate the Coulomb, the quadrupole and the magnetic dipole form factors. The transversal form factor $B(q)$ is only given by the magnetic dipole form factor F_M.

$g_\sigma^2/(4\pi) = 2.68$	$P_D[\%]$	$\mu_D[\mu_N]$	$Q_D[fm^2]$
Quark Model	5.23	0.850	0.266
Exp.	—	0.857	0.286

Table 1.
Deuteron properties for the σ-nucleon coupling constant $g_\sigma^2/(4\pi) = 2.68$. The D state admixture is given in % while the magnetic moment is indicated in units of nuclear magnetons $[\mu_N]$ and the quadrupole moment Q_D in units of $[fm^2]$. The first line gives the theoretical values, while the second line lists the experimental data.

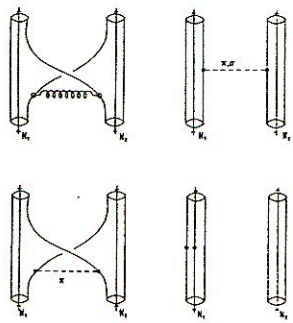

Fig.5.
Selection of diagrams included in the calculation of the deuteron wave function. One includes the one gluon exchange potential (OGEP) between all different quarks, pion exchange with and without antisymmetrization for the large distances and the exchange of the scalar and isoscalar σ meson between the quarks. The pion cloud is also included in each nucleon (intracluster pion exchange).

We first give the results in the impulse approximation shown in fig. 7.

The diagram of fig.7a can be also described phenomenologically on the nucleon level by introducing a suitable photon nucleon vertex function. But the quark exchange diagrams (b) and (c) cannot be included phenomenologically on the

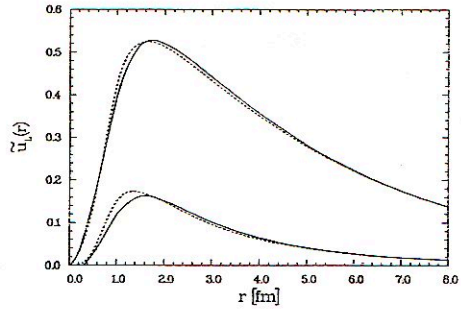

Fig. 6.
The deuteron S and D wave functions. Full curves: relative deuteron wave function in the quark cluster model; dashed curves: two-nucleon model wave functions calculated with the Paris potential (ref.18).

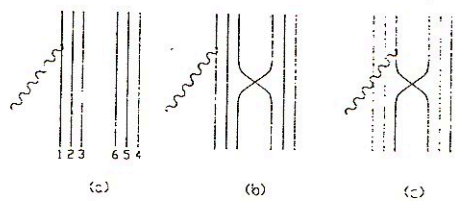

Fig. 7.
One body impulse current in the quark cluster model: (a) direct term, (b,c) quark interchange terms. The solid lines represent quarks and the wavy lines photons.

nucleon level. They represent genuine quark degrees of freedom. For the Coulomb and the quadrupole form factors the quark exchange diagrams of fig. 7 do not contribute appreciably and they are not measurable at the moment. But the magnetic dipole form factor seems to have a measurable effect.

Due to the large spin g-factors the spin magnetization current of the quark ex-

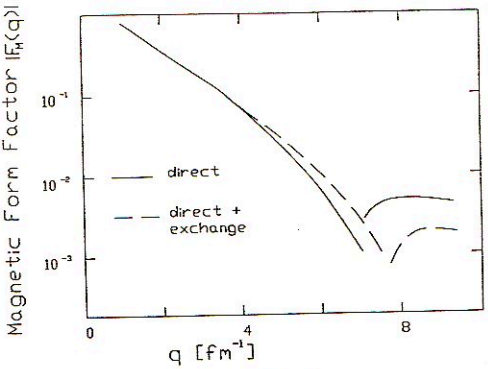

Fig. 8.

Magnetic form factor $|F_M(q)|$ as a function of the momentum transfer q for the direct impulse term (Fig. 7a; solid line) and the direct plus exchange terms (all diagrams in Fig. 7; dashed line).

change term is contributing appreciably as shown in Fig. 9. The spin exchange term as given by diagrams in Fig. .7 b,c can flip the spin of the nucleons and therefore these terms represent large spin magnetization currents. One sees in Fig. 9 that at momentum transfers above 6 to 7 fm^{-1} the differences could easily be detected. Thus elastic electron scattering on the deuteron and especially the transversal form factor can show genuine quark degrees of freedom.

Fig. 10 and Fig. 11 give the differential cross section calculated with the impulse terms only (Fig. 7a). Only the transversal form factor is sensitive to the quark exchange diagrams (Fig. 7b and 7c).

Fig. 12 shows in addition to the impulse diagrams of Fig. 7 also the two-body pion and gluon pair exchange diagrams in the quark cluster model.

The two-body exchange currents indicated in Fig. 12 can be calculated in two ways. Either one uses the minimal substitution

$$\mathbf{p}_i \rightarrow \mathbf{p}_i - \frac{e_i}{c}\mathbf{A} \tag{5}$$

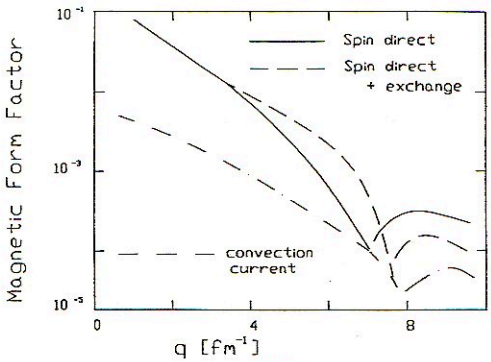

Fig.9.

Contributions to the magnetic form factor from the spin magnetization current (solid and dashed lines) and the convection current (dashed dotted line). The spin magnetization current is devided in the direct part (Fig. 7a; solid line) and the contributions from the direct and exchange parts (Fig.7b, 7c; dashed line). For the convection current contribution (dashed dotted line) the spin exchange terms do not contribute appreciably.

in the one gluon exchange potential or one calculates diagrams according to the Feynman rules. If one is consistent in the non-relativistic reduction one obtains the same results. (This twofold derivation of the two-body currents is a very useful check of the calculation.) Again the magnetic dipole form factor is most sensitive to the pion and gluon exchange currents with quark exchange (Fig. 12c-g). These results are indicated in Fig. 13.

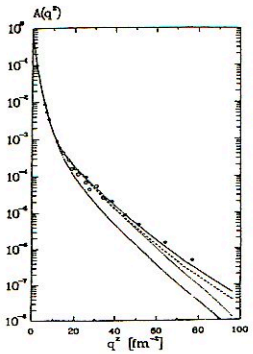

Fig.10.
Longitudinal form factor $A(q)$ from the elastic electron deuteron cross section (4) compared with the data. The theoretical calculation includes only the impulse approximation with quark exchange currents as shown in fig. 7, but no meson and gluon exchange currents (Fig. 12). This longitudinal form factor is not appreciably effected by the quark exchange diagrams of fig. 7b and 7c. The data are taken from ref. 19. The solid line gives the direct quark terms only (Fig.7a), while the dashed line includes also the quark exchange terms Fig. 7b and 7c.

4. QUARK MODEL AND THE MAGNETIC MOMENTS OF NUCLEI

To describe the magnetic moments and the elastic electron scattering of nuclei we start with the impulse approximation corresponding to Fig. 7 but now we have instead of two nucleons for the deuteron 16 nucleons for $^{16}0$. But still the photon exchange between the electron and the nucleus or the magnetic moment operator $\hat{\mu}$ interacts only with one quark. The interaction is given by the product of the vector potential A_μ and the single quark current J^μ.

$$H_{int} = -A_\mu J^\mu \tag{6}$$

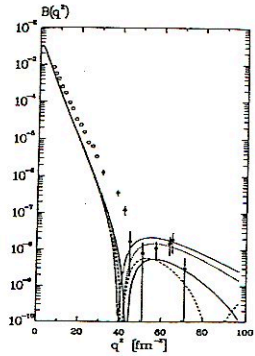

Fig. 11.

Transversal form factor $B(q)$ from elastic electron-deuteron scattering (4) compared with the data. The theoretical calculation shows the impulse approximation without and with exchange currents. The data are taken from ref. 19. The solid line gives the direct quark term only (fig. 7a), while the dashed line includes also the quark exchange terms (fig. 7b and 7c).

The one quark current operators

$$\begin{aligned} J_0 &= \sum_{i=q} e_i e^{i\mathbf{q}\mathbf{r}_i} \\ \mathbf{J} &= \sum_{i=q} \frac{e_i \hbar}{2m_i} [e^{i\mathbf{q}\mathbf{r}_i} \overrightarrow{\nabla}_i + \mathbf{q} \times \boldsymbol{\sigma}_i e^{i\mathbf{q}\cdot\mathbf{r}_i}] \end{aligned} \tag{7}$$

represent the charge of the different quarks with the momentum transfer q from the photon and their currents. The one quark magnetic operator is given by:

$$\hat{\boldsymbol{\mu}} = \sum_{i=q} \frac{e_i \hbar}{2m_i c} [\mathbf{l}_i + g_i \mathbf{s}_i] \tag{8}$$

in eqs. (7) and (8) the sums run over the quarks q. e_i is the charge of the different up and down quarks. m_i is the quark mass. The magnetic moment operator is later on more suitable derived from the currents.

$$\hat{\boldsymbol{\mu}} = \lim_{|\mathbf{q}|\to 0} \frac{\hbar}{2ci} \vec{\nabla}_q \times \mathbf{J} \tag{9}$$

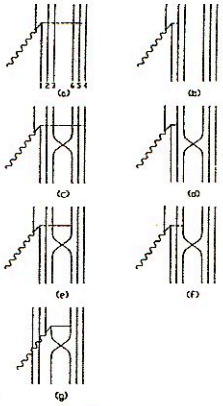

Fig.12.
The two-body pion and gluon pair currents in the quark cluster model: (b) direct inter cluster term, (c-g) quark interchange terms; the dashed line represents the pion or the gluon exchanged between quarks. For the gluon the matrix element represented by the diagram of Fig. 12a vanishes due to color selection rules (no color singlet gluons).

The currents (7) yield on the nucleon level one nucleon currents (the diagram of Fig. 7a) and two nucleon currents if one includes the antisymmetrization of the quarks. To make the calculation feasible we restrict ourselves always to the antisymmetrization of the quarks in two nucleons. In this way one obtains on the nucleon level atmost two-body currents. Further contributions to two-body currents one obtains due to meson and gluon exchange in the same way as in Fig. 12. The results shown here include only the two-body currents due to quark antisymmetrization the derivation of the two-body currents due to quark and gluon exchange without and with antisymmetrization on the quark level is still in progress.

The two-body nucleon currents corresponding on the quark level to Fig. 7 are again derived either by minimal substitution (5) or by using Feyman rules. With consistent non-relativistic reductions both procedures yield the same operators.

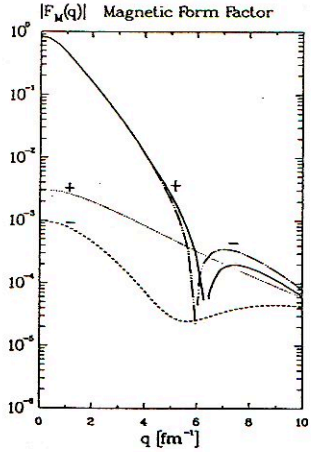

Fig.13.

Deuteron magnetic-dipole form factor as a function of the momentum transfer q. The dashed-double-dotted curve is the conventional impulse approximation; the dotted curve gives the pion pair exchange current without quark antisymmetrization. The dashed curve is the diagram with the pion exchange current with quark antisymmetrization. The gluon exchange currents give slightly smaller contributions and are not shown here. One sees that at high momentum transfers the pion exchange current with quark antisymmetrization is even larger than the usual pion exchange current without quark antisymmetrization.

Integration over the internal quark degrees of freedom yield then non-local two-body currents on the nucleon level.

$$J_\mu(\mathbf{r},\mathbf{r}';\mathbf{R};\mathbf{q})$$
$$\mathbf{r} = \frac{1}{6}[\mathbf{r}_1 + \mathbf{r}_2 + \mathbf{r}_3 - \mathbf{r}_4 - \mathbf{r}_5 - \mathbf{r}_6] \qquad (10)$$
$$\mathbf{R} = \frac{1}{6}[\mathbf{r}_1 + \mathbf{r}_2 + \mathbf{r}_3 + \mathbf{r}_4 + \mathbf{r}_5 + \mathbf{r}_6]$$

Here $\mathbf{r}$ and $\mathbf{r}'$ are the non-local distances between the two nucleons considered. $\mathbf{R}$ is the centre of gravity of these two nucleons. The nuclear wave function is chosen

to be a shell model Slater determinant. The short range correlations between the nucleons are important and are included solving the Bethe-Goldstone equation.

$$\left[\frac{\mathbf{p}_1^2}{2m_N}+\frac{1}{2}m_N\omega^2 r_1^2+\frac{\mathbf{p}_2^2}{2m_N}+\frac{1}{2}m_N\omega^2 r_2^2+Q(1,2)V_{N_1N_2}(\mathbf{r}_1,\mathbf{r}_2;\mathbf{R})\right]\psi_{\alpha\beta}(1,2)=E_{\alpha\beta}\psi_{\alpha\beta} \tag{11}$$

Here the non-local nucleon-nucleon interaction $V_{N_1N_2}$ is obtained using for the quark-quark interaction from Hamiltonian (1) the quark wave functions shown in Fig. 4 on the left hand side for the distances r and on the right hand side for r'. All the internal quark degrees of freedom are integrated out so that the nucleon-nucleon interaction depends only non-locally on the distance of the two nucleons on the left and on the right and on the centre of gravity of the two interacting nucleons R. Q (1,2) is the Pauli operator in the harmonic oscillator space. Fig. 14 shows relative ${}^1S$ and ${}^3S$ wave functions from the solution of the Bethe-Goldstone equation.

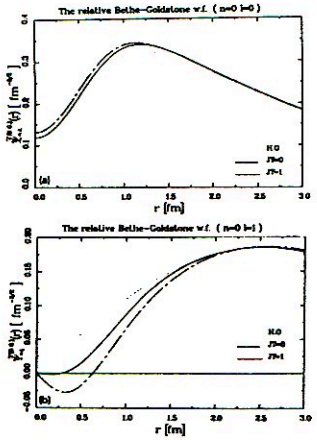

Fig. 14.

Relative harmonic oscillator S-wave function (dotted line) compared with the solution of the Bethe-Goldstone equation for ${}^3S$ (solid line) and ${}^1S$ (dashed-dotted line). One clearly sees the short-range correlations which stem here from quark degrees of freedom.

The electron nucleus cross section and especially the transversal form factor B(q) is now determined in the following way:

$$\left(\frac{d\sigma}{d\Omega}\right)_{eN} = \left(\frac{d\sigma}{d\Omega}\right)_{Mott}\left[A(q) + B(q)tg^2\frac{\vartheta}{2}\right]$$
$$with: \quad B(q) \propto q^2(1+q^2)|T^{magn.}_{JM}(q)|^2 \tag{12}$$
$$T^{magn.}_{JM}(q) = \frac{(-i)^J}{4\pi e}\int d\hat{q}[Y_J \times \mathbf{J}]^J_M$$

The magnetic moments are determined from the one-body operator (8) and the contributions from the two-body currents defined as in eq. (9).

$$\mu = \sum_{i=1}^{A} < Nucl.; JJ|\hat{\mu}_{iz}|Nucl.; JJ > \tag{13}$$
$$+ \lim_{q\to 0}\sum_{i<j} < Nucl.; JJ|\frac{\hbar}{2ci}\vec{\nabla}_q \times bfJ_{ij}|Nucl.; JJ >$$

From Fig. 15 one sees that the quark exchange effects cannot be seen in elastic scattering on nuclei with one proton or one neutron less or more than double closed shells. The situation is different for the magnetic moments as can be seen in table 2.

For the mass $A = 39$ system ^{39}K and ^{39}Ca one obtains a large effect due to quark exchange currents (Fig. 7b and c). Although the agreement with the experimental data is by that greatly improved, we won't not so much stress the better agreement but the fact that genuine quark degrees of freedom as contained in the graphs of Fig. 7b and c can be seen in magnetic moments. The fact that just the mass 39 system is so sensitive is due to the fact that the spin and the orbital contribution for the Schmid value cancel each other by a large part and due to the fact that the quark exchange current contributions (QEC) are roughly proportional to the mass.

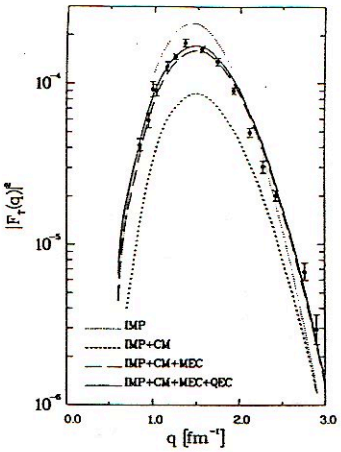

Fig.15.

Transversal form factor of ^{15}N as a function of the momentum transfer q *the dotted line gives the impulse approximation which describes the interaction of the elasticly scattered electron with only one nucleon. The dashed line is the impulse approximation plus the configuration mixing according to Arima and Horie (Ref. 6). The long dashed line includes the meson exchange currents calculated between the nucleons. The solid line also includes quark exchange effects.*

Fig. 7b and c can be seen in magnetic moments. The fact that just the mass 39 system is so sensitive is due to the fact that the spin and the orbital contribution for the Schmid value cancel each other by a large part and due to the fact that the quark exchange current contributions (QEC) are roughly proportional to the mass.

A	CM^6	MEC	QEC	EXP
15	5.5	7.2	−9.1	11.1
17	−16.9	15.5	1.6	1.3
39	42.2	−48.3	−20.9	−38.4

Table 2.
Isovector magnetic moments in nuclei with one proton or one neutron more than double closed shell nuclei. The values are given in percentages of the relative change to the Schmid value. 5.5 means an increase of 5.5 % of the Schmid value due to configuration mixing as first proposed by Arima and Hori (Ref.6) the isovector magnetic moment is calculated as the difference between the magnetic moments of nuclei with one proton and one neutron more or less than double closed shell nuclei.

5. CONCLUSIONS

In this invited talk we have essentially communicated three messages:

(i) A short range repulsion of the nucleon-nucleon interaction is not due to the hard or soft core in a static nucleon-nucleon potential but is due to many body symmetries of the 6-valence-quarks of the two interacting nucleons. At short distances the spatial symmetry is of [42] nature with the probability 8/9. This requests that one has at least two harmonic oscillator quanta in the relative wave function. That means one has a node in the interaction region which produces a hard core phase shift in the differential cross section.

(ii) In the elastic electron deuteron scattering genuine quark degrees of freedom can be seen in the transversal form factor which is proportional to the magnetic dipole form factor $F_{M1}(q)$. These quark degrees of freedom show up at momentum transfers above $5fm^{-1}$ or $1GeV/c$. They are essentially due to spin magnetization currents.

(iii) In finite nuclei one finds genuine quark effects which cannot be explained on the nucleon level for the isovector magnetic moments of nuclei one nucleon away from doubly closed shells. For the mass A=39 system the quark exchange currents due to the antisymmetrization of the quark wave function contribute 20 % to the Schmid value.

I would like to thank Dr's. A. Buchmann and Y. Yamauchi with whom this work has been performed. In the investigations reported in chapter 4 for finite nuclei the contributions of Prof. Akito Arima were also essential.

6. REFERENCES

1. A. Faessler, F. Fernandez, G. Lübeck, K. Shimizu, Phys.Lett.**112B** (1982)201; Nucl. Phys. **A402** (1983)555
2. M. Oka, K. Yazaki, Progr. Theor. Phys. **66** (1981)556 and 572
3. M. Oka, K. Yazaki, in Quarks and Nuclei, ed. W. Weise (World Scientific, Singapore) p. 489
4. K. Bräuer, A. Faessler, F. Fernandez, K. Shimizu, Z. Phys. **A320** (1985)609
5. K. Shimizu, Rep. Progr. Phys. **52** 1989)1
6. A. Arima, H. Horie, Progr. Theor. Phys. **11** (1954)509 and **12** (1954)623
7. K. Shimizu, Phys. Lett. **148B** (1984)418
8. F. Fernandez, E. Oset, Nucle. Phys. **A455** (1986)720
9. Y. Yamauchi, A. Buchmann, A. Faessler, Nucl. Phys. A **A494** (1989)401
10. A. Buchmann, Y. Yamauchi, A. Faessler, Nucl. Phys. **A496** (1989)621
11. Y. Yamauchi, A. Buchmann, A. Faessler, A. Arima, Nucl. Phys. **A526** (1991)495
12. A. Faessler, F. Fernandez, Phys. Lett. **124B** (1983)124
13. R. Arndt et al., Phys. Rev. **C15** (1977)1002
14. U. Straub, thesis University of Tübingen
15. A. Faessler, U. Straub, Ann. Physik **47** (1990)439; Nucl. Phys. **A483** (1988)686
16. A. Faessler, Nuclear and Particle Physics p. 238: Editors: C. J. Burden, B. A. Robson, 1990, World Scientific
17. A. Buchmann, H. Ito, Y. Yamauchi, A. Faessler, J. Phys. **G 14** (1988)1037
18. M. Lacombe et al., Phys. Lett. **B101** (1981)139
19. M. E. Elias et al., Phys. Rev. **177** (1969)2075; S. Galster et al., Nucl. Phys. **B 32** (1972)221; R. G. Arnold et al., Phys. Rev. Lett. **35** (1975)776; **58** (1987)1723

SPIN-DEPENDENT STRUCTURE FUNCTIONS OF NUCLEON AND NUCLEI

A. E. DOROKHOV
Joint Institute for Nuclear Research,
Head Post Office P. O. Box 79,SU-101000 Moscow, USSR
e-MAIL: DOROKHOV at THEOR.JINRC.DUBNA.RF

N. I. KOCHELEV and Yu. A. ZUBOV
High Energy Physics Institute, Academy of Sciences of Kazakhstan,
SU-480082 Alma - Ata, Kazakhstan

INTRODUCTION

Recently, common attention has been drawn to the so-called "spin crisis". There, the EMC has measured the proton structure function $g_1^p(x)$ and it is its first moment has been extracted[1]. Within the parton model this function is expressed via the quark distributions over helicity within a proton :

$$g_1^p(x) = \frac{1}{2}\sum_i e_i^2\,[q_+^i(x) - q_-^i(x)],$$

where $q_{+(-)}^i(x)$ is the probability that a quark of a flavour i has the helicity parallel (antiparallel) to the helicity of the proton. The integrals of the difference of the distribution functions:

$$\Delta q^i = \int_0^1 dx\,[q_+^i(x) - q_-^i(x)] \tag{1}$$

are connected with the matrix elements of the axial vector current between the baryon octet states which can be measured in the nucleon and hyperon β—decays and also in the elastic scattering of a neutrino off a proton. Joint analysis of these data produces the magnitude of the helicity carried by quarks[1]:

$$\Delta\Sigma = \Delta u + \Delta d + \Delta s = 0.12 \pm 0.24. \tag{2}$$

So, under generally accepted assumptions about $\mathbf{SU(3)}_f$ breaking, one can estimate the helicity of sea quarks[1]:

$$\Delta\Sigma^s = \Delta u^s + \Delta d^s + \Delta s^s = -0.95 \pm 0.16 \pm 0.23 \tag{3}$$

At the same time, it is known that the momentum fraction of the proton carried by sea quarks is small[2]:

$$p^s = \sum_q \int_0^1 dx\, x(q_+^s(x) + q_-^s(x)) \approx 0.074 \tag{4}$$

It is large violation of the **Ellis-Jaffe** parton sum rule[3] for the spin-dependent proton structure function $g_1^p(x)$ and the difference of an order between the magnitudes of the integrals, Eq. (3) and Eq. (4) has led to the "spin crisis".(see[4]). Almost zero value of helicity carried by quarks inside the proton determined from an analysis of the results[1] means that, contrary to naive expectation, the helicity carried by sea quarks is so large that it almost completely compensates for the helicity of valence quarks.

The anomalous large helicity of sea quarks has turned out extremely difficult to explain within the known parametrizations of the distributions of sea quarks[5]. Thus the question arises: what are the features of the parton distributions that allow to match so large sea polarization with its small momentum fraction?

A solution was suggested in our work[6] where it was noted that introducing a new Regge trajectory with a high intercept $\alpha(0) \approx 1$ caused by the Adler-Bell-Jackiw (ABJ) anomaly[7] and the Kogut-Susskind pole [8] (called further "anomalon") provides at least qualitative explanation of the experimental data on the structure functions of sea quarks. In work[6], within the nonperturbative **QCD** based on the model of the **QCD** vacuum as an instanton liquid[9] the x dependence of the distribution functions of sea quarks inside the proton has been considered. In the present work we discuss the nature of this trajectory and show that this trajectory defines not only the behavior of the spin-dependent sea quark structure functions in the region of small x but also some peculiarities of $pp-$ and $p\bar{p}-$ interactions and $p-$nuclei interactions at high energies .

STRUCTURE FUNCTIONS OF SEA QUARKS IN THE RANGE $X \to 1$

To find expressions of distributions, one uses the noncovariant perturbative theory (NCPT) in the system of infinite momentum. The distribution functions are connected with the light cone proton wave function expanded over free quark and gluon Fock states

$$| P >= | 3q > + | 3qq\bar{q} > + | 3qg > + ...$$

by the relation[10]

$$q_{f/p}(x) \propto \sum_n \int [dk_{\perp i}][dx_i]\, \delta(x - x_q) \cdot | \Psi_{(n)}(k_{\perp i}, x_i) |^2, \tag{5}$$

where $\Psi_{(n)}(k_{\perp i}, x_i)$ is the contribution of an n-particle component of the Fock state , $x_i = (k^0 + k^3)_i/(p_0 + p_3)$ is the fractional (light-cone) momentum of the proton carried by the $i-$th parton ($\sum_{i=1}^{n} x_i = 1$) and $k_{\perp i}$ is its transverse momentum ($\sum_{i=1}^{n} \vec{k}_{\perp i} = 0$).

As $x \to 1$, the contribution of a five-quark state $\Psi_5(k_{\perp i}, x_i)$ dominates in the sea quark distributions. The diagrams corresponding to this contribution within the instanton model of the **QCD** vacuum are presented in Fig. 1.

Fig. 1.The instanton contribution to the five-quark component of the nucleon wave function (+ (-) - instanton (anti-instanton)).

Instanton vertex is defined by the 't Hooft effective interaction[11]:

$$\begin{aligned} \mathcal{L}_{eff}^{inst} &= \frac{4\pi^2\rho_c^2}{3}\{\sum_{i\neq j}\int \frac{d^4k_1\, d^4k_2\, d^4k_3\, d^4k_4}{(2\pi)^{12}}\, \delta^{(4)}(k_1+k_2-k_3-k_4) \\ &\cdot \exp[-\rho_c \sum_{n=1}^{n=4} |\, k_n\, |]\, \bar{q}_{iR}(k_1)q_{iL}(k_3)\bar{q}_{jR}(k_2)q_{jL}(k_4) \\ &\cdot [1+\frac{3}{32}(1-\frac{3}{4}\sigma_{\mu\nu}^i\sigma_{\mu\nu}^j)\lambda_i^a\lambda_j^a] + (R \leftrightarrow L)\}, \end{aligned} \tag{6}$$

where the coupling constant is obtained by factorization of the N_f-fermion 't Hooft Lagrangian within the instanton liquid model[12], $q_{R,L} = [(1 \pm \gamma_5)/2]q$, $i,j-$ quark flavours, $\rho_c \approx 2\ Gev^{-1}$ is an average size of an instanton in the **QCD** vacuum[9].

It should be stressed that the vertex, Eq. (6), differs principally from the perturbative quark-quark vertex caused by the one-gluon exchange. First, opposite to the quark-gluon vertex the instanton-induced vertex flips the quark helicity, so that for the N_f- fermion vertex the helicity change is equal to $2N_f$. Second, the vertex, Eq. (6), is nonzero only in the case of quarks of different flavours. Thus, the quark sea produced by instantons inside the proton should not be exactly $SU_f(2)$-symmetrical.

In addition, since the instanton vertex, Eq. (6), changes the quark helicity by $2N_f$, then the total angular momentum conservation requires nonzero angular momentum of quarks in the intermediate state in Fig. 1. Then, it is obvious that the angular momentum projection should be equal to the helicity change at an instanton. This allows ones to estimate possible transverse momentum in a five-quark configuration by the relation:

$$\rho_c k_\perp \approx 2N_f. \tag{7}$$

So for $\rho_c \approx 2\ Gev^{-1}$, $N_f = 2$ one obtains $k_\perp \approx 2\ Gev$ which is essentially larger than average momentum of the valence quark inside the proton $k_\perp \approx 0.35\ Gev$.

In the integral, Eq. (5), the region[10] $\sum_{i=1}^{5} \frac{m_i^2+k_{\perp i}^2}{x_i} \approx M_p^2$ dominates. So one can put:

$$q_{I/p}(x) \propto A \int \frac{[dx_i]\ \delta(x - x_q)}{\left(M_p^2 - \sum_{i=1}^{5} \frac{m_{\perp i}^2}{x_i}\right)^2}, \tag{8}$$

where $m_{\perp q} = \sqrt{m_q^2 + k_{\perp q}^2}$ is the transverse mass of q-quark inside the proton.

Thus, the only five-quark configuration of the proton Fock state satisfies both the angular momentum and momentum conservation which contains at least two quarks with large transverse momentum. For this configuration from Eq. (8) one can easily obtain the asymptotics of the distribution functions:

$$q^s_{x\to 1} \propto \begin{cases} (1-x)^5 & m_{q\perp}^2 << M_p^2, \\ (1-x)^3 & m_{q\perp}^2 >> M_p^2, \end{cases} \tag{9}$$

So for the quark sea from light $u-$, $d-$, $s-$ quarks there are two regimes, Eq. (9), and for heavy $c-$, $b-$, $t-$ quarks there is one:

$$q^s_{x\to 1} \propto (1-x)^3.$$

The hard component of the quark sea produces very interesting consequences. Indeed, the experiments on charm production in the hadron interactions[13] produce the hard spectrum of charmed particles. At the same time, this spectrum is practically independent of the type of a hadron into which the charm is fragmented. The experiments on cumulative particle production off nuclei[14] also unambiguously indicate the hardness and similarity of spectra of all cumulative particles.

In our approach, these effects are easily explained by the fact that a quark with a large transverse mass provides a dominant contribution to the momentum of a hadron produced. Therefore, the spectra of secondary particles are almost completely defined by the structure functions of a hard quark and are independent of the fragmentation process.

Thus, we find the form of x-dependence as $x \to 1$ of the sea inside the proton

$$q^s_+(x)_{x\to 1} = P(x)(1-x)^n + N_1(x)(1-x)^5 + N_2(x)(1-x)^3, \tag{10a}$$

$$q^s_-(x)_{x\to 1} = P(x)(1-x)^n + 2N_1(x)(1-x)^5 + 2N_2(x)(1-x)^3\ , \tag{10b}$$

where the first terms of these relations describe the contribution of a quark sea due to a perturbative gluon ($n \approx 7$ within the quark-counting rule (see [15])), $P(x)$, $N_1(x)$, $N_2(x) \to$ *const* as $x \to 1$.

The difference between the coefficients in Eq. (10a) and Eq. (10b) comes from the fact that the sea quark helicity is antiparallel to the helicity of the valence quark off which the former is produced. Similarly, in our model it could be the substantial breakdown of $\mathbf{SU(2)}_f$ in the sea quark distribution functions as $x \to 1$: $\bar{d}_I(x) \approx 2\bar{u}_I(x)$ (I is the instanton part of Eq. (10a) and Eq. (10b)). Recently, the direct experimental

evidence of the d sea excess has appeared[16] *):

$$\int_0^1 dx\ (\bar{d}(x) - \bar{u}(x)) = 0.140 \pm\ 0.024.$$

In fact, the negative helicity of sea quarks and $\mathbf{SU}(2)_f$−breakdown of the sea is caused by the properties of zero fermion modes in the instanton field from which the Lagrangian, Eq. (6), is constructed.

STRUCTURE FUNCTIONS OF SEA QUARKS IN THE RANGE $X \to 0$ AND THE KOGUT-SUSSKIND POLE

As $x \to 0$ all quark and gluon configurations of the proton wave function are valuable and behavior of the distribution functions in this region is specified by the Regge asymptotics. Usually one assumes (see [15]) that the Pomeron exchange with intercept $\alpha_p(0) \approx 1$ dominates in the sum of the distributions $q^s\ (x) = q^s_+(x) + q^s_-(x)$, and hence:

$$\lim_{x\to 0} q^s(x) \propto 1/x, \tag{11}$$

whereas the difference $\Delta q^s\ (x) = q^s_+(x) - q^s_-(x)$ is specified by the A_1-meson trajectory with $\alpha_{A_1} \approx 0$, and therefore

$$\lim_{x\to 0} \Delta q^s(x) \propto const. \tag{12}$$

In fact, Eq. (12), which has been used in the analysis of experimental data by the EMC[1], is derived from the selection rule

$$\sigma(-1)^I G = -1 \tag{13}$$

for the Regge trajectories contributing to the structure function $g_1^p(x)$[15] (σ is signature). The well-known A_1−trajectory with $I = 1$, $\sigma = -1$, $G = -1$ satisfies this selection rule. However, it is obvious that this trajectory cannot contribute itself to the isosinglet anomalous combination $\Delta\Sigma(x) = \Delta u(x) + \Delta d(x) + \Delta s(x)$. In accordance with the rule, Eq. (13), the only Regge singularity capable to contribute to $\Delta\Sigma$ is that with quantum numbers $I = 0$, $\sigma = -1$, $G = 1$, $C = 1$.

In [6] we have suggested a new Regge trajectory with a high intercept $\alpha(0) \approx 1$ which allows us to obtain the singularity of the distribution functions as $x \to 0$. There it was also pointed out that the trajectory was probably related with the Kogut-Susskind ghost in QCD[8]. It cannot contribute to the structure function $g_1^p(x)$ as it causes the flip of the chirality of the proton (see Fig. 2) . However, the double-pole exchange can contribute to the Compton amplitude of the forward scattering off the nucleon, as in Fig 3, which is produced by quadrating the diagram of Fig 2b.

*)This result is apparently to be considered as a preliminary one because nuclear effects inside the deuteron can be essential (L.P. Kaptari, A.Yu. Umnikov private communication)

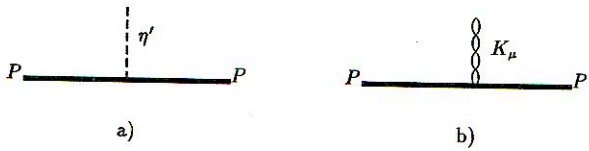

Fig. 2.The contribution to the divergence of axial-vector current of a) direct interaction of η'−meson, b) via the Kogut-Susskind pole.

In works, it was argued that the Kogut-Susskind pole effectively takes into account the contribution of heavy gluonic states to the correlator of hadron currents. Hence, we suppose that this pole is reggezied and its trajectory ("anomalon") contains gluonic states with odd spin. It is easy to see that the "anomalon" has the quantum numbers $\sigma = -1$, $P = +1$, $C = -1$, $I = 0$. The intercept of the new trajectory should obviously be equal to unity, $\alpha_A(0) = 1$, as $t \to 0$ we have the massless pseudo-vector pole.

From this it is easy to obtain x-dependence of the contribution of the "anomalon" to the structure function $g_1^p(x)$. Namely, the $A \otimes A$-cut corresponds to the diagram of Fig 3 and its contribution is

$$g_1^p(x)_{x\to 0} \to -a/(x \ln^2 x). \tag{14}$$

The minus sign in Eq. (14) has the principle meaning since it leads to lowering of the quark helicity inside the proton. Joining Eq. (10a), Eq. (10b) and Eq. (14) we obtain the expression for the singlet distribution functions of sea quarks over the helicity inside the proton

$$q_+^s(x) = \frac{A_P}{x}(1-x)^7 + \frac{1}{x \ln^2 x}[B(1-x)^5 + C(1-x)^3], \tag{15a}$$

$$q_-^s(x) = \frac{A_P}{x}(1-x)^7 + \frac{2}{x \ln^2 x}[B(1-x)^5 + C(1-x)^3], \tag{15b}$$

where the first terms of these relations describe the Pomeron contribution as $x \to 0$ and the quark sea due to a perturbative gluon as $x \to 1$ and the second terms describe the contribution of the $A \otimes A$-cut as $x \to 0$ (Fig. 3) and instantons as $x \to 1$ (Fig. 1).

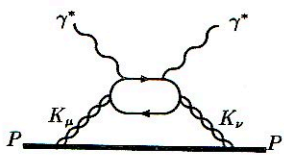

Fig. 3.The Kogut-Susskind pole contribution to the Compton effect off the proton.

From Eq. (15a) and Eq. (15b) we obtain the contribution of the ABJ anomaly to the spin-dependent distribution function in the form

$$g_1^p(x) = -\frac{1}{x \ln^2 x}[B_1(1-x)^5 + C_1(1-x)^3] \tag{16}$$

and to the proton momentum

$$\Delta p^s = \int_0^1 dx \, \frac{3}{\ln^2 x}[B_1(1-x)^5 + C_1(1-x)^3]. \tag{17}$$

Unfortunately, the EMC data at low x : $x < 0.05$ have large errors; so it is impossible to determine the constants B_1 and C_1 separately from the data[1]. In this case we do the following. It is obvious that the anomaly dominates at small x and essentially affects the value of the integral of $g_1^p(x)$:

$$I_p = \int_0^1 dx \; g_1^p(x). \tag{18}$$

If the anomaly were absent, then the Ellis-Jaffe sum rule would be correct[3]:

$$I_p^{EJ} = 0.175 \pm \; 0.018 \tag{19}$$

which corresponds to the quark helicity:

$$\Delta\Sigma^{EJ} = 0.60 \pm \; 0.12. \tag{20}$$

Recently, the work[18] has appeared where the estimation was derived :

$$\Delta\Sigma^{KZ} = -\frac{2N_f}{11N_c - 2N_f}. \tag{21}$$

In [18] the circumstance has been used that the change of the axial charge is related with the motion of the Dirac sea levels in the field of nonperturbative fluctuations (for example instantons). Then, the magnitude of the proton axial charge should not depend on the manner of regularization of the Dirac vacuum. By using this independence and some natural assumptions in[18] the model independent value, Eq. (21), has been derived. For $N_f = 3$ one has

$$\Delta\Sigma^{KZ} = -0.22, \tag{22}$$

which does not agree even in sign neither with Eq. (20) nor with the EMC number, Eq. (2). We think that this discrepancy is due to incorrect extrapolation of the EMC data into the small x region.

In order to overcome this difficulty one should obviously take into account the anomaly contribution , Eq. (16). In addition, its contribution to the integral, Eq. (18), should be such that the value, Eq. (22) , of the quark helicity be reproduced. Further, it is easy to show that the value of the integral , Eq. (18) , equal to

$$I_p^{KZ} \approx 0.086 \tag{23}$$

corresponds to Eq. (22). Then, from the difference of Eq. (19) and Eq. (23) we find the contribution of the anomaly to the integral, Eq. (18),

$$I_p^A \approx -0.089. \tag{24}$$

In Fig 4 we present our prediction of $g_1^p(x)$ satisfying Eq. (16), Eq. (23), and Eq. (24) with the parameterization[†]:

$$g_1^p(x) = -\frac{0.151}{x \ln^2 x}(1-x)^5 + 0.625(1-x)^{2.57}. \tag{25}$$

Here, the first term is the contribution of the anomaly; the second, which is regular over x , was determined from the fit of the EMC data in accordance with Eq. (25). This term corresponds to the valence quark contribution to $g_1^p(x)$.

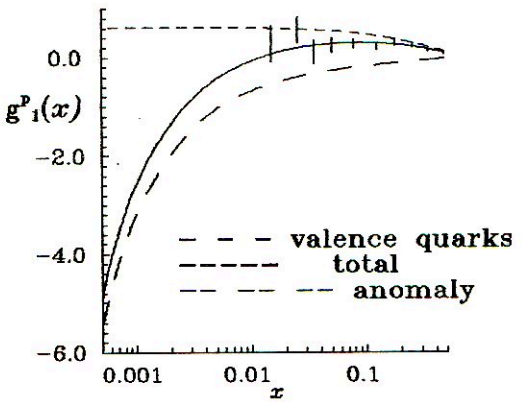

Fig. 4-Spin-dependent structure function $g_1^p(x)$. Continues line is the fit of EMC data by Eq. (25).

Under the parameterization, Eq. (25) , the contribution of the anomaly to the proton momentum, Eq. (17) , is equal to 2.7 % which is smaller than half a value of the proton momentum carried by sea quarks, Eq. (4) , (the rest 4.7 % is the contribution of the perturbative sea). Here, we should stress that as $x \to 0$ only the anomaly contribution to Eq. (25) allows us to match two numbers Eq. (22) and Eq. (4).

Thus, the analysis of the distribution functions of sea quarks performed within the nonperturbative QCD points out the necessity of introducing new Regge trajectory related with the Adler-Bell-Jackiw anomaly and the Kogut-Susskind pole ("anomalon") in the QCD. How to manifest this trajectory?

[†]The parameterization with the asymptotic form as $x \to 1$ $(1-x)^3$ gives essentially the same behavior.

Really, this trajectory should be naturally manifested in the processes of hadron-hadron scattering at high energies too. Now, the necessity of introducing the Regge trajectory with a high intercept additional to the Pomeron is intensively discussed[19, 20]. This is primarily connected with the necessity to explain the form of differential cross sections of elastic $pp-$ and $p\bar{p}-$ interactions at high transfers $\mid t \mid \geq 1\ Gev^2$. Namely, the experiment points out two salient facts: absence of a second diffractive minimum in pp interactions and existence of the shoulder in $p\bar{p}$ interactions at ISR energies and, second, independence of the differential cross section of energy at $\mid t \mid \geq 2\ Gev^2$.

Usually, these facts are explained by the contribution of the Odderon trajectory [20] with quantum numbers $\sigma = -1$, $P = -1$, $C = -1$. Within perturbative **QCD** the Odderon resembles the three-gluon exchange between hadrons. However, there arise some problems if the Odderon is applied to the data [21, 22].

Using the "anomalon" we arrive at a more natural explanation of these data. First, due to the double-spin flip helicity amplitude induced by "anomalon" the latter does not contribute to the total cross sections and thus the difference $\sigma_{pp}^{tot} - \sigma_{p\bar{p}}^{tot} \to 0$ as $\sqrt{s} \to \infty$. Further, we expect a very small slope α'_A of the "anomalon". It is connected with that this slope is defined by the size of an instanton while the slope of the Pomeron is related to the confinement radius. Thus, we have simple estimation $\alpha'_A/\alpha'_P \approx (\rho_c/R_{conf})^2 \approx 10^{-1}$. If as usual $\alpha'_P = 0.2{-}0.3$, then we have $\alpha'_A = 0.02{-}0.03$. Therefore, we can neglect the slope of the "anomalon".

Thus, the "anomalon" contribution to the amplitude of pp ($p\bar{p}$) scattering may be written as

$$T_A(t,s) = \mp\, \gamma_A(t)(\frac{s}{s_0}), \tag{26}$$

where the up (down) sign corresponds to pp ($p\bar{p}$) scattering. The residue in Eq. (26) should be related to the distribution of the axial charge inside the proton and therefore,

$$\gamma_A(t) \propto [G_A^{I=0}(t)]^2 \propto 1/[1 - t/M_A^2]^4, \tag{27}$$

where $M_A^2 \approx 1.4\ Gev^2$[23].

The Pomeron amplitude corresponds to the expression:

$$T_P(t,s) = i\gamma_P(t)(\frac{s}{s_0})^{\alpha_P(t)} \exp[-i\frac{\pi}{2}(\alpha_P(t) - 1)]\,, \tag{28}$$

where the Pomeron residue is related with the electromagnetic form factor of a nucleon[19]:

$$\gamma_P(t) \propto [G_{em}(t)]^2 \propto 1/[1 - t/M_p^2]^4, \tag{29}$$

where $M_p^2 \approx 0.71\ Gev^2$.

At large t the "anomalon" becomes dominant over the Pomeron ($M_A^2 > M_p^2$), which results in the observed change in the slope of the elastic cross sections of pp and $p\bar{p}$ scattering at $\mid t \mid \approx 1\ Gev^2$. Therefore, the absence of diffraction minima connected

with multi-Pomeron exchanges is explained by the fact that they remain under the large contribution of the "anomalon" at $\mid t \mid \geq 2\ Gev^2$.

Owing to the absence of the double-spin flip amplitude of Pomeron it does not interfere with the "anomalon", and therefore, the differential cross sections of $pp-$ and $p\bar{p}-$ interactions are

$$\frac{d\sigma}{dt} = \frac{1}{16\pi s^2}[\mid T_P \mid^2 + \mid T_A \mid^2]. \tag{30}$$

In Fig. 5 fits of the total and differential cross sections at high energies with the Pomeron and "anomalon" trajectories are presented. As we see, there is a satisfactory agreement with experiment in the regions $\mid t \mid \leq 1\ Gev^2$ and $\mid t \mid \geq 2\ Gev^2$. Note here that a small slope of the "anomalon" trajectory, $\alpha'_A \approx 0$, is needed for explaining the energy independence of elastic cross sections of $pp-$ and $p\bar{p}-$ interactions at $\mid t \mid \geq 2\ Gev^2$. Essential deflection is seen only in the region of the dip in pp at ISR energies but it seems to be of a very complicated nature due to secondary Reggeons and their cut-offs[19]; and its dynamics is a subject of our forthcoming study.

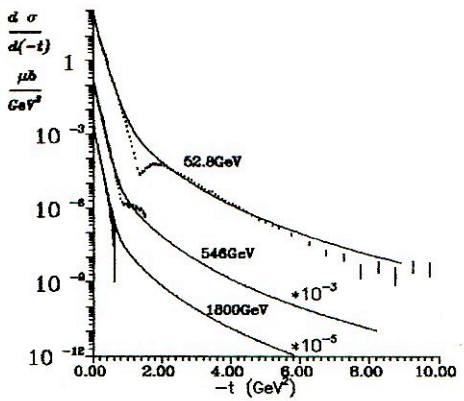

Fig. 5. Elastic pp and $p\bar{p}$ scattering at 52.8 GeV, 546 GeV, 1800 GeV. Data for $\sqrt{s} = 1800\ GeV$ are from[29]. The parameters are:
$\alpha_P = 1.08$, $\alpha'_P = 0.3$, $M_P^2 = 0.97\ GeV^2$, $\gamma_P(0) = 21.8$;
$\alpha_A = 1$, $\alpha'_A = 0$, $M_A^2 = 1.08\ GeV^2$, $\gamma_A(0) = 0.57$. .

In fact, at high energies two parts of structure functions of sea quarks, Eq. (15a) and Eq. (15b), correspond to two regions of transfers in the $pp-$ and $p\bar{p}-$ interactions. At $\mid t \mid \leq 1\ Gev^2$ the Pomeron dominates but at $\mid t \mid \geq 2\ Gev^2$ the "anomalon" does. The dominance of the "anomalon" at large transfers is clear since its contribution to the structure functions, Eq. (15a) and Eq. (15b), corresponds to the Fock state with large transfer momentum, Eq. (7).

CONCLUSION

Within the instanton liquid model of the **QCD** vacuum the parameterization of the distribution functions of sea quarks inside the proton is derived. It should be stressed that the instanton mechanism of resolution[24, 25] of "spin crisis" differs entirely from the perturbative explanation[26] based on the contribution of the **ABJ**-anomaly on polarized gluons. Within the perturbative mechanism a very large value of the angular momentum $\Delta G \approx 5$ carried by gluons is required, which is in turn difficult to understand within the well-working constituent three-quark model of the proton.

In our approach there is a natural way to generate negative helicity of sea quarks[24]. Namely, the quark helicity is flipped in the field of strong vacuum fluctuation - instanton. In this case, a quark-antiquark pair with a large relative angular momentum arises to compensate for the changes of helicity by $2N_f$ since the spins of sea and valence quarks are opposite to the spin of the original quark. Thus, our mechanism leads to a completely definite orientation of rotation of the quark-antiquark cloud within a constituent quark. However, the total angular momentum carried by a quark is unchanged, and this is the reason for the good results of the constituent quark model in the description of static properties of hadrons.

The analysis of the spin-dependent distributions of sea quarks indicates the necessity of introducing a new Regge trajectory related with the Kogut-Susskind pole. The specific features of dynamics of $pp-$ and $p\bar{p}-$ interactions at large transfers and high energies also require a trajectory additional to the Pomeron which does not die out with growing energy.

Note that probably there exists a direct experimental confirmation of the "anomalon".[‡)] For instance, the **OMEGA** Collaboration[27] has observed that the differential cross section of reaction $\gamma p \to b_1(1^{+-}, 1235)p$ at $E_\gamma = 40 \div 70$ *Gev* is almost energy independent although in quantum numbers the Pomeron cannot produce the contribution in this reaction. On the other hand, the "anomalon" can result in the constancy of the cross section in energy and in the slope over t about twice as small as the slope of the diffractive cone in elastic pp scattering at these energies, which has been observed in experiment [27].

Within our approach we can produce more natural explanation of hardness of charmed particles produced in the hadron interactions[13] and of cumulative particles produced off nuclei[14]. It is very interesting also to investigate the polarization process of proton scattering off deuteron to manifest new trajectory at low energy[§)] that it is possible in future at Dubna in the Laboratory high energies.

From our point of view the "anomalon" is also needed in order to explain anomalously large polarization phenomena in hadron-hadron processes at large transfers[28]. Thus, e.g., the three-anomalon vertex (3A) leads to the amplitude with single flip of helicity Φ_5 which does not die out with growing energy. Within the perturbative QCD this amplitude behaves as $m/\sqrt{s}$ where m is the quark current mass and therefore the perturbative QCD in principle cannot explain the anomaly in the scattering of polarized particles at high energies[28].

[‡)]The authors thank S. B. Gerasimov who drew their attention to this result.

[§)]A. Efremov, V. Karotkian Private communication

To provide a complete answer to the question of the existence of the new trajectory, which characterizes fundamental $U_A(1)$ symmetry of strong interaction, experimental efforts should be made along the following directions: first, precision measurement of the DIS spin-dependent proton structure function $g_1^p(x)$ in the region of small x; second, the measurement of the differential cross section of $\gamma p \to b_1(1^{+-}, 1235)p$ at $E_\gamma > 70$ *Gev*; third, investigation the process of polarized proton scattering off deuteron in order to manifest new trajectory at low energy. Thus we can hope that this new phenomenon forces low and high energies physics come into play simultaneously.

ACKNOWLEDGMENTS

The authors are sincerely thankful to S. B. Gerasimov,V. T. Kim, E. A. Kuraev, A.P. Samokhin, A.N. Shelkovenko, Yu. A. Simonov, B. V. Struminsky, M. K. Volkov, and L. L. Yenkowzky for fruitful discussions.

References

[1] EMC, J. Ashman et al. *Phys. Lett.* **B206** (1988) 364;
Nucl. Phys. **B328** (1990) 1.

[2] The CCFR Collab., C. Foudas et. al. *Phys. Rev. Lett.* **64** (1990) 1207.

[3] J. Ellis, R. L. Jaffe, *Phys. Rev.* **D9** (1974) 1444.

[4] R. L. Jaffe, A. Manohar, *Nucl. Phys.* **B337** (1990) 509 and references therein.

[5] G. Preparata, J. Soffer, *Phys. Rev. Lett.* **61** (1988) 1167;
G. Preparata, P.G. Ratcliffe, J. Soffer, *Phys. Rev. Lett.* **66** (1991) 687.

[6] A. E. Dorokhov, N. I. Kochelev *Phys. Lett.* **B259** (1991) 335.

[7] S.L. Adler *Phys. Rev.* **177** (1969) 2426;
J.S. Bell, R. Jackiw *Nuov. Cim.* **60A** (1969) 47.

[8] J. Kogut, L. Susskind *Phys. Rev.* **D11** (1975) 3594.

[9] E. V. Shuryak, *Phys. Rep.* **115** (1984) 151;
D. I. Dyakonov, V. Yu. Petrov *Nucl. Phys.* **B272** (1986) 457.

[10] S. J. Brodsky, C. Peterson, N. Sakai *Phys. Rev.* **D23** (1981) 2745.

[11] G. 't Hooft, *Phys. Rev. Lett.* **37** (1976) 8; *Phys. Rev.* **D14** (1976) 3432;

[12] N. I. Kochelev *Sov. J. Nucl. Phys.* **41** (1985) 291;
A. E. Dorokhov, N. I. Kochelev *Yad. Fiz.* **52** (1990) 214.

[13] The ACCMOR Collab., S. Barlag et. al. , *CERN report* CERN-ep/88-104 (1988); *Z. Phys.* **C46** (1990) 563.

[14] S. V. Bojarinov et al, *Yad. Fiz.* **45** (1987) 1472; *Yad. Fiz.* **50** (1989) 1605 (in Russian); Proc Int Conf *"Quark Matter 90"* Manton, 1990.

[15] B. L. Ioffe, V. A. Khose, L. N. Lipatov *Hard processes*, North-Holland, Amsterdam, **1** (1984) 61.

[16] NMC, D. Allasia et al, *Phys. Lett.* **B249**(1990) 366;
D. Allasia et al, *CERN report* CERN-EP/91-105 (1991).

[17] E. Witten *Nucl. Phys.* **B156** (1979) 269;
G. Veneziano *Nucl. Phys.* **B159** (1979) 213;
G't'Hooft *Phys. Rep.* **142** (1986) 357.

[18] J. H. Kühn, V. I. Zakharov *Phys. Lett.* **B252**(1990) 615.

[19] A. Donnachie, P. V. Landshoff, *Nucl. Phys.* **B123** (1983) 345; *Nucl. Phys.* **B231** (1984) 189

[20] P. Gauron, B. Nicolescu, E. Leader *Phys. Rev. Lett.* **54** (1985) 2656;
D. Bernard, P. Gauron, B. Nicolescu *Phys. Lett.* **B199** (1987) 125;
L. L. Yenkovsky, A. N. Shelkovenko, B. V. Struminsky *Z. Phys.* **C36** (1987) 496;
V. A. Petrov, A. P. Samokhin, *Phys. Lett.* **B237**(1990) 500.

[21] A. Donnachie, P. V. Landshoff, *Nucl. Phys.* **B348** (1991) 297.

[22] A. Donnachie, P. V. Landshoff *Z. Phys.* **C2** (1979) 55;
P. V. Landshoff, D. J. Pritchard *Z. Phys.* **C6** (1980) 69.

[23] V. Bernard, N. Kaiser, Ulf-G. Meissner *Phys. Lett.* **B237** (1990) 545.

[24] A. E. Dorokhov, N. I. Kochelev *Mod. Phys. Lett.* **A5** (1990) 55;
Phys. Lett. **B245** (1990) 609.

[25] S. Forte, *Phys. Lett.* **B224** (1989) 189; *Nucl. Phys.* **B331** (1990) 1.

[26] C.S. Lam, Bing-An Li *Phys. Rev.* **D25** (1982) 683;
A. V. Efremov, O. A. Teryaev *JINR preprint* Dubna E2-88-287;
G. Altarelli, G.G. Ross *Phys. Lett.* **B212** (1988) 391;
R.D. Carlitz, J.C. Collins, A.H. Mueller *Phys. Lett.* **B214** (1988) 229.

[27] The OMEGA Collaboration, M. Atkinson et al *Nucl. Phys.* **B243** (1984) 1.

[28] A.D. Krisch *Proc. VI Int Symp on High Energy Spin Physics*, Marseille, 1984 ;
S.M. Troshin *Proc. VI Int Symp on High Energy Spin Physics*, Protvino, 1986.

[29] E710 Collab. N. A. Amos et al. *FERMILAB-FN-562* (1991).

Рукопись сборника поступила в издательский отдел
21 января 1992 года

Редактор Э.В.Ивашкевич
Макет Т.Е.Попеко

Подписано в печать 23.04.92
Формат 60×90/16. Офсетная печать. Уч.-изд.листов 22,86
Тираж 200. Заказ 45269. Цена 6 руб. 86 коп.

Издательский отдел Объединенного института ядерных исследований
Дубна Московской области